University of Sheffield

Activity-dependent adaptation in single neurons in the *Drosophila* mushroom body

A thesis submitted in partial fulfilment of the requirements for the degree of Doctor of Philosophy

The University of Sheffield

Faculty of Science

School of Biosciences

By Thomas Christoper Cozens

Registration number: 210169391

September 2025

Acknowledgements

There are so many people to thank for all the support and guidance they have provided me throughout my PhD and beyond.

First, I would like to thank Andrew for being an incredible supervisor, teacher and mentor. I have learned so much over these 4 years and a lot of that is thanks to your patience and guidance. A students PhD experience is often defined by their supervisor and I am grateful to have had such an excellent one.

To all the placement and master's students who have worked in the lab over the years, I am grateful for all you have contributed to this work, for helping me learn how to be a good teacher and for teaching me so much in return.

To everyone in the lab past and present, I appreciate all the assistance (physical and mental) you have provided over so many experiments. In particular, thank you Melissa for so diligently taking care of my flies when I am away, Kat for sharing the struggle of antennal nerve dissection with me and thank you Greg for providing so much good advice.

To all my friends, thank you for providing an escape from constantly thinking about science and for your patience with me disappearing into my thesis these last few months.

To my parents, thank you for your support and constant encouragement these last 26 years. To Mum, thank you for helping me get through all my exams and for inspiring and nurturing my love of science. To Dad, thank you for being willing to help with any problem, no matter how far-fetched, and for all the thought-provoking conversations on long car journeys.

Finally, to Georgia, your love, patience and support has kept me sane these last few months. The one thing that has kept me on task is thinking about our future and all the amazing things we have yet to do together. The effort and care you put into everything in your life inspires me and I can only hope to one day be as good at spinning so many plates as you are.

Preface

This thesis and all associated results are my own work apart from the following exceptions which are also highlighted in the text where relevant:

- Connectome analysis in Figure 3.3 was performed previously by Kripi Mehra.
- All 18°C and 22°C ageing experiments displayed in Figure 3.10 were performed by Ya Yu Colin Wong.
- Half of the Reversal dissection and imaging experiments displayed in Figure 3.11 were performed by Ya Yu Colin Wong.
- Starvation and Sugar-only experiments displayed in Figure 3.12 were performed by Chaw C Yi, Ya Yu Colin Wong and I.
- Dissections and immunolabelling for α/β and α'/β' experiments were performed by Guy W Austin, Joseph Faulkner and Chaw C Yi.

This thesis has not previously been submitted to this or any other university.

Summary

How do neural circuits maintain stable function in the face of developmental changes and natural variability? Many neurons use homeostatic plasticity to adjust their activity to maintain a ‘set point’ level of activity. I investigate Kenyon cells, a population of ~2000 neurons that store olfactory associative memories in the Drosophila mushroom body. Our computational models suggest individual Kenyon cells should equalize the average level of activity across the population to avoid a few neurons responding to most odours while a minority are silent or respond very little. This would increase overlap between representations and impair learned odour discrimination. In this thesis I tested whether single Kenyon cells have activity-dependent compensation mechanisms to prevent such a situation. I tested this by artificially activating single Kenyon cells using the heat-activated cation channel TrpA. I find that in flies heated for 24-96 hours, TrpA-expressing γ Kenyon cells have fewer claws (dendritic input sites) than controls. However, the other two Kenyon cell subtypes, α’/β’ and α/β showed no such adaptation, suggesting different compensatory mechanisms exist between subtypes. Furthermore, this adaptation is not a result of early development flexibility but does disappear with significant age. I propose that this morphological change compensates for increased activity by reducing the number of excitatory inputs the cell receives and thereby decreasing Kenyon cell activity. This is supported by preliminary single cell live imaging experiments using the calcium indicator GCaMP, which showed that the activity of γ KCs hyperactivated for 24 hours is reduced. Together, these results reveal previously unidentified compensatory, potentially homeostatic, mechanisms in single Kenyon cells.

List of Abbreviations

2p	2 Photon
AIS	Axon initial segment
AMPAR	Type of glutamate receptor
AP	Action potential
APL	Anterior paired lateral
ASM	Anaesthesia resistant memory
BD	Binocular deprivation
BK	Big potassium channels
BRP	Bruchpilot
Ca^{2+}	Calcium
Cac	Cacophony (voltage-gated calcium channel)
CaMK	Calmodulin kinase (various types)
cAMP	Cyclic adenosine monophosphate
Cav	Voltage-gated calcium channels
ChAT	Choline acetyltransferase
CP	Critical period
DAN	Dopaminergic neurons
dNTP	Deoxynucleotide triphosphate
E/I	Excitatory/Inhibitory ratio
EPSP	Excitatory postsynaptic potential
FLP	Flippase protein
GABAR	GABA receptor
GCaMP	Genetically encoded calcium indicator
GFP	Green fluorescent protein
GLM	Generalized linear model
IEI	Inter-event intervals
IPSP	Inhibitory postsynaptic potential
K^+	Potassium
KC	Kenyon cell
KD	Knockdown
Kir2.1	Inward-rectifying potassium channel
KO	Knockout
Kv	Voltage-gated potassium channels
LH	Lateral horn
LTD	Long-term depression
LTM	Long-term memory
LTP	Long-term potentiation
MARCM	Mosaic analysis with a repressible cell marker
MB	Mushroom body
MD	Monocular deprivation
mEPSC	Miniature excitatory postsynaptic current
mEPSP	Miniature excitatory postsynaptic potential

MTM	Mid-term memory
Na^+	Sodium
NaChBac	Bacterial sodium channel
nAChR	Nicotinic acetylcholine receptors
Nav	Voltage-gated sodium channels
NMDAR	Type of glutamate receptor
NMJ	Neuromuscular junction
ORN	Olfactory receptor neurons
PCR	Polymerase chain reaction
PhTx	Philanthotoxin
RF	Receptive field
RRP	Readily releasable pool
SK	Small potassium channels
STM	Short-term memory
TeTx	Tetanus toxin light chain
TRESK	TWIK-related spinal cord K^+ channel
TrpA	Heat-sensitive cation channel
TTX	Tetrodotoxin

1. General Introduction

1.1. The dynamic brain: Learning networks and their significance

The ability to learn is shared across the animal kingdom and allows us to respond to changes in our environment and alter our behaviour accordingly. However, the complexity of learning varies dramatically. At the simplest level, single celled organisms like bacteria and acellular slime molds satisfy some of the criteria associated with learning. Both are capable of some level of habituation, what many would consider one of the most basic forms of learning, and slime molds can even solve mazes (Lyon, 2015; Nakagaki, Yamada and Tóth, 2000; Dussutour, 2021; Boisseau, Vogel and Dussutour, 2016). Even in these relatively simple systems each component of the system must be regulated to allow for continued adaptation. If one parameter is altered too far the consequences could be disastrous. How do the complex learning networks found in nervous systems achieve reliable outcomes on more 'difficult' tasks/behaviours, when so many parameters within the network are constantly in flux? Furthermore, is there something optimal about the structure and features of these networks that must be maintained to allow for continued sensory encoding/function. This is the overarching question of this work, but before delving deeper it is important to understand what learning networks are and discuss their core features.

When describing a concept as broad as learning networks it is best to start with a small and simple model and work our way up. The Perceptron (Rosenblatt, 1958) represents one of the earliest models of a learning network we have and at its most basic level is characterised by a single-layered architecture (Figure 1.1). In a single-layer perceptron the input layer is directly connected to the output layer and each connection between nodes has an associated weight. These weights determine the influence of a given input node on its associated output node and all weighted inputs are then summed. If they meet/exceed the required threshold the output node is activated; otherwise, it remains inactive. This model works well for tasks where the determining factors have a linear relationship, such as AND logic gates where the sum of ON inputs must reach a particular threshold to shift the output to active. However, it does not perform well when facing problems where the relationship between inputs and desired output is more complex, i.e. non-linear. It is also not what we would typically consider a 'learning network' when we envision brains or even complex machine learning models.

We get closer to 'true' learning networks when we examine the Multilayer Perceptron(Rosenblatt, 1958; Rumelhart, Hinton and Williams, 1986). The most obvious difference is the addition of one or more 'hidden layers' between the input and output layer

(Figure 1.1). Intermediate layer(s) allow the network to learn non-linear decision boundaries and tackle more complex problems with additional features. For example, when trying to predict the likelihood of an individual developing a disease, a Multilayer Perceptron can consider a combination of factors like age, genetics or lifestyle that don't necessarily have a linear relationship. The Multilayer Perceptron is comparable to the learning networks we find in nervous systems. For example, the mushroom body (MB), which is the focus of this work, has a 3-layered architecture that allows for efficient discrimination between odours. The intermediate layer made up of Kenyon cells (KC) allows the small number of odour input channels of ~50 (Couto, Alenius and Dickson, 2005) to be expanded into many possible odour representations. Additionally, this system can adjust the weights of synapses so that behavioural response to different odours can be altered when presented with changes in the valence of a given odour. This is where the learning part of the network comes in. In both computational models and nervous systems, a given network must be capable of storing new information so the system can respond to ever-changing inputs and produce logical outputs.

Ultimately, a multilayer perceptron is one type of learning network composed of a set of interconnected nodes, typically divided into a multilayered structure made up of: an input layer that brings in information, an intermediate layer that applies some non-linear transformation to that input, and an output layer that produces a range of responses which can be as simple as approaching or avoiding an odour. However, additional complexity exists within learning networks beyond what is apparent in their structure and connectivity. To achieve reliable processing at the connections between layers it is essential to maintain stability in key features necessary for the network to function, which is typically achieved via homeostatic plasticity. The exact features maintained within set limits vary between networks depending on the role of that system. The MB needs to be capable of effective odour discrimination and to do so the percentage of the expansion layer population (KCs) that respond to a given odour must remain low to ensure minimal overlap between representations; without this the fly may struggle to distinguish between reward- and punishment-associated odours, which could have disastrous consequences (Lin et al., 2014; Parnas, Manoim and Lin, 2024). Understanding of this extra complexity is only possible by observing network activity and how it responds to perturbations; through this we can identify what features must be maintained. Our recent modelling suggests that another target for regulation is the average activity of KCs across the population; if a small proportion of neurons have consistently high activity, this may predispose them to respond to most odours, while the remaining silent majority contribute to a much smaller number of representations

(Abdelrahman, Vasilaki and Lin, 2021). This model further suggests that a single cell mechanism to maintain a set level of activity on an individual neuron basis could prevent undesirable diversity in activity. Ultimately, it is currently unclear how much single neurons contribute to the function of a whole learning network, and whether adaptations at the single cell level are sufficient to allow continued function of these networks. This work explores the importance single neurons have in a larger network and how each neuron contributes to maintain efficient sensory encoding. The *Drosophila* mushroom body is the model system used to explore these ideas, with a particular focus on the Kenyon cells found in its intermediate/hidden layer. It is therefore important to begin by explaining why this model system was chosen, and to explain the structure and features we have discussed above, before we can grasp the importance of single KCs to this system.

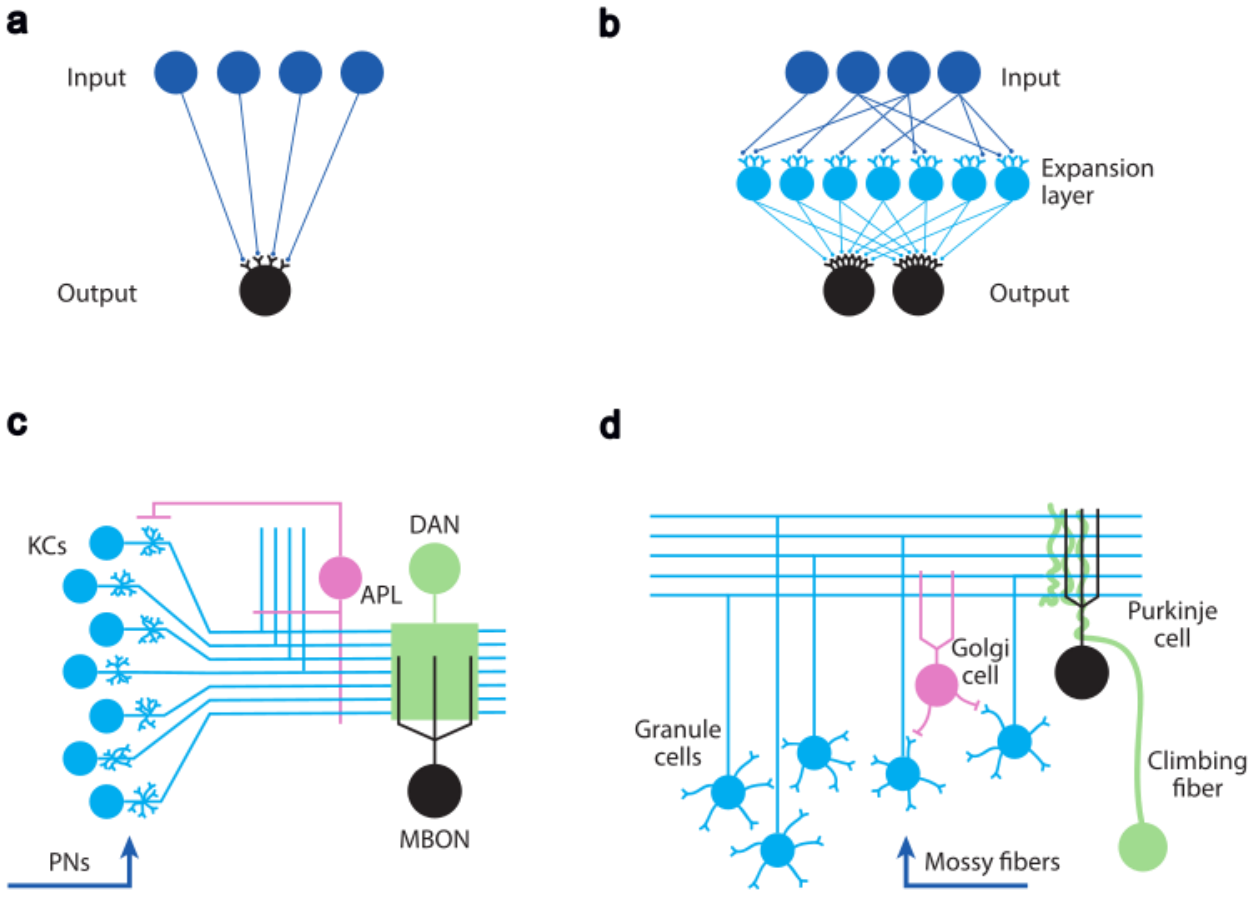

Figure 1.1: Learning networks. **a)** Schematic depiction of a single layer perceptron. Each input (dark blue) has an associated weight and these are summed at the output node (black). **b)** Multilayer perceptron. Addition of a hidden/intermediate expansion layer (light blue) allows non-linear processing of inputs to occur, enabling the network to tackle more complex problems. **c)** Mushroom body circuit. Input carrying odour information arrives via projection neurons (dark blue) and synapse with Kenyon cell (light blue) claws. The Anterior paired lateral neuron (pink) provides feedback inhibition to all Kenyon cells and maintains sparse coding. Kenyon cells synapse with mushroom body output neurons (black) in compartments along the lobes. Dopaminergic neurons (green) bring odour valence information to these compartments and drive plasticity to bias output in response to different odours. **d)** Cerebellar circuit. Input conveying motor/balance information arrives via Mossy fibres (dark blue). Similar to the Mushroom body these neurons synapse with an expansion layer composed of Granule cells (light blue). Golgi cells (pink) provide inhibition to this expansion layer. Parallel fibres from Granule cells synapse with Purkinje cells (black) and Climbing fibres (green) wrap around them bring motor error information and driving plasticity. Correct motor output leaves via Purkinje cells. The basic structure of these two circuits are remarkably similar. **Adapted from (Modi, Shuai and Turner, 2020).**

1.2. *Drosophila melanogaster* as a model organism

The focus of this work is the *Drosophila melanogaste*r Mushroom body, and this model system was chosen for several reasons. First their fast generation time allows for much larger sample sizes than you typically get in mammalian studies and the many stocks utilised for a single experiment are very easy to maintain. One of the primary reasons researchers use *Drosophila melanogaste*r is the species' unparalleled genetic access, which is a result of several groundbreaking innovations in this field. The first is the development of balancer chromosomes almost 100 years ago(Muller, 1918, 1927). Balancers prevent meiotic recombination between homologous chromosomes and therefore loss of any useful mutations/transgenes. This in combination with balancer homozygous lethality/sterility allows for the maintenance of mutant stocks for prolonged periods of time, an ability that is unmatched by any other model system. Balancers are also typically accompanied by mutations that induce noticeable markers/phenotypes like altered eye and wing shape or number of abdominal hairs; this feature makes it easy to track the presence of transgenes.

The ability to manipulate the *Drosophila* genome was further expanded by the development of several techniques that allow the insertion of single genes or gene constructs; first P-element mediated transformation where the vector inserts your transgene randomly on the genome (Rubin and Spradling, 1982), and later the more specific attb-P[acman] which allows you to insert the transgene at defined attb docking sites across all 4 chromosomes (Venken et al., 2006). Another innovation was the development of the (FLIP)-flippase recognition target (FRT) recombination system (Golic and Lindquist, 1989). This utilises a recombinase

found in yeast (*Saccharomyces cerevisiae*) that induces recombination between two flanking FRT sites, allowing for targeted deletion of endogenous genes or transgenes between these sites when a flippase is present to induce this. The GAL4/UAS system in yeast was discovered later and is used to induce targeted expression of genes in specific cell types (Brand and Perrimon 1993). This system involves the transcriptional activator GAL4 binding to Upstream Activating Sequences (UAS) which act as promoters for genes they are closely associated with; importantly transcription of the transgene only occurs when GAL4 binds. Random insertion of GAL4 with an associated promoter into the Drosophila genome has allowed the creation of many cell-specific lines. The beauty of this system is that when by chance a GAL4 sequence is closely associated with a gene that is specific to a subtype or set of subtypes, this can then be identified by combining that line with a UAS that promotes expression of a fluorescent protein; only the cells that produce GAL4 will be labelled (Tanaka 2008). Importantly, this technique has also massively expanded the capabilities of *Drosophila* circuit neuroscience. Previously, the measuring and manipulation of neurons was limited, typically involving direct electrophysiological manipulation, a method that is far easier in the much larger brains of mammalian models. This changed with the discovery and successive iteration of the genetically encoded calcium sensor GCaMP (Nakai, Ohkura and Imoto, 2001), which utilises a single GFP (G) bound to a calmodulin protein (CaMP) that has a binding affinity for Ca2+. Importantly, this fluorescent marker responds to changes in intracellular Ca2+ levels at timescales relevant for neural activity and generally correlates with changes in activity measured electrophysiologically (Jayaraman and Laurent, 2007; Chen et al., 2013). In tandem, techniques for the manipulation of neural activity were developed including utilising the heat sensitive cation channel dTrpA1, which opens in response to temperatures >25°C and induces increased activity in neurons (Hamada et al., 2008), and optogenetics (Zemelman et al., 2002; Deisseroth, 2010, 2011) which uses photosensitive proteins that induce changes in neural activity in response to the presence of light of specific wavelengths; the use of light allows for fast excitation and investigation into the relevance of firing patterns within neurons. Using GAL4/UAS with these techniques enables targeted measuring and manipulation of specific neuron subtypes without the need to use difficult techniques like electrophysiology. Several of these techniques were utilised in this work and will be discussed in further detail later.

Conditional expression of transgenes can be achieved when the GAL80 gene is incorporated. GAL80 represses GAL4, preventing it from binding to UAS and inducing expression of its associated gene. Its temperature sensitive form GAL80ts becomes non-

functional at >29C, which prevents it from repressing GAL4 (McGuire, Mao and Davis, 2004; Pilauri et al., 2005). This allows for temporal control of gene expression in specific cell types with the ability to switch genes On and Off by altering temperature and is relatively simple, only requiring an incubator or a water bath. Alternatively, GAL80 can be utilised in combination with the mosaic analysis with a repressible cell marker system (MARCM)(Lee and Luo, 2001) and the FLIP system to selectively label small populations or single cells of one subtype. This involves a FLP recombinase under control of a conditional promoter like a heatshock, with only cells that are currently undergoing mitosis having the necessary number of FRT sites to allow recombination. This recombination results in one daughter cell with both copies of GAL80 and one with no copies. Only subtypes that also have GAL4 present can then drive expression of your gene of interest. By altering length of heatshock, you can achieve fine control over the amount of labelling of the desired subtype. This method is integral to this work and as such will be covered in much greater detail later (Section 1.8, 2.2.1 and 3.2.1). By combining this method with knowledge of when different populations in the Mushroom body develop (Lee, Lee and Luo, 1999), you can attain targeted expression of transgenes in specific subpopulations with relative ease. Comparatively, genetic manipulation in mammals or stem cell models is much more difficult requiring techniques like pronuclear microinjection in embryos (Lin, 1966; Jaenisch, 1976; Jaenisch and Mintz, 1974) or the gene editing technology CRISPR/Cas9 (Jinek et al., 2012).

Genetic access alone is useless if the results of such studies cannot be extrapolated to other systems. However, Drosophila have proven their worth time and time again with many key genes and regulatory and signalling pathways first discovered in this species. The homeotic Hox genes integral to the patterning of the body plan across phyla was first discovered in Drosophila (Kaufman, Lewis and Wakimoto, 1980; Garber, Kuroiwa and Gehring, 1983; McGinnis et al., 1984), so were many key developmental genes that enabled researchers to identify orthologous pathways in humans (Nüsslein-Volhard and Wieschaus, 1980; Jürgens et al., 1984; Baker, 1988; Artavanis-Tsakonas, Matsuno and Fortini, 1995) and the K+ ion channel shaker, critical for afterhyperpolarization (Kaplan and Trout, 1969; Jan, Jan and Dennis, 1977; Ganetzky and Wu, 1982; Wu et al., 1983; Baumann et al., 1987; Kamb, Iverson and Tanouye, 1987; Papazian et al., 1987; Tempel et al., 1987). They also make excellent disease models as ~70% of disease-associated human genes have orthologues in the Drosophila melanogaster genome (Schneider, 2000; Adams et al., 2000; Reiter et al., 2001). The vastly different organ and immune systems do limit applications but the

comparative speed of trials and ease to manipulate still makes them an appealing model that is still being used today.

Importantly for this work, the field of learning and memory has made several advances pioneered by research in Drosophila. Discovery of key mutants like dunce (Dudai et al., 1976; Byers, Davis and Kiger, 1981) and rutabaga (Livingstone, Sziber and Quinn, 1984; Han et al., 1992; Levin et al., 1992) helped to unravel key biochemical pathways involving cAMP that underpin learning and memory across phyla and identified the Mushroom body as an important site of associative odour memory. The human brain contains ~86 billion neurons and the hippocampus, an important centre for learning and memory, possesses ~16 million of this total. In contrast, the Drosophila brain consists of ~100,000 neurons, of which the Mushroom body possesses ~2000 neurons, the majority of which are Kenyon cells. Studying learning networks at this scale allows us to uncover the fundamental principles of how representations are encoded, and effective learning is carried out. This is further supported by the now two complete connectomes in Drosophila, one hemibrain (Scheffer et al., 2020; Li et al., 2020b) and one whole brain (Dorkenwald et al., 2024; Schlegel et al., 2024). These advances have offered many insights, including previously unidentified neuron types and connections and allowed for more accurate predictions like neurotransmitters utilised by different cell types (Galili, Jefferis and Costa, 2022; Eckstein et al., 2024). Additionally, the existence of two completed connectomes and several partial connectomes (of opposing sex) allows comparisons to be made. The questions of how the structure of brains connect to behaviour has never before been supported by so much information and has already provided insights into the basis for sexually dimorphic behaviours (Stürner et al., 2025). It has also highlighted the level of variability in structure that can occur between individuals while still producing consistent behaviour between flies (Schlegel et al., 2024), an aspect of neuroscience that is only now being fully explored.

Connectomics can also be used to support and refine computational work modelling how networks like the Mushroom body function and was used to help develop the central hypothesis of this work (Abdelrahman, Vasilaki and Lin, 2021). The genetic access, array of tools for manipulation and recording, and insights provided by two connectomes make Drosophila a model that is easy to work with and capable of capturing more of the ‘whole picture’ of a learning network than in any other system. This work leverages many of these tools to understand the role single neurons have within this model centre for associative memory and more specifically how each one must adapt to allow for continued optimal

function of the network. Before going into the specifics of this hypothesis, it is first important to understand how the Mushroom body functions and the key features that enable it to do so.

1.3. The *Drosophila* Mushroom body

A learning network must be capable of converting a limited number of inputs channels into a large set of diverse patterns that correspond to the thousands of variations in stimuli found in the environment, succinctly known as pattern separation. This information must then be broken down into often simplistic responses, e.g., approach or avoid an odour, and these decisions must be accurately informed from the information processed upstream a high probability of the time for the organism to succeed. The *Drosophila melanogaste*r Mushroom body possesses a three-layered expand-converge architecture, which It uses to achieve the expansion of limited odour input into a more extensive set of odour representations which typically have an associated valence that drives behaviour (Figure 1.1). This structure is typical of several learning networks found in a variety of organisms and is theorised to be optimal for the encoding of sensory information (Albus, 1971; Stevens, 2015). The expanding part of this network, projection neuron (PN) to Kenyon cell (KC) synapses, appears to be involved in pattern separation. Around 150 uniglomerular PNs bilaterally project to the lateral horn and along the way synapse with ~2000 KCs in each hemisphere (Figure 1.2) (Strausfeld, Sinakevitch and Vilinsky, 2003; Caron et al., 2013; Schlegel et al., 2024). This expanding input in the MB achieves efficient stimulus separation and representation in several ways that will be discussed later. Around 2000 KCs converge onto 34 different Mushroom body output neurons (MBONs) (Aso, Hattori, *et al.*, 2014; Aso, Sitaraman, *et al.*, 2014) and the interactions at this layer appear to convert the large amount of specific odour information from KCs, into a limited set of behavioural outputs in response to different odours (Figure 1.2). Investigating the interactions at different layers of these structures can give important information not just on how odour is processed, represented and converted to behavioural output in *Drosophila*, but on learning networks in general and perhaps how features of interactions between neurons underlie learning and memory. I will briefly describe the theory and evidence on how these layers produce odour representations and their subsequent outputs, with particular emphasis on the key features of these interactions.

Olfaction in *Drosophila* begins in the antennae and maxillary palps in structures called sensilla which house 2-4 olfactory receptor neurons (ORNs) depending on sensillum type. There are ~50 ORN types corresponding to 50-60 odorant receptors which seem to determine the majority of ORN response dynamics (Couto, Alenius and Dickson, 2005; van der Goes van Naters and Carlson, 2007; Yao, Ignell and Carlson, 2005; Hallem, Ho and

Carlson, 2004; Hallem and Carlson, 2006). These dynamics include responding to the odorant molecule in varying concentrations with some ORNs having more specific affinities than others. Additionally, some odorants excite certain ORNs while inhibiting others and ultimately an odour is encoded in this first layer as the pattern of excitatory and inhibitory ORN responses.

Axons of ORNs expressing identical odorant receptor types converge onto the same glomerulus (Grabe et al., 2016), which are discrete neuropil compartments within the antennal lobe. These 54 glomeruli are the sites of interaction between ORNs and PNs, whose dendrites project into a glomerulus and receive monosynaptic input from one type of ORN ensuring odour specificity is maintained (Vosshall, Wong and Axel, 2000). There are ~1200 ORNs vs ~200 PNs, so why in these first 2 layers does the system transition to far fewer neurons (PNs) conveying odour information to the expansion layer? One possible advantage is reproducibility, with PNs spiking in response to odours more consistently than their cognate ORNs (Bhandawat et al., 2007) allowing the odour information carried to KCs to be more reliably transmitted than a direct connection between ORNs and KCs. Additionally, weaker ORN inputs to PNs are amplified allowing weaker odour stimuli or small increases in concentration to drastically increase PN spiking rate; these responses saturate at lower concentrations than ORNs though, meaning strong inputs are not amplified to the same degree. This layer also improves the speed at which odour information is conveyed with PNs depolarising quickly after a small increase in ORN spike rate and rapidly declining in spike rate themselves during the tonic phase of ORN responses (Bhandawat et al., 2007). The interaction at this layer also seems to produce more effective odour separation, likely due to ORNs of the same type innervating the same glomeruli allowing these inputs to be averaged across PNs within a single glomerulus. Overall, this increased separation of odours and reduced signal-to-noise ratio at the PN level ensures PNs from each glomerulus reliably carry information from separate odour channels where the signal from each odorant can then be massively expanded and translated into distinct representations within KCs.

The PN axons terminate in the lateral horn (Figure 1.2), an area involved in innate behavioural responses like feeding and courtship behaviours(Jefferis et al., 2007; Fişek and Wilson, 2014), but pass through the MB calyx on the way, where they form en passant synapses with KC dendrites/claws (Figure 1.2). Connectivity between PNs and KCs appears to be mostly random, but certain PN channels associated with ethologically relevant odours (e.g. food) are more likely to innervate the same KCs than chance (Caron et al., 2013; Zheng et al., 2020; Hayashi et al., 2022). Interestingly, this biased connectivity is evolutionarily

relevant, with species-specific over- and underrepresentation of glomeruli encoding ecologically relevant odours, especially in *D. sechellia* which feeds almost exclusively on noni fruit (Ellis et al., 2024). It is thought that the mostly random connectivity with biased inputs for relevant odours increases the prominence of those odours and improves the flies ability to generalize learning between odours from similar sources (Zavitz et al., 2021; Yang et al., 2023).

A KC claw ensheathes a single PN bouton and multiple claws synapse with one PN bouton, with each KC receiving input from an average of ~6-8 PN boutons (Figure 1.2) (Caron *et al.*, 2013). The KC axons collect into bundles that form the horizontal and vertical lobes of the MB based on KC type: γ, α/β and α'/β' (Figure 1.2). These types can be further divided into γ-main, α/β and α'/β' which reside in the main calyx and receive most of the olfactory input, and γ-dorsal and α/β-posterior which reside in the accessory calyx and receive inputs of other modalities like visual, gustatory and thermatosensory information (Li et al., 2020b). The MB is not a single unit but instead contains a diverse set of KC subtypes and local neurons that receive a range of information and contribute to the variety of odour memories that can be encoded.

Along the MB lobes KCs synapse with 34 MBONs split between 15 different compartments (Aso et al., 2014a); they do this with spines/boutons along their axons that synapse with MBON dendrites. Dopaminergic neurons (DANs) also present in these 15 compartments, which encode reward or punishment, induce long-term depression (LTD) at KC-MBON synapses when their activity is temporally paired with KC firing (Aso and Rubin, 2016). Collectively, the above structures make up the 3-layered expand-converge architecture of the MB.

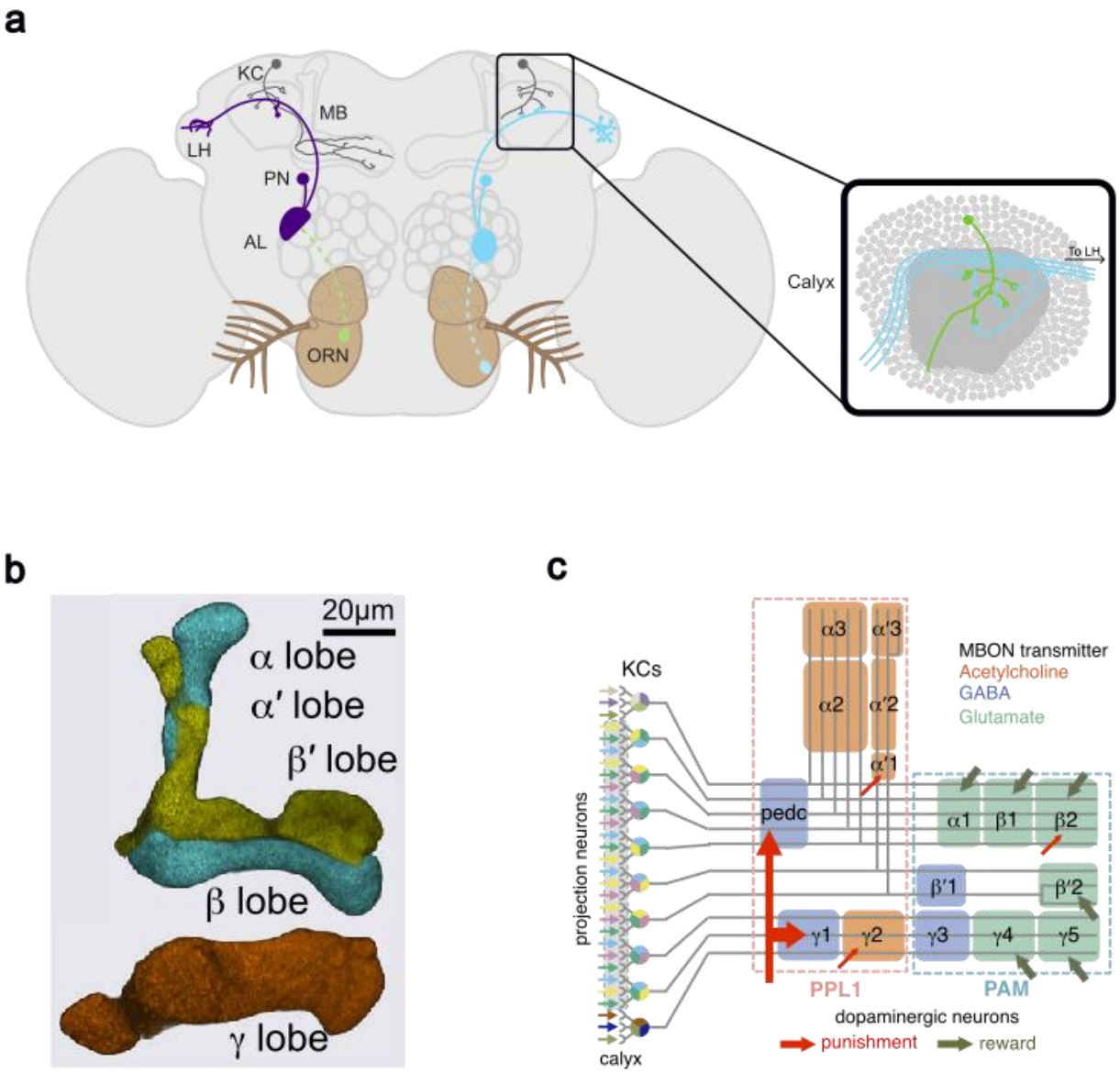

Figure 1.2: Anatomy of the Mushroom body (MB). a) Schematic diagram of the Drosophila olfactory system which begins with olfactory receptor neurons (ORNs) in the antennae. ORNs then project to the antennal lobe where odour information is transferred to projection neurons (PNs) at glomeruli. PNs project to the lateral horn (LH) but along the way form en passant synapses with Kenyon cell (KC) claws in the calyx. KCs then project through the MB lobes. Figure adapted from (Ellis et al., 2024). **b)** The subregions of the MB. KC subtype axonal projections are separated into different regions of the MB lobes. The γ lobe and pedunculus are shown separately below α/β and α'/β' lobes for clarity. Figure adapted from (Aso et al., 2014b). **c)** A schematic depiction of the MB compartments. The lobes of the MB can be divided into 15 compartments based on connections between KCs, mushroom body output neurons (MBONs) and dopaminergic neurons (DANs), which provide rewarding or punishing reinforcement depending on compartment. **Adapted from (Ellis et al., 2024) and (Aso et al., 2014a)**

1.4. Sparse coding in the Mushroom body

In *Drosophila* there are only ~50 ORN types (Couto, Alenius and Dickson, 2005), but a much larger number of odours within the environment. To detect as many odours as possible, the Marr-Albus model (Albus, 1971) suggests the middle layer of an expand-converge learning network achieves pattern separation via expansion recoding. This involves expansion of cell numbers in the intermediate layer, compared to inputs from the prior layer, as a way of combining receptive fields corresponding to generalised inputs from different sensory neurons. This is a common feature of many learning networks including artificial ones like the multilayer perceptron, where the expansion layer is referred to as the hidden layer. Aside from *Drosophila* this structure is found in the nervous systems of other organisms, including the mammalian hippocampus and cerebellum and the electrosensory lobe of weakly electric fish (Modi, Shuai and Turner, 2020). Expansion recoding allows the dense code at the input layer (ORNs/PNs), where a high proportion of neurons of a small total number are active, to be translated into a sparse code at the intermediate layer (KCs), where only a small proportion of a much larger number of neurons are active. In the case of *Drosophila*, because ORNs are broadly tuned and therefore will respond to most odours if they're present in a large enough concentration (Hallem and Carlson, 2006), this expansion and combination of receptive fields produces many specific representations in this layer that correspond to a large number of odours. Broad odour information passes from ORNs to the ~150 uniglomerular PNs to the ~2000 KCs to be separated out into these more specific representations of individual odours, with an individual odour only activating ~5-10% of KCs (Honegger, Campbell and Turner, 2011). The overlap of KC receptive fields produces very specific odour representation patterns, allowing for a much larger number of odours to be distinctly represented, each in a small number of neurons. Recalling the difference between single layer and multilayer perceptrons, the latter's ability to handle non-linear decision boundaries arises from the transformations occurring within its hidden/intermediate layer(s). Similarly, by increasing the dimensionality from a relatively limited set of odour inputs to a much larger number of possible odour representations, the intermediate layer makes it easier to linearly separate this information (Stevens, 2015; Litwin-Kumar et al., 2017). In this case odours fall into 2 classes, those with a positive valence that drive approach behaviour, and those with a negative valence that drive avoidance behaviour.

The valence of a given odour must be consistently updated so that any response is accurately informed by the information within the environment, e.g. detection of an odour indicates a potential food source. The establishment and updating of an odours associated

valence is driven by the interaction of dopaminergic neurons (DANs) and KCs at an individual MBON compartment. Of the 15 total MBON compartments, an individual compartment typically contains one MBON and one associated DAN which both synapse with KC boutons (Figure 1.2); most of these compartments have been identified as either promoting aversive or approach behaviours (Aso et al., 2014a, 2014b). When firing of KC boutons and a DAN occur concurrently, due to presentation of an odour and a rewarding/punishing stimulus respectively, LTD is induced at KC-MBON synapses (Hige et al., 2015; Handler et al., 2019). It is currently believed that this coincidence detection relies on odour-induced Ca^{2+} influx at the KC bouton and dopamine binding to Dop1R1 which triggers a Ca^{2+} dependent adenylyl cyclase called Rutabaga. The combination of these factors in a short span of time produces elevated cyclic AMP (cAMP) levels which induces plasticity presynaptically. This system is somewhat unique as within each compartment the DAN and MBON encode opposing valences; a ‘punishment’ DAN input is paired with an approach MBON output. So, when LTD occurs due to concurrent firing of a DAN and KC, it means that a reward associated odour induces depression at the aversive encoding KC-MBON synapses. The learned response to a given odour is then determined by the sum of aversive vs approach MBONs activated by KCs associated with that odour representation. The ‘correct’ synapses win out because they have the higher strength outputs compared to the incorrect ones that have previously undergone synaptic depression. In this way the many possible odour representations are split into 2 classes of behavioural response, avoid or approach an odour.

The translation of the many possible odour representations into distinct behavioural outputs begins to demonstrate the importance of sparse coding within the Mushroom body. Arrival of reward or punishment is reliably carried out by DANs and only induces plasticity when its activation occurs concurrently with that of associated KCs. This dynamic emphasises the importance of tightly regulated KC responses where either extreme in the proportion of the population that responds can have disastrous consequences. If the majority of KCs responded to each odour there would be little to distinguish one representation from another, resulting in a lack of appropriate and distinct behavioural responses for each odour. However, if an odour was only encoded by a single KC this would limit the number of potential odour representations to ~2000 (number of KCs), as it is the combinatorial activation of a small proportion of the population that allows for a massive expansion in the number of potential odours that can be stored in memory. Such a system would also be intolerant of any variation in response over time (noise). For example, if the cell failed to respond due to some small change in the odour like concentration present, the MB would be unable to encode this

information. Such a setup would make the system a lot less versatile in the number and variety of odours it could store. However, evidence suggests the MB response is fairly robust in the face of changing odour concentrations (Honegger, Campbell and Turner, 2011; Srinivasan et al., 2023). Additionally, the Mushroom body also needs to be able to generalize between similar odours. When concentrations of an odour vary naturally within the environment, the individual KCs that respond within the MB are likely very similar but not identical. It is important an individual can generalize between permutations of an odour when determining behavioural response, while 'ignoring' the intertrial variability in response caused by the inherent noisiness of the environment any sensory system must contend with. In actuality, it would appear the MB partially achieves these opposing goals of discrimination and generalization by utilising a coding strategy that incorporates cells with varying reliability in response. KCs that reliably respond to an odour are useful for discriminating between dissimilar odours, but uninformative when trying to be distinguish between similar odours where their responses are too overlapping. In contrast, those KCs that unreliably respond may aid in discriminating between similar odours, but only after extended training (Srinivasan et al., 2023); this is reinforced by several studies that demonstrate Drosophila are worse at discriminating between similar odours with a high level of overlap in KC representations (Campbell et al., 2013; Hige et al., 2015; Ahmed et al., 2023) . The MB is therefore a system that utilises sparse coding for odour discrimination but is not so sparse that it is not capable of generalizing associations to similar odours. A consequence of this is that it is worse at distinguishing between similar odours but is still capable of it if exposure to similar odours with opposing valences is prolonged.

The sparseness of this network is maintained through several key features of the MB. The first relates to the mostly random connectivity between PNs and KCs mentioned earlier, which ensures that each KC receives input from a distinct set of PNs and combined with expansion recoding ensures different odours induce responses in different KCs (Caron et al., 2013), Secondly, KCs have a high spiking threshold, requiring the majority of their associated PNs to fire to induce an action potential (Gruntman and Turner, 2013). Dual calcium imaging experiments (Li *et al.*, 2013) revealed that as number of PN axon terminals inputting to a single KC increased, so did the amplitude of the summed calcium signal across all the PNs required to induce an AP in said KC. If KC activation threshold remains the same, this could suggest that PNs scale their synaptic strength down as number of axon terminals increases as a way of maintaining a constant threshold. It is possible a certain threshold at this level is key for maintaining efficient stimulus separation. If this dropped too low the percentage of

KCs activated by a single odour would increase as fewer summated inputs would be required to induce an AP, resulting in less separation between individual odour representations.

Additionally, KCs receive feedback inhibition from the anterior paired lateral (APL) neuron, a large GABAergic inhibitory neuron in the MB (one per hemisphere). The APL synapses with all KCs in its associated hemisphere (Lin *et al.*, 2014) and feedback inhibition from the APL helps maintain sufficient sparse coding. Lin et al (2014) demonstrated that odour-evoked responses in KCs increased when APL synaptic transmission was blocked using temperature-sensitive shibire or tetanus toxin light chain (TeTx), whereas artificially activating the APL suppressed KC responses. Both these findings suggest the normal function of the APL is to maintain lower activity in KCs via feedback inhibition. Finally, they found that flies expressing shibire in the APL in both hemispheres demonstrated decreased discrimination between similar odours, with a higher correlation in activated KCs between these odours and an overall decreased sparseness. These findings suggest that the APL's role is to provide feedback inhibition to all KCs which aids in maintaining sparseness in this system

The establishment of this sparse network appears to be tightly regulated. Elkahlah *et al* (2020) used various ablation and neuron amplification methods in the developing larva to vary number of KCs and PNs. This consistently demonstrated that PNs increased the number of their presynaptic boutons during development in response to changes in PN or KC numbers, suggesting that the number of PN-KC synapses created during development may be optimal for sparse coding. In contrast, recent connectomics work (Schlegel et al., 2024) comparing the Hemibrain and Flywire connectomes discovered that increased γ KC number in one of the connectomes, likely due to differences in developmental feeding, was associated with a decreased number of PN boutons per KC. These seemingly opposing findings may be due to differences in exact timing of the potential perturbations that caused changes in KC number. However, both findings suggest there is something optimal about the connectivity in this structure that is necessary for effective stimulus separation.

Ultimately the dilemma of this structure is one of stimulus representation vs stimulus separation. The number of KCs activated by a given odour must remain low to allow representations to be separate from one another and result in distinct behavioural responses. However, a system that is 'too sparse' would be unreliable for detecting odours and potentially incapable of generalizing responses between them. This may suggest the existence of a 'Goldilocks zone' of sparseness where the system must keep responses finely tuned to allow effective stimulus separation while still allowing flies to generalize between similar odours and minimize the effects of intertrial noise.

1.5. Balanced Coding

Noise and variability are impossible to avoid in biological systems, as many factors are constantly in flux and require adjustment to maintain normal function. Homeostasis is a mechanism that allows maintenance of a stable internal environment in the face of an everchanging external one. Biological systems are not perfect though; ‘machinery’ breaks down over time and the feedback mechanisms utilised to return a variable to its set range can overshoot, leaving the system constantly in flux but hopefully within expected limits. Most neurons found in long-living mammals like humans are used for their entire lifespan but the half-life of the components within these cells, like ion channels or receptors, is much shorter (minutes-weeks) (Marder and Goaillard, 2006). It is therefore even more important that neurons are regulated to avoid runaway-variability. Homeostatic plasticity is used to compensate for natural changes in parameters like degradation of ion channels over time or addition of receptors associated with Hebbian plasticity to keep the neuron functioning as required. The term ‘as required’ is key here though as it is not always clear what extent of variability in parameters and associated noise in neuron responses is tolerable and indeed how much of it may actually be functional. It is important to distinguish the variability in parameters within a neuron type that influences its activity, to the differences in response dynamics between neurons of different types, which can be referred to as heterogeneity (Marder and Goaillard, 2006); examples of the benefits of heterogeneity can be easily found amongst the literature (Gjorgjieva, Drion and Marder, 2016; Marsat and Maler, 2010; Zeldenrust, Gutkin and Denéve, 2021). Similarly, there is growing evidence from modelling and experimental neuroscience that noise can improve information processing via stochastic facilitation (McDonnell and Ward, 2011). Stochastic resonance is one observed form of facilitation and posits that an optimal level of noise amplifies weaker signals that would usually be subthreshold. Computational modelling even supports the idea that stochastic facilitation may improve encoding of memory (Caston et al., 2022). The key question is what level of variability is tolerable/functional and in what contexts may neuronal similarity be more appropriate? How does a learning network like the MB balance similarity and variability and what mechanisms might it use to reinforce this?

To begin to answer this question a member of our lab previously created a rate-coding model of the MB (Abdelrahman, Vasilaki and Lin, 2021), with PN activity simulated as a saturating nonlinear function of ORN activity taken from real recordings of odour responses to 110 odours (Hallem and Carlson, 2006). Three parameters were considered for all 2000 KCs:

Number of excitatory inputs (N) from a randomly selected set of the total PNs, the strength of each of these inputs (W), and a spiking threshold (θ). The feedback inhibition from the APL was simplified to be the sum of all KC excitation and was represented as pseudofeedforward inhibition to avoid complexity of modelling temporal dynamics. KC response to a given odour was determined by the sum of all excitatory inputs minus inhibitory inputs and threshold, with any activity below the threshold converted to 0 e.g. silent. All these factors were scaled to ensure ~10% of KCs respond to each odour in line with experimental evidence of sparse coding in this system (Honegger, Campbell and Turner, 2011). To simplify the output of a given response from KCs, only two MBONs were modelled, one representing approach and the other avoid. As mentioned earlier, depression of KC-MBON synapses associated with the 'wrong' outcome occurs when firing of KCs responding to the odour and DANs responding to the odour valence coincides (Aso et al., 2014a; Hige et al., 2015; Aso and Rubin, 2016). In the model, input odours were randomly split so that 50% were reward associated and the other 50% were punished. KCs responding to a rewarded odour weakened their synapses onto the avoid MBON and vice versa for those responding to punished odours. 'Behavioural' response of the model was then determined by the comparative activity of the avoid vs approach MBON with the greater winning. Finally, the accuracy of all variants of this model was represented by the fraction of correct decisions to noisy versions of the trained odours (e.g. with PN activities shuffled). With this setup, the impact of inter-KC variability could begin to be assessed (Figure 1.3a).

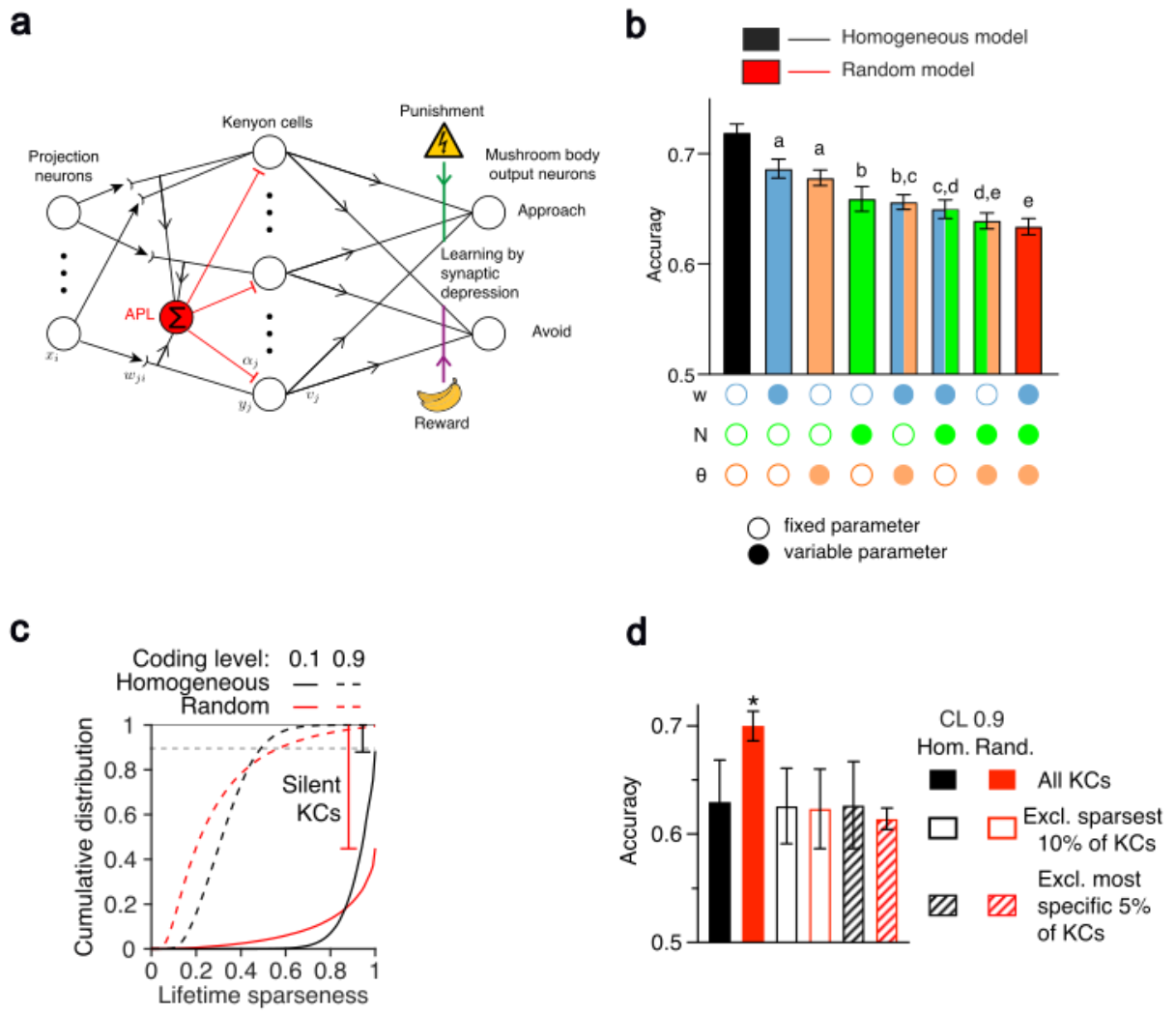

Figure 1.3: A Mushroom body network model. a) Schematic of the MB network model. Input layer represented by PNs that relay downstream odour information to KCs. These connections are random and receive feedforward inhibition from the APL neuron. Repertoire of MBONs simplified to just two, one approach neuron and one avoid. Reinforcement signals from DANs also simulated in this model and induces depression of KC and MBON synapses as has been observed. **b)** Model fly's performance. Each model varies one of three additional parameters from left to right, synaptic weight (w), KC spiking threshold (θ) and number of inputs per KC (N). The homogenous model (black) has no variability between any parameters and has the best performance, determined by accuracy of response to noisy versions of trained odours. The random model (red) with variability in all three parameters performs the worst. Significant difference between bars indicated by distinct letters above the bars, with those that share annotations being non-significant. **c)** Cumulative distribution of lifetimes sparseness across the model KC population. Under enforced sparse coding (0.1) the majority of KCs in the homogenous model have high lifetime sparseness (>0.8), while the random model has a much larger proportion of KCs with low lifetime sparseness; a high percentage of this population is also silent. Under dense coding conditions (0.9) the lifetime sparseness of these models is much more even, although it is slightly higher in the random model. **d)** Removing most valence-specific or sparsest KCs, under dense coding conditions, abolishes increased performance of the random model. Significant increase in random model accuracy represented by red bar with *. **Adapted from (Abdelrahman, Vasilaki and Lin, 2021)**

Initially eight model variants were created: a “homogenous” model with all three parameters identical across KCs and then 7 models with an increasing number of these parameters varied in different combinations; the final model had inter-KC variability in all three parameters and is called the “random” model due to the lack of any relationship in this variability between parameters (Figure 1.3b). Importantly, variability in N, w and Θ was biologically realistic, having been obtained from experimentally measured distributions of these factors (Turner, Bazhenov and Laurent, 2008; Caron et al., 2013). Comparing these models demonstrated that as inter-KC variability increased (e.g. number of parameters with realistic variability) the model performed worse (Figure 1.3b). The homogenous model performed the best, supporting the idea that variability within the MB may not be desirable and that it may benefit from constraining variability within set limits. However, it is unclear why increased inter-KC variability would worsen performance. The improved performance of the homogenous model may imply it is more effective at linearly separating representations into punished or rewarded odours. If we envision the MB as a 2000-dimensional space, the goal of this system is to ‘draw’ a dividing line that effectively separates activity of punishment-associated KCs from reward-associated ones. Two factors that may influence how effectively the MB can achieve this is angular distance and the dimensionality of your representations. Angular distance relates to how similar the patterns of activity across all 2000 KCs is between two different representations and dimensionality relates to how much the full 2000-dimensional space in the MB is being utilised. Methods developed previously (Turner, Bazhenov and Laurent, 2008; Litwin-Kumar et al., 2017) were used to assess these factors contributions to performance but although low in the sparse code model, they were equally low in the high performing dense code model. It is likely these factors do influence the MBs ability to distinguish between odours of opposing valence, but in this instance, it would appear it may not be responsible for poor performance when inter-KC variability is high.

Given the variability in parameters is completely random (while constrained within biological limits) another possibility is that some KCs by chance are always active while the remaining majority are silent. For example, if by chance 10% of KCs had low spiking thresholds, high number of excitatory inputs, high strength of excitatory or low strength of inhibitory inputs or some combination of these that drastically increases the chance the neuron will fire, it is possible this small minority could respond to the majority of odours. Counter variability resulting in low spiking probability in the remaining neurons, combined with feedback

inhibition from the APL decreasing this further to try and maintain sparse coding (Lin et al., 2014), could result in a high number of neurons that are silent to most/all odours. We can now introduce our second measure of sparseness: “lifetime sparseness” which refers to how selectively neurons respond to stimuli. Maximal lifetime sparseness would mean a given neuron would only respond to one stimuli (score 1 on the model), while minimal sparseness would result in a neuron that responds equally to all stimuli (score 0 on the model) (Willmore and Tolhurst, 2001). Lifetime sparseness and population sparseness (the % of neurons that respond to a given stimuli as described earlier) are not necessarily correlated. In this instance, because the random model is constrained to have high population sparseness (only 10% of KCs active in response to any given odour), it is possible that low lifetime sparseness in the random model is responsible for its poor performance; if the same 10% of neurons respond to all odours while all other neurons are silent (or similar scenarios that aren’t as extreme) it would still satisfy the sparse coding requirement but there would be little distinction between odour representations. Approximately 80% of KCs had a high lifetime sparseness (between 0.85 and 1) and very few silent KCs under sparse coding conditions (Figure 1.3c). Under the same conditions, the random model demonstrated much more variability in lifetime sparseness with a small number of KCs ranging from ~0.4-0.7 and greater than 50% of neurons were completely silent (Figure 1.3c). In a dense coding background, inter-KC variability conveys improved performance on the random model. Removal of 10% of KCs with the highest lifetime sparseness in this background resulted in decreased performance (Figure 1.3d), suggesting variability is only beneficial as it produces some KCs that have high specificity to a small number of odours. Collectively this modelling suggests that inter-KC variability is bad for performance in the MB, primarily because it decreases lifetime sparseness and therefore decreases the distinction between representations. Although the homogenous model has performed best so far it is unlikely any biological system could fix neurons across a population to have identical parameters, so it was next asked if adding a compensatory mechanism to restrain inter-KC variability would rescue poor performance of the variable models.

Two compensatory mechanisms were trialled, with the first utilising an activity-independent mechanism where variability in some parameters are compensated by changes in another. In this instance, KCs adjusted their synaptic weights to adjust for variability in their threshold or number of excitatory inputs (Figure 1.4a). A correlation was applied to these parameters so that any variability in N or Θ, with a distribution matching that of the aforementioned experimentally observed values, was associated with a change in w. For example, if the

number of excitatory inputs in a KC are high, the weight of those inputs will be lowered so that each input is now weaker. Conversely, if number of inputs are very low, then the weights of those inputs are increased. Importantly, the distribution of synaptic weights across all KCs was constrained so that it matched those observed experimentally. This compensatory mechanism rescued the model's performance so that it performed better than the random model but still performed worse than the homogenous model (Figure 1.4a). This modelled compensation seems effective for improving discrimination between odours yet still doesn't perform as well as a perfectly fixed system. Does this mean inter-KC variability limits biological systems or is it possible an alternative mechanism could increase performance further?

The second compensatory mechanism may hold the answer. These models introduced activity-dependent tuning of parameters, where every KC has a target activity level (with a margin of $\pm$6%). Three different models were trialled where each can only adjust one parameter (spiking threshold, inhibitory weights or excitatory weights) and all other parameters were set to match the distribution observed previously (Figure 1.4a). This can be best understood by envisioning a scenario where spiking threshold is low and number of excitatory inputs is high, leaving the neuron more active than its target range. In the model where the strength of synapses (excitatory weights) is the tuned parameter, the weights of all inputs would be scaled down to reduce probability of firing. All three compensatory models matched or outperformed the homogenous model depending on the difficulty of the task (Figure 1.4a-b).

Interestingly, this compensation also reduced variability in lifetime sparseness to lower levels than that seen in the homogenous model, while mean sparseness was similar between models (Figure 1.4c). This reduced variability may influence performance because a greater proportion of the 2000 KCs specifically respond to a small number of odours increasing their chance of responding only to rewarded or punished odours. In contrast, the homogenous model contained some individual KCs that achieved a greater lifetime sparseness than that seen in the homeostatic model, but some who ranked far lower. This suggests that at least in this model, it is more important that the majority of KCs respond to a limited number of odours than have a population with a few individuals who are extremely specific in the stimuli they respond to. Comparisons in distribution of parameters in the 3 homeostatic models to experimentally measured variation was also performed (Figure 1.4d-f). This revealed that tuning excitatory input weights resulted in a distribution of these parameters most closely matching experimental evidence. In contrast, spiking threshold was much more variable

suggesting that tuning of weights alone may be sufficient to restore KC activity to an average level but adjusting threshold is not. Further exploration of the inhibitory tuning model revealed many inhibitory weights were negative (meaning excitatory), which is not currently thought possible in the MB (Inada, Tsuchimoto and Kazama, 2017). This also implies that any strategy involving adjustment of inhibitory weights must also compensate with changes in other parameters.

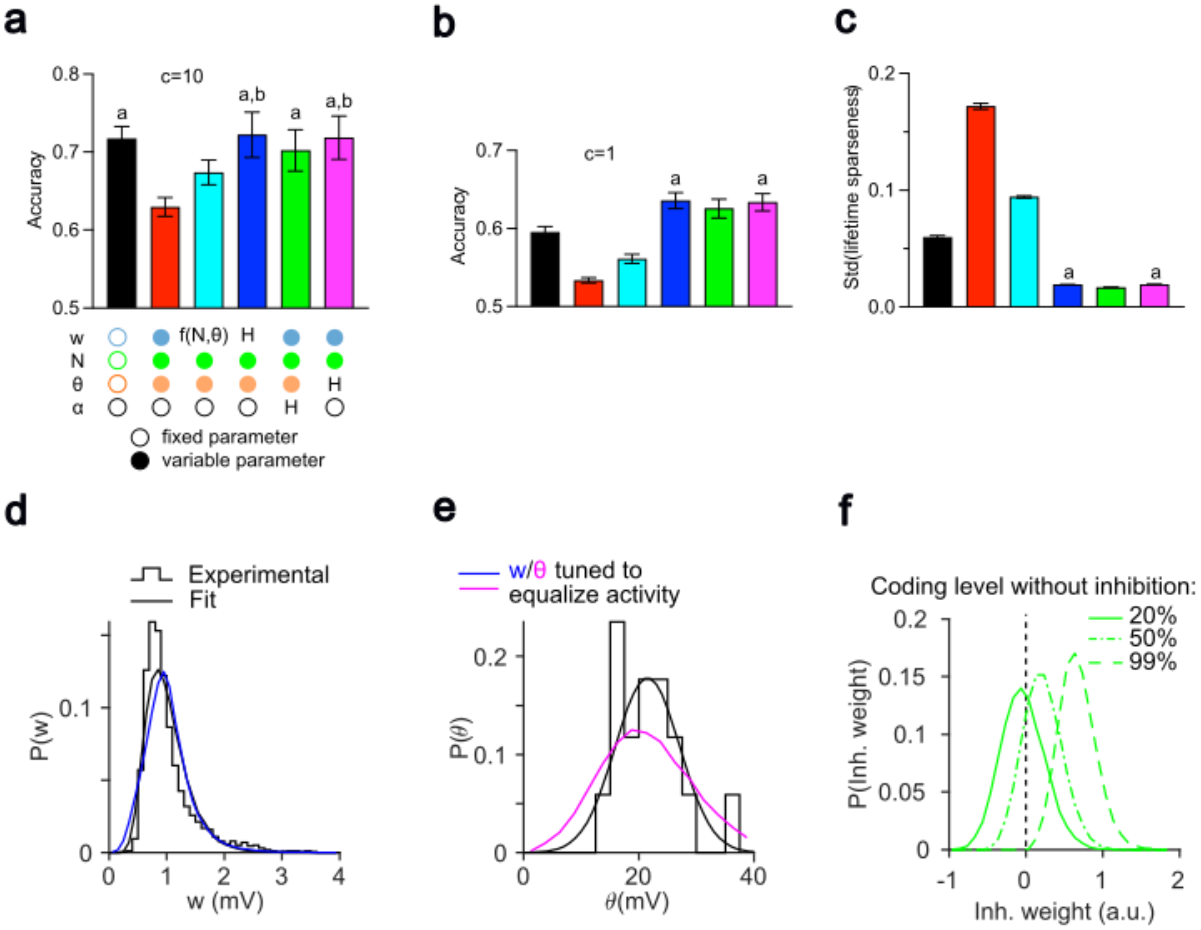

Figure 1.4: Activity-dependent vs activity-independent compensation. a) Parameter compensation rescues performance. Poor performance caused by inter-KC variability in the random model (red) is rescued by compensation in parameters. In the activity-independent model (cyan) setting excitatory weight (w) according to number of inputs (N) and spiking threshold (Θ) partially improves performance but still performs worse than the homogenous model (black). In the three activity-dependent models (blue, green and magenta), adjusting w, inhibitory weight (α) and Θ respectively to restore activity to a set level, produces a performance equal to or greater than the homogenous model; H indicates the adjusted parameter in these models. **b)** Performance advantage of the activity-dependent models is more apparent when the task is more difficult; difficulty increased by making decision making more stochastic (c=1). **c)** Both activity-independent and activity-dependent compensation decreases lifetime sparseness variability. This is most pronounced in the activity-dependent model, where lifetime sparseness Std falls below values observed in the homogenous model. In panels a-c, shared letters above bars indicates groups are not significantly different from each other; all other comparisons significant. **d-f)** Comparison of the distribution in 3 activity-dependent model parameters to experimentally measured variation. **d)** Tuning of excitatory weights results in distribution most closely matching measured variation. **e)** Adjusting Θ produced variation much larger than observed values. **f)** Model tuning inhibitory weights was most distinct from experimental measurements, with some negative weight values, which has not been observed in the Mushroom body. Only model with a 99% coding level without inhibition had more accurate inhibitory weights. **Adapted from (Abdelrahman, Vasilaki and Lin, 2021)**

The above model demonstrates that activity-dependent compensation in parameters underlying spiking probability would be an effective strategy to combat the effects of inter-KC variability on performance. However, is there any experimental evidence to support such a compensation mechanism? Although no research so far has identified any mechanism in the adult MB, thanks to the development of the hemibrain connectome (Scheffer et al., 2020; Li et al., 2020b) we can look for correlations that may support this idea. This dataset allowed identification of the number of excitatory and inhibitory inputs across KCs and an approximation of the weights of these inputs by using synapse number per input (estimated from close association of T bars and postsynaptic densities) as a proxy (Figure 1.5a). This falls in line with findings that the number of synaptic counts correlates well with total synaptic contact area between neurons in *Drosophila* larva (Barnes, Bonnéry and Cardona, 2022) and area positively correlates with EPSP amplitude in studies of the mammalian cortex (Holler et al., 2021). As predicted by the model, the number of excitatory inputs was negatively correlated with the approximate weight of each input across all KC subtypes. For each PN input there were 6-15% less synapses across inputs for an individual, compared to 22% for the activity-independent model and 18% for the homeostatic model (Figure 1.5b-i). It is important to acknowledge that in the activity-dependent model they were only able to adjust one parameter (the model tuning weights of excitatory inputs is relevant in this case), so this may further support the idea that multiple parameters are finetuned to achieved desired

activity level. One way to reduce probability of firing is to place dendritic inputs further away from the axon initial segment (AIS)(Williams and Stuart, 2003). Estimating the location of the AIS (using the peduncle as a guide) in connectome analysis revealed only γ-main and αβ-c KCs demonstrated a positive correlation between number of PNs per KC and distance from these inputs to the peduncle. Finally, there was a strong positive correlation between the number of excitatory and inhibitory synapses, suggesting multiple compensatory strategies targeting different parameters may be utilised in the MB to decrease inter-KC variability.

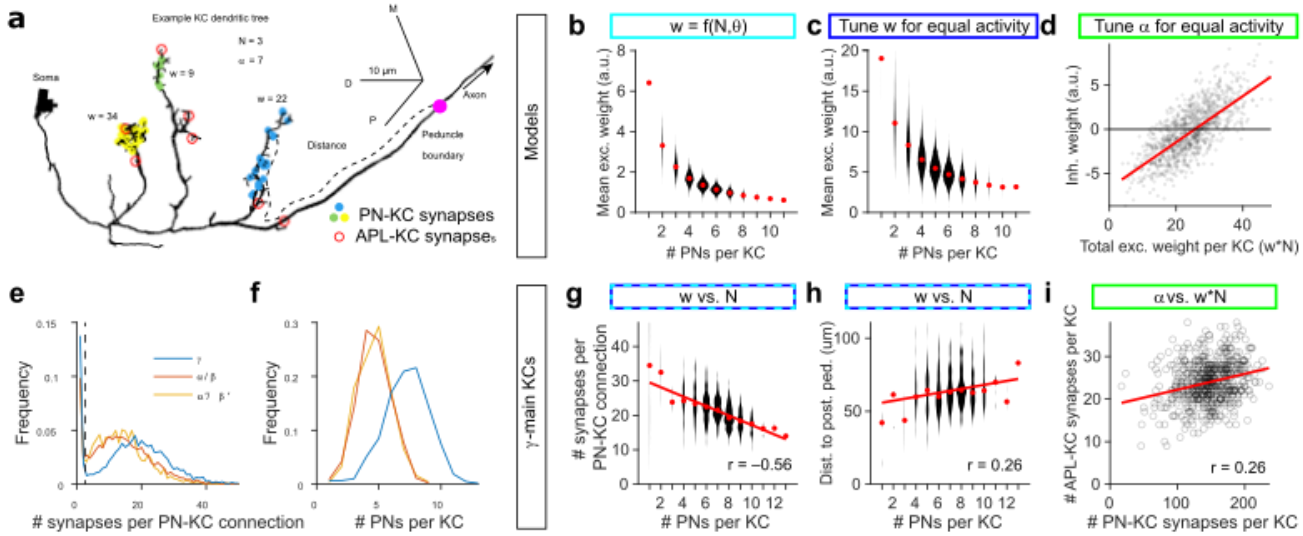

Figure 1.5: Connectome parameter correlations that support homeostatic compensation. **a)** Example α/β KC recreated from connectome dataset. Synapses from three distinct inputs from PNs to KCs represented by blue, green and yellow dots and the 7 APL-KC synapses are shown with red circles. The magenta dot shows the starting boundary of the peduncle. The w value next to each input represents their weight, estimated by number of synapses per input. **b-d;g-i)** Evidence of existing balance between parameters in the Drosophila MB. **b-c)** In both the activity-independent model (cyan) and activity-dependent model (blue) compensation produces an inverse correlation between the number of excitatory inputs per KC and the weight of each input (e.g. a KC with very few inputs would have a higher mean excitatory weight across all inputs). **d)** In the model that adjust inhibitory weights to equalize activity across KCs, there is a strong correlation between inhibitory weight and the total excitatory weight per KC (note negative inhibitory weights). **e)** Distributions of the number of synapses per PN-KC connection, dotted line indicates threshold where anything below was not included in connectome analysis and were marked as annotation errors. **e-f)** KC subtypes that do not receive exclusively odour input were removed from analysis, leaving only γ-main α/β and α'/β'. Connectome analysis shows these subtypes have distinct distributions in the number of PNs per KCs, with α/β and α'/β' near identical, whereas γ-main KCs have on average a higher number of PN inputs. From g-i only γ-main analyses are shown. **g)** Similar to the model, an inverse correlation was observed in connectome analysis of γ KCs. **h)** Distance from the peduncle was also positively correlated with number of PNS per γ KC. **i)** In the connectome γ KCs also show a correlation between inhibitory weight (number of APL synapses per KC) and excitatory weight (number of PN-KC synapses per KC).

I have covered this model in great detail because the questions raised by its findings directly link to the hypotheses underpinning this work. It identifies inter-KC variability as a factor that may need to be controlled for to prevent decreased ability to distinguish between odours. The model further suggests that the impact of variability on lifetime sparseness may be the source of decreased performance, and this may arise when parameters across the population reach opposing extremes. In particular, if a small number of KCs respond indiscriminately to presented stimuli, while many others remain silent, this reduces the MBs ability to linearly separate odours with opposing valences because too many of these representations become overlapping. Furthermore, it shows some connectomic evidence that an expected correlation exists between parameters supporting either activity-independent or activity-dependent compensation. However, concrete examples of homeostatic plasticity occurring in the adult mushroom body are rare. We have previously identified that KCs adapt to excess inhibition from the APL by increasing their responses to odours (Apostolopoulou and Lin, 2020), suggesting some homeostatic compensation has occurred but the exact source of this is unclear. It is notable that this study examines the whole MB, recording odour responses across all KCs which makes it difficult to distinguish between adaptation on a network vs single cell level. If the activity-dependent model is correct and KCs adjust for changes in one parameter that pushes them out of a desired activity level by fine tuning others, it is likely that every KC would have to have some intrinsic mechanism to drive this; it seems unlikely that network level regulation or signalling could drive the adaptation of parameter levels in every cell to ensure few neurons stray too far from the average. This conundrum was the inspiration for my primary research questions. Principally, do KCs have a single-cell homeostatic mechanism to maintain an average level of activity across the population? However, it first seems appropriate to understand our options. Now we have evidence for homeostatic plasticity in the MB, and it is predicted to be computationally important for learning, let us examine it in a broader context. What forms does homeostatic plasticity take and what parameters are commonly adjusted across phyla to maintain the normal functioning of the network? Furthermore, what differences are there in homeostatic plasticity strategies/end goals? Do all systems want to achieve minimal inter-neuron variability or do the defined limits of what is tolerable vary depending on the function of a given network?

1.6. Homeostasis and synaptic plasticity

The theory of homeostasis originated in the late 19th century with the work of the French physiologist Claude Bernard (Bernard, 1885) who proposed ‘higher animals’ were in a close

relationship with their external environment and used it to inform the stability of the ‘internal milieu’. The term homeostasis would not be used until later when the physiologist Walter B. Cannon (Cannon, 1929) developed the idea of “physiological regulation of normal states” and would propose that biological factors must be kept within narrow limits as opposed to completely fixed values. However, the discovery of homeostatic plasticity wouldn’t come until much later and first some important groundwork in Hebbian plasticity would need to be laid to facilitate this later discovery. Donald Hebb originally proposed that neurons closely associated with each other who fire together undergo a physical change that makes future coordinated activations stronger; this is commonly summarized as “Neurons that fire together, wire together” (Hebb, 1949). Findings supporting Hebb’s theory of plasticity would come later with work in the rabbit hippocampus identifying long-term potentiation (LTP) in activity of postsynaptic neurons induced by high frequency stimulation (Bliss and Lomo, 1973) and discovery of long-term depression (LTD) in the rabbit cerebellum (Ito and Kano, 1982). These mechanisms scale the strength of synapses between neurons whose activity is coordinated to increase or decrease the responsiveness of the postsynaptic neuron to the presynaptic neuron.

Without a limiting factor, both mechanisms of Hebbian plasticity can result in potentially network destabilizing positive feedback loops (Miller and MacKay, 1994; Abbott and Nelson, 2000). Coincidental activation of neurons induces strengthening of synapses which increases the chance that those neurons will fire in close association again, which results in further potentiation ad infinitum and hyperactivity. Conversely, prolonged low frequency stimulation of postsynaptic neurons weakens synapses, but this can similarly lead to an endless positive feedback loop and hypoactivity. These ‘infinite’ loops are constrained by biological factors, like the maximum number of channels or receptors that can exist on a neuron, suggesting the existence of ceilings and floors to potentiation and depression. However, it is the comparative patterns of activity of neurons in response to different stimuli or internal processing that allows us to encode distinct representations. If the majority of neurons in a network reached a maximum active state, it is possible there would be little to distinguish these neurons from each other as such unchecked potentiation might spread. Of course this does not typically occur in biological circuits, and this suggested the existence of a homeostatic mechanism to constrain the effects of natural variability in neuron parameters as well as Hebbian plasticity positive feedback loops. The first evidence of homeostatic plasticity was in lobster neurons, where isolation from inputs in culture resulted in a transition to tonic firing patterns but a later restoration of their original burst activity (Turrigiano, Abbott and Marder, 1994). These

neurons demonstrated an ability to adapt their conductance's to maintain stable activities, termed intrinsic homeostasis. It was then later established that neurons could scale their synaptic strength in response to prolonged hypo- or hyperactivity in a proportionate manner, so the relative balance of the different synaptic strengths across the neuron are maintained (Turrigiano et al., 1998); this is termed synaptic homeostasis. Hebbian and homeostatic plasticity likely work synergistically to allow learning-associated changes in synaptic strength while keeping activity/parameters within 'expected range'. We will discuss this balancing act later when reviewing the goals of homeostatic plasticity.

A mechanism essential to homeostasis of all types is negative feedback. This requires (1) a sensor that allows the system to track changes in the biological variable being regulated, (2) a comparator that calculates the error representing the difference between the current level of the variable and the set range, (3) a controller that interprets this error and determines the correction required, and (4) an effector that produces this correction and brings the variable back within range thereby closing the loop (Modell et al., 2015; Michetti and Benfenati, 2024). In the previous section we alluded to the contributions of these elements without directly discussing them. For example, in (Abdelrahman, Vasilaki and Lin, 2021) both activity-independent and activity-dependent compensatory models were created agnostic to the exact biological mechanisms used to sense and induce changes in parameters. However, when trying to determine which of these models is closer to the real mechanisms used in the MB, it is important to consider what molecular mechanisms may map onto the different elements of any potential negative feedback loop (s). In the activity-dependent model, the sensor(s) needs some way of detecting direct changes in the cell's average level of activity. In the mammalian cortex, level of Ca^{2+} influx has been implicated as a sensor of altered average activity; changes to influx appear to induce up-/downregulation of calcium-dependent signalling pathways that converge to scale synaptic strength up or down to restore average activity (Ibata, Sun and Turrigiano, 2008; Seeburg et al., 2008; Seeburg and Sheng, 2008; Hu et al., 2010; Fu et al., 2011). Interestingly, some modelling work has also demonstrated that utilising Ca^{2+} as an activity-sensor that influences relative production and degradation of ion channels proves effective for regulating intrinsic excitability within set range (O'Leary et al., 2014). Conversely, work on the *Drosophila* neuromuscular junction (NMJ) has revealed that inhibition of postsynaptic receptors results in increased Ca^{2+} influx presynaptically necessary for enhanced neurotransmitter release (Müller and Davis, 2012) and this appears to result from changes in number/function of calcium channels (Zhao, Dreosti and Lagnado, 2011). The combination of these results would suggest that intracellular

Ca^{2+} can act as both sensor and effector in homeostatic plasticity, but this may be diverse across cell types.

Reactive oxygen species (ROS) are another potential activity sensor in homeostatic plasticity. Neuronal hyperactivity causes elevated levels of ROS at presynaptic terminals in both mammals and Drosophila (Hongpaisan, Winters and Andrews, 2004; Oswald et al., 2018), and artificially increasing ROS at the NMJ is both necessary and sufficient to induce homeostatic structural changes, like increased bouton number and decreased dendritic arbour length, similar to those caused by hyperactivity (Oswald et al., 2018). This structural plasticity is required for homeostatic changes in larval motor behaviours and artificially decreasing ROS using Catalase prevents compensatory changes in synaptic transmission. Importantly, these experiments identified a highly conserved ROS sensor DJ-1β, that is also necessary for homeostatic structural changes and may sit in a pathway responsible for mediating activity-dependent alterations in synaptic number and structure (Kim et al., 2005; Martín-Peña et al., 2006; Meulener et al., 2006; Kim et al., 2009; Jordán-Álvarez et al., 2012; Lin, Prahlad and Wilson, 2012; Ariga et al., 2013). Calcium-dependent proteins and ROS interact with each other at mitochondria, suggesting there may even be a level of communication between activity-sensing pathways relying on Ca^{2+} and ROS respectively (Hongpaisan, Winters and Andrews, 2004)

This work is not an investigation into the mechanisms used to sense changes in activity. Instead, the aim is to identify any parameters that may be adjusted in response to alterations in average activity of single neurons, which may suggest the existence of an intrinsic activity-dependent homeostatic mechanism. In (Abdelrahman, Vasilaki and Lin, 2021), synaptic strength, number, inhibitory weight and spiking threshold were all suggested as potential targets for compensation. However, within the literature there are many ways to achieve changes in these parameters and alternative targets/changes that can also be used to achieve homeostatic adaptation. It is important to consider the forms that homeostatic plasticity can take as this will allow for identification of the possible target parameters for homeostatic plasticity in the *Drosophila* MB.

1.7 Types of homeostatic plasticity

As is typically the case in biology there are many ways to categorize homeostatic plasticity. Here I will divide homeostatic plasticity on two characteristics: first, how neurons maintain a

set level of activity, either through acting on the intrinsic excitability of the cell or through scaling synaptic strength up or down (or both). A particular emphasis will be placed on activity-dependent compensations in the neuron's morphology because of its relevance to this project's findings. The second division is whether the plasticity occurs in single cells or at a network level, although as will become clear there is a large amount of overlap in this; even neurons that utilise cell-autonomous regulation can still improve network function as demonstrated in the model in (Abdelrahman, Vasilaki and Lin, 2021). A distinction will also be made between activity-dependent plasticity that occurs during development and adulthood, as the findings of this project relate specifically to adult adaptations.

1.7.1 Intrinsic homeostatic plasticity

Intrinsic homeostatic plasticity involves mechanisms that act on the cells intrinsic excitability to restore it within a set range that is necessary for the cell or network to function. It can involve alterations in the composition of ion channels expressed across the cell, or changes to neuron morphology like adjustment of the axon initial segment (AIS) position. Necessarily, these changes occur through signalling pathways that may be activity-dependent or independent. To test how neurons adjust their excitability the system must be perturbed, which usually involves the application of ion channel blockers, genetic manipulation or isolation in culture to increase/decrease activity, alter the conductance of specific ion channels or remove the typical inputs these cells receive. The first experiments demonstrating homeostatic plasticity used electrophysiological recordings of isolated cultured neurons, which revealed that even without the presence of their usual rhythmic input, neurons recovered their burst activity upon depolarization after 3-4 days (Turrigiano, Abbott and Marder, 1994). However, this does not reveal how conductance's are being altered, although it is likely that many different strategies can be used to achieve this depending on species and cell type. Staying with lobster stomatogastric ganglion neurons, later experiments tested their response to artificially increasing the expression of Shal (MacLean et al., 2003), one of the voltage-dependent K^+ channels in the Shaker family responsible for the repolarising I_A current; in these neurons this current assists in regulating rhythmic firing and spike frequency (Tierney and Harris-Warrick, 1992). This increased expression of repolarising K+ channels would typically result in reduced excitability and firing frequency but despite increased I_A current amplitude, activity was unchanged in these neurons due to a correlated enhancement of the inward I_H current, suggesting the existence of a homeostatic mechanism to maintain intrinsic excitability. Intriguingly, expression of a non-functional Shal

mutant also resulted in an increase in I_H despite no change in I_A amplitude, demonstrating this adaptation may be activity-independent. The existence of both activity-dependent and activity-independent homeostatic mechanisms in one neuron type suggests multiple strategies and pathways may be used to achieve a set activity level. This could suggest some level of crosstalk between the two or these neurons may have developed multiple approaches that have different goals (maintain activity level and maintain balance in ion channel expression) but produce a consistent result.

In the lobster model system, it is clear that adjusting ion channel composition is critical for regulating intrinsic excitability, but is this true across organisms? Cultured rat visual cortex neurons with their spontaneous activity blocked by Na+ channel blocker tetrodotoxin (TTX) for 48 hours demonstrate similar adaptations (Desai, Rutherford and Turrigiano, 1999); they show increased firing frequency and lowered spiking threshold. Utilising a range of molecules that block different ion channels and their associated currents (TEA, cadmium, 4-AP, caesium) revealed that this adaptation is achieved through an increase in Na^+ currents and decrease in persistent/repolarizing K^+ currents, suggesting blocking activity can cause an increase in Na^+ channels and decrease in specific K^+ channels. Similar effects are observed in hippocampal slices, where activity blockade with TTX causes increased expression of voltage-gated Na^+ channels that return to normal levels 1 day after cessation of TTX, demonstrating excitability can be scaled in both directions by, at least partially, manipulating levels of Na+ channels (Aptowicz, Kunkler and Kraig, 2004). Sodium channels appear to be a common homeostatic lever across organisms. Elevated activity in Drosophila motor neurons decreases mRNA levels of para (Mee et al., 2004), the voltage-gated sodium channel discovered in Drosophila. Blocking synaptic vesicle release results in an opposing increase in para mRNA, demonstrating this adaptation too is bidirectional. Interestingly this appears to be regulated by the transcriptional repressor pumilio (pum) whose mRNA levels correlate with para during manipulations and when overexpressed is sufficient to increase both para mRNA and amplitude of $I_{Na.}$ This highlights a potential homeostatic effector that mediates alterations in excitability and appears to be conserved in mammals where it has been shown to bind voltage-gated sodium channel transcripts (Driscoll et al., 2013).

Manipulating voltage-gated sodium channel number appears to be an effective way of directly regulating spiking threshold and therefore activity of a neuron, but there are many other potential targets that can alter intrinsic excitability. There are a variety of potassium channels, many of which were originally discovered in *Drosophila* as covered in section 1.2. There are broadly speaking three classes of potassium channel: (1) Voltage-gated (or

calcium-gated) channels K_v which typically open in response to depolarization and are responsible for the repolarization of the membrane, (2) inwardly-rectifying potassium channels K_{ir} which are responsible for setting and stabilizing the resting membrane potential and in shaping the action potential, (3) tandem pore domain potassium channels typically referred to as leak channels which are constitutively open and allow continuous K+ efflux and also contribute to maintaining the cells resting potential (Armstrong and Hille, 1998; Kuang, Purhonen and Hebert, 2015).

K_v channels have already been implicated in some of the mechanisms discussed above (Desai, Rutherford and Turrigiano, 1999) working in parallel with a homeostatic mechanism that adjusts voltage-gated sodium channels, which logically follows given their often opposing effects. There are many types of K_v channels that vary in temporal dynamics and whose mosaic of expression across cell types contribute to their distinct firing pattern and intrinsic excitability (Johnston, Forsythe and Kopp-Scheinpflug, 2010). For example in rat models of epilepsy, a pathology associated with dysregulated homeostatic plasticity (Lignani, Baldelli and Marra, 2020), individuals with induced seizures/hyperactivity demonstrate altered localization of somatodendritic Kv2.1 (delayed rectifier) channels in cortical and hippocampal pyramidal neurons (Misonou et al., 2004); channels shift from a clustered organization to a more uniform distribution rapidly (~5 minutes). This reorganization is mediated by Kv2.1 dephosphorylation and Ca^{2+} influx and calcineurin activation is necessary and sufficient for both this and the relocation of these channels. This is accompanied by a shift in voltage-dependent activation of potassium current resulting in a higher proportion of channels open during rest and depolarization and likely a greater K^+ efflux, theoretically counteracting the increased excitability. Similar manipulations/pathologies also homeostatically reduce neuronal firing rates suggesting this mechanism is functionally involved in pathological conditions (Park et al., 2006; Misonou et al., 2004; Misonou, Mohapatra and Trimmer, 2005; Mohapatra et al., 2009; Misonou et al., 2005; Romer et al., 2014; Romer, Deardorff and Fyffe, 2016). TRESK (TWIK-related spinal cord K+ channel) are a type of leak potassium channel abundantly expressed in neurons of the trigeminal and dorsal root ganglia in the spinal cord and contribute extensively to their background K^+ currents (Dobler et al., 2007; Liu et al., 2013). Prolonged hyperactivity in a seizure model of hippocampal CA3 neurons revealed these channels may be partially responsible for termination of seizures as part of a calcium-dependent homeostatic mechanism (Huang et al., 2021b). Sustained depolarization activates these channels which in turn appear to partially contribute to depolarization-induced shunting

inhibition (DShI), a process which reduces excitability via increased current flowing out of the cell, making it less likely that graded potentials reach the AIS.

Many of the above examples further demonstrate the importance of Ca^{2+} in regulating homeostatic plasticity, but what about calcium-activated potassium channels like BK (big potassium) and SK (small potassium)? Another potential homeostatic lever to use to adjust to altered excitability is to change action potential duration. In cultured cortical neurons blocking spikes for 24-48 hours results in longer action potential durations (Li et al., 2020a). This increased duration requires alternative splicing of one of the BK transcript exons and relies on voltage-gated calcium currents and associated pathways. Intriguingly, blocking APs produces temporary depolarizations in dendritic spines which are sufficient to trigger voltage-gated calcium channels and allow greater Ca^{2+} influx, which go on to activate calcium-dependent signalling proteins that induce alternative splicing. Not only does this research demonstrate that regulation of BK channels is another way of homeostatically adjusting intrinsic excitability but highlights a clear Ca^{2+} signalling pathway responsible for this adaptation. As will become clear, these pathways are prevalent in many homeostatic mechanisms. It is also worth mentioning that this mechanism appears to use the same machinery utilised in Hebbian plasticity mechanisms (Deisseroth et al., 2003; Ma et al., 2014) suggesting it may be co-opted for both Hebbian and homeostatic plasticity depending on context. Given the critical role of calcium in homeostatic plasticity, it logically follows that calcium channels are yet another lever for regulating intrinsic excitability. Intracellular calcium levels are particularly critical for regulating neurotransmission and as such we will discuss these channels with synaptic homeostatic plasticity (1.7.2) as they play a big role in this process.

Altering distribution of ion channels represents another method of adjusting intrinsic excitability to compensate for perturbation, as we have already alluded to (Misonou et al., 2004); redistribution of channels in the AIS may be particularly effective. The AIS is a region of the neuron dense with voltage-gated channels (especially Na_v) and is typically where graded potentials are summed and APs initiated (Bender and Trussell, 2012); because of this role any change in ion channel distribution/expression here is likely to heavily influence neuron spiking probability. For example, chronic depolarization of hippocampal neurons in culture induces Na_v to move away from the soma effectively reducing firing probability by increasing the distance currents have to propagate before reaching the AIS to initiate an AP (Grubb and Burrone, 2010); this mechanism also appears to be calcium dependent (Evans et al., 2013). This form of homeostatic plasticity appears to vary based on neuron type, with

chronic depolarization in the olfactory bulb resulting in a shifting of the AIS proximally in inhibitory interneurons and distally in non-inhibitory neurons (as observed previously in excitatory neurons) (Chand et al., 2015). These opposing changes in neurons of different polarities begins to allude towards the differences in mechanisms of homeostatic plasticity between neuron types. A potential issue arises in theories of compensation if all neurons, both excitatory and inhibitory, adjust their activity in a self-centred manner e.g. compensate for hyperactivity by decreasing intrinsic excitability or scaling strength of relevant synapses down(Michetti and Benfenati, 2024); decreased activity in excitatory neurons would be countered by decreased inhibition of these neurons. This demonstrates why it may be necessary for different neuron types to use distinct homeostatic rules and mechanisms. The length of the AIS and distribution of different voltage-gated ion channels across it (Na_V, K_V, Ca_V) are not only important for adult homeostatic plasticity, but may help define the intrinsic excitability of different neurons during development and therefore establish their role within the network (Bender and Trussell, 2012). There is more than one way to compensate for changes in activity outside neurons set range. We have seen that intrinsic homeostatic plasticity can be spatially specific but there is another way to achieve an even more targeted level of adaptation.

1.7.2 Synaptic homeostatic plasticity

As is the case with Hebbian plasticity, neurons are capable of adjusting the strength of their synapses, although in homeostatic plasticity the goal is to adapt to prolonged increased/decreased activity from particular inputs. This synaptic homeostasis typically takes two forms, altering of postsynaptic sites or changing neurotransmission at the presynapse, both with the aim of altering the probability of successful information transfer from one synapse to the other; ultimately these changes inform spiking probability in the postsynaptic neuron.

1.7.2.1 Presynaptic homeostatic plasticity

First, let's start with presynaptic neurons and close off the discussion of ion channel adaptations with a focus on voltage-gated calcium channels (Ca_V). These channels regulate the influx of Ca^{2+} into the presynaptic bouton, typically occurring on arrival of an AP, and therefore contribute to neurotransmission, signalling pathways and transcription and translation. These channels are regulated in a variety of ways (Catterall, 2000; Tedford and Zamponi, 2006; Catterall and Few, 2008; Dolphin, 2009; Currie, 2010; Lipscombe, Allen and

Toro, 2013) and unsurprisingly they are implicated in both Hebbian and homeostatic plasticity (Voglis and Tavernarakis, 2006; Frank, 2014b). For example, the cacophony gene encodes L-type voltage-gated calcium channels at the Drosophila neuromuscular junction (NMJ), which are presynaptic synapses between motor neurons and muscle fibres conserved across organisms (Jan and Jan, 1976a, 1976b). The influx of Ca^{2+} via these channels triggers a pathway involving Synaptotagmin and the Snare complex that induces vesicle fusion and therefore release of neurotransmitter (Perin et al., 1990; Schiavo et al., 1996; Geppert et al., 1994; Fernández-Chacón et al., 2001). Homeostatic plasticity at the NMJ was first characterised in experiments where postsynaptic glutamate receptor deletion was combined with constitutive PKA expression, which induces an initial decrease in muscle responses to single vesicles (quantal size) and depends on postsynaptic PKA activity (Petersen et al., 1997; Davis et al., 1998; DiAntonio et al., 1999); this perturbation is partially compensated for by an increase in the amount of neurotransmitter being released. Partial loss of the voltage-gated calcium channels cacophony (cac) blocks this homeostatic adaptation and expression of these channels is modulated during synaptic homeostasis (Frank et al., 2006; Frank, Pielage and Davis, 2009; Gratz et al., 2019). Calcium imaging has revealed the aforementioned manipulation induces an increase in presynaptic calcium influx that requires voltage-gated calcium channels (Müller and Davis, 2012). Calcium and calcium-dependent proteins interact with many other members part of the SNARE complex, and several of these are also implicated in homeostatic plasticity at the NMJ. For example, several structural changes are induced by homeostatic plasticity here, which relies on alterations to proteins like Bruchpilot (BRP) and an associated increase in the size of the presynaptic cytomatrix (Weyhersmüller et al., 2011), a dense protein scaffold that is required for efficient vesicle release (Siksou et al., 2007). Research at the NMJ therefore supports the critical role of Ca_V channels as part of a complex set of signalling pathways regulating Ca^{2+} influx, communication between neurons and muscle fibres and structural changes (Frank, 2014a).

The story is similar in mammalian synapses, where much work on cortical cultures and in vivo has investigated presynaptic bouton-centred homeostatic plasticity and the role of calcium. Both pharmacological silencing via TTX and blockade of the glutamatergic receptor AMPAR via PhTX reveal a compensatory increase in the readily releasable pool (RRP) of vesicles available, increased release probability and increased size of the presynaptic bouton, and this adaptation requires L-type voltage-gated calcium channels (Murthy et al., 2001; Thiagarajan, Lindskog and Tsien, 2005). Additionally, an experiment using SyGCaMP2 and SypHy (a reporter of vesicle fusion) revealed that decreased activity of cultured

hippocampal neurons causes an increase in Ca^{2+} influx and increased activity induces an opposing change (Zhao, Dreosti and Lagnado, 2011). Furthermore, this adaptation decreases the probability of vesicle release without significantly changing the maximum amount of vesicle present at these boutons, elucidated by high frequency stimulation (Rosenmund and Stevens, 1996). The relationship between Ca^{2+} influx and probability of vesicle release can be described by a "third-power law", meaning for example if calcium influx doubles, the probability of vesicle release increase proportionately to this by a factor of 8 (Zhao, Dreosti and Lagnado, 2011) and this closely matches what has been observed at other synapses (Katz and Miledi, 1970; Sinha, Wu and Saggau, 1997). Importantly, this suggests that the target of this homeostatic adaptation is calcium influx itself and not another mechanism that could be used to alter probability of a vesicle release. This further demonstrates how critical regulating presynaptic intracellular Ca^{2+} is for homeostatic adjustments of vesicle release. It also at least partially explains many of the changes at the postsynaptic bouton that occur during homeostatic plasticity we will now discuss.

1.7.2.2 Postsynaptic homeostatic plasticity

The strength of a synapse can also be adjusted through alterations in the expression and distribution of receptors and ion channels. The first evidence of synaptic scaling in rat visual cortex neurons demonstrated postsynaptic neurons were capable of bidirectional adjustment of synapse strength (Turrigiano et al., 1998); blocking activity resulted in a compensatory increased miniature excitatory postsynaptic current (mEPSC) amplitude whereas blocking inhibition produced a decreased mEPSC amplitude after 48 hours. This changed response is at least partially due to alterations in number and function of receptors and has been observed across multiple neuron types and systems (Desai et al., 2002; Stellwagen and Malenka, 2006; Goel and Lee, 2007; Kim and Tsien, 2008; Ibata, Sun and Turrigiano, 2008; Knogler, Liao and Drapeau, 2010). Importantly these changes aren't accompanied by perturbation to Hebbian plasticity, demonstrating homeostatic adaptations can occur while short-term plasticity is maintained. (Watt et al., 2000; Wierenga, Ibata and Turrigiano, 2005). In particular the glutamate receptor AMPA is a common target of homeostatic plasticity mechanisms. AMPA receptor subunit GluR2 (but not GluR1 or GluR3) is necessary and sufficient for synaptic scaling in the rat visual cortex following TTX or monocular deprivation, and GluR2 AMPARs accumulate at the synapse after these manipulations (Gainey et al., 2009). In contrast, GluR1 is required for LTP in the visual cortex (Watt et al., 2004). These findings suggest that distinct forms of plasticity are managed by different pathways which is

further supported by findings these subunits utilise and bind to different trafficking and scaffold proteins (Shepherd and Huganir, 2007). To bring this full circle, the pathway that induces increased GluR2-AMPAR expression at synapses appears to partially depend on reduced postsynaptic Ca^{2+} influx and subsequent reduced activation of the calcium/calmodulin dependent protein kinase IV (CaMKIV) (Ibata, Sun and Turrigiano, 2008).

Although homeostatic plasticity has been extensively studied at the Drosophila NMJ, there has also been important research of central neurons that match many of the findings observed in mammalian central synapses. The major excitatory neurons in Drosophila are cholinergic (Gu and O'Dowd, 2006) which makes investigations of homeostatic plasticity at these sites a good comparison for mammalian glutamatergic synapses and the cholinergic neurons that are also found in these systems. Blocking nicotinic acetylcholine receptors (nAChR) for 24 hours using curare increased the amplitude of mEPSCS and increased Dα7-subunit-containing nAChRs of neurons in culture (Ping and Tsunoda, 2011); this upregulation was also observed in adult brains. In motor neurons and PNs this inactivity also caused an upregulation in number of Shal voltage-gated potassium channels but required a 1h recovery period unlike changes in number of nAChRs. This adaptation in potassium channels counteracts the overexcitation induced by increased nAChR expression, returning mEPSPs recorded to control levels. Secondary homeostatic upregulation of potassium channels is induced by Ca2+ acting via CaMKII and may partially rely on increased influx through Dα7-nAChRs counterparts (Albuquerque et al., 2009; Gotti et al., 2009). These findings demonstrate coordination of counter homeostatic mechanisms that may allow for tighter control of activity within a neurons set range by preventing the first adaptation from perturbing activity too far. Note this reliance on receptor subunit-specific and calcium-calmodulin dependent mechanisms is remarkably similar to what we discussed earlier (Ibata, Sun and Turrigiano, 2008), although the competing nature of this homeostatic mechanism is unique.

This begins to build a picture of a series of presynaptic and postsynaptic alterations that depend on intracellular calcium to sense changes in a neurons average activity and activate pathways that produce changes in neurotransmitter release probability, number of ion channels and expression of receptors all of which can result in an adjustment in postsynaptic responses; importantly, changes in intracellular Ca^{2+} is not always the first step, demonstrating variability in mechanisms between neuron type and species. All this then impacts on the probability of information being transferred from presynaptic neuron to postsynaptic neuron and its spiking probability. This may be combined with further changes in

intrinsic homeostasis that increase/decrease the chance an EPSP has of making it to the AIS through changes in the morphology and distribution of channels across this region.

To return briefly to the model proposed in (Abdelrahman, Vasilaki and Lin, 2021) there were several key parameters suggested as targets for homeostatic compensation in KCs: Number of inputs (N), the strength of inputs (w), and spiking threshold (θ). We have covered above adaptations in the strength of inputs through changes in neurotransmission, expression of receptors and key ion channels through a series of diverse signalling pathways. Spiking threshold compensation has also been discussed and occurs through changes to intrinsic excitability by altering number and distribution of ion channels and morphological plasticity in AIS location relative to dendrites. So far, I have avoided exploring homeostatic plasticity that involves changes in number of inputs and have only alluded to structural changes at synapses. This is not due to lack of importance, in fact these adaptations are highly relevant to this work. Findings of alterations in density (e.g. fewer or greater spines per neuron) and volume (smaller/larger spines) of dendritic spines are commonplace in mammalian models of homeostatic plasticity (Moulin, Rayêe and Schiöth, 2022). In contrast, experiments demonstrating homeostatic changes in dendrite number in Drosophila are limited, although there is a good deal of evidence highlighting adjustment in size and structure of the presynaptic bouton and postsynaptic active zone of many neurons, NMJ and ORNs as chief examples (Goel et al., 2019; Rozenfeld et al., 2023); the next section will discuss these in detail. Finally, we have alluded to the importance of many key signalling pathways in regulating homeostatic plasticity here without a detailed discussion of their individual relevance. Aside from a few examples, these will mostly be covered in the Discussion where possible regulators of the adaptations observed in this work will be proposed (5.3).

1.7.3 Morphological homeostatic plasticity

1.7.3.1 Synaptic structure homeostatic plasticity

We have focused on the physiological changes that occur during homeostatic synaptic scaling, e.g. alterations in mEPSC amplitude and frequency, and the changes in receptor and ion channel expression and distribution that drive this. It logically follows that these adaptations may also be accompanied by structural modifications to synapses. For example, increased synaptic size appears to positively correlate with synaptic strength, and this association may be partially due to a larger pool of readily available vesicles at bigger

presynaptic active zones and increased size of the postsynaptic density, which allows for a greater number of receptors on the membrane, and therefore a larger mEPSC amplitude (Murthy et al., 2001). Experiments using prolonged AMPAR blockade of hippocampal neurons supports this idea, as homeostatic adaptations to this perturbation increase vesicle pool size and turnover rate, and increase incorporation of GluR1-AMPARs at the postsynapse (Thiagarajan, Lindskog and Tsien, 2005). Interestingly, recruitment of GluR1-AMPARs was targeted to the largest synapses and is driven partially by replacement of GluR1/GluR2 heteromeric AMPARs with no observed changes in spine number. Similar to previous results, decreased Ca^{2+} influx via voltage-gated calcium channels are necessary for both presynaptic and postsynaptic changes (Thiagarajan, Lindskog and Tsien, 2005). Blockade of activity for 48 hours in hippocampal pyramidal neurons using TTX causes a compensatory increase in volume of affected spines that is reversible when activity is restored (Hobbiss, Ramiro-Cortés and Israely, 2018). Homeostatic changes in mEPSC amplitude and spine size were compared at several timepoints (0 h,24 h,48 h,72 h) which revealed a linear scaling of mEPSC amplitude but an initial supralinear increase in spine volume compared to control spines, that becomes linear at 72 hours. This may suggest modifications initially ‘overshoot’ their target and correct later, which is typical of many homeostatic negative feedback loops. Intriguingly, this homeostatic adaptation also appears to facilitate Hebbian plasticity, with LTP induction in these neurons lasting significantly longer than control counterparts but occurring preferentially at smaller spines. Smaller spines that have undergone homeostatic plasticity grow more, demonstrate greater LTP than controls and have lower thresholds for Hebbian plasticity. However, specificity of LTP is lost in these neurons, as neighbouring spines also demonstrate increased volume (Hobbiss, Ramiro-Cortés and Israely, 2018). These findings demonstrate significant interaction between structural changes caused by homeostatic plasticity and those induced by Hebbian plasticity which may allow for cooperation between inputs and integration of information from distinct synapses into the same engram via clustering (Govindarajan et al., 2011; Kleindienst et al., 2011; Makino and Malinow, 2011; Fu et al., 2012; Yadav et al., 2012; Hobbiss, Ramiro-Cortés and Israely, 2018).

Similar changes in synapse structure and volume have also been observed in the visual cortex, where visual deprivation via retinal lesions is often used to block activity. Complete bilateral visual deprivation results in an increased mEPSC amplitude in visual cortical neuron slices and an associated increase in spine size (Keck et al., 2013). The increase in mEPSC amplitude and spine size over time show paralleled timings and magnitude supporting the

multiplicative relationship between these factors. Interestingly, similar increases in spine size are also observed in a subclass of visual inhibitory neurons expressing spines and both are dependent on tumour necrosis factor-alpha (TNF-α) which has been previously implicated in synaptic scaling via AMPAR upregulation (Stellwagen and Malenka, 2006; Steinmetz and Turrigiano, 2010). Spine size increases were most prevalent on dendritic branches that had lost spines after visual deprivation in both inhibitory and excitatory neurons and appears to preferentially occur at these branches and not across the whole neuron. A model comparing branch-specific and global synaptic scaling found that normalizing synaptic weights within a branch resulted in higher mutual information between stimulus and output, meaning postsynaptic neurons reliably respond and encode the stimulus from the presynaptic neuron (Barnes et al., 2017). Collectively, this evidence suggests that morphological homeostatic adaptations have a spatial specificity within a branch, but compensations are not necessarily targeted to single spines.

Morphological plasticity is not limited to mammalian systems and has also been observed in the *Drosophila* NMJ. It is well established that reducing synaptic vesicle sensitivity of the NMJ postsynapse using PhTx, induces a rapid (10 minute) homeostatic increase in vesicles released by the presynaptic neuron (Frank et al., 2006); what structural changes accompany this plasticity? Bruchpilot (BRP) is a key scaffolding protein of the Active zone important for organizing vesicle release machinery (Kittel et al., 2006) and this role makes it a likely target for homeostatic plasticity. Homeostatic increase in number of release-ready vesicles at the NMJ is associated with increased expression of BRP at these synapses and an enlargement of the Active zone (Weyhersmüller et al., 2011). The Active zone is an extensive structure and incorporates many proteins in addition to BRP like RIM-binding protein (RBP), Unc13a, Unc18 and Syntaxin-1A who all play roles in regulating synaptic release and several of which are part of the SNARE complex (Kittel et al., 2006; Liu et al., 2011; Acuna, Liu and Südhof, 2016; Böhme et al., 2016; Reddy-Alla et al., 2017; Sakamoto et al., 2018; Südhof, 2012; Walter, Böhme and Sigrist, 2018); it logically follows these may also be targets for homeostatic mechanisms. PhTx application causes increased expression of BRP, RBP, Unc13A and Syntaxin-1a at Active zones, and these changes are further amplified in neurons lacking Glur2A (Böhme et al., 2019). Importantly, this adaptation occurs within minutes of activity blockade but is only necessary for chronic increases in quantal content, suggesting these structures are established quickly to ensure long-term consolidation of homeostatic plasticity; in contrast Unc13A is required for rapid presynaptic homeostatic plasticity. (Böhme et al., 2019). It is likely that interplay between RIM, RBP, Unc13A and BRP may be highly

conserved across organisms and several of these proteins have been implicated in synaptic plasticity of both types (Dulubova et al., 2005; Lu et al., 2006; Deng et al., 2011; Camacho et al., 2017; Castillo, 2012; Müller et al., 2012; Hu, Tong and Kaplan, 2013; Müller, Genç and Davis, 2015; Michelassi et al., 2017).

To alter the number of vesicles ready for release, the NMJ uses mechanisms that modulate Active zone structure and polymerization of F-actin. In *Drosophila,* development of spatially coordinated Active zones and postsynaptic glutamate receptors (aka “nanocolumns” (Biederer, Kaeser and Blanpied, 2017)) depends on the antagonism between Neuroligin 1 and 2 (Nlg1, Nlg2) and associated presynaptic proteins Syd-1 and Spinophilin (Spn) (Ramesh et al., 2021). Nlg1 and Syd-1 promote Active zone assembly and AMPAR-GluR2A incorporation through BRP accumulation, while Nlg2 and Spn drive Active zone maturation and restrain the incorporation of these receptors; crosstalk between these antagonistic regulatory modules drives pre- postsynaptic matching. Furthermore, Spn also drives BRP incorporation during presynaptic homeostatic plasticity at the NMJ and similar to prior results Spn alone is also required for the maintenance of this plasticity and not for the initial rapid compensation of mEPSC amplitude (Böhme et al., 2019; Turrel et al., 2022; Ramesh et al., 2023). The antagonism between Spn and Syd-1 also seems to extend to presynaptic homeostatic plasticity, where their interaction sets the limit of Active zone remodelling and associated functional changes, which is partially achieved through regulation of F-actin accumulation and stabilization at these synapses (Nakanishi et al., 1997; Ryan et al., 2005; Chia, Patel and Shen, 2012; Ramesh et al., 2023). F-actin synapse accumulation may block vesicle exocytosis (Aunis and Bader, 1988; Bleckert, Photowala and Alford, 2012; Wu and Chan, 2022) which can be countered by Mical, a protein which drives oxidation and destabilization of actin and has been found to be necessary for presynaptic homeostatic plasticity at the NMJ (Orr, Fetter and Davis, 2017; Wu et al., 2018; Orr, Fetter and Davis, 2022). Interestingly, presynaptic homeostatic plasticity deficiency in Spn KD mutants is rescued by Syd-1 presence, Mical overexpression and block of actin polymerization separately (Ramesh et al., 2023). Furthermore, Spn mutants have fewer synaptic vesicles close to the Active zone and don’t demonstrate the typical homeostatic increase in readily releasable pools of vesicles (Ramesh et al., 2023). While not as obvious as changes in number or absolute volume of spines, these homeostatic compensations at the NMJ demonstrate an alteration in the size and organization of structures inside presynaptic boutons which directly impacts vesicle release.

Although there is little direct evidence of homeostatic mechanisms in the MB, several key proteins involved in presynaptic homeostatic plasticity are important for olfactory memory. For example, both Unc13A and BRP are upregulated across the MB after paired olfactory conditioning and knockdown (KD) of BRP in α/β and α'/β' KCs, but not γ, strongly suppresses midterm memory (MTM) with no effect on short-term memory (STM) (Turrel et al., 2022). Additionally, both BRP and Spn KDs in the MB resulted in deficits in anaesthesia-sensitive memory (ASM) but not anaesthesia-resistant memory (ARM) (Turrel et al., 2022; Ramesh et al., 2023). This collectively suggests that Active zone remodelling is important for some types of olfactory memory and not others and with other evidence suggests that regulation of actin depolymerization is also key for presynaptic plasticity across organisms (Krucker, Siggins and Halpain, 2000; Frambach et al., 2004; Kramár et al., 2006; Ganeshina et al., 2012; Lamprecht, 2016). More importantly for this work, both these mechanisms are required for presynaptic homeostatic plasticity in the *Drosophila* NMJ, so it is not a large leap in logic to propose they may also be implicated in homeostatic plasticity in the MB too. In fact, sleep deprivation has been found to elevate levels of BRP presynaptically in KC axonal lobes and raise Cac and Syd1 levels across the MB; in contrast increasing sleep decreases the amount of BRP in KCs (Weiss and Donlea, 2021). It has been proposed that one of the roles of sleep is to permit the brain to undergo homeostatic synaptic downscaling to allow continued learning-associated plasticity and prevent a 'ceiling' being reached (Tononi and Cirelli, 2003, 2006, 2014). There is evidence that sleep deprivation increases the expression of several synaptic proteins and increases the size/number of synapses (Gilestro, Tononi and Cirelli, 2009; Dissel et al., 2015; de Vivo et al., 2017; Spano et al., 2019; Gisabella et al., 2020); these results include the MB specifically where sleep deprivation or extended periods awake causes an increase in the volume of γ KC presynaptic terminals (Bushey, Tononi and Cirelli, 2011). While this does not represent direct evidence of homeostatic structural changes in the MB, the role that sleep may play in homeostasis combined with evidence to changes in these proteins during learning-associated plasticity, support the idea that structural homeostatic plasticity may be possible in the MB.

1.7.3.2 Synaptic number homeostatic plasticity

An additional potential compensation to hyper- or hypoactivity is to add or remove synapses. At the simplest level, removing a synapse completely removes one input channel and theoretically should decrease the postsynaptic neuron's chance of spiking. Following this logic, adding a new synapse should increase the neurons' chance of spiking through virtue of

more inputs to sum together for a potential AP. However, change in number of inputs could be considered an extreme adaptation when considering the information that is being lost or gained. If we use the example of KCs, if they lost 2 of their 6 claws, there is a good chance this could result in them becoming unresponsive to an odour due to loss of input from its associated PN(s). Conversely, if a KC formed new claws with a novel PN, although this may increase the neurons' chance of firing, it also may result in alterations to the odours that KC encodes. It is also possible that morphological changes interact with other homeostatic mechanisms in unpredictable ways. In this section we will discuss the evidence for homeostatic alterations in synapse number and touch on why the simple model described above may not capture the full effects of these changes.

Early research revealed that a compensatory change in number of synapses may take place. (Kirov and Harris, 1999) pharmacologically blocked synaptic transmission in hippocampal slices and discovered an increase in the number of dendritic spines. Conversely neurons that undergo hyperactivity during epilepsy or in models of excitotoxicity, demonstrate a reduction in the number and size of spines (Paul and Scheibel, 1986; Müller et al., 1993; Segal, 1995; Drakew et al., 1996; Jiang et al., 1998). Intriguingly, loss of spines was also accompanied by a loss of F-actin at existing spines and appears to be sensitive to the calcium-sensitive protein calcineurin (Halpain, Hipolito and Saffer, 1998). This provides some potential regulators in this mechanism, which are implicated in other homeostatic mechanisms we have already discussed.

Later evidence now supports the functional benefits of adaptation in number of spines. Earlier we discussed visual deprivation as a method of perturbing activity of the visual cortex, but this technique is quite broad and cuts off all input to the visual system. Making small focal lesions in the retina allows observation of adaptations in a limited area of the visual cortex, and interestingly this silenced area begins to respond to new stimuli from lesion-adjacent receptive fields (RFs) (Kaas et al., 1990; Heinen and Skavenski, 1991; Gilbert and Wiesel, 1992). It is now clear this occurs through an increase in number of spines with new presynaptic neurons. Excitatory visual pyramidal neurons show a threefold increase in spine turnover 1 month after focal retinal lesion, with 91% of original spines in this group replaced after 2 months (Keck et al., 2008); the same change was not observed in animals that were completely visually deprived. Interestingly, there was no broad changes to dendritic architecture, showing that adjusting only spines is sufficient to restore activity to this area and suggesting these neurons can obtain new RFs by forming synapses with those neurons already in close contact with them. Supporting this, electron microscopy and modelling show

that dendrites in mouse cortex have enough axons close by for neurons to reorganise their connectivity just from changes to spine number (Stepanyants, Hof and Chklovskii, 2002). A subset of inhibitory neurons with spines in the visual cortex respond to both focal retinal lesion and full visual deprivation by reducing their number of spines and boutons, also through adjustment of base spine turnover rate after only 72 hours (Keck et al., 2011). This adaptation seems to represent a more obvious homeostatic change, albeit to compensate for loss of activity in the network, i.e. reduce total inhibition to boost excitation in the visual cortex. It is important to acknowledge this data collectively is not direct evidence of homeostatic plasticity, i.e. an activity-dependent change that restores a previous level of activity but represents a structural remodelling that allows neurons to start responding to new stimuli. What this does demonstrate is that cortical neurons have the capability to adjust their morphology in response to perturbations in activity; whether the same mechanisms apply to more typical activity blockade methods remains to be seen.

Chronic TTX application of cultured hippocampal slices causes synaptic upscaling of both AMPAR and NMDAR mediated mEPSCs (Arendt, Sarti and Chen, 2013). Unexpectedly, this also causes new spines that only express NMDARs and not AMPARs to be created and are therefore theoretically functionally silent given the NMDAR voltage block. Induction of LTP in these neurons revealed an increased LTP magnitude in TTX treated slices, and this appears to be partially due to incorporation of AMPARs at the previously silent synapses (Arendt, Sarti and Chen, 2013). Unsurprisingly, this further demonstrates the interaction between homeostatic and Hebbian plasticity, showing that LTP drives AMPAR expression and therefore activation of the silent synapses created by homeostatic mechanisms. It is possible that this priming of the neuron for future enhanced Hebbian plasticity, represents a more complex homeostatic mechanism where increased activity is not achieved immediately, but amplifies future synaptic strengthening.

The development of optogenetics has allowed for targeted activity manipulations and unsurprisingly is useful for investigations of homeostatic plasticity. In particular, it has been used to great effect to explore cell-autonomous homeostatic plasticity by chronically activating small populations of neurons. For example, (Goold and Nicoll, 2010) labelled CA1 neurons in slice culture with Channelrhodopsin, and performed electrophysiological recordings on them and adjacent non-labelled control neurons after exposure to pulses of blue light for 12 and 24 hours to induce chronic hyperactivity. This resulted in a homeostatic depression in AMPAR and NMDAR currents that may be partially due to intrinsic excitability changes in neurons, as they required greater depolarization to elicit an AP. The changes to

AMPAR/NMDAR currents were not due to adaptations in probability of release at the presynaptic neuron or increased inhibition via enhancement of IPSCs. However, postsynaptic neurons demonstrated a decreased number of spines, which suggests elimination of synapses may be partially responsible the decreased mEPSC frequency observed in these neurons (Goold and Nicoll, 2010). A similar stimulation protocol in CA1 neurons of freely-moving mouse, caused the same reduction in NMDAR- and AMPAR-mediated mEPSCs and decrease in volume and number of spines (Moulin et al., 2019). Interestingly, these changes also impaired establishment of LTP in these neurons and facilitated LTD, demonstrating homeostatic plasticity effects the thresholds for Hebbian plasticity.

Slightly different homeostatic adaptations occur in sparsely labelled CA1 and granule cell hippocampal neurons after 10 minutes of high frequency optogenetic stimulation, instead of 24 hours, that is similar to activity observed in vivo (Mendez et al., 2018). In contrast to the previous experiment, these neurons demonstrated differential regulation of excitatory and inhibitory synapses, with increased inter-event intervals (IEI) of mEPSCs but decreased IEI in mIPSCs. The ratio of evoked EPSCs to IPSCs also decreased, which overall suggests these neurons decrease excitation and increase inhibition in response to a period of high activity. These adapted responses appear to be partially driven by a reduction in number of excitatory synapses which, with results that show similar manipulations increase the number of inhibitory synapses at CA1 neurons (Flores et al., 2015), suggests the rate at which spines of different polarities are removed and added is a target of homeostatic plasticity (Mendez et al., 2018). Adjustment of spine numbers is reversible (Goold and Nicoll, 2010; Flores et al., 2015; Mendez et al., 2018), only occurs after high frequency stimulation and requires protein synthesis (Mendez et al., 2018). Interestingly, this adaptation does not require either of the glutamatergic receptors, but is blocked by blockade of L-type voltage-gated calcium channels and is dependent on regulation of GABAR anchoring protein regulation through the calcium-dependent protein CaMKII at inhibitory synapses (Flores et al., 2015; Mendez et al., 2018); this further implicates intracellular Ca^{2+} levels as an activity sensor and effector of homeostatic plasticity. Similar morphological adaptations are observed in hippocampal granule cells in vivo. These neurons are known to encode fear memory and cells that undergo this homeostatic adaptation demonstrate enhanced extinction memory when highly activated during memory recall (Mendez et al., 2018). The implication is that homeostatic plasticity reduces the reactivation of the full engram during recall and in doing so simultaneously strengthens the extinction trace. Combined with evidence from (Moulin et al., 2019), this is further proof of the critical role homeostatic plasticity plays in influencing

Hebbian plasticity, although it is unclear whether this is ‘intended’ or just a functional consequence of structural changes that were meant to reduce total activity.

Differences in homeostatic adaptations, morphological or otherwise, may be partially explained by different protein expression patterns between time points. For example, there is very little overlap in proteins expressed at 2 and 24 hours after homeostatic adaptation, but there is significant crossover in targets at the same timepoints for both up- and downscaling, suggesting opposing homeostatic adaptations may act through differential regulation of some of the same pathways (Dieterich et al., 2006; Schanzenbächer et al., 2016; Schanzenbächer, Langer and Schuman, 2018). Interestingly, although the proteins targeted at 2 and 24 hours were different, there were similarities in their function. For example, voltage-gated calcium channels were targeted at both time points but the exact channel subunit being regulated was distinct between groups. Furthermore, many of the functional protein groups regulated at both timepoints and in both treatments are implicated in several of the structural homeostatic adaptations we have discussed so far, including proteins involved in the synaptosome, dendritic spines and the actin cytoskeleton (Schanzenbächer et al., 2016; Schanzenbächer, Langer and Schuman, 2018). This analysis highlights several candidates for homeostatic sensors and effectors that may play key roles in morphological homeostatic plasticity and in homeostatic plasticity overall.

MicroRNAs are also a candidate for homeostatic effector as they can regulate the stability of mRNAs and therefore influence translation success (Kosik, 2006; Guo et al., 2010). Chronic hyperactivity in hippocampal culture in the presence of a transcriptional blocker revealed several mRNAs involved in synapse and morphological processes that are regulated post-transcriptionally (Cohen et al., 2011). A sequence analysis of these mRNAs revealed that many of them have miRNA binding sites, of which the brain-enriched miR-485 site was particularly prevalent. Importantly, this experiment produced direct evidence of miR-485 regulation of morphological homeostatic plasticity, as levels of this miRNA increase after chronic activity, and its overexpression reduces overall number of spines and increases the proportion of this total that are immature. Furthermore, miR-485 overexpression also caused reduced clustering of GLuR2-AMPARs at the synapse and inhibition of endogenous miR-485 induced an increase, suggesting this miRNA also plays a role in receptor trafficking (Cohen et al., 2011). Although distinct timepoints were not tested in this experiment, homeostatic regulation of key target mRNAs through miRNAs may further explain differences in the type of morphological plasticity over time, with early adaptations potentially utilizing post-transcriptional modulation more than later ones where protein synthesis plays a larger role; of

course it is also possible that just like the different protein expression profiles discussed above, distinct miRNAs regulate different mRNAs across multiple timepoints.

By now it is clear that there are some inconsistencies in homeostatic adaptations in number of spines. In particular, opposing activity perturbations are both capable of causing a reduction in number of spines (Moulin, Rayêe and Schiöth, 2022), which doesn't logically follow if spine loss or gain is a simple way of reducing or increasing activity respectively. A recent study has attempted to establish the rules homeostatic synaptic scaling uses and explain this observed diversity in morphological plasticity (Lu et al., 2025). They discovered differences in physiological adaptations in response to distinct NBQX concentrations. Furthermore, low concentrations caused an increase in the number of spines, while high concentrations reduced spine number, demonstrating there is a non-monotonic relationship between activity and morphological adaptations. These differences in activity-dependent changes in synapse number could be explained by a biphasic plasticity rule where partial vs complete loss of activity utilise distinct homeostatic structural mechanisms; neural network simulations support this conclusion (Lu et al., 2025).

Findings of homeostatic changes in number of synapses is mostly confined to mammalian systems, as has been noted in an extensive review of relevant literature (Moulin, Rayêe and Schiöth, 2022); in fact the majority of experiments focus on excitatory neurons in the rodent hippocampus and cortex (Moulin, Rayêe and Schiöth, 2022). By comparison, findings of homeostatic changes in synapse number in **adult** *Drosophila* are much rarer. One relevant example is work by (Kremer et al., 2010) who investigated the structural changes in PN-KC connections, termed microglomeruli (Yasuyama, Meinertzhagen and Schürmann, 2002; Leiss et al., 2009), in response to loss of activity in a small number of PNs. This perturbation caused an increase in number and volume of microglomeruli associated silent PNs which was due to an increase in the size of the postsynaptic domain and in the density of the presynaptic active zones. These effects were inverted in PNs expressing synaptic fusion blocker TeTx, suggesting distinct mechanisms may regulate structural homeostatic adaptations depending on the nature of the perturbation (Kremer et al., 2010). Important for our central question, the **number** of microglomeruli was also affected in both these manipulations, demonstrating that homeostatic activity-dependent alteration in the number of synapses is possible in the MB. However, silencing of this subset of PNs used a driver that is expressed 18h after puparium formation (Jefferis et al., 2004), meaning they were silent during a developmental period. Silencing during this key critical period (CP) may affect refinement of microglomeruli (Ganeshina, Vorobyev and Menzel, 2006), which could suggest

alterations observed in this experiment represent a perturbation of this refinement process and not a form of adult homeostatic plasticity. In fact, we will now see that activity-dependent morphological adaptations are quite common in the neurons of developing mammals and *Drosophila*, suggesting these circuits are more flexible when they are being initially established. The question is do any of these mechanisms translate to adult plasticity?

1.7.4 Critical periods in activity-dependent plasticity

The term 'developmental homeostatic plasticity' is complicated to unpack, as evidence of activity perturbations of neurons during development is often conflicting and doesn't always appear to be homeostatic; that is the changes observed don't always seem to restore activity to a 'set level' and can often lead to dysfunction of a circuit in later life. Furthermore, only during certain periods of development are neurons capable of activity-dependent plasticity. These timepoints are referred to as critical periods (CPs), as originally described by the Hubel lab (Wiesel and Hubel, 1963; Hubel and Wiesel, 1970; Hubel, Wiesel and LeVay, 1977), and during these CPs different populations of neurons are acutely sensitive to experience. The original example of this is in ocular dominance columns of the visual cortex, which respond to monocular deprivation by reducing the size of these columns in the deprived eye and enlarge the columns of the non-deprived eye, but this adaptation is much reduced when it occurs outside of the CP (Antonini and Stryker, 1996; Antonini, Fagiolini and Stryker, 1999; Fagiolini and Hensch, 2000; Hensch, 2005; Morishita and Hensch, 2008; Hensch and Quinlan, 2018). In this section we will discuss why activity-dependent plasticity is limited to critical periods, whether these changes are homeostatic or disturb the establishment of set points, how these differ from the mostly adult homeostatic plasticity we have discussed so far, and the evidence of critical periods in the Drosophila MB and its relevance to this work.

To identify the purpose of critical periods, it is important to understand what is achieved during the normal functioning of these developmental timepoints before describing what happens when they are perturbed. We have already described the ocular dominance plasticity that occurs in response to monocular deprivation (MD), and the period this occurs coincides with maturation of visual acuity in normal circuits (Movshon and Van Sluyters, 1981; Fagiolini et al., 1994; Cancedda et al., 2004); unsurprisingly MD decreases visual acuity suggesting a disruption of visual acuity development (Boothe, Kiorpes and Carlson, 1985; Prusky and Douglas, 2003). In normal development, cortical ocular dominance does

not differ between hemispheres without monocular deprivation (Sato and Stryker, 2008) which raises the question of what purpose plasticity in ocular dominance actually serves in an unperturbed system? In other words, why are these areas susceptible to experience-informed plasticity at this stage? Research by (Wang, Sarnaik and Cang, 2010) hypothesized the purpose of this plasticity is to match the orientation responsiveness of neurons to stimuli across hemispheres. This idea was supported by work demonstrating the preferred stimulus orientations of cortical neurons is similar across the two eyes (Hubel and Wiesel, 1962; Nelson, Kato and Bishop, 1977; Ferster, 1981; Bridge and Cumming, 2001), suggesting it is necessary to integrate these binocular stimulus-specificities at some point during development and experience dependent plasticity during the CP may be used to achieve this. Investigation before and after the onset of the ocular dominance CP revealed that there is a large disparity in orientation responsiveness between the two eyes pre CP, whereas post CP and into adulthood this orientation specificity of individual neurons in the binocular zone is very similar for both eyes (Wang, Sarnaik and Cang, 2010). Importantly, both dark rearing and MD of these animals during the CP blocked binocular matching of orientation preference and, in conjunction with previous results, they demonstrated this matching plasticity requires NMDAR activation, providing a potential mediator for visual experience-driven matching between the two eyes (Sato and Stryker, 2008; Wang, Sarnaik and Cang, 2010). Finally, MD of animals for the full CP and restoration of visual input after, still left orientation preference between eyes significantly mismatched, demonstrating this CP is necessary for establishment of matching binocular orientation selectivity. MD in adults did not result in binocular mismatch, but dark rearing animals from birth to the typical end of the CP revealed that binocular responsiveness was completely mismatched, but returned to expected adult levels after 6-7 days of vision; in line with previous results this demonstrates the CP can be delayed by dark rearing animals (Cynader and Mitchell, 1980; Fagiolini et al., 2003; Wang, Sarnaik and Cang, 2010). Overall, this highlights one purpose of CPs is to utilise experience to shape activity and specificity of neurons before onset of adulthood.

It is still unclear from the normal function of this CP, whether the associated adaptations are homeostatic. mEPSCs in layer four visual cortex excitatory neurons decrease in amplitude during the CP, an effect prevented by dark rearing (Desai et al., 2002). Furthermore, MD in the initial period eye opening usually occurs, representing the start of the CP and effectively blocking a massive increase in input, also results in an increase in mEPSC amplitude in the monocular cortex. It is unclear whether this change is homeostatic, as although activity increases after a prolonged blockade of input, control animals usually demonstrate a

decrease in mEPSC amplitude during this period, suggesting this manipulation may block typical developmental changes. Interestingly layer 2/3 visual cortex neurons demonstrate a similar adaptation but at a later timepoint demonstrating the existence of separate CPs for these areas (Daw et al., 1992; Stern, Maravall and Svoboda, 2001; Desai et al., 2002). The changes to layer 4 neuron activity in response to MD during this CP appear to be mediated by an increase in the strength of excitatory connections and a decrease in inhibitory connection strength in these neurons (Maffei, Nelson and Turrigiano, 2004). Theoretically this would increase the sensitivity of these neurons to any input they do receive but again these changes are at odds with those normally observed during development. The visual deprivation induced plasticity in layer 2/3 neurons persists into adulthood, but theoretically these adaptations should be homeostatic later once these neurons set activity is established, e.g. in development the activity ‘target’ is moving while in adulthood it should be stable. Dark rearing animals long past the end of the ocular dominance plasticity CP (P35 and P95) causes a reversible increase in mEPSC amplitude similar to that observed during CP disruption, and both rely on synaptic scaling (Goel and Lee, 2007). However, the nature of this scaling appears to be different between development and adulthood (Desai et al., 2002; Goel and Lee, 2007). During development the relative strengths of synapses are maintained during scaling, while in adulthood this is not the case, suggesting Hebbian plasticity at these synapses could be disrupted. Furthermore, this implies the homeostatic mechanisms utilised at these different time points are different, highlighting a key difference in homeostatic plasticity between adulthood and development.

This still leaves doubt on whether visual deprivation induced changes during CPs represents functional homeostatic plasticity. MD during CPs causes shifts in ocular dominance cortical excitability, first decreasing this areas response to the deprived eye but later increasing responsiveness to the open eye (Frenkel and Bear, 2004). This demonstrates the biphasic nature of this adaptation, as initial reduced responsiveness appears to be caused by an LTD-like mechanism (Yoon et al., 2009) and plasticity with inhibitory neurons (Maffei et al., 2006; Maffei, Lambo and Turrigiano, 2010), while the source of later potentiation in response was initially unclear. By tracking the changes in excitatory postsynaptic strength of layer 2/3 visual cortex neurons during the CP, (Lambo and Turrigiano, 2013) discovered changes in postsynaptic strength were first depressed and later potentiated, and this potentiation was present in both monocular and binocular regions. Importantly, later postsynaptic changes increase responsiveness to both the open and deprived eye in layer 2/3 neurons, suggesting this may represent a more typical homeostatic restoration of responsiveness. Interestingly,

both biphasic changes in postsynaptic strength seem to require GluA2 C-tail interaction, a intracellular binding site for various proteins that helps regulate the localization and function of AMPARs at synapses, and this subunit has been previously implicated in both synaptic scaling (Gainey et al., 2009) and some forms of LTD (Yoon et al., 2009). Finally, the potentiation phase of this adaptation also involves increased intrinsic excitability of these neurons, suggesting both intrinsic and synaptic homeostatic mechanisms are utilized here (Lambo and Turrigiano, 2013). Overall, this evidence supports the idea that a range of plasticity mechanisms are at play during this visual CP, including homeostatic plasticity, and these changes appear similar to those observed in adulthood. However, there is still some uncertainty in the goal of homeostatic plasticity during CPs, as they adaptations don't seem to restore activity to those observed during normal development. It is possible that the extreme nature of the manipulation, losing vision from one or both eyes, leaves the system in an impossible situation where it attempts to adapt in a way that will never restore activity/responsiveness to control levels.

These findings are not limited to sensory systems, where it is logical that typical sensory input is used to tune responsiveness of neurons, so they are well prepared to respond to these inputs in adulthood. There is a CP for Drosophila motor neuron development 11-19h after egg laying (AEL), which appears to be integral for the transition from spontaneous contractions of body wall muscles to coordinated and mature larval peristalsis which coincides with onset of APs in these neurons (Baines and Bate, 1998; Crisp et al., 2008; Crisp, Evers and Bate, 2011). High frequency optogenetic stimulation of motor neurons during this CP is sufficient to increase seizure recovery time after electric shocks and reduce seizure threshold several days after stimulation; the same findings were observed when using optogenetic inhibitory tools (Giachello and Baines, 2015). Both of these features are similarly observed in the Drosophila seizure bang-senseless (bss) mutant, where it was also discovered that changes in temperature during this CP influence motor development suggesting these neurons are sensitive to environmental changes (Ganetzky and Wu, 1982; Kuebler and Tanouye, 2000; Parker et al., 2011). Notably, interventions that counter perturbations in activity during this CP restore normal adult phenotype (Giachello and Baines, 2015). Collectively, this demonstrates that any disruption of normal activity during this CP is sufficient to increase susceptibility and recovery to seizures. However, this doesn't reveal what the normal function of this CP is and why during this period neurons are sensitive to experience. Alterations in activity in dorsal motoneurons through optogenetic activation during CPs, or by blocking synaptic activity, causes changes to intrinsic firing properties of

these neurons (spontaneous rhythmic currents) that persist into adulthood and correlate with increased seizure susceptibility (Baines et al., 2001; Rohrbough and Broadie, 2002; Giachello and Baines, 2015). As discussed earlier, epilepsy and seizures are theorised to result from dysfunctional network homeostatic plasticity (Lignani, Baldelli and Marra, 2020), so these observed changes may represent activity that is no longer being regulated within homeostatic limits. This suggests that the role of this particular CP is to establish homeostatic set points for these neurons, where typical excitatory input helps to shape these limits in a way that is compatible with your environment (e.g. temperature), but extreme manipulations result in dysfunction (Giachello and Baines, 2015, 2017).

Importantly for this work, there is also evidence of CPs in the Drosophila MB, which may give us insight into potential overlapping homeostatic mechanisms. First, we have already described the work from (Kremer et al., 2010) where silencing a select number of PNs from 18h after puparium formation to adulthood results in a morphological adaptation of the microglomeruli structure and size in adulthood. This period includes one of three defined CPs in Drosophila, the adult post-eclosion CP, where experience has been shown to influence the development of the olfactory system for up to 2-5 days post eclosion (Dombrovski and Condron, 2021; Devaud, Acebes and Ferrús, 2001; Devaud, Keane and Ferrús, 2003; Devaud et al., 2003). Prolonged exposure to odours during this CP causes a stimulus-dependent decrease in volume of different glomeruli that is odour-specific and accompanied by a change in behavioural response (Devaud, Acebes and Ferrús, 2001; Devaud, Keane and Ferrús, 2003; Devaud et al., 2003); importantly these changes are not possible outside of the first week of *Drosophila* adult life. Distinct glomeruli in the antennal lobe have different odour specificities as a result of their cognate ORNs, and these appear to explain the odour-specific nature of adaptations during this CP (Hallem, Ho and Carlson, 2004; Couto, Alenius and Dickson, 2005; Hallem and Carlson, 2006). For example, the CO_2-specific glomerulus in the antennal lobe demonstrates a reversible increase in volume in response to prolonged CO_2 exposure during this CP, while other glomeruli are unaffected (Sachse et al., 2007). This shows these changes are not a result of CO_2 exposure but represent an activity-dependent mechanism. What changes are responsible for alterations in glomerular volume? Prolonged ethyl butyrate (EB) exposure during this CP causes a decrease in innervation from EB-ORNs to their cognate glomeruli (decreased ORN synapse number) and an associated decrease in glomerulus volume (Sachse et al., 2007; Das et al., 2011; Golovin et al., 2019); outside of this CP EB exposure causes no change in glomerular volume. Furthermore, silencing EB and CO_2 responsive ORNs extends the structural plasticity in their cognate glomeruli beyond the

usual closure of the CP (Chodankar et al., 2020). Importantly, this effect is specific to their associated glomeruli suggesting regulation of CP is governed partially by ORN activity and occurs at a local level and not across the whole antennal lobe (Chodankar et al., 2020). Overall, this demonstrates the existence of a CP in the Drosophila olfactory system where prolonged odour exposure induces long lasting habituation of local circuits through diverse changes to ORN, LN and PN morphology and responses. It is important to note that this is not evidence of developmental homeostatic plasticity and actually involves learning-associated changes to circuits.

Whether KCs are also capable of these changes during development is unclear. (Kremer et al., 2010) demonstrated structural changes in PN-KC synapses that appear to involve an increase in size of the postsynaptic domain, but the exact nature of this morphological plasticity is still unclear. Ultimately, the existence of a CP in the first 2-4 days of adult life in Drosophila highlights the need to be cautious of activity-dependent homeostatic changes that may occur during this window and suggests we should test outside of this if we want to confirm the existence of an adult intrinsic homeostatic mechanism in KCs.

1.7.5 Single cell vs Network homeostatic plasticity

Most of the evidence of homeostatic plasticity we have covered so far has focused on activity perturbations of networks using pharmacological or broad genetic interventions that effect whole populations. However, due to the inherent difficulty of targeting single neurons, very few experiments have investigated homeostatic plasticity at this level. The model in (Abdelrahman, Vasilaki and Lin, 2021) suggests that if KCs compensate on the individual level, this is optimal for maintaining lifetime sparseness. Is there any precedent for neurons using cell-intrinsic mechanisms in homeostatic plasticity? This section will focus on evidence of single cell homeostatic plasticity and explore the differences between compensations here and at the network level.

Recording and manipulation of single cells is difficult, especially in mammalian systems, but there are experiments that achieve one or both of these. (Burrone, O'Byrne and Murthy, 2002) first demonstrated single cell homeostatic changes by sparsely transfecting a small number of hippocampal neurons in slice culture with the inward-rectifier potassium channel Kir2.1. Single neurons expressing Kir2.1 are much less excitable and require larger currents to reach firing threshold, but crucially this manipulation still allows the rest of the network to retain 'normal' activity. Neurons repressed before synapse formation have fewer inputs, but

this can be prevented by global TTX application to silence all neurons; this suggests neurons preferentially form connections with more active neurons during development. In contrast, expressing Kir2.1 in single neurons when synapses are fully formed causes an increase in mEPSC frequency and homeostatic increase in vesicle pools terminating on these neurons. Importantly, this returns firing rates to control levels, demonstrating the existence of a cell-intrinsic homeostatic mechanism. Fine pharmacological manipulation is also possible and was utilised by (Ibata, Sun and Turrigiano, 2008) where TTX was locally applied to pre- or postsynaptic regions of single cortical neurons. When used to block postsynaptic firing of a neuron, this caused increased AMPA accumulation at synapses, similar to what is seen when TTX is applied globally. This synaptic scaling is mediated through decreased calcium influx and subsequent reduced activation of CaMKIV, which is localized to the soma and is a transcriptional regulator (Soderling, 1999; Ibata, Sun and Turrigiano, 2008); decreased CaMKIV activation induces a decrease in gene transcription. Collectively, this suggests neurons detect changes in their activity through reduced calcium influx and then through calcium-dependent pathways increase AMPAR transcription to scale up the strength of synapses. Importantly, only changes to the neurons postsynaptic firing were sufficient to induce these changes, while blocking a set of presynaptic inputs only produced slight increase in AMPAR accumulation which appears to be mediated by decreased firing as a result of fewer graded potentials. Overall, this evidence demonstrates cell-autonomous homeostatic mechanisms that respond to deviations in their own activity sensed via changes in intracellular Ca2+, a common homeostatic sensor; the idea that Ca2+ can act as an activity sensor and comparator is well supported by modelling we have already discussed (O'Leary et al., 2014).

Cell-autonomous changes can also cause compensatory changes in neuron morphology. As mentioned earlier, sparsely labelling CA1 neurons in culture with Channelrhodopsin to increase cell-autonomous excitation causes a homeostatic decrease in mEPSC amplitude and frequency, which appears to be partially mediated by a decrease in the number of spines; similar findings were observed by (Moulin et al., 2019) and these cell-autonomous changes impacted Hebbian plasticity thresholds. High frequency optogenetic activation for only 10 minutes causes a compensatory increase in number of inhibitory synapses and a decrease in excitatory synapses 24 hours later (Mendez et al., 2018). Collectively, this demonstrates that synaptic scaling mechanisms capable of removing and adding spines can be cell-intrinsic and respond to changes in the cells firing rate. E/I ratio may also be regulated at the individual cell level. Activating a small number of layer 2/3 visual cortex neurons with

Channelrhodopsin revealed that although the amplitudes of EPSCs and IPSCs varied between neurons, the ratio of EPSC to IPSC amplitude was highly correlated (Xue, Atallah and Scanziani, 2014). Neurons with artificially reduced (increased) activity receive less (more) inhibition from Parvalbumin interneurons, an effect specific to the manipulated neuron and not neighbouring neurons, demonstrating cell-autonomous activity-dependent E/I balancing (Xue, Atallah and Scanziani, 2014). Furthermore, there is some disparity in forms of single-cell homeostatic plasticity observed even within a system, making it more difficult to establish consistent cell-autonomous homeostatic mechanisms. A lot of this can likely be explained by differences in neuron type and area which are more likely to have diverse homeostatic mechanisms, as differing set points within these systems may be important for their function. The type of manipulation also has an impact, both amplitude of activity increase/decrease and the timescale of these perturbations. For example, (Lu et al., 2025) demonstrated that mildly blocking excitation increased spine density while totally blocking excitation decreased spine density. Such biphasic plasticity could explain variations in results between neurons activated for different timeframes. Ultimately, single neurons are more flexible and complex than simple manipulations would necessarily imply and may contribute differently to adaptations on the network level over time.

It is unclear whether the cell-autonomous changes we discussed so far are sufficient to achieve homeostatic plasticity at the network level. It is possible that network homeostasis regulates factors that only exist at the circuit level and therefore may not have set values in individual neurons. Two potential factors are population firing rate and synchrony of this firing across the network, which may be necessary to maintain in order for normal network function to continue. In hippocampal cultures, after 2 days of chronic activity suppression, the population firing rate returns to the previous baseline but ~90% of individual neurons have different firing rates compared to their pre-perturbation baseline rate (Slomowitz et al., 2015). This shows that firing rates are homeostatically regulated at the network level but not on an individual basis, suggesting this form of homeostatic plasticity may not be cell-autonomous. Furthermore, increased inhibition causes an initial increase in network firing synchrony, followed by a homeostatic return to baseline levels that is mirrored at the single cell level. However, single neurons demonstrate large variation in this compensation with some significantly changing the fraction of their spikes in bursts, while others were unchanged (Slomowitz et al., 2015). This may suggest there is not a set point for this metric in individual neurons, and the target is network-orientated, e.g. the goal is network synchrony not restoration of single cell firing rates. The findings of this paper suggest hippocampal neurons

have a network-orientated set target, as they compensate to restore the population average firing rate and not the single cell rate. This is supported by evidence that the population of neurons encoding representations changes significantly over time, suggesting large changes in involvement of single neurons is tolerable (Liberti et al., 2016). Overall, these findings may suggest that achieving network homeostatic plasticity requires regulation and communication at the circuit level and cannot just rely on individual neurons compensating for changes in their own set points.

Some evidence suggests that cell-autonomous changes may be sufficient to achieve network homeostasis. MD in freely behaving juvenile rats at p23-p26 caused a reduction in V1 average firing rate in the deprived hemisphere that slowly returns to baseline over several days (Hengen et al., 2013, 2016). Interestingly, in this system the firing rate of individual neurons also returned to their baseline level, despite large variation in these rates across the population, differing by several orders of magnitude (Hengen et al., 2016). This suggests that network activity can be maintained purely through cell-autonomous homeostasis of firing rate, but the individual firing rate set points between neurons have large variation.

Another network feature that may be maintained by homeostatic plasticity is criticality. Critical networks are theorised to operate at the edge between highly coordinated and weakly coordinated population activity, a state which optimises its ability to process and transmit information (Shew and Plenz, 2013; Cocchi et al., 2017). There is evidence that cortical networks are critical (Beggs and Plenz, 2003; Gireesh and Plenz, 2008), but (Ma et al., 2019) discovered a criticality set point within the intact visual cortex which is a target of homeostatic plasticity. The visual cortex operates close to criticality under normal conditions and perturbing activity using MD revealed that deviation and recovery of this criticality is much quicker than firing rate homeostasis of excitatory neurons (Hengen et al., 2013, 2016; Ma et al., 2019). This demonstrates criticality is homeostatically regulated but suggests that excitatory neuron firing rate rebound is not responsible for this restoration (Ma et al., 2019). However, the timescale of criticality homeostasis does more closely match firing rate drop and rebound in inhibitory neurons (Hengen et al., 2013; Keck et al., 2013), which could suggest inhibitory neuron cell-autonomous firing rate homeostasis is responsible for maintaining network criticality. Modelling suggests that precise excitatory-inhibitory connectivity is sufficient to produce a critical network. Importantly, these models also suggested the delay in excitatory neuron firing rate homeostasis is due to initial disinhibition as inhibitory neurons concurrently lower their own activity, suggesting homeostatic mechanisms at the individual neuron level may act at the same timeframe but initial

disinhibition counters rapid return of baseline firing rate in excitatory neurons (Ma et al., 2019). Later analysis and modelling suggests that firing rate homeostasis in excitatory and inhibitory neurons relies on intrinsic homeostatic plasticity, while synaptic scaling is necessary for recovery of network synchrony (Wu et al., 2020). This suggests that distinct homeostatic mechanisms contribute to homeostasis of different network features. Importantly, although it doesn't directly demonstrate cell-autonomous changes are sufficient to achieve full network homeostatic plasticity, it does demonstrate that certain features can be maintained by intrinsic plasticity across a population as suggested by MB modelling work (Abdelrahman, Vasilaki and Lin, 2021).

Network homeostasis appears to differ depending on the function of the network and the associated set points of the features required for its function. Modelling suggests that in the Drosophila MB inter-KC variability must remain low for effective odour discrimination; this is to avoid a small percentage of KCs responding to the majority of odours, while the majority of the population remains silent resulting in little distinction in the KCs responding to separate odours (Abdelrahman, Vasilaki and Lin, 2021). It is also already well known that the MB utilises sparse coding and likely has to maintain a balance between too many or too few KCs responding to any given odour, to avoid too much generalization or too little (Lin et al., 2014; Parnas, Manoim and Lin, 2024). The function of the MB is to effectively discriminate between odour representations and ensure the valence of those representations are reliably encoded. Our prior modelling work suggests that one of these network features, lifetime sparseness, is a target for homeostatic plasticity, but this may be achieved by compensation of cell-intrinsic parameters to ensure the activity across the KC population is roughly equal (Abdelrahman, Vasilaki and Lin, 2021). Previous experimental evidence from our lab has demonstrated that KCs respond to prolonged inhibition from the APL partially through increasing their excitation and partially through decreased APL activation (Apostolopoulou and Lin, 2020). Furthermore, unpublished data suggests that global hyperactivity of KCs is compensated for by reduced activation of KCs and this may be partially mediated by reduced voltage-gated sodium channel expression (G. Bergmann, unpublished results). However, both these experiments utilised whole population manipulation and recordings, making it difficult to determine whether compensations in activity could result purely from cell-autonomous changes or whether network activation may utilise unique homeostatic mechanisms. In fact, manipulation and recording of single neurons in vivo to investigate homeostatic mechanisms is rare. Many of the experiments we have discussed in this section activate and record from single neurons in culture or record from single cells in vivo but utilise more global manipulations. In this

sense, the Drosophila model system provides us with a powerful tool to target and record from single cells and compare any homeostatic adaptations to those we have previously observed at the network level.

1.8 Manipulation and recording of single KCs

In this work I use several different genetic techniques to achieve labelling of single KCs to hyperactivate them, visualise their morphology and later record their activity. Previous work from our lab indicated there are subtype differences in KC homeostatic adaptations (Apostolopoulou and Lin, 2020; G. Bergmann, unpublished results), so I used MARCM to label single cells within each subtype (γ, α/β and α'/β')(Lee and Luo, 2001; Wu and Luo, 2006). This technique relies on a genotype containing both ubiquitously-expressed GAL80 and a GAL4 driver for the cell type of interest; the Gal80 blocks Gal4 action and therefore prevents population wide expression of any transgenes under the control of UAS. When a heatshock-sensitive flippase (FLP) is activated, homologous recombination occurs between FRT sites adjacent to GAL80 on sister chromosomes. This technique only produces labelling when cells are dividing as it allows two copies of GAL80 to be segregated to one daughter cell while the other now only contains GAL4 and is therefore free to drive expression of UAS-associated genes (Figure 1.6). Importantly, the heatshock is performed during development when cells are dividing so you must know when your cell type of interest develops. Fortunately, the developmental timings of the different KC subtypes are well characterized (Figure 1.7)(Lee, Lee and Luo, 1999) which allowed us to investigate differences in homeostatic adaptations between γ, α/β and α'/β' KCs.

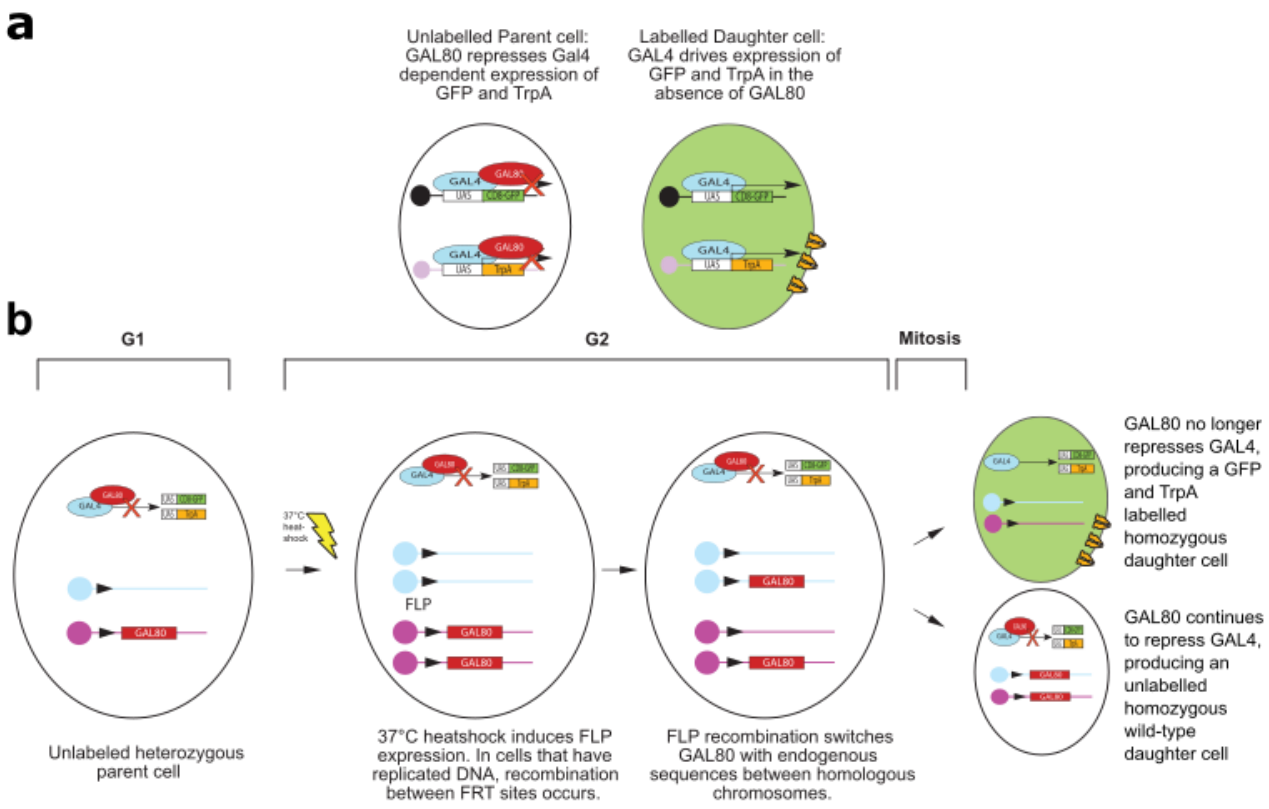

Figure 1.6: Using MARCM to sparsely label single cells. a) GAL4-UAS system with GAL80. GAL4 drives expression of transgenes under the control of a UAS sequence; in this work TrpA and GFP are expressed to visualise cells and artificially increase their activity. GAL80 represses GAL4 action and is ubiquitously expressed so parent cell is unlabelled. MARCM produces a daughter cell with no copies of GAL80, allowing expression of transgenes. **b)** MARCM mechanism. All cells start unlabelled due to ubiquitous expression of GAL80. When flies are raised to 37°C a heat-sensitive FLP is activated and induces recombination between homologous chromosomes at FRT sites adjacent to GAL80 sequence. Only cells that are currently dividing segregate two copies of GAL80 into one daughter cell and no copies into the other cell. This technique achieves sparse labelling of subtypes expressing GAL4 and produces one daughter cell labelled with your transgene, or more if heatshock time is increased. Adapted from (Wu and Luo, 2006).

To investigate single cell morphological adaptations, I used MARCM to label single KCs with GFP to visualize any changes in dendrite number or structure and to allow me to trace these neurons, and dTrpA1 to hyperactivate them. TrpA is a heat-sensitive non-specific cation channel which, when artificially expressed in neurons, increases their activity in a temperature-dependent manner (Hamada et al., 2008; Apostolopoulou and Lin, 2020). Here I incubate adult flies at 31°C, for varying timeframes, to chronically activate single cells and compare morphological adaptations at different timepoints and across subtypes. To confirm whether these adaptations are homeostatic I utilised a similar line expressing TrpA with the

latest GCaMP (GCaMP8m)(Zhang et al., 2023). As described earlier (Section 1.2), GCaMP fluoresces when bound to calcium which allows it to respond to changes in intracellular Ca2+ levels at timescales relevant for neural activity and generally correlates with changes in activity measured electrophysiologically (Nakai, Ohkura and Imoto, 2001; Jayaraman and Laurent, 2007; Chen et al., 2013). Here I use it in combination with Two-photon imaging (Denk, Strickler and Webb, 1990) to measure changes in calcium response after prolonged hyperactivation, and thus determine the physiological changes associated with morphological adaptations. Specifically, I use antennal nerve stimulation similarly to previous work (Groschner et al., 2018), to activate the whole MB and measure evoked calcium responses at different stimulation strengths and compare across timepoints similar to our morphological data.

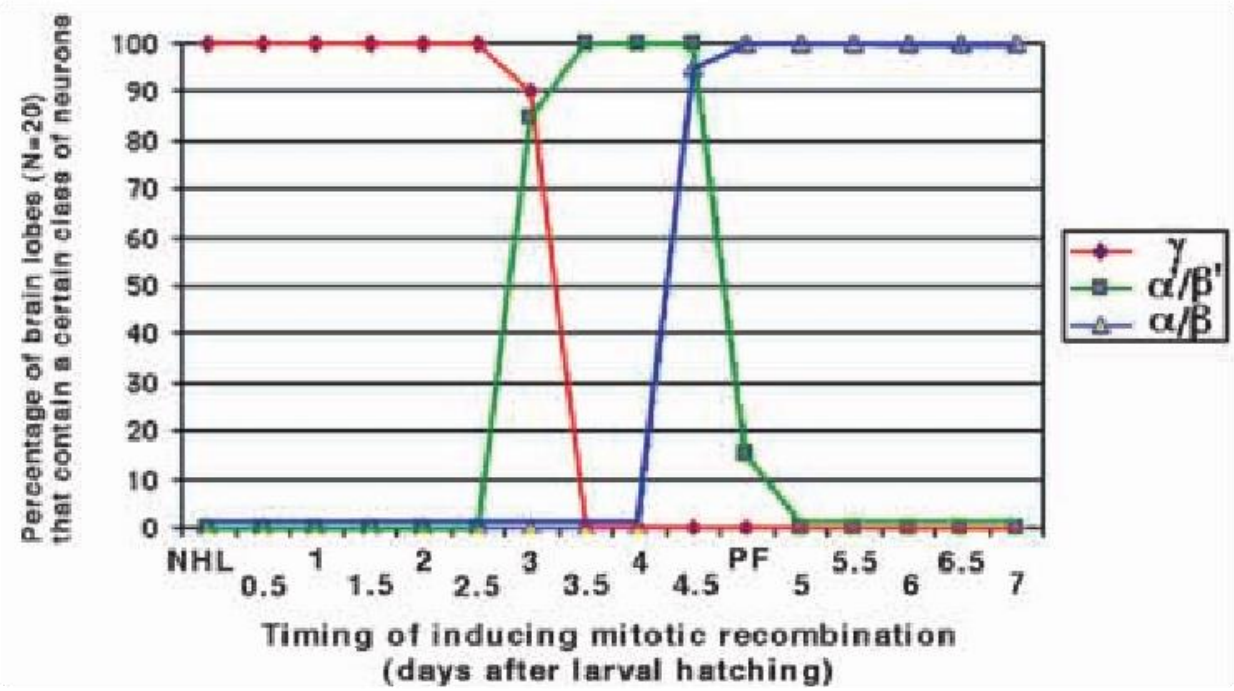

Figure 1.7: Developmental timings of Kenyon cell (KC) subtypes. Newly hatched larvae (NHL) were heatshocked at various timepoints to induce mitotic recombination in cells of the developing MB. The percentage of brain lobes containing different classes of neurons in the adult was measured. Graph shows three developmental windows for the different KC subtypes with some overlap. γ KCs (red) are the only subtype dividing for the first ~2 days post larval hatching and their development only finishes at ~3.5 days. At ~2.5 days post hatching α'/β' KCs (green) begin to develop, showing the first of two transition points where mitotic recombination produces labelling of γ and α'/β' neurons. The second transition point begins at ~4 days post hatching when α/β KCs (blue) begin to develop and from ~5 days onwards these are the only subtype that continues to develop. Adapted from (Lee, Lee and Luo, 1999).

Overall, these techniques give me the unique ability to identify homeostatic adaptations at the single cell level and confirm whether some of the compensations theorised in our previous model (Abdelrahman, Vasilaki and Lin, 2021) occur.

1.9 Focus of this thesis

It is essential that KCs have a roughly equal level of activity across the population to ensure lifetime sparseness of these neurons is fairly even. Noise is inevitable in biological systems and natural variation/drift in parameters over time could allow a minority of KCs to always be active while the remaining cells in the population are silent or respond to very few odours. Without homeostatic adaptations to counter this, these changes would result in the inability to discriminate between odours due to too much overlap in associated representations of the neurons that encode them. However, although we know the MB is capable of global homeostatic plasticity in response to network perturbations (Apostolopoulou and Lin, 2020; G. Bergmann, unpublished results), there is currently no direct evidence of single cell homeostatic adaptations in KCs. Our models suggest that homeostatic adaptations at the single cell level may be necessary to ensure optimal MB function by preventing unequal KC population activity. Additionally, it was unclear from our prior modelling work whether such adaptations are activity-dependent or activity-independent (Abdelrahman, Vasilaki and Lin, 2021). This work addresses these questions, by chronically activating single KCs using TrpA and identifying any associated homeostatic adaptations.

The question of whether single KCs have an adult intrinsic homeostatic mechanism can be divided into further sub-questions. Firstly, do single KCs adapt their morphology in response to chronic activation? I have already discussed the ample evidence that homeostatic mechanisms often involve changes in morphology. This can include altering the AIS length or distance from dendrites to adjust the chance graded potentials will reach this area and initiate an AP (Grubb and Burrone, 2010; Evans et al., 2013; Chand et al., 2015). It is also possible that KCs could adjust the size or number of their inputs as seen in homeostatic adaptations of mammalian spines. By scaling synapse strength or altering number of inputs, neurons can influence the amplitude and frequency of miniature currents which similarly influence the neurons probability of firing (Murthy et al., 2001; Keck et al., 2013; Hobbiss, Ramiro-Cortés

and Israely, 2018). There are also many established differences in the function and mechanisms of different KC subtypes, including in network homeostatic plasticity in the MB (Apostolopoulou and Lin, 2020) suggesting intrinsic mechanisms between subtypes may differ. To answer all these questions, I used high resolution confocal microscopy to capture single KCs labelled with GFP in detail, allowing me to trace them and analyse their morphology. Furthermore, my use of MARCM allowed me to target specific subtypes so I could compare changes in their morphology. Finally, by incubating adult flies at 31°C for various lengths of time I could identify any temporal changes in homeostatic morphological adaptations.

Secondly, do single KCs demonstrate homeostatic changes in their activity after prolonged activation? Although identifying morphological changes induced by hyperactivity is useful, we cannot know whether they are homeostatic without identifying compensatory changes in the neuron's activity. I expected that chronic activity caused by prolonged TrpA activation would cause an initial increase in the KCs activity, followed by a compensatory decrease to restore activity to a set level. To answer this question, I chronically activated single KCs expressing GCaMP8m to measure changes in evoked calcium influx in response to whole MB activation. This allowed me to identify changes in the amplitude and shape of calcium response and determine whether associated morphological changes are homeostatic.

2. Materials and Methods

2.1 Materials

2.1.1 Fly rearing

Most fly lines were stored at 25°C. Some stocks were kept at 18°C for long-term maintenance but when required were moved back to 25°C. Offspring for the single cell morphology experiment in Chapter 3 were initially raised at 25°C and then moved to 22°C after heatshock to prevent TrpA activation. Offspring for the single cell physiology experiment were initially treated the same as flies in Chapter 3, but after issues with TrpA were identified (see 4.2.6) were instead incubated at 18°C after heatshock. All flies experienced a 12 hr light /12 hr dark cycle and were kept in vials containing fly food following the recipe seen in Table 2.1 excluding Starved and Sugar-only flies. Starved flies were raised as normal but incubated at 31°C on 1% agar with filter paper soaked in 125µl dH_2O in line with previous work (Tully et al., 1994; Yu, Akalal and Davis, 2006), while Sugar-only flies were given filter paper soaked in 125µl 5% glucose.

Table 2.1. Fly food recipe given to all flies excluding Starved and Sugar-only flies.

Ingredient	Measurement
H_2O	1L
10% Nipagin in Absolute Ethanol	25ml
Propionic Acid	4ml
Agar	8g
Dried Yeast	18g
Malt Extract	80g
Medium Cornmeal	80g
Molasses	40g
Soya Flour	10g

2.1.2 Fly lines used in Chapter 3-Morphological experiments

All fly lines used to investigate activity-dependent morphological adaptations in Chapter 3 can be seen in Table 2.2.

Table 2.2 Fly lines used in Chapter 3

Fly line	Purpose	Availability/ Citation
hsFLP,UASCD8GFP;; FRT82,tubP-GAL80/TM3,Sb; OK107	MARCM parent line labelling single KCs	(Lee and Luo, 2001) Bloomington: 44408
w;; FRT82	Control parent line labelling single KCs	(Xu and Rubin, 1993) Bloomington: 2050
UAS-dTrpA1/CyO; FRT82/TM3,Ser	Experimental parent line labelling single KCs and hyperactivating them with TrpA	Created by the Lin lab
UAS-Dα7mCherry/CyO; FRT82/TM3,Ser	Original control parent line labelling Dα7-nicotinic receptors with mCherry	FRT82 line created by the Lin lab. Original UAS-Dα7mCherry line: (Fayyazuddin et al., 2006).
UAS-dTrpA1,UAS-Dα7mCherry/CyO; FRT82/TM3,Ser	Original experimental parent line labelling Dα7-nicotinic receptors with	Created by the Lin lab

	mCherry and labelling KCs with TrpA	
UAS-dTrpA1	Heat sensitive non-specific cation channel	(Rosenzweig et al., 2005) Bloomington: 26263
OK107-GAL4	GAL4 driver that labels the MB	(Connolly et al., 1996) Bloomington: 854
UAS-Dα7mCherry	Labels the Dα7 subunit of nicotinic receptors.	(Fayyazuddin et al., 2006) Created by the Lin lab?

2.1.3 Fly lines used in Chapter 4-Physiological experiments

All fly lines used to investigate physiological adaptations to prolonged hyperactivity in Chapter 4 can be seen in Table 2.3

Table 2.3. Fly lines used in Chapter 4

Fly line	Purpose	Availability/ Citation
hsFLP; Sp/CyO; Sb/TM6b,Tb	Db hsFLP line used in first single cell live imaging line attempt	Made by Dr Andrew Lin

hsFLP; UAS-GCaMP6f/CyO; R13F02-GAL4/TM6b,Tb	Parent line-first single cell live imaging attempt	Created by me
tubp>GAL80>/CyO; Sb/TM3,ser	Parent line-first single cell live imaging attempt	(Gao et al., 2008)
tubp>GAL80>, UAS-mCherry/CyO; Sb/TM3,ser	Parent line-first single cell live imaging attempt with mCherry for labelling morphology	(Gao et al., 2008; Kakihara et al., 2008) Created by the Lin lab
UAS-GCaMP6f(attp40)	Fluorescent calcium indicator	(Chen et al., 2013) Bloomington: 42747
R13F02-GAL4	Labels all KCs-used in both live imaging genotypes	(Jenett et al., 2012)
hsFLP,tubp-GAL80,-neoFRT19A	Original hsFLP FRT19A line	(Lee, Lee and Luo, 1999) Bloomington: 5132
hsFLP,tubp-GAL80,-neoFRT19A; If/CyO; Sb/TM3-Ser	Double balanced hsFLP+FRT19A MARCM line-used to create single cell live imaging line	Created by me

hsFLP,tubp-GAL80,-neoFRT19A; UAS-GCaMP8m, UAS-mCherry/CyO; R13F02-Gal4	Labels single KCs with GCaMP and mCherry	Created by me
y,w,-neoFRT19A	Original FRT19A line	(Xu and Rubin, 1993) Bloomington: 1744
y,w,-neoFRT19A;If/CyO	Control FRT19A line for single cell live imaging	Created by me
y,w,-neoFRT19A;UAS-dTrpA1/CyO	Experimental FRT19A line for single cell live imaging which includes TrpA	Created by me
Or83b-GAL4 (Orco)	Labels ORNs/antennal nerve.	(Wang et al., 2003) Bloomington: 26818
UAS-jGCaMP8m(attp5)	Newest generation of fluorescent calcium indicator	(Zhang et al., 2023) Bloomington: 92591

2.1.4 Equipment list

Equipment used throughout this work are listed in Table 2.4

Table 2.4. Equipment used and associated vendors

Equipment	Vendor

Manual control variable speed pump-Perfusion system. 120S/DM2	Watson Marlow Fluid Technology Solutions, Falmouth, UK
Scientifica Patchstar Micromanipulator	Scientifica, East Sussex, UK
Narishige PC-10 Dual stage glass Micropipette puller lab	Narishige Group, Tokyo, Japan
Digitimer Constant current isolated stimulator, Model DS3	Digitimer, Welwyn Garden City, UK
Narishige Micro Forge MF-900	Narishige Group, Tokyo, Japan
Leica S8APO stereomicroscope	Leica, London, Uk
Scientifica Perfusion temperature controller	Scientifica, East Sussex, UK
PHCbi Cooled incubator MIR-154-PE	PHCbi, Tokyo, Japan
Grant Instruments Water bath	Grant Instruments, Cambridge, UK
Almore Electra waxer 220 Volt	Almore International, Hickory North Carolina, USA
Bio-Rad power PAC 300	Bio-Rad, Hercules California, USA
Syngene NuGenius XE	Syngene, Cambridge, UK
Zeiss LSM 880 Airyscan confocal	Zeiss, Oberkochen, Germany
Zeiss LSM 980 Airyscan confocal	Zeiss, Oberkochen, Germany
Mai Tai eHP DeepSee Ti:S laser	Spectra-Physics, Mountain View California, USA
GO-5000M-USB camera	Jai, Hovedstaden, Denmark
Thorlabs Shutter controller SC10	Thorlabs, Newton New Jersey, USA
Sutter Moveable Objective microscope	Sutter Instrument, Novato California, USA
Sutter Resonant scan box MDR-R	Sutter Instrument, Novato California, USA

Microscope movement controller MPC200	Sutter Instrument, Novato California, USA
DSP controller LC.400 (1-Channel)	Npoint, Middleton Wisconsin, USA
Pockels amplifier 350-80LA	Conoptics, Danbury Connecticut, USA
PXIe-1073	National Instruments, Austin Texas, USA
VWR Tube Rotator 20rpm with Adjustable Angle Rotisserie 444-0502 Jencons(VWR)	The LabWorld Group, Rotheram, UK
Series 20 Plain Platform, Model P-1 Harvard Apparatus catalog # 640277	Harvard Apparatus, Holliston Massachusetts, USA

2.1.5 Recipes and Reagents

2.1.5.1 External Solution

For all live imaging experiments flies were perfused with external solution that closely matches the usual physiological environment of haemolymph; this ensures the normal cellular activity of neurons is maintained. The recipe for external solution was based on previously published methods where it was used for functional imaging and electrophysiology (Murthy and Turner, 2013; Groschner et al., 2018). Table 2.5 shows the concentrations/measurements of reagents used to create 1000ml of external solution.

Table 2.5 Recipe for 1000ml of External solution and associated issue number and vendor

Ingredient	mM	ml or mg for 1000ml	Vendor	Issue Number
KCl	3	3 ml 1 M stock	Sigma, Burlington,	10735874

			Massachusetts, USA	
$CaCl_2$	1.5	1.5 ml 1 M stock	Sigma, Burlington, Massachusetts, USA	21115-100ML
$MgCl_2$	4	4 ml 1 M stock	Sigma, Burlington, Massachusetts, USA	M1028-100ML
TES	5	1.14625 mg	Sigma, Burlington, Massachusetts, USA	T5691-100G
NaCl	103	6.01932 mg	Sigma, Burlington, Massachusetts, USA	S7653-1KG
$NaHCO_3$	26	2.18426 mg	Sigma, Burlington, Massachusetts, USA	S6014-1KG
$NaH2PO_4$	1	0.11998 mg	Sigma, Burlington, Massachusetts, USA	S5011-100G
Trehalose	8	3.02664 mg	Sigma, Burlington,	T9531-100G

			Massachusetts, USA	
Glucose	10	1.8016 mg	Sigma, Burlington, Massachusetts, USA	G8720-1KG

2.1.5.2 Antibodies and reagents for fixation and immunolabelling

A list of the antibodies used for whole brain immunolabelling and their associated concentration, vendor and purpose can be found in Table 2.6.

Table 2.6. Details of antibodies used in whole brain immunolabelling

Antibody	Concentration	Purpose	Vendor
Chicken anti-GFP (Abcam-ab13970)	1:1000	Label GFP to enhance existing GFP signal	Abcam, Cambridge, UK
Mouse anti-Choline Acetyltransferase (chAT) (DSHB ChAT4B1)	1:200	Label PN boutons	DSHB, University of Iowa, Iowa City, USA
Mouse anti-Bruchpilot (BRP) (DSHB-NC82)	1:100	Label the MB lobes	DSHB, University of Iowa, Iowa City, USA

Goat anti-chicken Alexa Fluor 488 (ThermoFisher, A-32931)	1:1000	Alexa Fluor 488 secondary antibody for improved visualization of GFP.	ThermoFisher Scientific, Waltham Massachusetts, USA
Goat anti-mouse Alexa Fluor 546 (ThermoFisher, A-11072	1:1000	Alexa Fluor 546 secondary antibody for improved visualization of either MB lobes or PN boutons.	ThermoFisher Scientific, Waltham Massachusetts, USA

2.1.5.3 Other reagents

For live recording, both whole MB and single KCs, Carbogen gas (95% O_2, 5% CO_2) was bubbled through external solution to provide O_2 and balance the pH. For antennal nerve stimulation, the silver electrode was first immersed in bleach to create a chloride coat on the electrode. The details for both these reagents can be found in Table 2.7

Table 2.7. Reagents used in live imaging and antennal nerve stimulation

Reagent	Reference	Vendor
Carbogen gas	131-J	BOC, Sheffield, UK
Bleach (sodium hypochlorite)	425044	Sigma

2.2 Methods

2.2.1 Heatshock protocol

To label KCs using MARCM, offspring in vials were placed in a 37°C water bath and submerged so that all embryos/larvae were surrounded by water. In all conditions and across both morphological and physiological experiments, vials were heated for 35 minutes to ensure high probability of labelling only single neurons. After heatshock vials were dried and then placed in a 22°C incubator to avoid premature activation of neurons in TrpA-expressing KCs. However, flies used for data displayed in Figure 4.10 and 4.12 were instead moved to an 18°C incubator after heatshock after potential issues with 22°C activating TrpA were identified. To label different subtypes, flies were heatshocked 2 days (γ), 4.5 days (α'/β') and 7 days (α/β) after parental egg laying, in line with the previously characterised development timings of these subtypes (Lee, Lee and Luo, 1999) (Figure 1.7).

2.2.2 TrpA activation

To hyperactivate TrpA-expressing KCs, adult flies were collected after eclosion, placed into new vials and moved to a 31°C incubator; aged flies (Chapter 3.2.4) were first moved to 22°C or 18°C after eclosion before being incubated at 31°C (See Figure 3.9a and 3.10a). In most experiments flies were collected and placed in the 31°C incubator at ~12pm and were dissected within 1-3 hours once that conditions respective period of TrpA activation was complete; flies were always kept at 31°C until just before dissection. In the 12 hour and 6 hour 31°C conditions (Figure 3.6 and 3.7) flies were placed in a 22°C incubator programmed to switch to 31°C at 12am and 6am respectively; flies were then dissected at ~12pm. Apart from the Starved and Sugar-only conditions, all flies were incubated at 31°C in vials containing food with the recipe displayed in Table 2.1.

2.2.3 Whole brain dissection and Immunolabelling

Flies were first placed on ice for ~2 minutes until immobile, before being placed in 70% ethanol for ~30 seconds to remove the cuticle hydrophobic coating. They were then moved to a Sylgard dish containing PBS, where forceps were used to remove the brain from the cuticle and any remaining tracheal tissue to ensure no obstructions in later imaging. Brains were then fixed at room temperature in 4% paraformaldehyde for 20 minutes and then underwent two quick washes in PBST (0.3% Triton X-100 in PBS) and a further three 20 minute PBST washes.

In experiments using immunolabelling (brains imaged on the Zeiss Airyscan confocal), after washes brains were then blocked in 5% goat serum in PBST for 30 minutes and were then incubated in primary antibody (5% goat serum PBST solution) for 2-4 days at 4°C. After this period, brains underwent two more PBST quick washes and a further three 20 minute PBST washes, before being transferred into a secondary antibody solution (5% goat serum PBST) and incubated for a further 2-4 days at 4°C. Another two quick washes and three 20 minute washes in PBST were performed, and then brains were mounted in Vectashield anti-fade mounting medium on glass slides posterior side up to improve visualisation of the calyx during imaging; a coverslip was placed over brains with nail polish at its edges to seal it. Dilutions of different antibodies can be seen in Table 2.6. Dissection and immunolabelling protocol was adapted from (Wu and Luo, 2006). Eppendorf tubes containing brains were rotated during fixing, washing and labelling steps (VWR Tube Rotator 20rpm with Adjustable Angle Rotisserie 444-0502) to ensure whole brain penetration.

2.2.4 Whole brain imaging protocol (2-photon and Airyscan confocal)

Brains were initially imaged on a 2-photon (2p) microscope before I later switched to the Zeiss LSM 880 and LSM 980 Airyscan confocal microscopes due to their superior lateral and axial resolution (Wu and Hammer, 2021); the majority of images used for morphological analysis were taken on an Airyscan confocal. The stochastic nature of MARCM often resulted in several KCs labelled per hemisphere and/or KCs on both hemispheres labelled; z stacks from both hemispheres were taken if they contained 1-4 KCs and only when KCs could be distinguished from each other within a hemisphere. Z stacks of the calyx were captured with an image window adjusted to include only KC dendrites, cell body and the beginning of the axon so the approximate location of the AIS could later be estimated when tracing neurons. KC subtype was visually confirmed in γ and α/β KCs before performing a z stack, while a stack of the axon (2µm slice interval) was captured in α'/β' KCs to allow later confirmation of subtype (see Chapter 3.2.8). 2p stacks had a slice interval of 0.5µm (512x512), with Mai Tai laser (Table 2.4) set to 910nm to maximise signal from GFP; both green and red channel (channel 1 and 2) were captured when KCs also expressed Dα7-mCherry to try and identify nicotinic receptors. Airyscan stacks had a slice interval of 0.16µm (Plan-Apochromat 63x oil immersion lens/1.4 NA DIC M27; super resolution) and 488nm laser line was used (KCs were immunolabelled with Goat anti-chicken-Alexa Fluor 488); when BRP or chAT were labelled (Secondary antibody: Goat anti-mouse Alexa Fluor 546) an identical z stack was captured after the first using a 561nm laser line. On both microscopes, power and gain were altered to

maximise signal while decreasing noise. Airyscan images were processed using Airyscan joint deconvolution (da Costa, Ralf Engelmann, Martin Gleisner and Lutz Schäfer, Olivia Prazeres, 2021).

2.2.5 Claw counting and associated criteria

Images were analysed in FIJI and claw count was recorded using the “Cell counter” plugin; all filenames were blinded to avoid bias when analysing them. KCs have many dendritic structures, but not all of these are claws so I developed a criteria for distinguishing between the different classes of dendrites to improve consistency of claw counting. I used hemibrain connectome reconstructions (Scheffer et al., 2020), which includes approximations of synapse identity based on proximity and the presence of T bars, to distinguish between claws and other structures. From this starting point I characterised 4 classes of dendrites: Class 1/Twigs, Class 2/Branches, Class 3/Simple Claws, Class 4/Complex Claws; a description of each class can be seen in Table 2.8 and examples can be seen in Figure 3.3. These classes can be divided into non-claw dendrites (Class 1 and 2) and claw-dendrites (Class 3 and 4), with the latter being of particular interest as they are the primary excitatory input to KCs and therefore may be implicated in homeostatic plasticity. Disconnected structures were considered debris or a result of non-specific labelling and were not counted. If a significant proportion of structures were disconnected from the neuron, the image was omitted due to high likelihood of damage occurring during dissection or fixing/labelling/mounting.

Table 2.8 Claw counting Criterion. Blue shading indicates non-claw dendrites while purple shading indicates claw-dendrites.

Class	Description
1 (Twig)	Thin short single dendrites that extend off primary neurite or secondary branches
2 (Branch)	Longer dendrites that may demonstrate limited branching (1-2 branches). Sometimes appear to possess a claw shape but have a much smaller volume.
3 (Simple Claw)	Dendrites that usually have a thick claw protrusion; examples without claw shape still demonstrate a significant volume at the end.

4 (Complex Claw)	More elaborate structures than simple claws, often possessing multiple 'simple claw-like' structures (Butcher et al., 2012) If distance between claws is =>10µm they are two simple claws, otherwise they are part of the same complex claw. Claws that extend separately from the primary neurite are always considered distinct claws.

2.2.5 Tracing protocol and morphological analysis

After claw counting was performed, I created skeletons of individual KCs using the simple neurite tracer (SNT) plugin on FIJI (Arshadi et al., 2021); images with multiple KCs where dendrites were too overlapping to trace separately were excluded. SNT allows semi-automation of tracing when selecting between points on the neurite/dendrite. I used the A* search algorithm auto-tracing feature, to find the lowest-cost path along the neurite between the selected start and end points; before confirming this trace, I evaluated the accuracy of the automated path and, if required, selected new points closer together to most closely match the real neurite. I first traced the primary neurite from the end of the soma to the start of the AIS based on approximation of entry into the pedunculus, indicated by position in the calyx and by curve of the primary neurite. Then I added branch points off of the primary neurite to trace connecting dendrites of all 4 classes (claw and non-claw dendrites); additional forking points were added on these dendrites depending on branching complexity. Non-claws were traced to the very end of the dendrite, while claws were traced from branching point to the start of the claw (Figure 3.13), as tracing the structure itself as a single path was not possible due to its complexity. Once all neurites had been traced, they were tagged depending on type: the primary neurite was marked as "Basal Dendrite", both simple and complex claws were tagged as "Apical Dendrite" and class 1's and 2's were left as "Undefined". Finally, I traced the length of the soma branching off of the primary neurite, so its position could be used for analysis. To further improve the accuracy of tracing, I used SNT's Refine Paths feature on all traces and selected both types of refinement: "Assign fitted radii" and "Snap node coordinates". Snap node coordinates fits a circular cross-section at each node along a

traced neurite and snaps the node to the centroid of this section, producing a trace that more accurately follows the centre line of the neurite. Assign fitted radii then takes the radius of the fitted circle to estimate the thickness of the traced neurite based on pixel intensity. I set the maximum radius of this circle to 10 pixels as this most closely matched the ~size of neurites while avoiding immunolabelling artifacts or adjacent structures from being included in the fit; the soma path was excluded from the fitting process. I used SNT's built in "Measure Path(s)" function to determine the length of the primary neurite and all dendrites; I then recorded the average and sum of these lengths for claws and non-claw dendrites separately.

2.2.6 Single cell live imaging dissection and antennal nerve stimulation

Fly preparation and antennal nerve dissection

Vials containing a single fly were placed on ice for ~5 minutes until immobile, after which the fly was moved onto foil on our Custom-made perfusion chamber (Series 20 Plain Platform, Model P-1 Harvard Apparatus catalog # 640277). The fly was pinned in the supine position with the thorax inserted into a hole in the foil to prevent movement and the abdomen, wings and legs fixed with wax. A window was then cut on the other side of the foil and the head was pushed through. The foil was then refolded underneath the head and the proboscis fixed with wax to ensure the head would remain in position and as stationary as possible during recording. External solution was then pipetted into the holder ducts to ensure all exposed tissue was covered. Using fine forceps, a surgical window was cut in the cuticle at the back of the head around the ocelli, and any obstructing tracheal tissue and glial sheath were removed to improve visualisation of the MB lobes and calyx. The stage/holder was then placed under the 2p microscope and carbogen (95% Oxygen/5% CO2) was constantly bubbled through external solution using a perfusion pump to achieve consistent solution recirculation. The brain was located using the widefield pathway on the microscope (Sutter Moveable Objective Microscope) before switching to the 2p pathway and illuminating with the Mai Tai laser (Table 2.4) set to 1040nm to visualise single KC mCherry labelling. If there was no labelling present the brain was abandoned, otherwise the antennae (if both hemispheres were labelled) were dissected between the Scape and Pedicel segments to reveal the exposed nerve. Technique was adapted from (Groschner et al., 2018).

Electrode preparation and antennal nerve suction

Prior to dissection a silver electrode was immersed in bleach for ~10-15 minutes to chloride the wire to make it stable. The electrode was then inserted into a glass pipette/electrode containing ~15µl of external solution with a 40µm pore at the end and attached to the electrode arm (Scientifica electrode arm Table 2.4); the electrodes were connected to a Digitimer constant current isolated stimulator. After antennal nerve dissection, the fly was placed back under the 2p and the glass electrode was lowered into position close to the antennal nerve of the hemisphere about to be stimulated. An attached 60ml syringe was then used to suction the nerve into the electrode and the ground electrode was fixed in place in the external solution close to the fly. Perfusion was then started again as described earlier. For flies recorded at 17°C (See Chapter 4.2.6 and 4.2.7) external solution was suspended in an ice-water bath. Extended perfusion tubing was used and a significant portion of its length was also surrounded by ice just before delivery to the fly to reach 17°C; this was confirmed by Scientifica temperature sensor placed close to the fly submerged in external solution.

Two-photon setup and recording

The 2p setup for recording calcium responses included a Ti:Sapphire laser (Mai Tai eHP DS, Spectra-Physics) set to 910 nm, which was attenuated by a Pockels cell controller connected to a voltage amplifier (model 350-80LA, Conoptics). The laser was then focused onto the sample using a 1.0 NA 20X objective (Olympus) after being directed by a galvo-resonant scanner (model MDR-R, Sutter). Emitted fluorescence was detected by GaAsP photomultiplier tubes (model PS-2LV, Hamamatsu Photonics) and amplified with a TIA-60 (Thorlabs). A piezo objective stage (nPFocus400, nPoint) and ScanImage 5 software were used to control the volume imaging. For single Kenyon cell recordings, a FastZ stack was acquired to capture as much of the neuron as possible during antennal nerve stimulation. Each stack consisted of 20 slices with a 1–2 µm interval, beginning at the highest Z position where the Kenyon cell was visible and extending towards the beginning of the axon. The recording was performed at a resolution of 256x256 pixels. In hemispheres containing multiple KCs, calyx recording was only performed if neurons could be distinguished easily. Dendrites were always stimulated/recorded first, followed by associated axons in the same hemisphere; in α/β KCs the α and β lobes were recorded separately. In brains with both hemispheres labelled, the hemisphere with the strongest signal was usually recorded from first as there was a chance flies may die during extended recordings. Electrode was detached and re-suctioned to the opposite antennal nerve before recording from its

associated hemisphere. All recordings used maximum laser power (~27.5mW) due to the dim nature of single KC GCaMP8m signal.

Antennal nerve stimulation details

LabVIEW software was used to externally trigger antennal nerve stimulation from the Digitimer constant current isolated stimulator. The stimulation was set to 1mA with a pulse length of 0.1 seconds, a stimulus train duration of 0.5 seconds, and an inter-stimulus interval of 20 seconds. Calcium responses and morphology were captured simultaneously by recording from channels 1 and 2 respectively, to aid in subsequent analysis. Specific frequencies and timings of stimulation are detailed in Tables 2.9 and 2.10.

Table 2.9. Regular onset antennal nerve stimulation. The onset of pulses and their associated frequencies are shown.

Stimulation Time (s)	Stimulation Frequency (Hz)
5	120
25.5	100
46	80
66.5	60
87	40
107.5	20
128	10
148.5	4
169	2

Table 2.10. Delayed onset antennal nerve stimulation. The onset of pulses and their associated frequencies are shown.

Stimulation Time (s)	Stimulation Frequency (Hz)
40	120
65.5	100
86	80
106.5	60
127	40
147.5	20
168	10
188.5	4
209	2

2.2.7 Two-photon whole MB trialling different currents

The 2p microscope settings were identical to those described in Section 2.2.6 with a few key differences adapted for whole-brain imaging. Due to the absence of mCherry labelling, only a single channel was used for GCaMP signal recording. To capture a representative mushroom body response, single-plane images of the horizontal lobe were acquired instead of a Z-stack, as volume recording was not necessary. The laser power was significantly lower (18–20%) than in single-cell experiments because the signal from the whole mushroom body was much stronger.

To test the effect of varying stimulus intensity, a range of currents were applied in pseudorandomized order to the antennal nerve. The stimulation timings and frequencies remained consistent with the parameters detailed in Table 2.9. A subset of the following currents were tested on each fly: 2 µA, 5 µA, 10 µA, 30 µA, 100 µA, 150 µA, 200 µA, 300 µA, 1000 µA, and 3000 µA. Not all currents were tested across all flies due to the preliminary nature of these experiments.

2.2.8 Whole MB and single neuron temperature recordings

The two-photon microscope settings for both whole-Mushroom Body (MB) and single Kenyon Cell (KC) temperature response recordings were identical to those described in Sections 2.2.6 and 2.2.7.

For whole-MB temperature responses, flies were initially recorded at room temperature (~22°C). The bath temperature was then increased to 31°C using a Scientifica Perfusion temperature controller with a perfusion pump to circulate the heated external solution. Once the target temperature of 31°C was reached, the heater was switched off and recording continued until the bath temperature returned to 22°C.

For single-KC temperature responses, the fly holder and external solution were first cooled to approximately 17°C using ice as described in Section 2.2.6. The temperature was then increased to 31°C by a combination of activating the heater and repositioning the external solution tubing to no longer pass through the ice. Once 31°C was reached, the heater was switched off, and the external solution and tubing were re-immersed in the ice bath to cool the fly back down to approximately 17°C. The recording was then concluded.

2.2.9 PCR genotyping

Genomic DNA was isolated from single flies to confirm the presence of specific genes and recombination events. For DNA extraction, a Squishing buffer (10mM Tris-HCL, 1mM EDTA, 25mM NaCl, Ph 8.0) containing 200µg/ml Proteinase K was prepared. A single whole fly was added to the solution and a pipette tip was used to squish it and expose neural tissue. Once completed the fly was incubated at 37°C for 30 minutes to facilitate protein digestion by Proteinase K. The solution was subsequently heated to 95°C for 3 minutes to inactivate the enzyme.

Polymerase chain reaction (PCR) was performed using the extracted genomic DNA. Each 50 µl reaction contained the following components: 5 µl of 10X CoralLoad buffer, 1 µl of dNTPs (thawed on ice), 1 µl each of two primers (forward and reverse), 3 µl of genomic DNA, 0.25 µl of Taq Polymerase (which was constantly kept in an ice box) and 38.75 µl dH_2O.

The PCR thermal cycling program was as below:

1. Initial denaturation: 15 minutes at 95°C.
2. Cycling (35 cycles):
    a. Denaturation: 15 seconds at 95°C.

b. Annealing: 30 seconds at a temperature optimised for the specific primers (ranging from 50°C to 65°C).
c. Extension: An extension time at 72°C was calculated based on expected product size (~1 minute per KB of expected size).

3. Final extension: 10 minutes at 72°C.

PCR products were visualised using agarose gel electrophoresis. A 1% agarose gel was prepared with Sybr Safe (5 µl per 50ml of agarose solution) for DNA staining. Gel was placed in a TAE bath and samples were loaded into wells. The gel was run at 100V for ~20-30 minutes to separate DNA fragments by size. Details for all reagents used can be found in Table 2.11

Table 2.11. Details of reagents for genotyping of single flies

Reagents	Reference No.	Vendor
Proteinase K	P2308-10MG	Sigma, Burlington Massachusetts, USA
Taq DNA Polymerase Kit	201205	Qiagen, Manchester, UK
dNTPs	15393189	ThermoFisher Scientific, Waltham Massachusetts, USA

The following recombinants were created for use in this work:

1. UAS-GCaMP8m, UAS-mCherry (used in single cell live imaging genotype in Chapter 4).
2. Mb247-LexA, LexAOP-TrpA (positive control for whole MB temperature responses in Chapter 4).
3. LexAOP-jRGECO1A, UAS-TrpA (crossed to single cell live imaging genotype to confirm lack of whole MB response in Chapter 4).

See table below for primer sequences used for genotype verification.

Table 2.12. Primer sequences used for PCR reactions to confirm recombination

Relevant Transgene	Forward Primer Sequence	Reverse Primer Sequence	Annealing Temperature
UAS-GCaMP8m	GGGAAAACTCCCGGTTCCAT	ATGACGGTGCCCAACTCTTT	60°C
UAS-mCherry	ATGGTGAGCAAGGGCGAGGAG	CTTGTACAGCTCGTCCATGCCG	60°C
Mb247-LexA	CCGTGATCACATCAGCCAGA	AATACGTGCGACAACGACCT	60°C
TrpA	CACCATCTGGTTCGGCTCAT	TACCTTAGAGCTTTAAATCTCTGTAG	51°C
jRGECO1A	TGAATAATGCCGCCGTCCTC	GGACGAGCTGTACAAGGGAG	60°C

2.3 Analysis

2.3.1 Analysis of single cell calcium responses

Single KC calcium responses to antennal nerve stimulation were initially analysed in FIJI. Motion artifacts were corrected by registration. The Freehand selection tool was used to draw ROIs around the cell's soma and dendrites in each z-slice; the dimmest area across slices with no KCs present was used as a background ROI. The change in calcium fluorescence over time, or ΔF/F was then calculated:

1. $F(t) = F_{ROI}(t) – F_{Background}(t)$
    - The raw fluorescence signal over time (F(t)) is calculated by subtracting the background fluorescence ($F_{Background}$) from the fluorescence across the multi ROI including all sections of the KC (F_{ROI}); t indicates time of the entire recording.
2. $F0(t) = F_{mean}(t)$ over the pre-stimulus window
    - The baseline calcium fluorescence (F0(t)) was calculated from the mean of the corrected fluorescence signal ($F_{mean}(t)$) over a user-defined pre-stimulus window. This provides a stable baseline against which changes in fluorescence can be measured. For all antennal nerve stimulation, the baseline was

calculated separately in Igor from the 5 seconds pre stimulus for each stimulation frequency (2.3.2)

3. $\Delta F/F = [F(t) – F0(t)]/F0(t)$

Change in fluorescence over time (ΔF/F) is calculated over time and used to generate traces for individual KCs; for antennal nerve stimulation steps 2 and 3 were performed in Igor Pro (Wavemetrics), all other live imaging experiments used FIJI to calculate ΔF/F before exporting to Igor for plotting.

For whole MB antennal nerve responses, the same ΔF/F calculation was used, but an ROI was drawn around the MB (either the whole calyx or horizontal lobe). Similarly, for whole MB and single neuron temperature recordings, the same ΔF/F calculations were applied. When responses were exported to Igor, they were also plotted against time and the associated temperature of the fly (determined by sensor close to the fly), which allowed the change in calcium response to different temperatures in TrpA flies to be determined.

2.3.2 Statistical analysis

Graphs and statistical analysis were performed on GraphPad Prism 10 with the following exceptions: All calcium response traces (Chapter 4) were created in Igor Pro (Wavemetrics) and all Generalized Linear Models (GLM) were performed in Python. Significance on graphs is indicated in the following format: *P<0.05, **P<0.01, ***P<0.001. For claw and non-claw counts and path length analysis, QQ plots and Homoscedasticity plots were performed first to assess normality and equivalence of variance respectively. As most groups demonstrated unequal variances on a Homoscedasticity plot, I instead performed a GLM (Gaussian family) to determine the effect of genotype and condition on claw counts and path lengths, including a full interaction term. To account for heteroscedasticity, robust standard errors was calculated using the HC3 method. Significant differences between the same genotype were evaluated across conditions as well as comparing between genotype within a condition using a Wald test post hoc comparisons with Holm-Sidak multiple comparisons correction. Both genotypes of the following conditions were analysed together for claw counts, non-claw counts and path length: 22°C 4 days, 31°C 6 hours, 31°C 12 hours, 31°C 1 day, 31°C 4 days, Older flies and Reversal. The conditions Aged 18°C, Aged 22°C and 31°C 1 day were separately compared in their own GLM as were 31°C 1 day Starved flies, 31°C Sugar only flies and 31°C 1 day flies. a/b and a’/b’: Unpaired t test with Welch’s correction was used to compare between genotypes within each subtype

After ΔF/F of calcium responses was determined in FIJI and responses were plotted in Igor (2.3.1), to determine the peak response to each frequency I measured the average ΔF/F between 0 and 0.5 seconds after the start of each stimulation. The baseline for each response was calculated at 5 seconds before stimulation onset (2.3.1) and the mean calcium response was calculated over the peak response window for all frequencies so that they could be compared across genotype and condition. The mean peak calcium responses at the highest stimulation frequency (120Hz) of both genotypes was compared using a 2-way ANOVA, with the following comparisons between conditions:

1. Calyx recordings: 22°C 1 day, 31°C 6 hours, 31°C 1 day, 31°C 4 days.
2. Axon recordings: 22°C 1 day, 31°C 6 hours, 31°C 1 day, 31°C 4 days.
3. α/β: 31°C 1 day Calyx, 31°C 1 day alpha lobe (beta lobe excluded due to inconsistent responses and poor sample size).
4. Calyx recordings: No ice regular onset, No ice delayed onset, Ice regular onset, Ice delayed onset
5. Calyx recordings: 18°C 1 day and 31°C 1 day-Raised at 18°C

For the comparison of responses between genotypes across all stimulation frequencies, a nonlinear saturating curve was fitted to the average peak responses for each genotype. This curve, similar to a Hill function (Weiss, 1997), used the following equation:

$$y = k * \frac{x}{b+x}$$

Parameter **k** represents the saturation point, while **b** indicates the slope, or the rate at which the saturation point is reached. This model, a simplified version of a previously described model (Olsen, Bhandawat and Wilson, 2010), was selected as it adequately captured the relationship between KC responses and stimulation frequency with the fewest possible parameters. To determine if the responses of different Cntrl and TrpA were significantly different, an extra sum-of-squares F-test was performed. This test compares the fit of a single, simplified model applied to all data with the fit of two separate models, each fit to Cntrl and TrpA responses. A significant F-test result indicates that the separate models provide a significantly better fit to the data than the single model, suggesting a significant difference between genotype.

3. Morphological adaptations as a mechanism of homeostatic plasticity

3.1 Introduction

In our previous work (Abdelrahman, Vasilaki and Lin, 2021) adaptations in several morphological parameters were proposed as potential compensatory mechanisms; primarily altering the number of inputs per KC. Although correlations between parameters in the connectome suggest some of these adaptations could occur (Figure 1.5)(Scheffer et al., 2020), there is currently no evidence that adult KCs alter their morphology as a homeostatic mechanism. Furthermore, previous unpublished results (Lily Bolsover) discovered that altering activity of KCs using the bacterial sodium channel NaChBac causes drastic changes in the morphology of these neurons, making their dendrites more tortuous. Based on these findings, and the evidence of morphological homeostatic plasticity in other systems (Section 1.7.3), I decided to investigate whether single KCs change their morphology in response to prolonged activation. My primary aim in this chapter was to identify whether hyperactivating KCs with TrpA for prolonged periods produced any changes in the number or length of excitatory inputs (claws) across all three subtypes. Secondary to this I wanted to determine whether any changes were reversible, as you might expect if adaptations are homeostatic, and determine if factors like energy and protein availability had any impact on observed adaptations.

3.1.1 Precedent for using TrpA

To address the first of my primary questions, “do single KCs adapt their morphology in response to prolonged activation?”, I increased the activity of single cells by artificially expressing the temperature sensitive cation channel TrpA. This protein was used partially because our previous findings of homeostatic plasticity in the whole MB utilised TrpA (Apostolopoulou and Lin, 2020; G. Bergmann, unpublished results), allowing for comparison between any potential findings. Furthermore, TrpA is commonly used for activity manipulation in Drosophila (for example: Das et al., 2011; Lin et al., 2014), and therefore the response profile of neurons expressing TrpA is fairly well defined. This channel is closed at 22°C but begins to open around 25°C, reaching maximal conductance at ~31°C (Hamada et al., 2008). Additionally, the manipulation is relatively simple, only requiring an incubator, which allows automated control of on and offset of neuron activity.

One potential downside of using TrpA is its lack of spatial specificity and fine temporal control. TrpA is theoretically expressed relatively uniformly across the cell and therefore is incapable of targeted activation of specific areas of the neuron (e.g. dendrites vs axon). Furthermore, the opening and closing of the channel is too slow to allow generation of single spikes, or trains of spikes followed by activity cessation, unlike optogenetic tools like CsChrimson (Deisseroth, 2011; Aso et al., 2014a). There are advantages to those manipulations, however for this experiment I only had two basic requirements. First, I needed to achieve chronic activation of neurons and our previous work demonstrated its effectiveness at this (Apostolopoulou and Lin, 2020; G. Bergmann, unpublished results). Second, I needed to achieve an extreme activation of the neuron to determine if homeostatic plasticity is even possible in KCs, as this has not yet been shown at the single cell level. Through the combination of TrpA and MARCM I could achieve both these requirements while keeping the manipulation relatively simple with few potential parameters that could influence the exact activity pattern of the neuron. In contrast, for optogenetic manipulations I would need to consider the frequency and intensity of light and test effectiveness of light penetration through the cuticle, while the effect of temperature on the activity of TrpA-expressing neurons is already well defined. I will go into more detail on this later, when reviewing the conclusions from both the morphological and physiological results.

3.2 Results

3.2.1 Achieving labelling of single Kenyon cells

To identify potential morphological adaptations to prolonged hyperactivity, I used MARCM to label single cells with TrpA and visualized them using GFP (and immunolabelling with an anti-GFP primary antibody with Alexa fluor 488 green secondary). However, this technique is stochastic and relies on heatshock induced flippase expression to induce homologous recombination in cells actively dividing, producing a labelled and unlabelled pair of daughter cells. In order to consistently label only a few KCs, I tested a series of heatshock timings as the longer a heatshock is, the more FLP protein produced and the higher the likelihood neurons divide with FLP present resulting in GAL80 recombination; too short and I may consistently label nothing at all, while too long may result in whole MB labelling, or KCs that overlap leaving me unable to count their claws. I started with a long heatshock time of 2 hours to confirm the genotypes effectiveness; this consistently resulted in whole MB labelling in both hemispheres (Figure 3.1). I then tested a 40 minute heatshock duration and discovered this was effective at labelling only a few KCs, however, there was still often 3-4

cells present. Dropping the heatshock time to 35 minutes consistently produced 1-3 cells labelled so this time was used for all experiments (Figure 3.1).

The majority of images in which number of claws on KCs were counted only contained 1 KC per brain, but I did not throw out images that did not satisfy this criteria. Even after trialling heatshock times the number of brains dissected, fixed, labelled and imaged that contain KCs that can be analysed is relatively low. If we consider just the main γ KC timepoints (22°C 4 days, 31°C 4 days,1 day, 12 hours, 6 hours and Older flies) of the ~621 brains dissected, only 148 were able to be successfully counted (a ~24% success rate). This low rate is due to a variety of factors which includes lack of any labelled KCs, whole MB labelling (likely due to labelling of a neuroblast), damage to KCs during dissection, or too many KCs in close proximity to each other making it impossible to distinguish neurons; the success rate is even lower in α'/β' KCs due to the inconsistent labelling of this subtype (see Results 3.2.8). As a result of this low success rate, I also counted claws of KCs in brains containing multiple neurons, either in separate hemispheres or to a maximum of four per hemisphere. I hypothesized that the this few KCs in the same hemisphere would be unlikely to significantly influence the activity of each other or the APL, similar to what occurs at the whole MB level (Lin et al., 2014; Apostolopoulou and Lin, 2020). However, to confirm this I compared the control claw count of hemispheres containing single γ KCs to those with 2 or more across conditions. I also did the same with TrpA claw counts in only groups with a significant decrease in claws after hyperactivation (31°C 4 days and 1 day). Neither of these comparisons revealed any significant differences between each other (Figure 3.1), suggesting first, that the counting itself is not affected by the presence of multiple cells in the image and second, that the claw loss adaptation I will discuss later is not different when only a few KCs are activated vs just one.

a

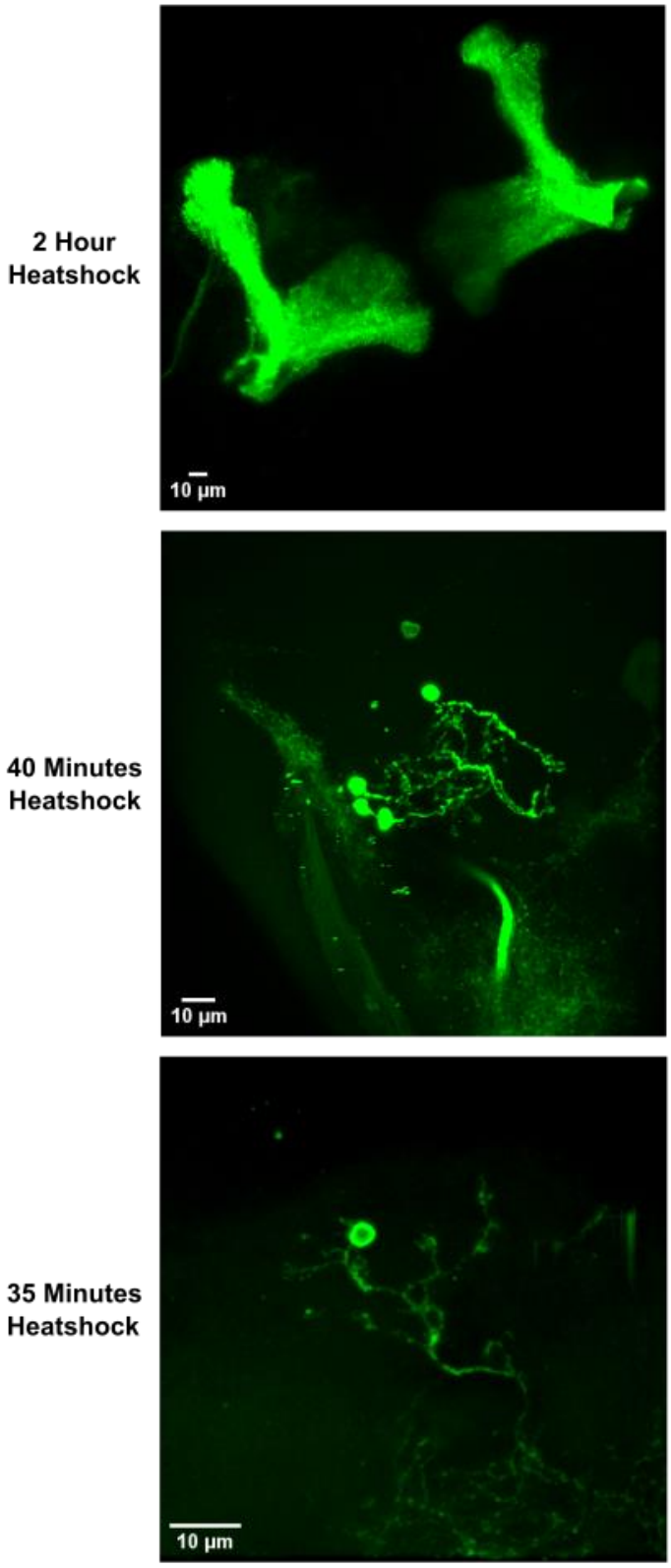
2 Hour Heatshock
10 µm
40 Minutes Heatshock
10 µm
35 Minutes Heatshock
10 µm

b

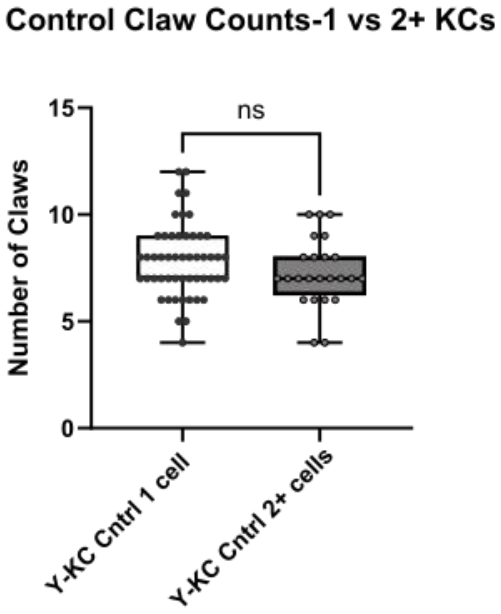
Control Claw Counts-1 vs 2+ KCs
Number of Claws
15
10
5
0
ns
Y-KC Cntrl 1 cell
Y-KC Cntrl 2+ cells

c

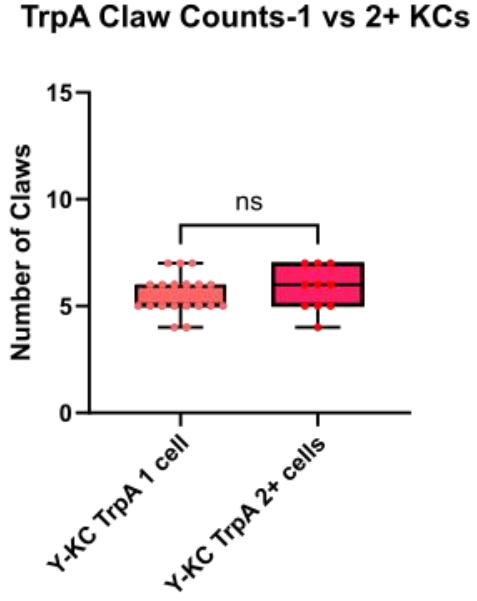
TrpA Claw Counts-1 vs 2+ KCs
Number of Claws
15
10
5
0
ns
Y-KC TrpA 1 cell
Y-KC TrpA 2+ cells

Figure 3.1. Identifying reliable heatshock timing for labelling single Kenyon cells a) Labelling effectiveness in 3 different heatshock timings. The top panel shows the brain of a fly heatshocked for 2 hours, which results consistently in whole MB labelling. Middle panel shows the brain of a fly heatshocked for 40 minutes, which produces labelling of only a few cells but consistently labels 3 per hemisphere, making it more difficult to distinguish and count claws of individual KCs. Bottom panel shows the brain of a fly heatshocked for 35 minutes; this timing consistently produces labelling of only 1 KC per hemisphere and therefore was used for all morphological experiments. All brains were from control flies. Scale bar at bottom left represents 10μm. b) Graph of mean number of claws in control γ KCs across conditions (22°C 4 Days, 31°C 4 Days, 31°C 1 Day, 31°C 12 hours, 31°C 6 hours and Older flies) in hemispheres containing 1 KC vs 2 or more. Individual data points are displayed on associated boxplot which shows the median and interquartile range. Error bars represent the standard deviation of each group. From left to right: Cntrl 1 KC (n=51), Cntrl 2+ KCs (n=24). Significance was evaluated using an unpaired t test with Welch's correction. *P<0.05, **P<0.01, ***P<0.001. c) Graph of mean number of claws in TrpA γ KCs across claw loss conditions (31°C 4 Days and 31°C 1 Day) in hemispheres containing 1 KC vs 2 or more. Individual data points are displayed on associated boxplot which shows the median and interquartile range. Error bars represent the standard deviation of each group. From left to right: TrpA 1 KC (n=19), Cntrl 2+ KCs (n=10). Significance was evaluated using an unpaired t test with Welch's correction.

3.2.2 Developing claw counting criteria

Preliminary analysis of single KCs activated for 4 days appeared to show a reduction in their number of claws. However, I quickly noticed that several other non-claw dendrites were present in images, and without a means to distinguish between these structures and claws, consistency in counts was low. The initial experimental genotype (hsFLP, UASCD8GFP; UASTrpA, UASDα7mCherry/Cyo; FRT82, Gal80/Tm3-Sb; OK107) labelled the Dα7-subunit of nicotinic receptors with mCherry as a method of marking KC claws, which should express these receptors unlike other dendrites (e.g APL-KC synapses) (Parnas, Manoim and Lin, 2024). However, labelling was dim and inconsistent, with only occasional spots in the calyx appearing even in whole MB labelling; due to its lack of effectiveness nearly all experiments used a genotype without this labelling. To attempt to categorically distinguish between claws and non-claws, I later used the primary antibody anti-chAT and a red secondary label to stain against the enzyme choline acetyltransferase (chAT). This enzyme synthesizes acetylcholine and so should be expressed strongly in PN boutons which are cholinergic (Parnas, Manoim and Lin, 2024). However, although effective at labelling these boutons, the number of boutons and diffuse nature of the signalling made it too difficult to determine whether KC dendrites were claws or other dendrites, as most structures were in close proximity to a bouton (Figure 3.2).

To solve this issue and provide consistency in counts across KCs, I developed a criteria for distinguishing between the different dendrite types. Fortunately, during our previous work we analysed the Drosophila hemibrain connectome (Scheffer et al., 2020), and utilised reconstructions of all KCs to investigate correlations in parameters (Abdelrahman, Vasilaki and Lin, 2021). These reconstructions used T-bars to approximate synapses, and the close proximity of PN inputs to them, to characterise claws; this included distinguishing between inputs from different PNs (Figure 3.3). Visualizing reconstructions allowed me to establish key differences in morphology between claws and non-claw dendrites, which informed the creation of a classification criteria. In particular, I divided KC dendrites into four classes: Class 1's (Twigs) which are small processes that are mostly uniform in their volume and extend minimally from their origin, Class 2's (Branches) which can extend from their origin point in similar lengths to claws and typically have enlarged volume at their end, Class 3's (Simple Claws) which demonstrate a typical claw shape, and Class 4's (Complex Claws) which are typically larger than simple claws, have a more complex morphology and often appear to be comprised of multiple claw like structures (Figure 3.3). Based on connectome reconstructions and their associated localization of PN-KC synapses, I divided these four classes into two groups, claws (class 3 and 4) and non-claw dendrites (class 1 and 2).

Upon initial creation of criteria, I reviewed my previous counts and identified that the original inconsistency in counts seemed to arise from two issues. The first was that I was often mischaracterizing class 2's as 3's and vice versa, which produced too much variety in claw counts across images. To ensure I distinguished between these two types a majority of the time, I composed a list of differences along with example images that could be referred to

a

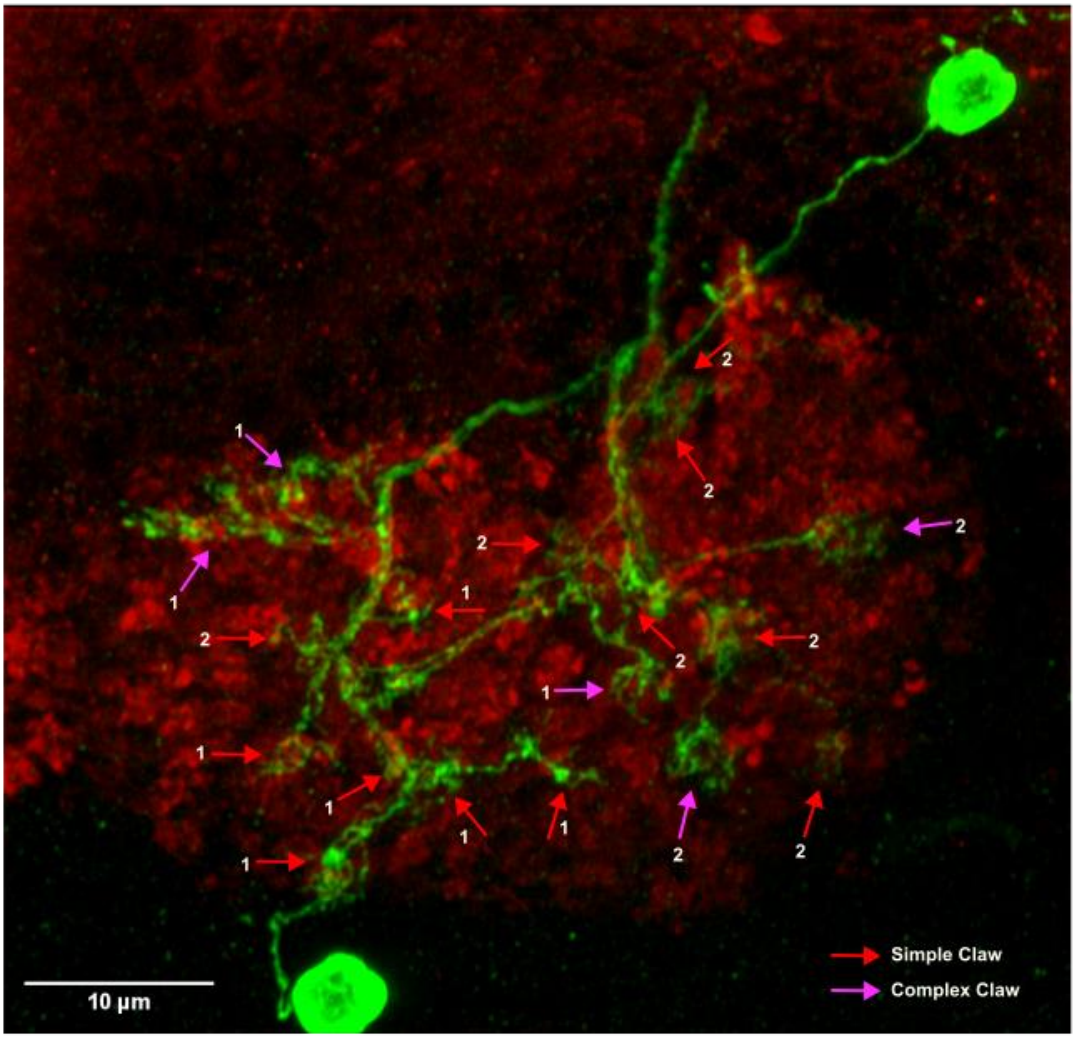

Figure 3.2. a) Ineffectiveness of chAT labelling to identify KC claws. Kenyon cells labelled in green and cholinergic PN boutons labelled in red. Two types of claws are labelled with separate arrows, simple claws (red) and complex claws (magenta). There are two KCs in this image, left cell (1) and right cell (2). Although distinction between 2 KCs is not clear on this 2D image, they can be distinguished in the 3D Z-stack. Calyx is clearly marked by red PN bouton expression area. Within the calyx bouton labelling is fairly uniform and not useful for distinguishing claws from non-claw dendrites. Scale bar represents 10µm.

when counting is performed. The key difference is that class 2's are typically not as large as class 3's and persist across fewer slices with smaller areas per slice. Importantly 'claw shape' is not a consistent predictor of class 3 identity, as several class 3's lack this feature, likely due to the viewing angle of the z stack. Furthermore, class 2's can demonstrate a claw shape

(Figure 3,3), but this limited branching is distinct from the large area that simple claws and complex claws demonstrate.

The second issue is my previous counts made no distinction between simple claws and complex claws, meaning a single complex claw was often characterised as multiple claws; this likely contributed to my increased average claw counts compared to previous findings (Caron et al., 2013) and our connectome analysis (Abdelrahman, Vasilaki and Lin, 2021). The characterisation of complex claws has been previously established (Butcher et al., 2012) and can also be seen in connectome reconstructions (Figure 3.3). These class 4's are often more elaborate than simple claws, either completely lacking a claw shape or appearing to be composed of multiple claws (Figure 3.3). The class 4's lacking a claw shape are easier to characterise as they are fairly uniform and extend across much larger areas than class 3's. However, the complex claws composed of several claw structures are more difficult to distinguish. On connectome reconstructions we can differentiate between these groups on the identity of the PNs they synapse with, e.g. if they synapse with different PNs they are different claws (Figure 3.3). However, as established our method does not provide a way to visualize these synapses effectively. So how can we distinguish multiple simple claws from single complex claws? In an attempt to improve consistency, I used the Freehand line and measurement tools on FIJI and trialled maximum distances along the neurite between 'claws' for them to be considered distinct simple claws and not part of one complex claw. Preliminary analysis revealed that a threshold distance between claws of greater than or equal to 10μm produced control γ KC claw counts closest to those observed in the connectome; counts were only of γ-main KCs which almost exclusively receive olfactory inputs (Scheffer et al., 2020) (Figure 3.3). It is important to note that this threshold does not represent a real biological distance that separates KCs interacting with distinct PNs, but was created to increase consistency while counting and bring control claw counts down to be more in line with the connectome (Scheffer et al., 2020) and consensus in the field (Caron et al., 2013). In a similar vein, I observed that very few claws originating separately from the primary neurite interacted with the same PNs. To account for this, I added an exception to the 10 μm threshold for claws originating from distinct points on the primary neurite. Most claws on a single KC synapse with distinct PNs but do occasionally synapse multiple times with the same bouton. Our experiments have no way to distinguish this possibility, and furthermore it is unclear what the functional reason for synapsing multiple times with a single PN bouton is. I will discuss the implications of this in this section's conclusions, but for simplicity and consistency these claws are always counted separately.

Developing this criteria made counts more consistent and was sufficient to allow others to reproduce my findings. Furthermore, to improve my ability to distinguish between claws, especially in neurons with more convoluted overlapping branching, after my initial experiments I switched to using the Airyscan confocal instead of the 2-photon microscope. Specifically, the Airyscan provides a better Z spatial resolution (Zipfel, Williams and Webb, 2003; Huff, 2015; Doi et al., 2018) which, in combination with its joint deconvolution processing (da Costa, Ralf Engelmann, Martin Gleisner and Lutz Schäfer, Olivia Prazeres, 2021), allowed me to more easily distinguish between claws that were closely associated with each other. All counting was performed blind to the genotype of KCs, ensuring I applied criteria without bias.

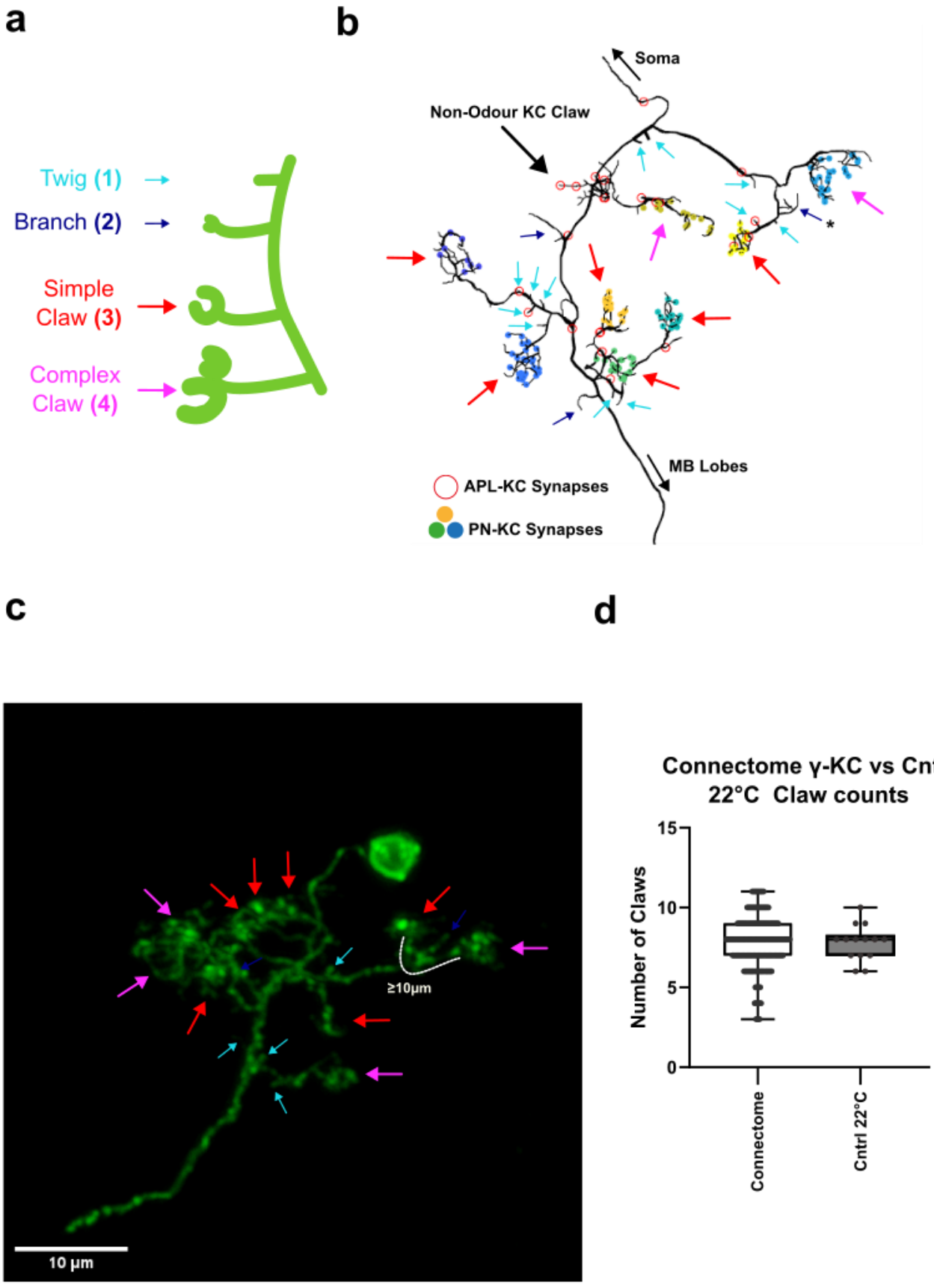
a
Twig (1)
Branch (2)
Simple Claw (3)
Complex Claw (4)
b
Soma
Non-Odour KC Claw
MB Lobes
APL-KC Synapses
PN-KC Synapses
c
≥10µm
10 µm
d
Connectome γ-KC vs Cntrl
22°C Claw counts
Number of Claws
15
10
5
0
Connectome
Cntrl 22°C

Figure 3.3. Kenyon cells counting criteria. **a)** Cartoon depicting examples of the 4 types of dendrite in my classification system: Class 1/Twig, Class 2/Branch, Class 3/Simple Claw, Class 4/Complex Claw. Colours and arrows correspond to labels in b-c. **b)** Example γ KC connectome reconstruction. This reconstruction only includes dendrites, with the direction of the soma and axonal projections to the MB lobes labelled. Synapses from distinct PNs are marked with different colours, while synapses from the APL are highlighted with a red circle. Arrows of different colours depict different classes of dendrites. Only synapses from odour PNs are marked, so non-odour KC claw likely represents synapses with gustatory or visual input. * Depicts a class 2 that has the basic claw shape of a simple claw and could be difficult to distinguish in my images. Key difference is the comparative size of these structures-class 2's are much smaller. **c)** 2-photon image of a 22°C Cntrl γ KC. Different classes of dendrite are labelled. White dotted line shows 2 claws that are further than 10μm apart along the neurite and so are classed as distinct claws and not one complex claw. Worth noting that compared to connectome there are far fewer class 1's, likely due to the lower spatial resolution of light microscope images vs electron microscope images from connectome. Scale bar is 10μm. **d)** Boxplot of γ KC connectome mean claw count (white; n=150) vs 22°C Cntrl counts (grey;n=14). Individual data points are displayed on associated boxplot which shows the median and interquartile range. Error bars represent the standard deviation of each group. **Connectome analysis was performed by Kripi Mehra**.

3.2.3 Prolonged TrpA activation causes a reduction in the number of claws in γ Kenyon cells

Firstly, MARCM was used to label single γ KCs with GFP and TrpA (only in experimental flies) as described in the previous section. Flies were then incubated at 31°C for 4 days to induce prolonged hyperactivity and a control set of flies were kept at 22°C at the same time to confirm any changes were induced by activity increase and not presence of TrpA alone. After 4 days whole brains were quickly dissected, fixed and immunolabelled with anti-GFP to improve visualization of KCs (see 2.2.3 for detail). Once applied to slides, brains were imaged on a 2p or Airyscan confocal and a Z stack across the calyx was performed to capture dendrite morphology in detail, but was ended approximately where the axon entered the pedunculus; this was done to minimize image time and allow for images with high spatial resolution which would be impossible if attempting to capture the whole neuron, with axons that extend across the MB. The identify of these neurons as γ KCs was visually confirmed and noted through the lack of axonal projections into the vertical lobe of the MB, a key feature that makes these neurons distinct from other subtypes (see Results 3.2.8). The morphology of neurons was then visually analysed and compared to identify differences between control and TrpA flies.

Interestingly, γ KCs activated for 4 days demonstrate a reduction in the number of claws (combined simple and complex claw counts) (Figure 3.4). Importantly TrpA flies kept at 22°C

for 4 days showed no change in number of claws, demonstrating this change is due to prolonged activity. One possibility is that these claws are not completely removed but are just partially retracted or reduce their number of synapses and associated volume. To determine if this was true, I also counted the number of non-claw dendrites (combined twig and branch counts) and compared between control and TrpA flies. However, there was no differences in these counts across any groups (Figure 3.4), suggesting these dendrites don't represent intermediate stages between immature and mature synapses, as seen in mammalian spines, but are their own unique structures. Their exact purpose is unclear, with some in connectome reconstructions possessing APL-KC synapses, but many do not; it is possible they synapse with other neuron types present in the MB but that is beyond the scope of this research.

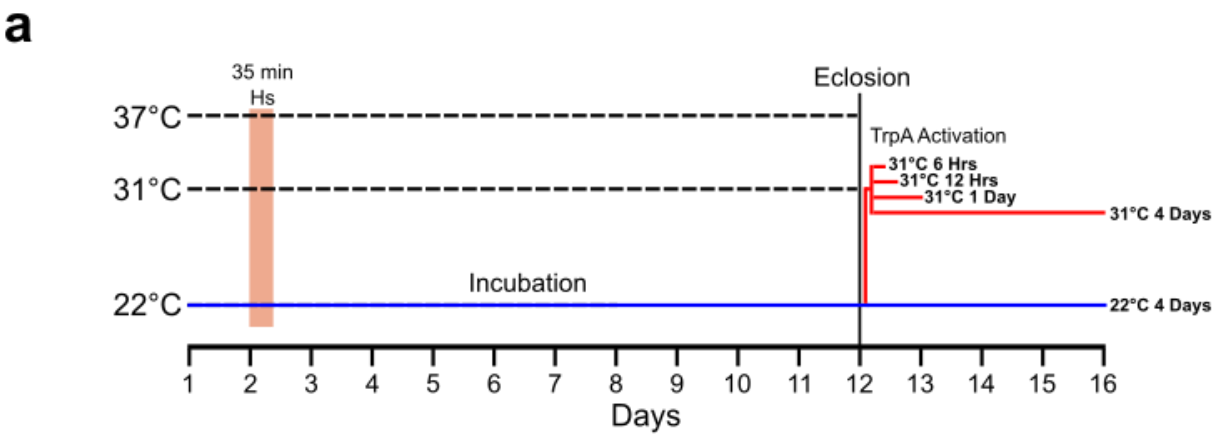
a
35 min
Hs
Eclosion
37°C
31°C
22°C
TrpA Activation
31°C 6 Hrs
31°C 12 Hrs
31°C 1 Day
31°C 4 Days
Incubation
22°C 4 Days
1 2 3 4 5 6 7 8 9 10 11 12 13 14 15 16
Days

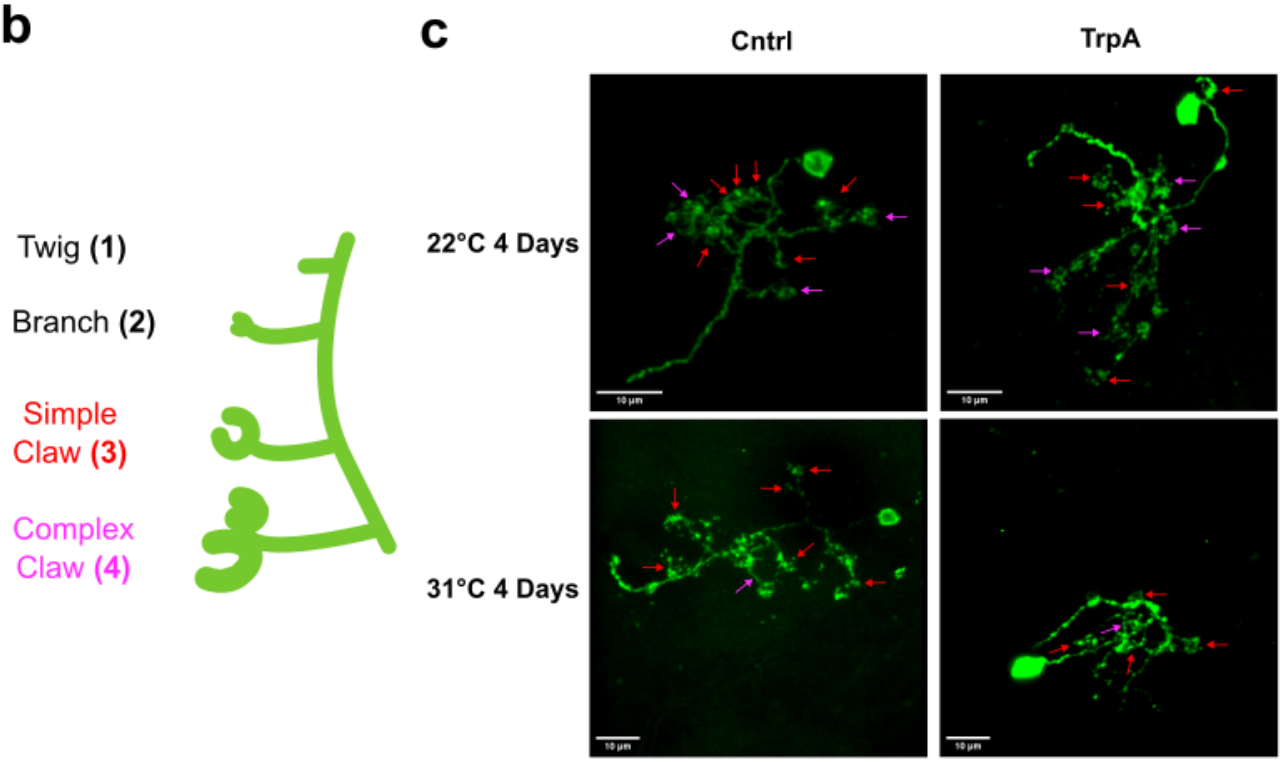
b
Twig (1)
Branch (2)
Simple Claw (3)
Complex Claw (4)
c
Cntrl
TrpA
22°C 4 Days
31°C 4 Days

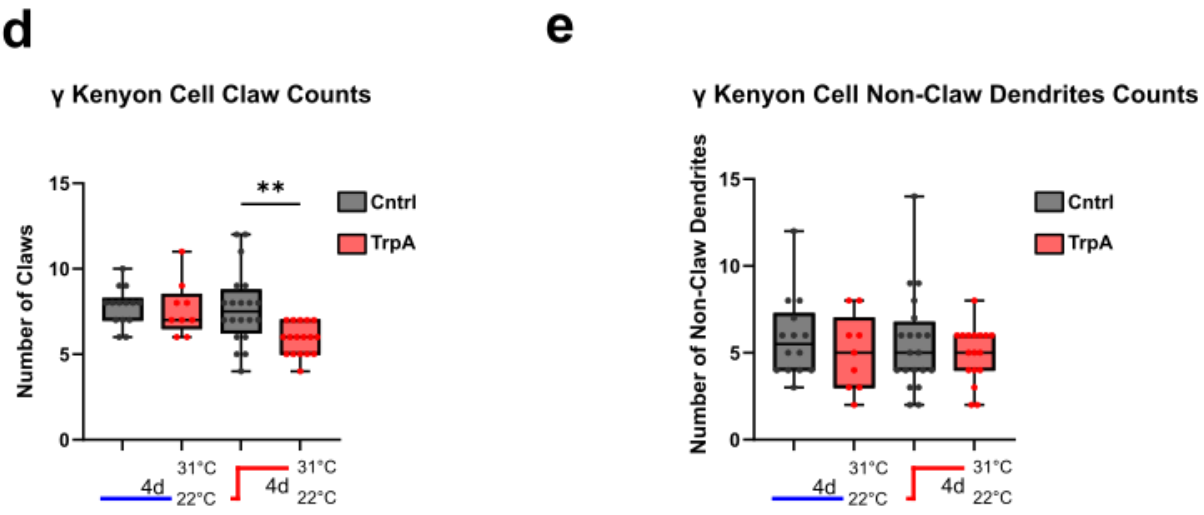
d
γ Kenyon Cell Claw Counts
Number of Claws
15
10
5
0
**
Cntrl
TrpA
4d
31°C
22°C
4d
31°C
22°C
e
γ Kenyon Cell Non-Claw Dendrites Counts
Number of Non-Claw Dendrites
15
10
5
0
Cntrl
TrpA
4d
31°C
22°C
4d
31°C
22°C

Figure 3.4. Kenyon cells hyperactivated for 4 days reduce their number of claws. **a)** Heatshock and incubation protocol for labelling γ KCs. To achieve labelling of single γ KCs vials were heatshocked (Hs) 2 days after egg laying based on developmental timings of this subtype previously established (Lee, Lee and Luo, 1999). Flies were then raised at 22°C until eclosion (~12 days after egg laying). After eclosion flies were then incubated at 22°C for 4 days in the control condition or at 31°C at various timepoints to activate TrpA and test the effect of different periods of hyperactivity on KC dendrite morphology (6 hours, 12 hours, 1 day, 4 days). At the end of the incubation period flies were dissected, fixed and immunolabelled before being later imaged. **b)** Schematic depiction of the different dendrite classes found on KCs. **c)** Example single KCs from 22°C and 31°C 4 days conditions of both genotypes (Cntrl and TrpA). Simple claws are labelled with a red arrow, and complex claws are labelled with a purple arrow. Scale bar in bottom left of images represents 10μm. **d)** Graph of mean number of claws in γ KCs heated for 31°C or 22°C for 4 days. Individual data points are displayed on associated boxplot which shows the median and interquartile range. Error bars represent the standard deviation of each group. From left to right n= Cntrl 22°C 4 Days (13 flies, 14 KCs), TrpA 22°C 4 Days (7 flies, 9 KCs), Cntrl 31°C 4 Days (19 flies, 20 KCs), TrpA 31°C 4 Days (14 flies, 17 KCs). *P<0.05, **P<0.01, ***P<0.001, Generalized Linear Model (GLM) with HC3 heteroscedasticity-consistent standard errors and Wald test post hoc comparisons with Holm-Sidak multiple comparisons correction. **e)** Graph of mean number of non-claw dendrites. Groups, n and statistical analysis as in d.

To determine when exactly this adaptation occurs, I hyperactivated KCs at several other timepoints, successively decreasing the incubation period at 31°C (Figure 3.4). Interestingly one day of TrpA-induced hyperactivity is also sufficient to induce a reduction in number of claws (Figure 3.5). Furthermore, 31°C 1-day TrpA claw counts do not significantly differ from those observed in the 31°C 4 days condition, demonstrating there is no change in the number of claws between 1 day of hyperactivity and 4 days. Importantly, this does not rule out other adaptations occurring during this period, but it seems this reduction in number of claws may have a lower limit. This could suggest that the mechanism responsible for this change has an opposing process that prevents further removal of claws, or there is a biological ‘floor’ for the required number of claws on a KC. In contrast, TrpA flies incubated at 31°C for both 12 hours and 6 hours do not demonstrate a significant reduction in their number of claws (Figure 3.5; Figure 3.6). However, the 12-hour group does appear to show a trend of decreased claw count and decreased non-claw dendrite count. Upon further examination this effect appears to be driven by a higher mean claw count in the control 12-hour group, which significantly differs from the 31°C 1-day controls. A similar significant difference also exists between the non-claw dendrite counts of these conditions. This is supported by the fact that 12 hour TrpA claw counts are significantly higher than those observed in both 1 day and 4 day TrpA flies, suggesting the increased Cntrl claw counts may be a result of increased variability in counts within this group. When comparing within

condition both 31°C 12-hours and 6-hours TrpA flies show no difference in non-claw counts, further demonstrating these dendrites are functionally distinct to claws. Collectively, these results suggest that prolonged hyperactivity for longer than 12 hours is required to induce a loss of claws. However, the logic behind claw removal is unclear. TrpA is theoretically expressed uniformly across KCs (Hamada et al., 2008), so no one claw should be more active than another, making it unlikely only the most active claws are being removed. Furthermore, flies were collected soon after eclosion so it is possible that this adaptation is a result of early flexibility during a CP and not homeostatic plasticity.

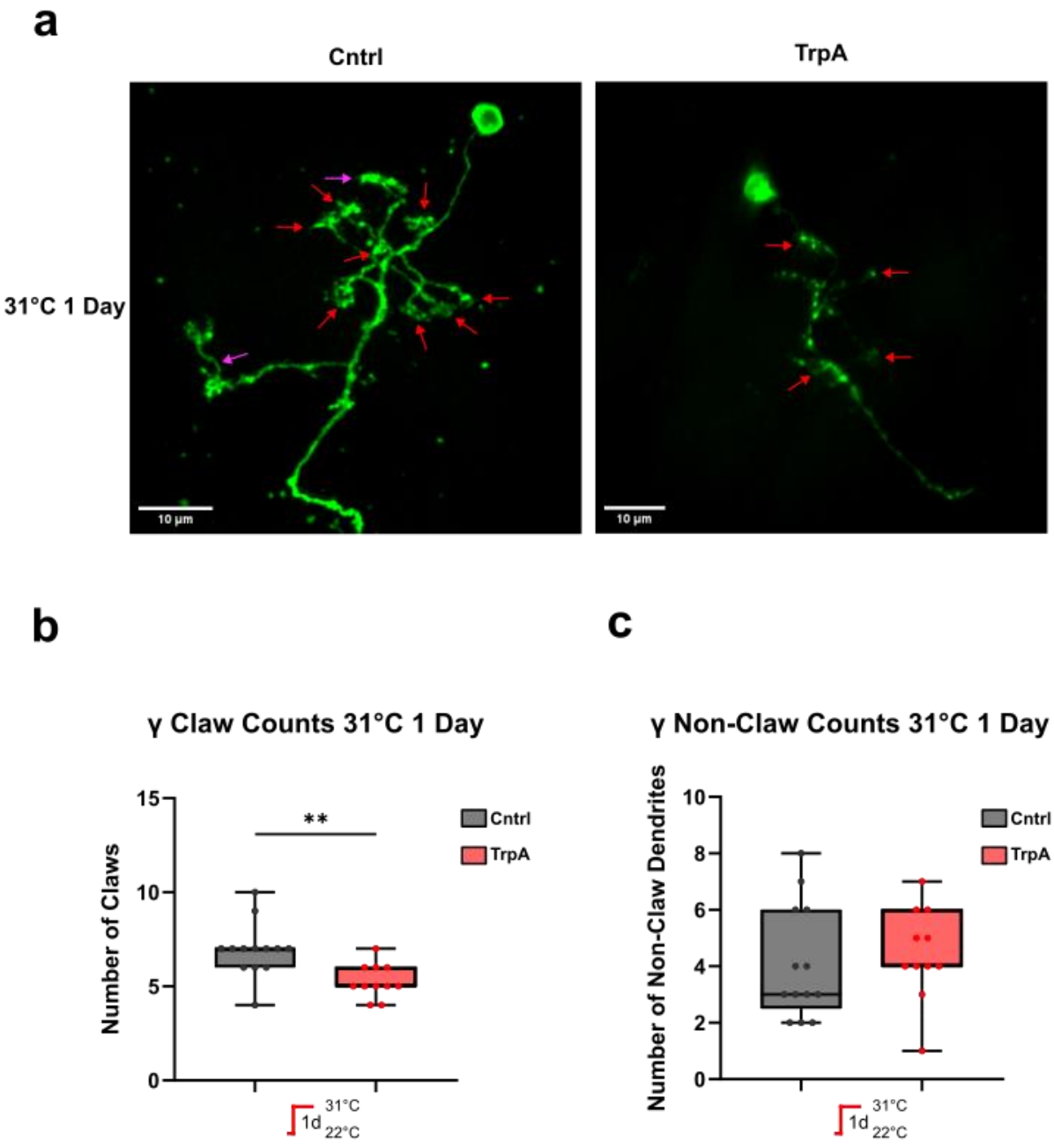

Figure 3.5. Kenyon cells hyperactivated for 1 day also reduce their number of claws. **a)** Example single KCs from 31°C 1 day condition (Cntrl and TrpA). Simple claws are labelled with a red arrow, and complex claws are labelled with a purple arrow. Scale bar in bottom left of images represents 10µm. **b)** Graph of mean number of claws in γ KCs heated for 31°C 1 day. Individual data points are displayed on associated boxplot which shows the median and interquartile range. Error bars represent the standard deviation of each group. From left to right n= Cntrl 31°C 1 Day (11 flies, 13 KCs), TrpA 31°C 1 Day (9 flies, 11 KCs). *P<0.05, **P<0.01, ***P<0.001, Generalized Linear Model (GLM) with HC3 heteroscedasticity-consistent standard errors and Wald test post hoc comparisons with Holm-Sidak multiple comparisons correction. **c)** Graph of mean number of non-claw dendrites. Groups, n and statistical analysis as in b.

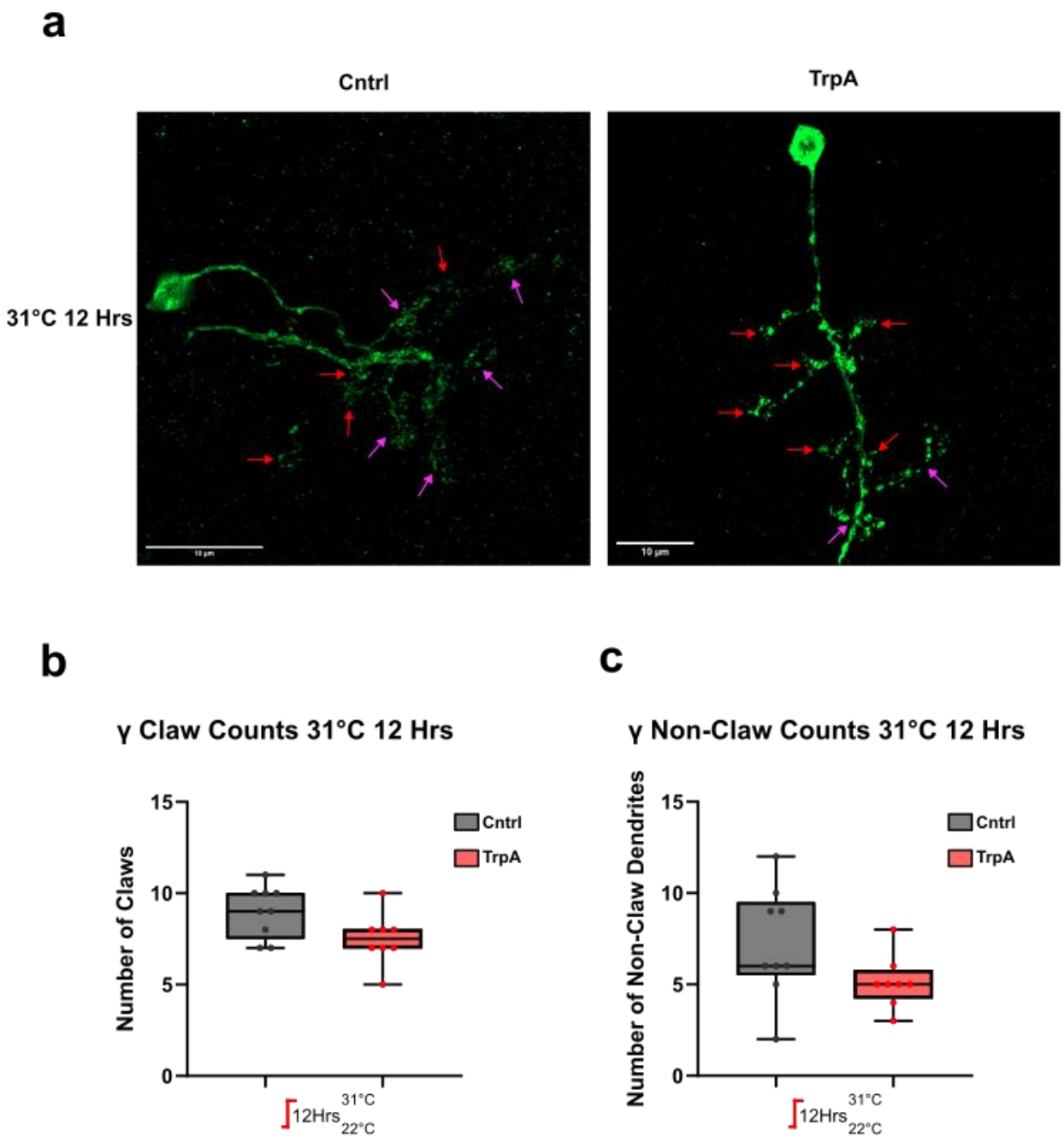

Figure 3.6. Kenyon cells hyperactivated for 12-hours do not reduce their number of claws. **a)** Example single KCs from 31°C 12 hours condition (Cntrl and TrpA). Simple claws are labelled with a red arrow, and complex claws are labelled with a purple arrow. Scale bar in bottom left of images represents 10µm. **b)** Graph of mean number of claws in γ KCs heated for 31°C 12 hours. Individual data points are displayed on associated boxplot which shows the median and interquartile range. Error bars represent the standard deviation of each group. From left to right n= Cntrl 31°C 12 hours (5 flies, 9 KCs), TrpA 31°C 12 hours (7 flies, 8 KCs). *P<0.05, **P<0.01, ***P<0.001, Generalized Linear Model (GLM) with HC3 heteroscedasticity-consistent standard errors and Wald test post hoc comparisons with Holm-Sidak multiple comparisons correction. **c)** Graph of mean number of non-claw dendrites. Groups, n and statistical analysis as in b.

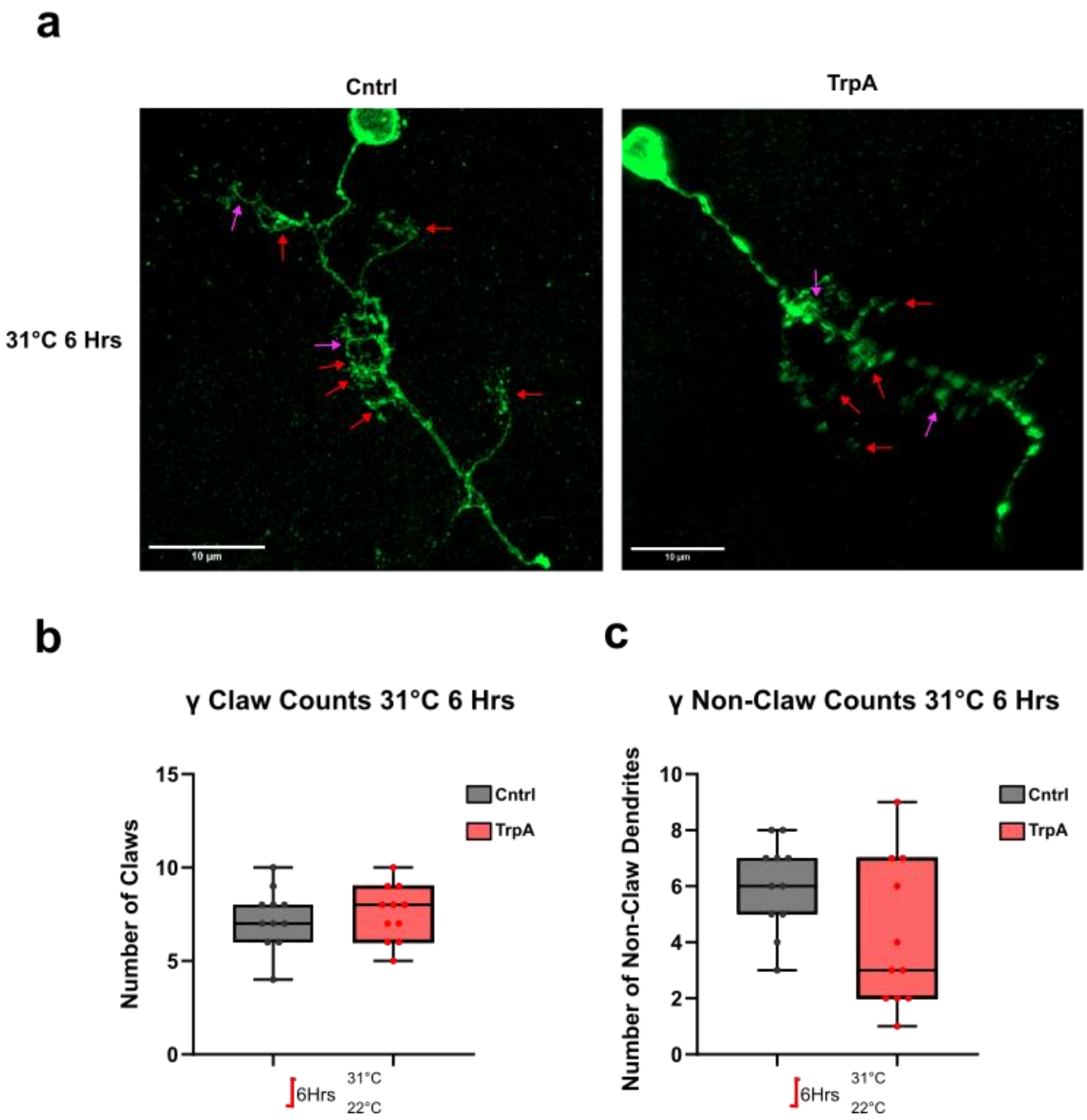

Figure 3.7. Kenyon cells hyperactivated for 6-hours also do not reduce their number of claws. **a)** Example single KCs from 31°C 6 hours condition (Cntrl and TrpA). Simple claws are labelled with a red arrow, and complex claws are labelled with a purple arrow. Scale bar in bottom left of images represents 10μm. **b)** Graph of mean number of claws in γ KCs heated for 31°C 6 hours. Individual data points are displayed on associated boxplot which shows the median and interquartile range. Error bars represent the standard deviation of each group. From left to right n= Cntrl 31°C 6 hours (10 flies, 11 KCs), TrpA 22°C 6 hours (9 flies, 11 KCs). *P<0.05, **P<0.01, ***P<0.001, Generalized Linear Model (GLM) with HC3 heteroscedasticity-consistent standard errors and Wald test post hoc comparisons with Holm-Sidak multiple comparisons correction. **c)** Graph of mean number of non-claw dendrites. Groups, n and statistical analysis as in b.

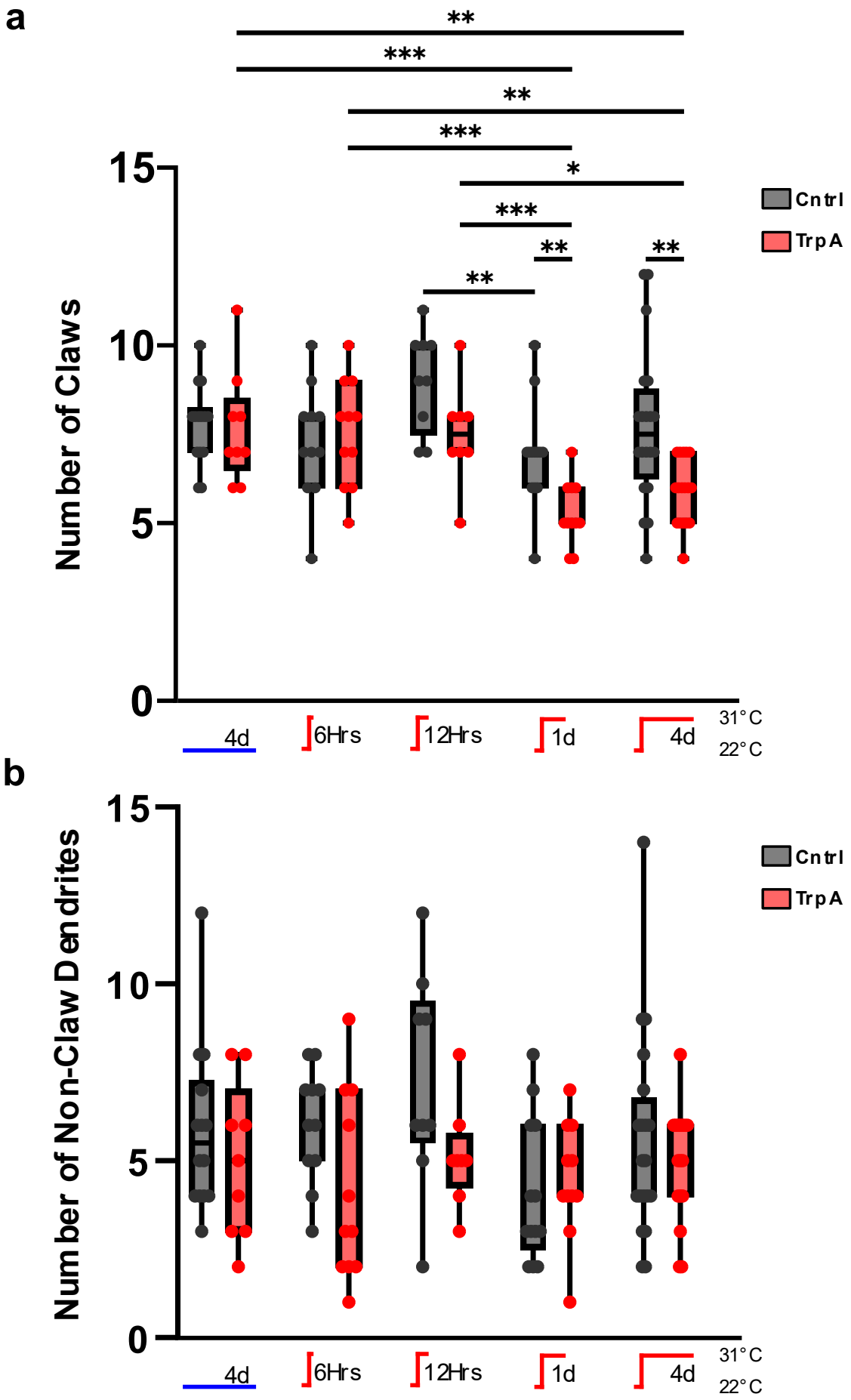
a
**
***
**
***
*
***
**
**
**
15
10
5
0
Number of Claws
Cntrl
TrpA
4d
6Hrs
12Hrs
1d
4d
31°C
22°C
b
15
10
5
0
Number of Non-Claw Dendrites
Cntrl
TrpA
4d
6Hrs
12Hrs
1d
4d
31°C
22°C

Figure 3.8. γ **Kenyon cell claw counts summary**. **a)** Graph of mean number of claws in γ KCs across all timepoints. Individual data points are displayed on associated boxplot which shows the median and interquartile range. Error bars represent the standard deviation of each group. From left to right n= Cntrl 22°C 4 Days (13 flies, 14 KCs), TrpA 22°C 4 Days (7 flies, 9 KCs), Cntrl 31°C 6 hours (10 flies, 11 KCs), TrpA 22°C 6 hours (9 flies, 11 KCs), Cntrl 31°C 12 hours (5 flies, 9 KCs), TrpA 31°C 12 hours (7 flies, 8 KCs), Cntrl 31°C 1 Day (11 flies, 13 KCs), TrpA 31°C 1 Day (9 flies, 11 KCs), Cntrl 31°C 4 Days (19 flies, 20 KCs), TrpA 31°C 4 Days (14 flies, 17 KCs) . *P<0.05, **P<0.01, ***P<0.001, Generalized Linear Model (GLM) with Gaussian family and HC3 heteroscedasticity-consistent standard errors and Wald test post hoc comparisons with Holm-Sidak multiple comparisons correction. **b)** Graph of mean number of non-claw dendrites across all timepoints. Groups, n and statistical analysis as in a.

3.2.4 This adaptation is not just a result of early adult flexibility

It is possible the loss of claws after 1-4 days prolonged hyperactivity is a result of early adult flexibility during the CP 2-4 days post eclosion (Dombrovski and Condron, 2021; Devaud, Acebes and Ferrús, 2001; Devaud, Keane and Ferrús, 2003; Devaud et al., 2003). In fact, this adaptation may not actually be a loss of claws but could result from TrpA KCs growing fewer claws than they usually would during this period. To test this assumption, after eclosion I left flies at 22°C for 4 days before moving them to a 31°C incubator for another 4 days (Figure 3.9). By this point these older flies should be out of the early-adult CP, which allowed me to determine whether the observed effect is due to loss of claws or reduced claw growth. There is still a significant difference in claw counts between control and TrpA flies in older flies, and similarly no difference in number of non-claw dendrites. This demonstrates that (1) the adaptation likely results from loss of claws and (2) this loss does not require early adult flexibility.

These results don’t completely rule out the idea that this adaptation may only be possible early in life. It is still plausible that this potential homeostatic effect, which allows large scale restructuring of the cell’s morphology, is possible earlier in life but begins to fade as flies age. Additionally, there is evidence that mammalian neurons undergo large scale alterations in morphology as they age (Dickstein et al., 2013) and it is also known dysregulation of homeostatic plasticity occurs during this time (Taylor and Jeans, 2021; Radulescu et al., 2023). To test whether this is true, a master’s student (Ya Yu Colin Wong) aged flies for 30 days at 22°C before incubating them at 31°C for 1 day (Figure 3.10). This revealed that much older flies appear to lose the ability to reduce their claws, with no significant difference in claw

count between control and TrpA flies or between Aged 22°C controls and 31°C 4 day controls (p=0.999 and p=0.809) (Figure 3.10). 30 days at 22°C is equivalent to ~21 days at 25°C (Linford et al., 2013) so these flies are less than halfway through their average lifespan. Therefore it is unclear whether the loss of this adaptation means that the prior older fly results only demonstrate claw loss because of early adult flexibility or whether aged KCs lose many homeostatic mechanisms as reported in other systems (Radulescu et al., 2023). Intermediate timepoints between 8 days and 30 days post eclosion would need to be tested to identify when exactly KCs lose this mechanism.

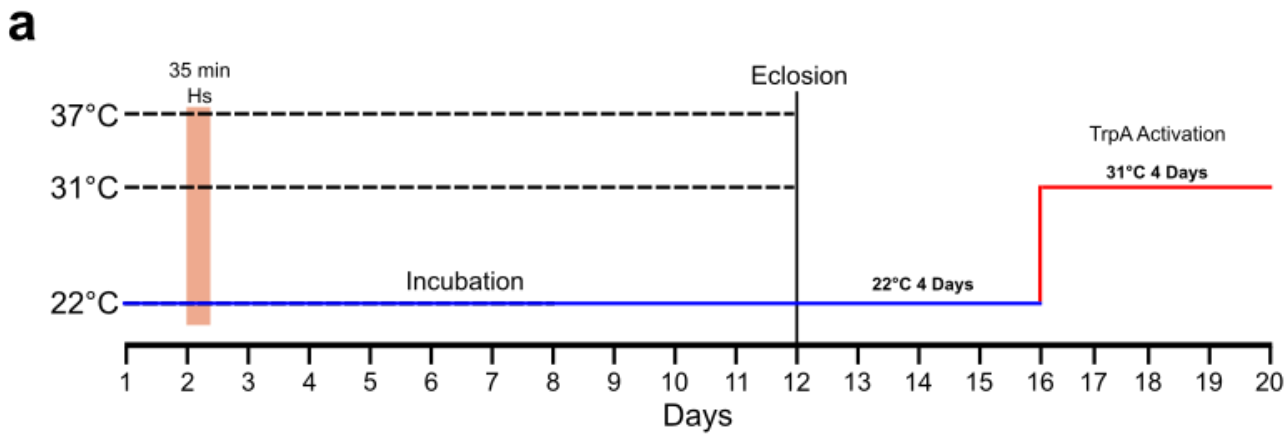
a
35 min
Hs
Eclosion
37°C
31°C
22°C
TrpA Activation
31°C 4 Days
Incubation
22°C 4 Days
1 2 3 4 5 6 7 8 9 10 11 12 13 14 15 16 17 18 19 20
Days

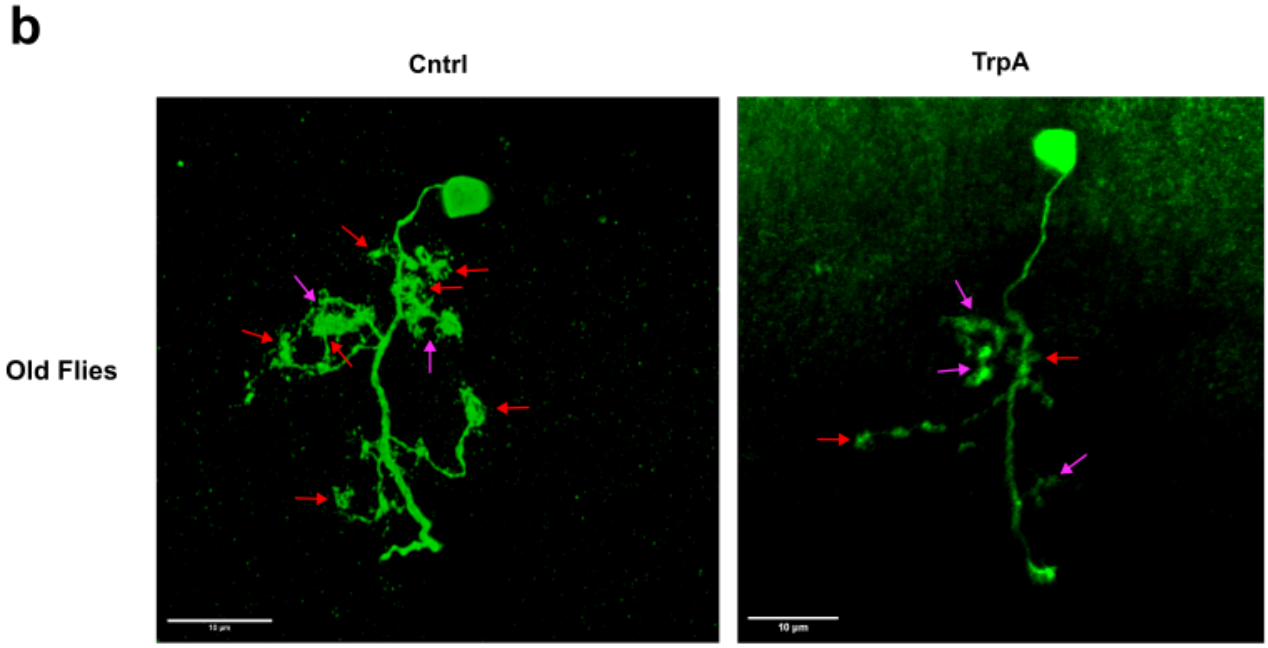
b
Cntrl
TrpA
Old Flies

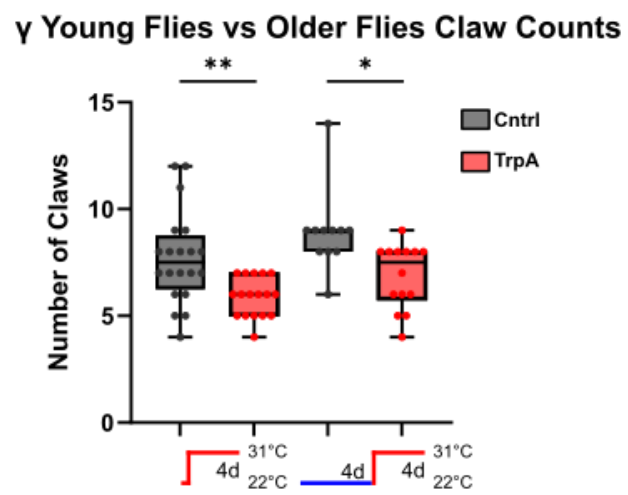
c
γ Young Flies vs Older Flies Claw Counts
**
*
Number of Claws
15
10
5
0
Cntrl
TrpA
4d
31°C
22°C
4d
4d
31°C
22°C

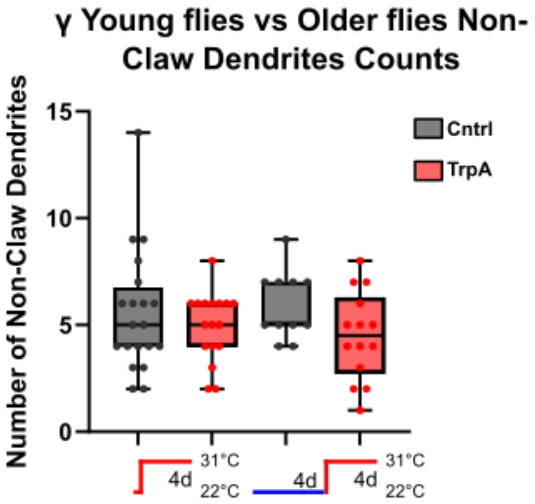
d
γ Young flies vs Older flies Non-Claw Dendrites Counts
Number of Non-Claw Dendrites
15
10
5
0
Cntrl
TrpA
4d
31°C
22°C
4d
4d
31°C
22°C

Figure 3.9. Older fly γ KCs still lose claws after 4 days of hyperactivity. **a)** Heatshock and incubation protocol for Older flies. As before flies were heatshocked 2 days after egg laying to label γ KCs. Flies were then raised at 22°C until eclosion (~12 days after egg laying). After eclosion flies were then incubated at 22°C for 4 days and then moved to 31°C for a further 4 days. At the end of the incubation period flies were dissected, fixed and immunolabelled before being later imaged. **b)** Example single KCs from Older flies' condition (Cntrl and TrpA). Simple claws are labelled with a red arrow, and complex claws are labelled with a purple arrow. Scale bar in bottom left of images represents 10μm. **c)** Graph of mean number of claws in older γ KCs compared to 31°C 4 day flies. Individual data points are displayed on associated boxplot which shows the median and interquartile range. Error bars represent the standard deviation of each group. From left to right n= Cntrl 31°C 4 Days (19 flies, 20 KCs), TrpA 31°C 4 Days (14 flies, 17 KCs), Older Cntrl (11 flies, 11 KCs), Older TrpA (14 flies, 14 KCs). *P<0.05, **P<0.01, ***P<0.001, Generalized Linear Model (GLM) with Gaussian family and HC3 heteroscedasticity-consistent standard errors and Wald test post hoc comparisons with Holm-Sidak multiple comparisons correction. **d)** Graph of mean number of non-claw dendrites in Older flies compared to 31°C 4 day flies. Groups, n and statistical analysis as in c.

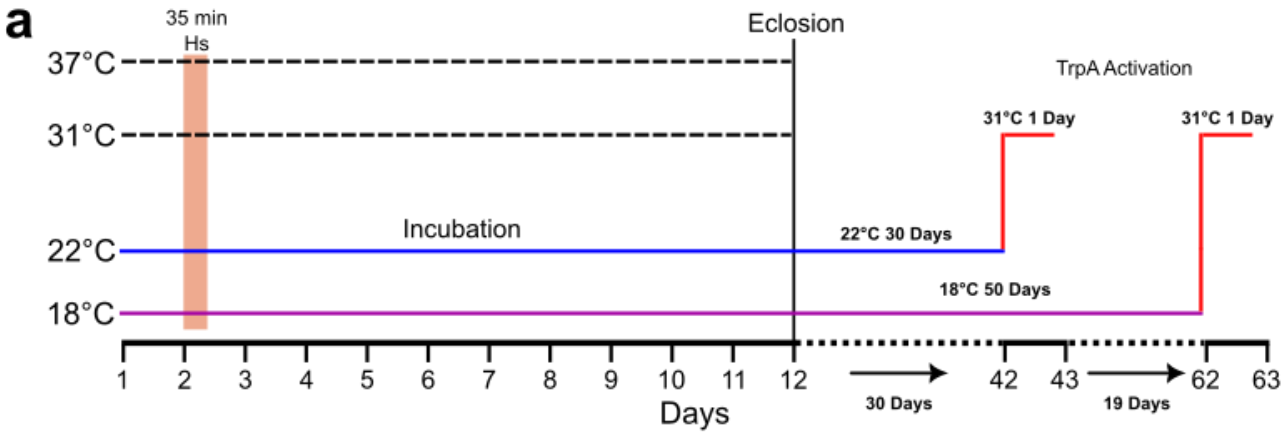

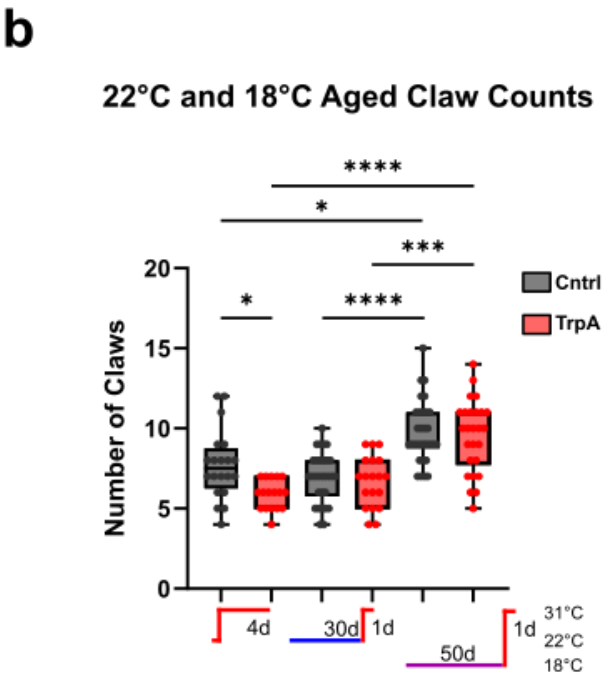

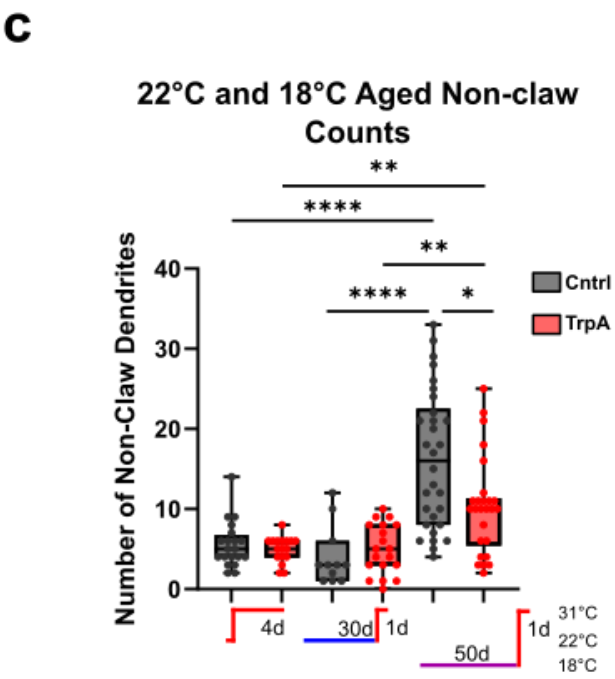

Figure 3.10. Aged fly γ KCs no longer capable of claw loss. **a)** Heatshock and incubation protocol for Aged 22°C and 18°C flies. As before, flies were heatshocked 2 days after egg laying to label γ KCs. Aged 22°C flies were raised at 22°C until eclosion (~12 days after egg laying). After eclosion flies continued to be incubated at 22°C for 30 days and then were moved to 31°C for a further 1 day. Aged 18°C flies were raised at 18°C until eclosion (~16 days after egg laying). After eclosion flies continued to be incubated at 18°C for 50 days and then were moved to 31°C for a further 1 day. At the end of the incubation period flies were dissected, fixed and immunolabelled before being later imaged. **b)** Graph of mean number of claws in Aged 22°C and Aged 18°C compared to 31°C 4 day flies. Individual data points are displayed on associated boxplot which shows the median and interquartile range. Error bars represent the standard deviation of each group. From left to right n= Cntrl 31°C 4 Days (19 flies, 20 KCs), TrpA 31°C 4 Days (14 flies, 17 KCs), Aged 22°C Cntrl (11 KCs), Aged 22°C (19), Aged 18°C Cntrl (30), Aged 18°C TrpA (26). *P<0.05, **P<0.01, ***P<0.001, ***P<0.0001, Generalized Linear Model (GLM) with Gaussian family and HC3 heteroscedasticity-consistent standard errors and Wald test post hoc comparisons with Holm-Sidak multiple comparisons correction; comparisons were performed within condition and between all Cntrls and all TrpA's separately. **c)** Graph of mean number of non-claw dendrites in Older flies compared to 31°C 4 day flies. Groups, n and statistical analysis as in c. **All experiments were performed by Ya Yu C Wong**

Due to some concerns surrounding TrpA's activating temperature, Ya Yu Colin Wong also raised flies at 18°C, collected them after eclosion and continued to keep them at 18°C for 50 days before moving them to 31°C for 1 day. We were concerned that the TrpA channel may be slightly open at 22°C, making labelled KCs slightly active during development; more on this issue in Section 4. Similar to Aged 22°C flies, Aged TrpA 18°C flies that were hyperactivated for 1 day show no significant difference in claw number compared to controls. As before, it is possible this is due to loss of homeostatic mechanisms with age or that KCs are only capable of this adaptation earlier in life. It is also worth considering that although 1 day may not be sufficient to induce claw loss in Aged flies, it is possible that hyperactivating neurons for longer may be required to induce this adaptation. Surprisingly, these flies raised at 18°C also show significant differences in both Cntrl and TrpA claw and non-claw dendrite counts compared to Aged 22°C and 31°C 4 day flies. Overall, these average counts are significantly higher in 18°C flies, although there is a small significant difference in non-claw counts between Cntrl and TrpA flies within this condition. It is clear that this overall increase is likely nothing to do with TrpA activation as both conditions are much higher than in flies incubated at 22°C and 31°C. The most likely reason for this drastic difference is probably being at 18°C during development as it has been previously shown that Drosophila neurons grow more synapses when developing at cooler temperatures (Kiral et al., 2021). This factor

will need to be considered when discussing results in Section 3 as if TrpA is still open at 22°C it makes an 18°C incubation potentially problematic.

3.2.5 This adaptation is not reversable

I next wanted to determine whether loss of claws was reversible. To do this I incubated flies at 31°C for 1 day before moving them back to 22°C for a further day (Figure 3.11). This revealed that TrpA flies still demonstrate a decreased claw count after a 1 day recovery period (Figure 3.11). As with other conditions, there was still no change in non-claw dendrite count (Figure 3.11). There are two possible explanations for this. The first, is that loss of claws is an extreme solution to continued hyperactivity that other mechanisms may not have been able to reverse. Loss of claws may represent an end point in a homeostatic pathway or set of pathways containing many less extreme mechanisms that attempt to restore the neurons set activity. Claw loss may be a ‘last resort’ and because the breakdown of claws is costly and the recreation/formation of new claws likely even more so, this adaptation is not reversable. Alternatively, it is possible that a longer period without TrpA activation is required to allow restorative mechanisms to take effect or may require perturbations that completely silence the cell before these mechanisms are activated. At the very least these experiments reveal that claws are not easily restored and raises some further interesting questions about how homeostatic loss or increase in number of claws would influence the neurons activity.

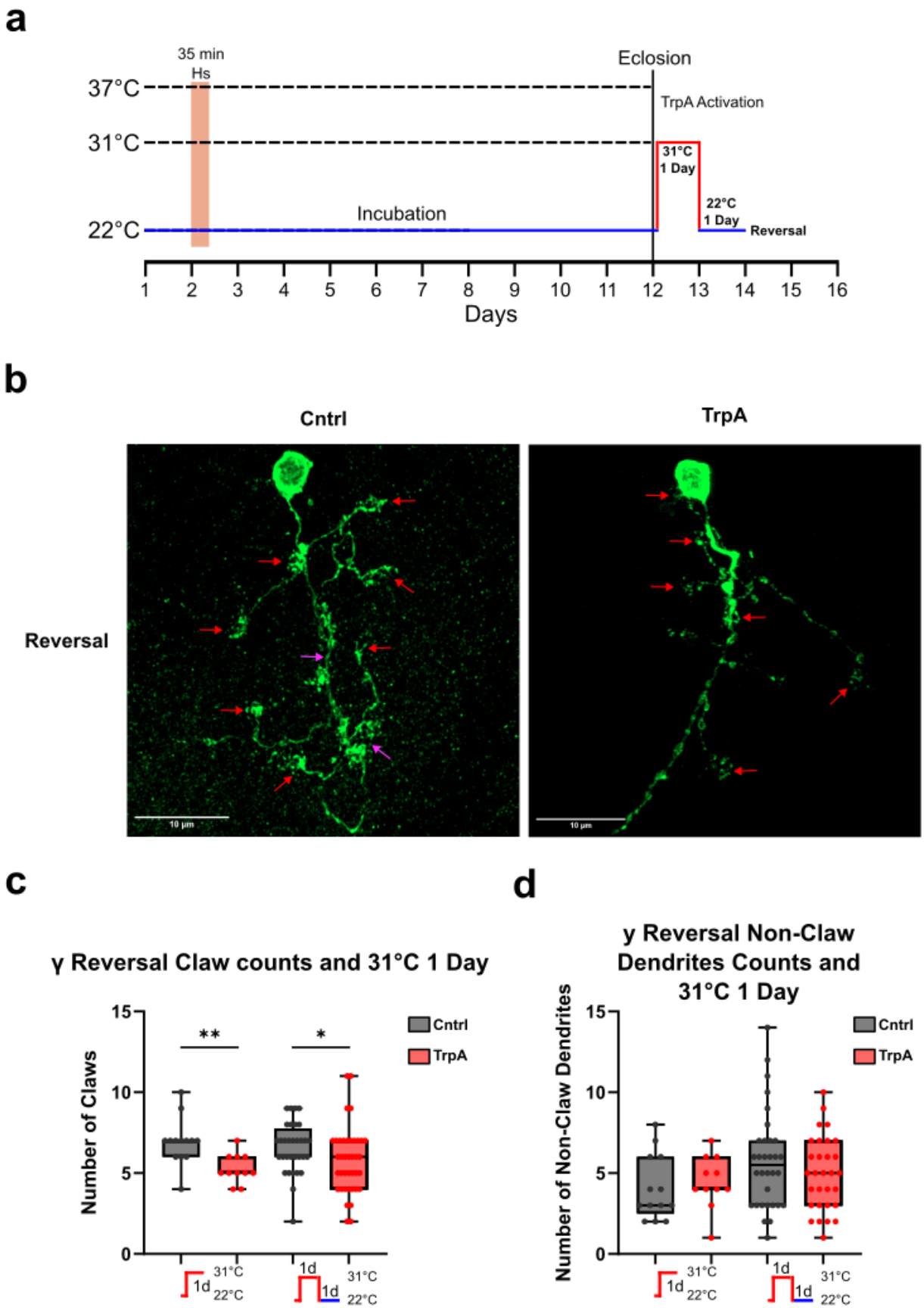
a
35 min
Hs
Eclosion
37°C
31°C
22°C
TrpA Activation
31°C
1 Day
22°C
1 Day
Reversal
Incubation
1 2 3 4 5 6 7 8 9 10 11 12 13 14 15 16
Days
b
Cntrl
TrpA
Reversal
10 µm
10 µm
c
γ Reversal Claw counts and 31°C 1 Day
Number of Claws
15
10
5
0
**
*
Cntrl
TrpA
1d
31°C
22°C
1d
1d
31°C
22°C
d
γ Reversal Non-Claw Dendrites Counts and 31°C 1 Day
Number of Non-Claw Dendrites
15
10
5
0
Cntrl
TrpA
1d
31°C
22°C
1d
1d
31°C
22°C

Figure 3.11. Claw loss adaptation is not reversible. **a)** Heatshock and incubation protocol for Reversal flies. As before, flies were heatshocked 2 days after egg laying to label γ KCs. Aged 22°C flies were raised at 22°C until eclosion (~12 days after egg laying). After eclosion flies were moved to 31°C for 1 day and then moved back to 22°C for a further day. **b)** Example single γ KCs from Reversal condition (Cntrl and TrpA). Simple claws are labelled with a red arrow, and complex claws are labelled with a purple arrow. Scale bar in bottom left of images represents 10µm. **c)** Graph of mean number of claws in Reversal flies compared to 31°C 1 day flies. Individual data points are displayed on associated boxplot which shows the median and interquartile range. Error bars represent the standard deviation of each group. From left to right n= Cntrl 31°C 1 Day (13), TrpA 31°C 1 Day (11) Cntrl Reversal (32), TrpA Reversal (30). *P<0.05, **P<0.01, ***P<0.001, Generalized Linear Model (GLM) with Gaussian family and HC3 heteroscedasticity-consistent standard errors and Wald test post hoc comparisons with Holm-Sidak multiple comparisons correction. **d)** Graph of mean number of non-claw dendrites in Reversal flies compared to 31°C 1 day flies. Groups, n and statistical analysis as in c. **Half of the dissection and imaging experiments were performed by Ya Yu C Wong**

3.2.6 Starvation and sugar only diet prevent activity-dependent reduction in claws

Continuing along the lines of the theoretical energy intensive requirements of completely removing claws, we also wanted to determine whether this adaptation would be prevented by loss of incoming sugar and protein. To test this a placement student, master's student and I starved flies after eclosion by placing them in 1% agar vials on filter paper containing 125µl dH2O for 1 day at 31°C (Figure 3.12) (Chaw C Yi, Ya Yu C Wong**)**. Additionally, to separate out fly's requirement for new protein vs sugar for energy production, we performed a sugar only condition; flies were placed in 1% agar vials on filter paper containing 125µl glucose solution. This revealed that Sugar only flies no longer reduce their claws after prolonged hyperactivation (Figure 3.12). In contrast, completely Starved flies still show a slight non-significant reduction in their number of claws (p=0.0735) (Figure 3.12) with no significant interaction between genotype and condition on a GLM (p=0.199). This weaker effect could suggest that under starved conditions the mechanism which drives claw removal is partially suppressed, enough to reduce the likelihood of claw removal in response to hyperactivity but not to prevent it entirely. This could further imply that new protein is partially required for the mechanism responsible and this has some support in the literature. For example, It is already well established that protein synthesis is required for memory formation across organisms (Park and Kaang, 2019; Wang et al., 2023). Furthermore, we have already discussed that alterations in protein expression and synthesis of new relevant proteins (e.g. AMPARs) is required for homeostatic plasticity in mammalian circuits (Dieterich et al., 2006; Arendt, Sarti and Chen, 2013; Schanzenbächer et al., 2016; Mendez et al., 2018; Schanzenbächer,

Langer and Schuman, 2018). However, it is currently unknown whether the same is true in Drosophila. Further complicating matters, TrpA flies in the Sugar only condition completely lose the ability to remove claws. These flies are lacking protein, but that is also true of the Starvation condition and yet they show distinct effects. The lower sample size in the Sugar only condition could be limiting our ability to detect an effect, but preliminary findings show a clear lack of difference between Cntrl and TrpA flies (Figure 3.12). It is possible complete starvation activates distinct pathways that interact with claw loss mechanisms differently than loss of protein alone, although why this would be the case is unclear.

It is important to acknowledge that the starvation condition does not block protein synthesis and instead likely reduces the availability of key amino acids that may be required for pathways required for claw loss. Additionally, the length of starvation tested (1 day) is probably not sufficient to deplete energy stores, leaving us unable to determine whether this may play a role in claw removal. Previous work has suggested that energy availability may play a role in determining the balance of aversive vs appetitive memory formation (Plaçais and Preat 2013; Jiang, Foyard, and van Rossum 2024). KCs also utilise adjacent glial cells to sustain aversive memory under starvation conditions, further supporting the idea that energy is an essential requirement for plasticity in these neurons (Silva et al., 2022). This last result in particular is important as it supports the idea that 1 day starvation is not sufficient to deplete these neurons energy stores. Ultimately, these results preliminarily suggest that protein may be partially required for activity-dependent loss of claws. Further experimentation (3.33) is required to confirm this relationship.

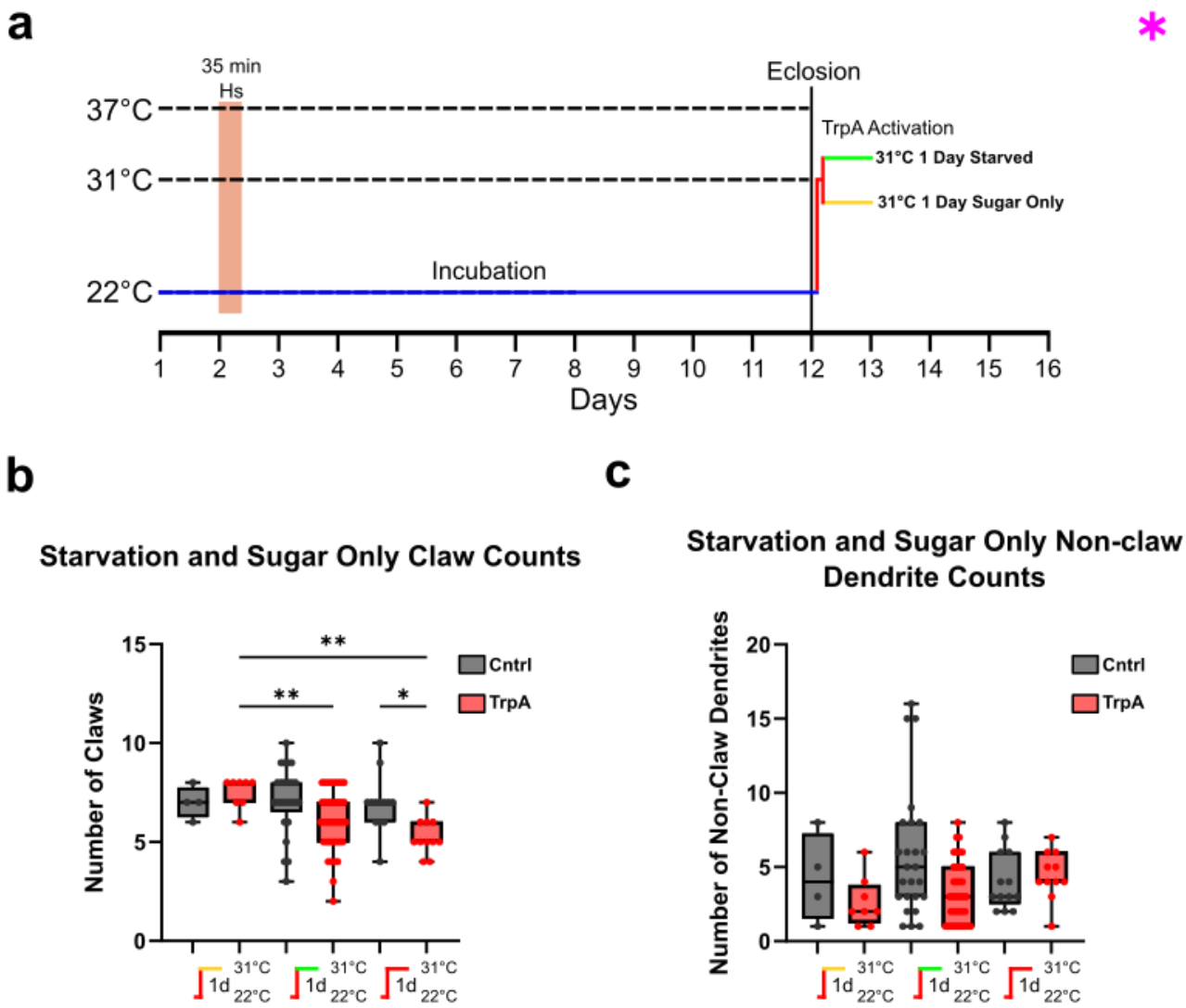

Figure 3.12. Claw loss adaptation requires new protein. **a)** Heatshock and incubation protocol for Reversal flies. As before, flies were heatshocked 2 days after egg laying to label γ KCs. Starved flies were moved to a 31°C incubator and placed in 1% agar vials, on filter paper with 125µl of dH2O. Similarly, Sugar only flies were moved to the 31°C incubator but were placed in 1% agar vials on filter paper with 125µl of glucose. After 1 day at 31°C both were dissected, fixed and labelled. **b)** Graph of mean number of claws in Starved and Sugar only flies compared to 31°C 1 day flies. Individual data points are displayed on associated boxplot which shows the median and interquartile range. Error bars represent the standard deviation of each group. From left to right n= Cntrl Sugar only (4 KCs), TrpA Sugar only (8 KCs), Cntrl Starved (25), TrpA Starved (38) (Cntrl 31°C 1 Day (13 KCs), TrpA 31°C 1 Day (11 KCs). *P<0.05, **P<0.01, ***P<0.001, Generalized Linear Model (GLM) with Gaussian family and HC3 heteroscedasticity-consistent standard errors and Wald test post hoc comparisons with Holm-Sidak multiple comparisons correction. **c)** Graph of mean number of non-claw dendrites in Starved and Sugar only flies compared to 31°C 1 day flies. Groups, n and statistical analysis as in c. **Experiments were performed by Chaw C Yi, Ya Yu Colin Wong and I.**

3.2.7 Does length of dendrites inform which claws are removed?

To ascertain if the morphology of claws or overall dendrites may be influencing the 'choice' of which claws are removed, I traced individual KCs using the simple neurite tracer (SNT) plugin on FIJI (Arshadi et al., 2021); some images with multiple KCs were not traced due to difficulty of overlapping dendrites. I used this software to semi-automate the tracing of KCs to produce skeletons of each neuron (Figure 3.13) that could then be analysed further (Methods). Neurons were traced from the end of the soma to the start of the AIS based on approximation of entry into the pedunculus and forking points were then created to trace dendrites branching off the primary neurite. To further improve the accuracy of tracing, I used SNT's Refine Paths feature on all traces and then used SNT's built in analyses to analyse these traces and investigate their morphology further.

One potential basis for claw removal could be the length of claw dendrites, with claws that are shorter or longer being removed before others. For example, shorter dendrites could be removed first because it is easier for the cytoskeletal machinery to retract them, e.g. overall fewer proteins to remove/degrade. Alternatively, if we assume the goal of this adaptation is homeostatic and therefore any changes need to act to reduce activity, it is possible degrading shorter claws while sparing longer ones could result in a decreased spike likelihood. Leaving the neuron with only claws above a certain length, would mean the total mean distance EPSPs now have to travel to reach the AIS could increase, potentially reducing probability of summation. The combination of fewer claws and a longer mean distance for EPSPs at these claws to propagate would theoretically be quite powerful at reducing the neurons activity, assuming no opposing adaptations occur. To determine if length influences this mechanism, I compared the mean and summed length of claw and non-claw dendrites. Mean claw length did not significantly differ between control and TrpA flies incubated at 31°C for 4 days (Figure 3.6) or in the 22°C 4 day control condition (Figure 3.14). Summed length of 31°C 4 day TrpA flies did significantly differ to controls, but this is expected given they have fewer claws (Figure 3.15). The non-claw mean and summed path lengths also did not significantly differ in TrpA flies raised at 31°C. Furthermore, 31°C 1 Day TrpA flies show no difference in mean or summed claw or non-claw length compared to controls, supporting the idea that path length does not influence which claws are removed.

Control flies raised at 22°C have significantly lower mean non-claw lengths than 22°C TrpA flies and 31°C 4 day control flies. The lack of any difference between TrpA 22°C flies and all other TrpA flies across conditions suggests this effect is primarily driven by a lower Cntrl non-claw count. Therefore, it is unlikely this represents a real biological difference unless

incubation at 22°C during adulthood reduces the length of these dendrites in a temperature-dependent manner, and this is countered by neuron activity driven by slight TrpA channel opening; this assumes this channel is partially open at 22°C, which is not supported by previous results (Hamada et al., 2008; Lin et al., 2014; Apostolopoulou and Lin, 2020) but is possible given findings in Section 4. Without any additional evidence this conclusion seems unlikely and for now it is reasonable to conclude that the 'decision' of which claws to remove is not driven by the length of claws.

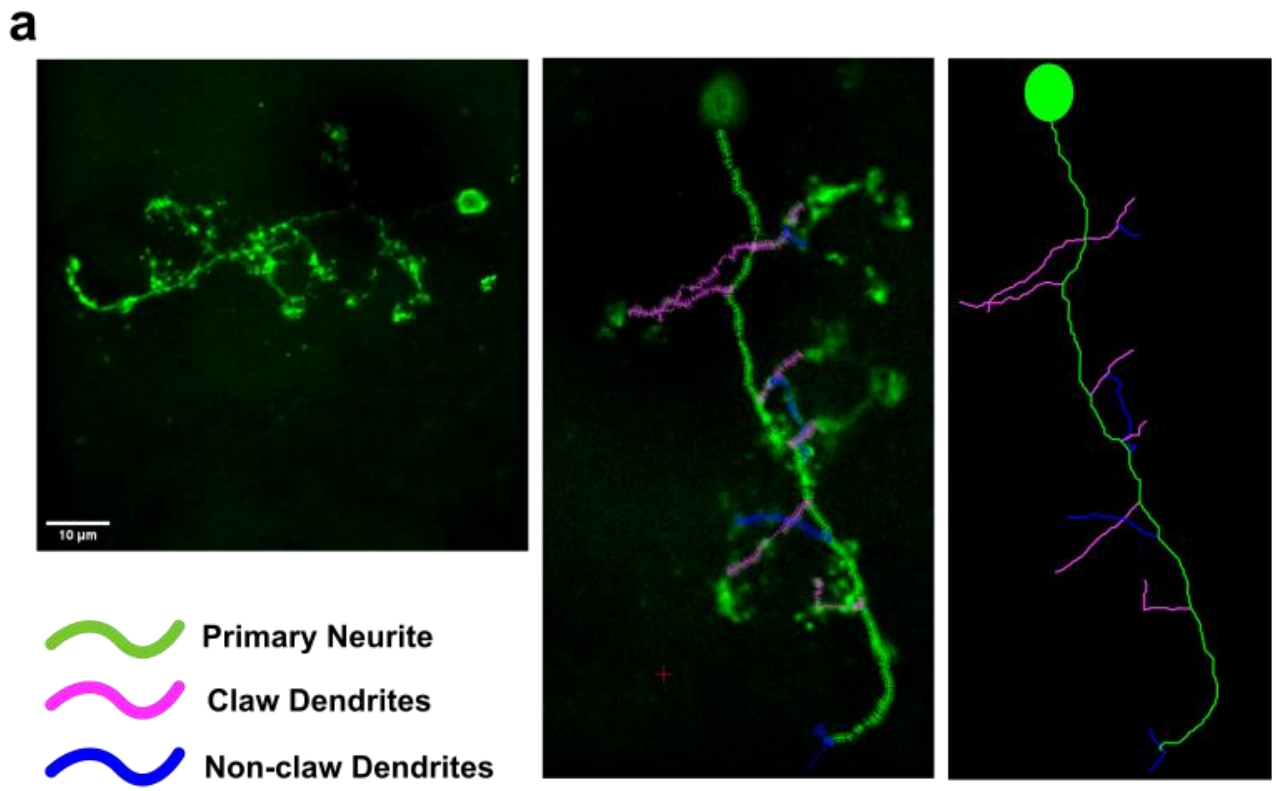

Figure 3.13. Kenyon cell tracing and skeleton creation method a) Example KC and associated trace. Primary neurite (green) is traced first from the end of the soma to the ~beginning of axon entry into pedunculus. Fork points are created from the primary neurite from which associated claw (magenta) and non-claw (blue) dendrites can be traced. Paths are refined and filled via SNTs Assign fitted radii and Snap node coordinates feature, results seen in panel 2. Measurements are then taken from this final trace. Panel 3 shows the trace alone without associated image. Scale bar in bottom left of panel 1 represents 10µm.

a

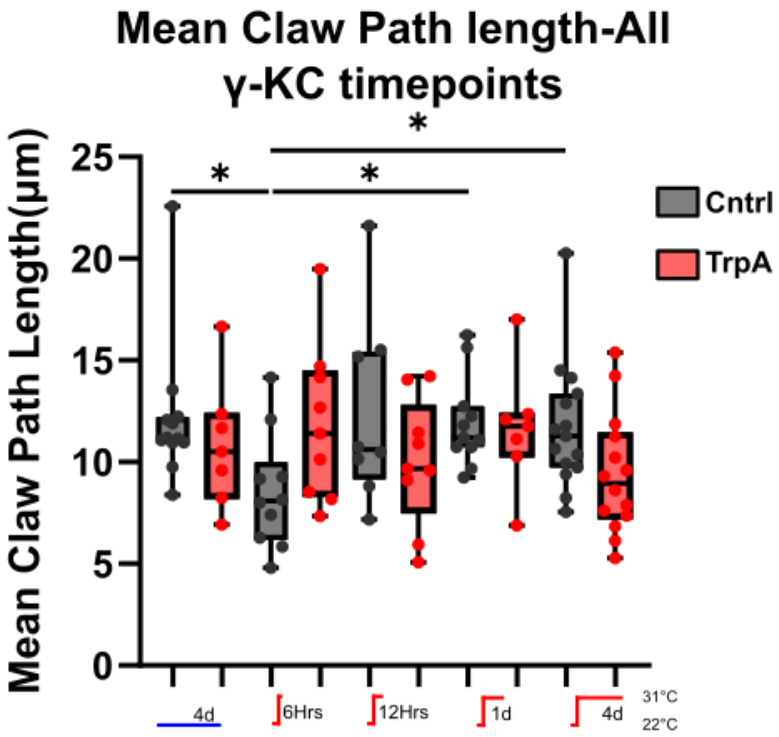
Mean Claw Path length-All
γ-KC timepoints
Mean Claw Path Length(μm)
25
20
15
10
5
0
*
*
*
Cntrl
TrpA
4d
6Hrs
12Hrs
1d
4d
31°C
22°C

b

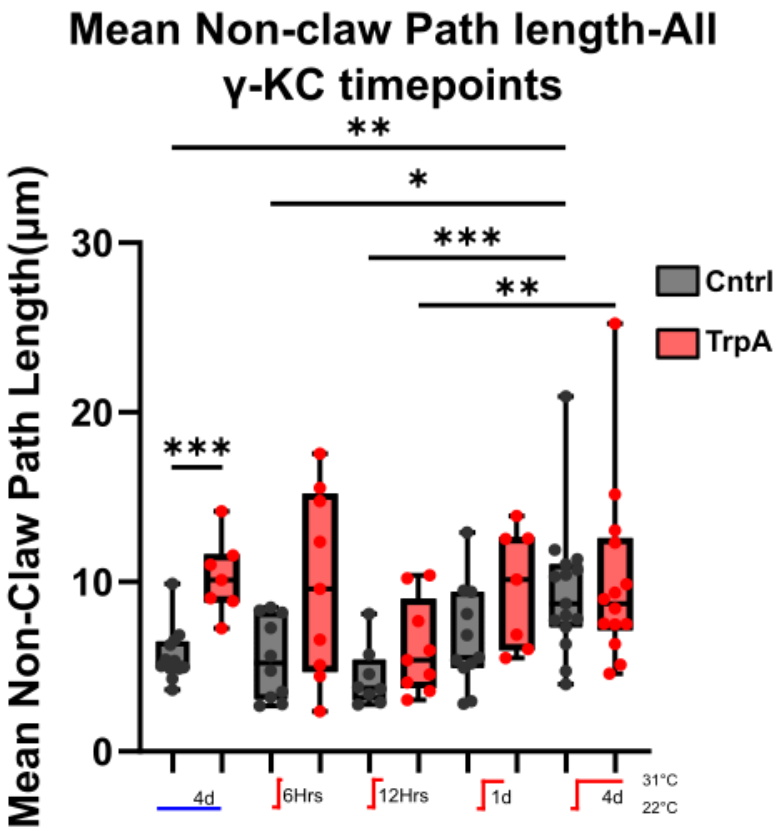
Mean Non-claw Path length-All
γ-KC timepoints
Mean Non-Claw Path Length(μm)
30
20
10
0
**
*
***
**
***
Cntrl
TrpA
4d
6Hrs
12Hrs
1d
4d
31°C
22°C

Figure 3.14. Tracing Kenyon cells hyperactivated for 1-4 days reveals no difference in mean path length of remaining claws. **a)** Graph of mean claw path length in γ KCs at all timepoints; control (grey) and TrpA (red) flies; conditions represented by associated figures beneath x axis. Individual data points are displayed on associated boxplot which shows the median and interquartile range. Error bars represent the standard deviation of each group. Images containing multiple KCs were sometimes not traced due to difficulty of overlapping dendrites. From left to right n= Cntrl 22°C 4 Days (11 flies, 12 KCs), TrpA 22°C 4 Days (7 flies, 7 KCs), Cntrl 31°C 4 Days (15 flies, 15 KCs), TrpA 31°C 4 Days (12 flies, 14 KCs), Cntrl 31°C 6 hours (9 flies, 10 KCs), TrpA 31°C 6 hours (7 flies, 9 KCs), Cntrl 31°C 12 hours (4 flies, 8 KCs), TrpA 31°C 12 hours (8 flies, 9 KCs), Cntrl 31°C 1 day (9 flies, 11 KCs), TrpA 31°C 1 day (6 flies, 7 KCs). *P<0.05, **P<0.01, ***P<0.001, Generalized Linear Model (GLM) with HC3 heteroscedasticity-consistent standard errors and Wald test post hoc comparisons with Holm-Sidak multiple comparisons correction. **b)** Graph of mean non-claw dendrite path length in γ KCs. Groups, n and statistical analysis for all graphs match those seen in a.

Although activity-dependent claw loss does not occur at other timepoints, is it possible that these KCs may adjust the length of dendrites without claw loss? For example, claws may be retracted first before being degraded, which would show up as a lower mean claw length in these KCs. Control flies incubated at 31°C for 6 hours have a mean claw path length significantly lower than control flies at 22°C 4 days, 31°C 1 day and 31°C 4 days but not 31°C 12 hours (Figure 3.14). Additionally, although not significant after correction, these flies seem to demonstrate slightly lowered mean path length than their TrpA counterparts, further supported by the high degree of similarity between TrpA 31°C 6 hour flies and TrpA flies at all other timepoints (Figure 3.14). Furthermore, the mean length of non-claw dendrites in both 6 and 12 hour controls is significantly lower than 31°C 4 day controls and, although not significant, appear to be lower than 1 day controls also (Figure 3.14). Importantly, although both 31°C 6 hour and 12 hour flies experience shorter periods of hyperactivity than 31°C 1 day flies, these flies are all ~the same age. After eclosion all flies are collected close to 12pm and put in the incubator, which starts at 22°C for 12 hour and 6 hour flies, and switches to 31°C 12 and 6 hours before dissection respectively; the 1 day flies are incubated at 31°C the whole time. This means that the differences we see between these groups are not caused by any differences in when neurons are activated during development but relates purely to the length of neuron activation. Furthermore, given the 6 hours Cntrl is only marginally significantly different, while the non-claw counts seem inconsistent across conditions, it is possible these also do not represent meaningful biological variation. In conjunction with the 22°C 4 day non-claw dendrite length findings, this may suggest the criteria for these 2 classes of dendrite is not strict enough and needs further refining. Ultimately, these results

suggest that claw and non-claw dendrite length is not altered in any significant way and does not inform the decision on which claws are removed.

a

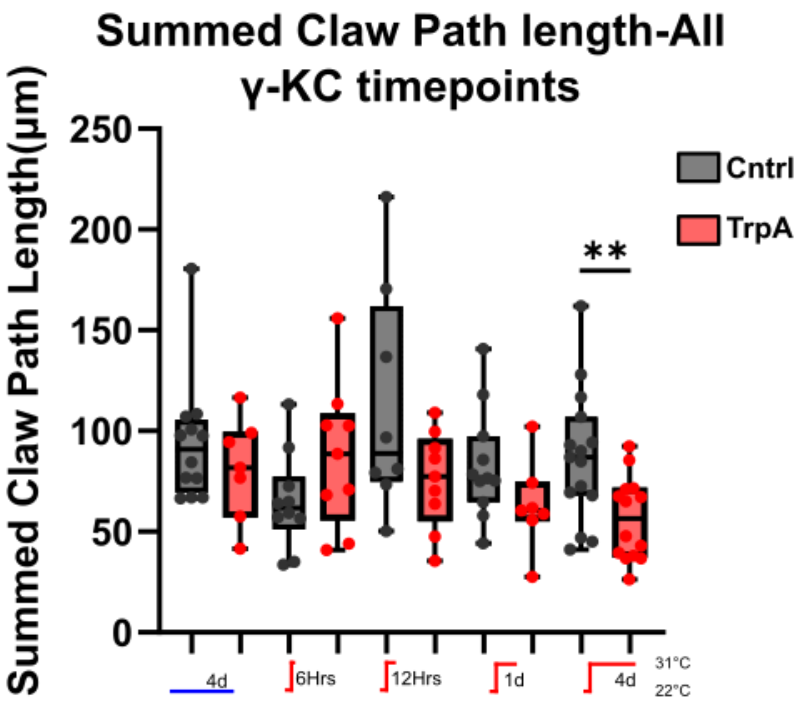

b

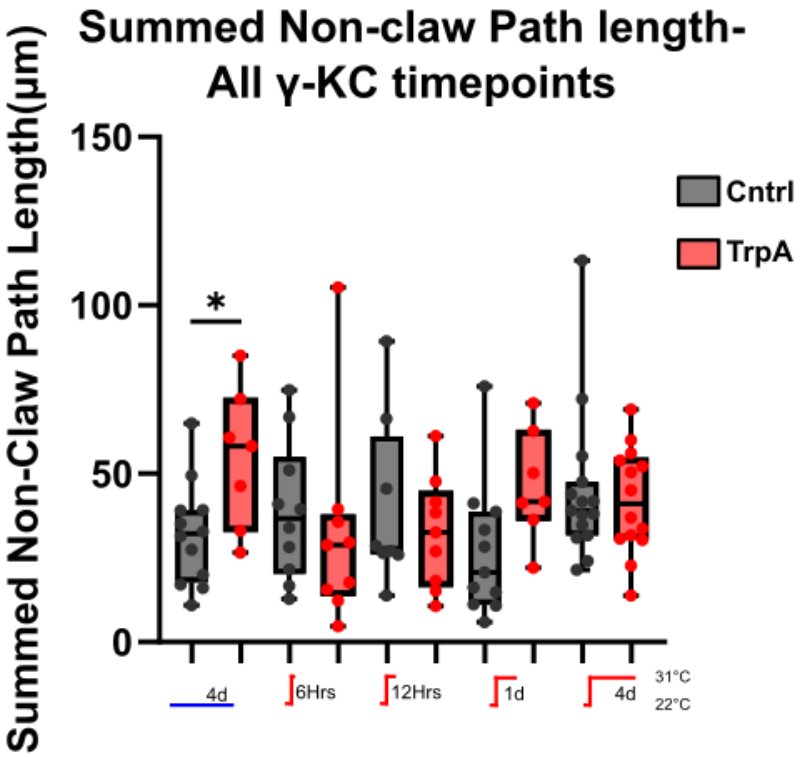

Figure 3.15. Tracing Kenyon cells hyperactivated for 1-4 days reveals no difference in summed path length of remaining claws. **a)** Graph of summed claw path length in γ KCs at all timepoints; control (grey) and TrpA (red) flies; conditions represented by associated figures beneath x axis. Individual data points are displayed on associated boxplot which shows the median and interquartile range. Error bars represent the standard deviation of each group. Images containing multiple KCs were sometimes not traced due to difficulty of overlapping dendrites. From left to right n= Cntrl 22°C 4 Days (11 flies, 12 KCs), TrpA 22°C 4 Days (7 flies, 7 KCs), Cntrl 31°C 4 Days (15 flies, 15 KCs), TrpA 31°C 4 Days (12 flies, 14 KCs), Cntrl 31°C 6 hours (9 flies, 10 KCs), TrpA 31°C 6 hours (7 flies, 9 KCs), Cntrl 31°C 12 hours (4 flies, 8 KCs), TrpA 31°C 12 hours (8 flies, 9 KCs), Cntrl 31°C 1 day (9 flies, 11 KCs), TrpA 31°C 1 day (6 flies, 7 KCs). *P<0.05, **P<0.01, ***P<0.001, Generalized Linear Model (GLM) with HC3 heteroscedasticity-consistent standard errors and Wald test post hoc comparisons with Holm-Sidak multiple comparisons correction. **b)** Graph of summed non-claw dendrite path length in γ KCs. Groups, n and statistical analysis for all graphs match those seen in a.

3.2.8 Both α/β and α'/β' Kenyon cells do not demonstrate activity-dependent morphological adaptations

So far, I have only discussed activity-dependent adaptations in γ KCs, but are similar adaptations possible in the two other KC subtypes α/β and α'/β'? To test this my placement students and I (Guy, W Austin, Joseph Faulkner and Chaw C Yi) used MARCM with an altered heatshock protocol to label single α/β or α'/β' KCs with TrpA and GFP. Based on the timepoints at which these subtypes begin to develop (Lee, Lee and Luo, 1999) we heatshocked flies at 7 days to label α/β KCs and 4.5 days post-egg-laying to label α'/β' KCs (Figure 3.16). We then incubated both groups at 31°C for 4 days and imaged them as before to identify any potential morphological adaptations. The 7 days heatshock consistently produced brains only labelled with α/β KCs but this was not true in α'/β'-KCs. The heatshock window was more complicated for this subtype, as the beginning of their developmental window overlaps with the end of γ KC development, while the end overlaps with the start of α/β development. This is further complicated by the fact that flies heatshocked within a vial are not exactly the same age. Crosses were flipped twice a day, meaning there was an 8-16 hour window for the parents to lay eggs. Furthermore, even flies that originate from eggs laid at the same time will not develop at exactly the same speed. This means that the heatshock does not occur at a precise developmental point but within a ~16 hour window e.g. 2 days and 16 hours at maximum vs 2 days exactly. This was not a problem with the other subtypes, which were labelled correctly the majority of the time, but the developmental window where α'/β' KCs are the only subtype dividing is quite small (~12 hours). A heatshock at 4.5 days post-egg-laying was most effective but this still labelled both γ and α/β KCs in many brains.

To account for this issue whole neuron images were taken after single cell Z-stacks were captured, so the subtype of the cell could be identified; this was only performed when the axonal projection had a vertical lobe, as α/β and α'/β' KCs share this feature making them more difficult to distinguish. Additionally, we later used the anti-BRP antibody NC82, which labels active zones in neurons and thus reveals the morphology of the whole MB (Fouquet et al., 2009; Hamanaka and Meinertzhagen, 2010). This allowed us to see which vertical and horizontal lobe projections were localized to and more accurately characterise their subtypes.

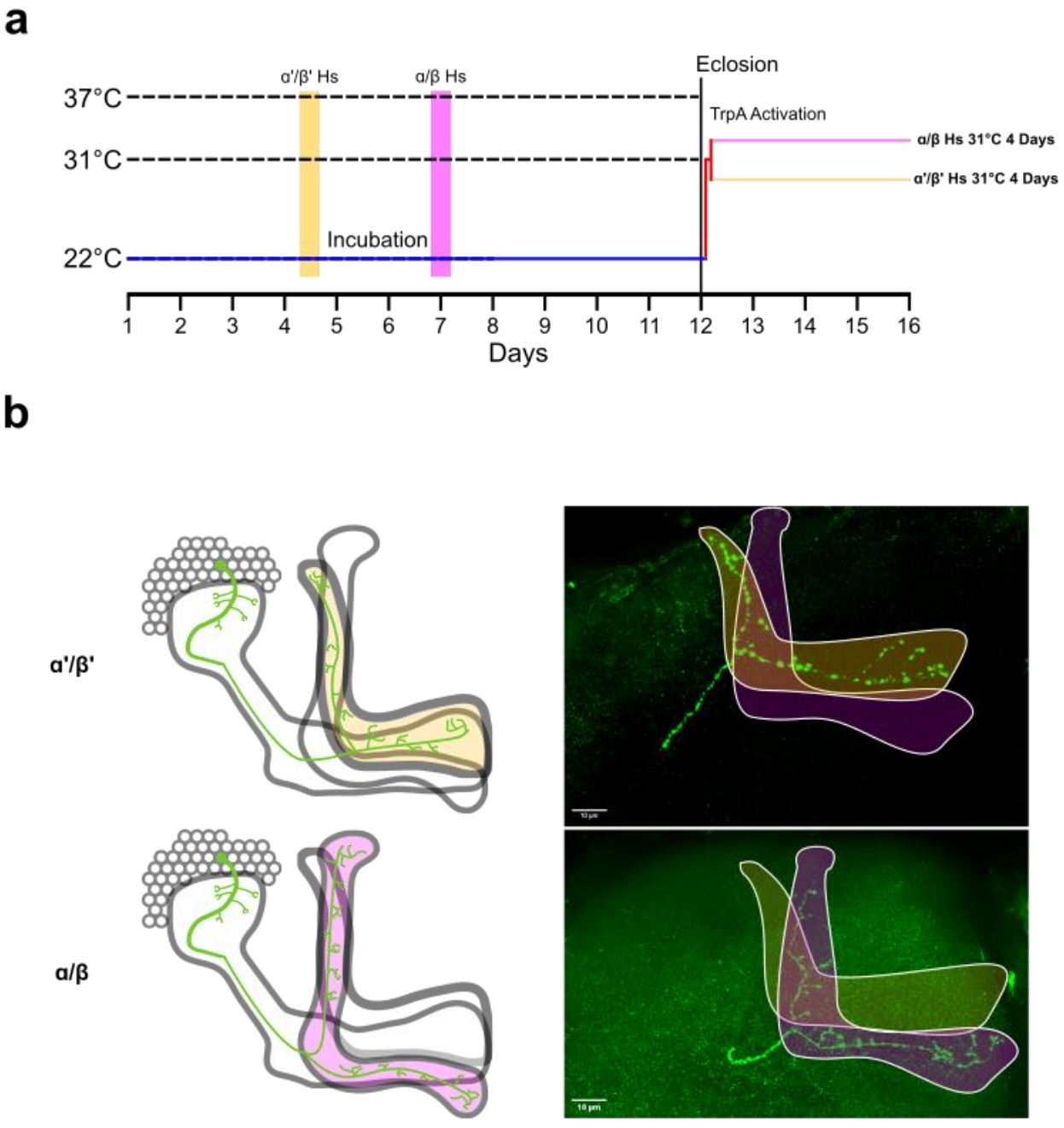

Figure 3.16. α/β and α'/β'-KC Heatshock **protocol and identification**. **a)** Heatshock and incubation protocol for α/β and α'/β'-KCs. To label α/β KCs flies were heatshocked 7 days post-egg-laying. To label α'/β'-KCs flies were heatshocked 4.5 days post-egg-laying. Flies of both subtypes were then moved to 31°C for 4 days to induce prolonged KC activation. After 4 days at 31°C both were dissected, fixed and labelled. b) Identifying KC subtype with whole neuron images. Whole neuron images of 4.5 day heatshock flies were visually analysed to identify which regions of the MB they are localized to. Schematic diagram on the left depicts the organisation of the α'/β' lobes (yellow) vs the α/β lobes (purple). Scale bar in bottom left represents 10μm.

Claw count analysis of both subtypes revealed that TrpA flies show no significant difference in claw number compared to controls (Figure 3.17). Furthermore, neither show any differences in their non-claw dendrite counts (Figure 3.17), demonstrating that these dendrites are likely functionally unrelated in this subtype too. However, the lack of this adaptation does not mean these subtypes don't alter their morphology in other ways in response to increased activity. Similarly to γ KCs, I traced these neurons using SNT on FIJI and analysed their path lengths so I could compare between genotypes. This revealed there are also no differences in length of claw or non-claw dendrites between TrpA and Cntrl flies in both these subtypes (Figures 3.18 and 3.19). This suggests both these subtypes do not adjust these particular aspects of their morphology in response to prolonged periods of hyperactivity. However, this doesn't rule out other adaptations, like alterations to volume of claws, number of synapses per claw or spiking threshold, none of which were measured in this work, although results in Section 4 hint at possible changes in some of these.

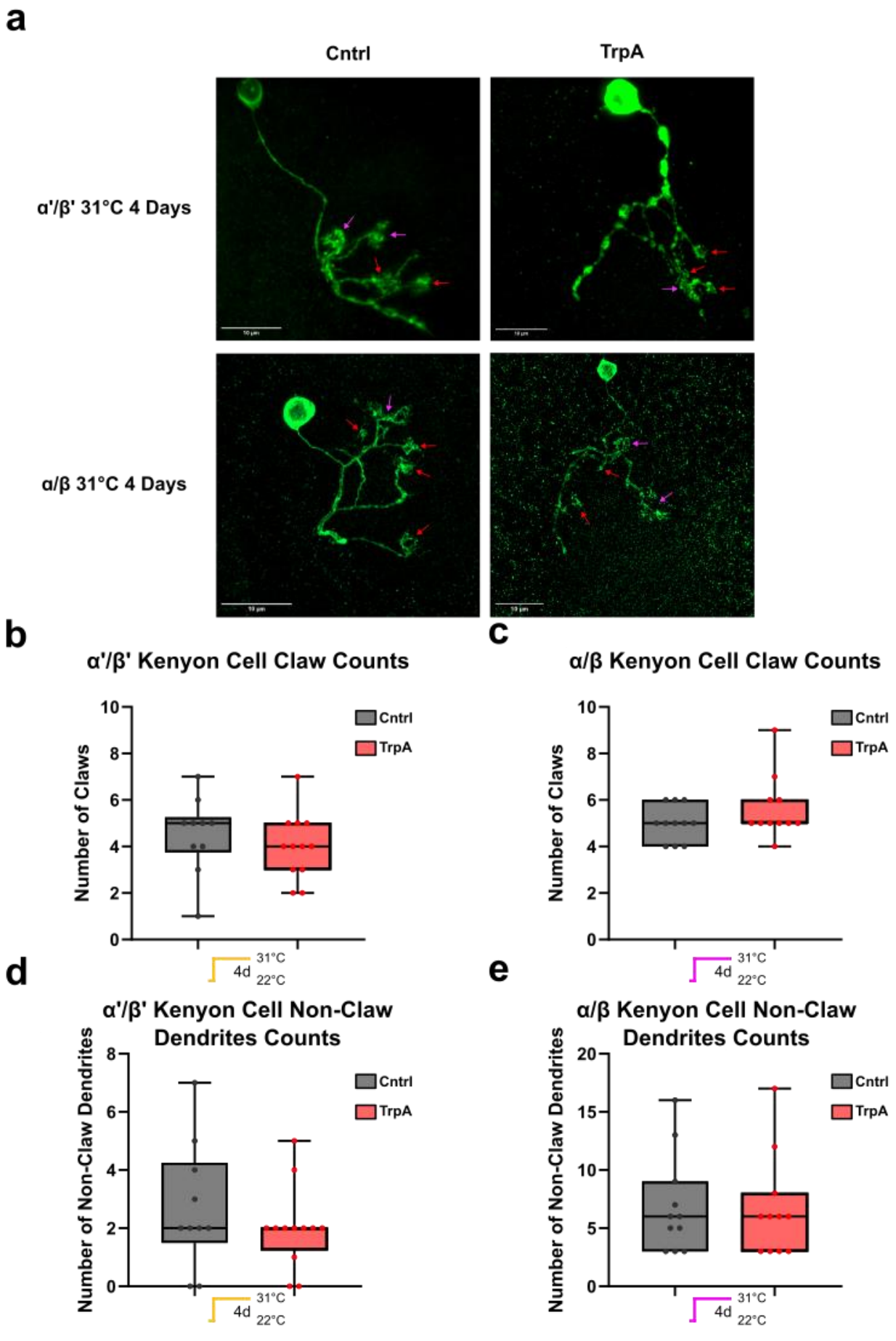
a
Cntrl
TrpA
α'/β' 31°C 4 Days
α/β 31°C 4 Days
b
α'/β' Kenyon Cell Claw Counts
Number of Claws
Cntrl
TrpA
31°C
4d
22°C
c
α/β Kenyon Cell Claw Counts
Number of Claws
Cntrl
TrpA
31°C
4d
22°C
d
α'/β' Kenyon Cell Non-Claw Dendrites Counts
Number of Non-Claw Dendrites
Cntrl
TrpA
31°C
4d
22°C
e
α/β Kenyon Cell Non-Claw Dendrites Counts
Number of Non-Claw Dendrites
Cntrl
TrpA
31°C
4d
22°C

Figure 3.17. **α/β and α'/β'-KCs do not reduce their number of claws after prolonged hyperactivity. a)** Example single γ KCs from α/β and α'/β'-KCs (Cntrl and TrpA). Simple claws are labelled with a red arrow, and complex claws are labelled with a purple arrow. Scale bar in bottom left of images represents 10μm. **b-c)** Graph of mean number of claws in α/β and α'/β'-KCs. Individual data points are displayed on associated boxplot which shows the median and interquartile range. Error bars represent the standard deviation of each group. From left to right n= Cntrl α'/β' (10 KCs), TrpA α'/β' (12 KCs), Cntrl α/β (11 KCs), TrpA α/β (11 KCs). *P<0.05, **P<0.01, ***P<0.001. Unpaired t test with Welch's correction was used to compare between genotypes within each subtype**. d-e)** Graph of mean number of non-claw dendrites in α/β and α'/β'-KCs. n and statistical test used are the same as in b-c. **Dissections, fixation and immunolabeling were performed by Guy, W Austin, Joseph Faulkner and Chaw C Yi**

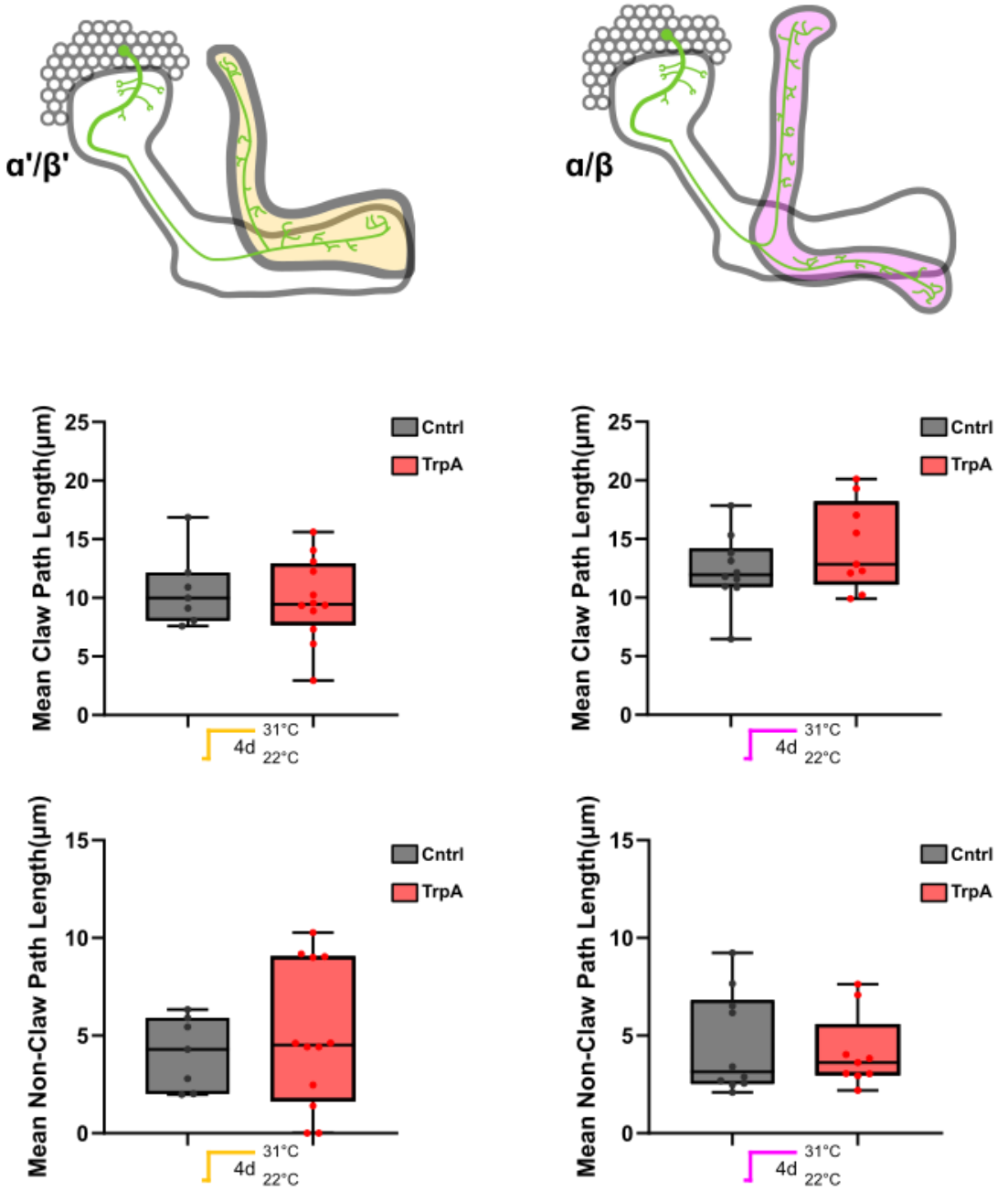

Figure 3.18. **α/β and α'/β'-KCs do not alter their mean claw dendrite length after prolonged hyperactivity. a-b)** Graph of mean claw path length in α/β and α'/β'-KCs. Individual data points are displayed on associated boxplot which shows the median and interquartile range. Error bars represent the standard deviation of each group. From left to right n= Cntrl α'/β' (7 KCs), TrpA α'/β' (12 KCs), Cntrl α/β (10 KCs), TrpA α/β (9 KCs). *P<0.05, **P<0.01, ***P<0.001. Unpaired t test with Welch's correction was used to compare between genotypes within each subtype**. c-d)** Graph of mean path length of non-claw dendrites in α/β and α'/β'-KCs. n and statistical test used are the same as in b-c. **Dissections, fixation and immunolabeling were performed by Guy, W Austin, Joseph Faulkner and Chaw C Yi.**

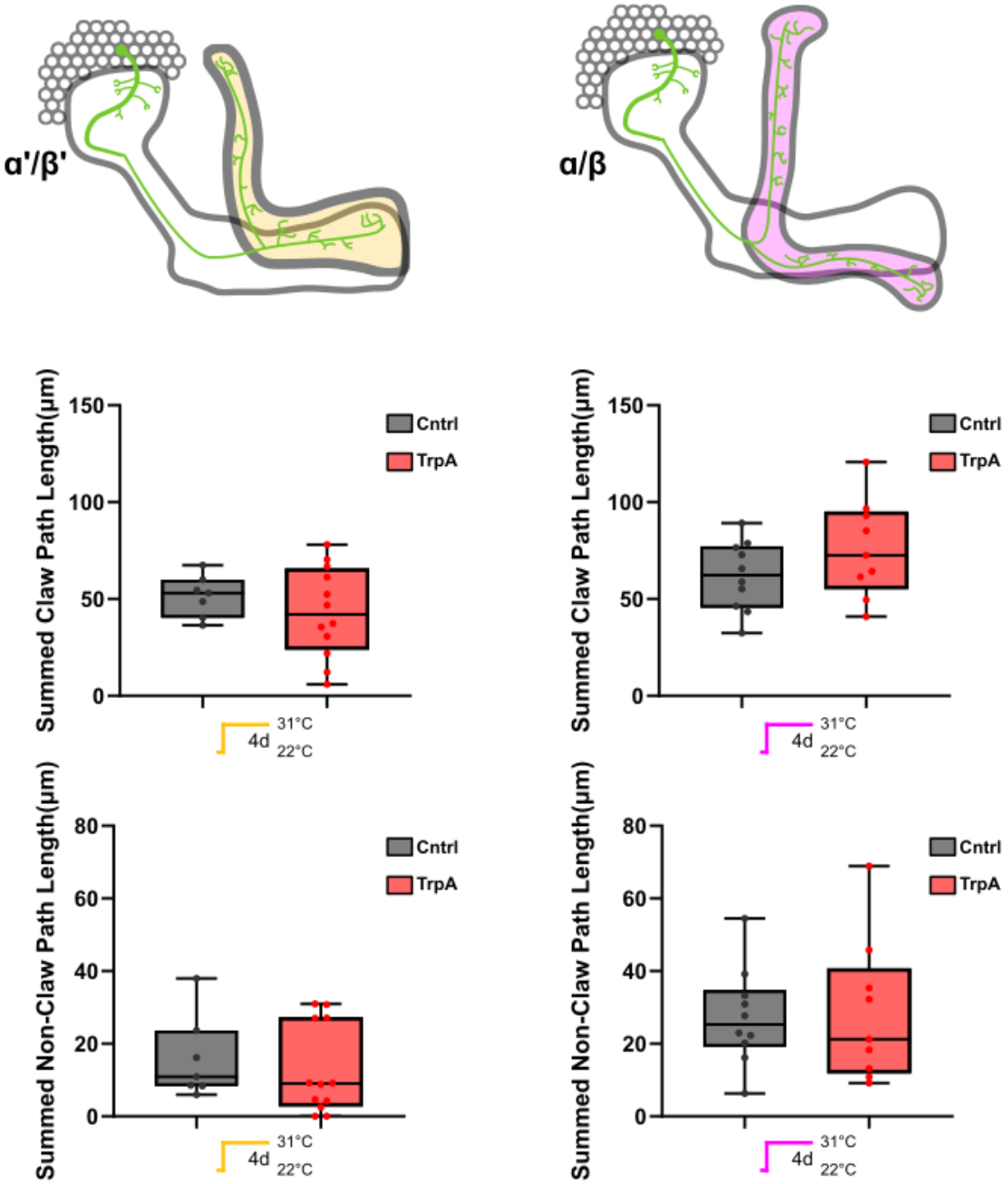

Figure 3.19. The total length of α/β and α'/β'-KC claws also doesn't change after prolonged hyperactivity. a-b) Graph of summed claw path length in α/β and α'/β'-KCs. Individual data points are displayed on associated boxplot which shows the median and interquartile range. Error bars represent the standard deviation of each group. From left to right n= Cntrl α'/β' (7 KCs), TrpA α'/β' (12 KCs), Cntrl α/β (10 KCs), TrpA α/β (9 KCs). *P<0.05, **P<0.01, ***P<0.001. Unpaired t test with Welch's correction was used to compare between genotypes within each subtype**. c-d)** Graph of summed path length of non-claw dendrites in α/β and α'/β'-KCs. n and statistical test used are the same as in b-c. **Dissections, fixation and immunolabeling were performed by Guy, W Austin, Joseph Faulkner and Chaw C Yi.**

3.3 Discussion

3.31. γ KCs demonstrate an activity-dependent reduction in number of claws

I have identified a previously unreported activity-dependent reduction in number of claws in KCs. This adaptation occurs after 1-4 days of prolonged hyperactivity induced by TrpA activation through incubating flies at 31°C. This adaptation does not occur after 6-12 hours of activity, suggesting claw removal begins to occur sometime between 12 and 24 hours and is not significantly altered by a further 3 days of activity. Further investigation revealed that claw dendrites do not 'become' non-claw dendrites as these counts are not significantly different between genotypes. This demonstrates that by 1 day of 31°C, claw removal has already been achieved, with no sign of any 'intermediate' dendrites. Investigating the morphology of these cells further supports this conclusion. One possibility is these claws maintain their volume (meaning they are still counted at the 6 and 12 hour timepoints) but have started to be retracted. However, the mean length of claws in TrpA-overactivated KCs is not significantly different from controls suggesting no retraction mechanism has begun. Furthermore, this also demonstrates these neurons do not alter their length in response to prolonged activity independently to loss of claws. Length of remaining claws in 31°C 4 day and 1 day TrpA KCs is not significantly different to controls, suggesting this does not inform the decision of which claws are removed. This currently leaves the factor that determines a claws removal unclear. However, my current morphology analysis does not measure changes in branching complexity, which could be another factor influencing claw removal. For example, this mechanism could target claws on more complex branches (containing multiple claws) for removal, resulting in more 'simple' branches in TrpA neurons; claws on the same branch may synapse with the same PN bouton, making loss of just one claw more 'tolerable'. Future work should perform a Sholl analysis on existing traces to identify any differences in branching complexity between control and TrpA KCs.

In a more ethologically realistic section, we could imagine that removal of a specific claw would be informed by the increased EPSC amplitude or frequency of that claw. In our previous modelling work, we hypothesized that without a homeostatic mechanism to counter single neuron activity drift beyond their setpoint, these neurons may respond to too many odours and in combination with converse decreased activity of a large percentage of the total KCs, this may decrease the ability of the MB to discriminate between odours (Abdelrahman, Vasilaki and Lin, 2021). For example, if these neurons through natural variability have 1 claw

that becomes more active, this increases the neurons chance of firing, which also means any other weak signalling from the other PNs which would usually not result in a spike would be enhanced; this could represent noise produced by ORNs which are spontaneously active in the absence of odours (Joseph, Dunn and Stopfer, 2012). The high spiking threshold of KCs (Gruntman and Turner, 2013) would usually prevent spontaneous ORN and subsequent PN firing from going further, but it is possible that a significant increase in activity in one claw would be sufficient to bypass the neurons threshold. In this scenario, removing this claw may achieve restoration of the neuron's activity to its previous set point (likely in conjunction with other compensatory mechanisms).

It is important to acknowledge that if one KC's activity increased, this would mean very little for the actual encoding of a single odour, which is usually represented by 100-200 KCs (Honegger, Campbell and Turner, 2011). This work is trying to identify whether homeostatic mechanisms on the single cell level are possible, and, if they exist, these mechanisms in turn should maintain a roughly equal level of activity across the population, which should prevent the scenario described in Chapter 1.5 where a small percentage of the population respond to the majority of odours, while the rest remain silent.

One important consideration is what the removal of a claw actually means, as this does not represent a simple reduction in the neuron's activity. If we turn to mammalian literature, we have already discussed that many neurons across circuits can achieve reduction in their number of spines in response to the increased activity of said spines (Stepanyants, Hof and Chklovskii, 2002; Keck et al., 2008; Goold and Nicoll, 2010; Keck et al., 2013). However, spines and claws are distinct in their importance. A single spine is one of ~10,000 across the neuron depending on the exact cell type (Tjia et al., 2017), so losing just one or 2 spines represents no significant loss of information. Removing spines from specific dendrites, actually represents a reduction in the amplitude of signal the neuron is receiving from the particular presynaptic neuron synapsing with those spines. In contrast, KCs removing single claws may represent a complete loss of information from the associated PN it was previously synapsing with. There are two possible conclusions we can draw from this. The first is that the 'trade-off' of losing the odour information from one PN vs being active beyond your set point favours returning activity to normal levels. If our modelling is correct (Abdelrahman, Vasilaki and Lin, 2021) and allowing activity to drift across the population is disastrous for odour discrimination, this could make sense as responding to one or even 2 fewer odours may not significantly affect the flies ability to distinguish between odours. However, if my reversal data is true and these neurons are incapable of restoring these claws once they are

removed, this adaptation occurring across the population could be disastrous. In a situation where over time all KCs at some point become too active and remove 1-2 of their claws, this would theoretically have a significant impact on odour encoding, representing a loss of many different PN inputs, even with the existence of a potential ‘floor’ preventing further claw removal. Given that the natural variation that increases the responsiveness of these claws is theoretically essentially random, this would also be ethologically problematic as flies may later encounter odours that by chance the network has reduced its responsiveness to and cannot restore. Longer reversal periods would need to be trialled in future to confirm if the number of claws could be eventually restored or if this adaptation really is set in stone.

One potential factor driving the decision of claw removal is whether a KC has multiple claws that synapse with the same PN. We know that this is fairly common through analysis of γ KCs in the hemibrain connectome (Scheffer et al., 2020), but the question is would this mechanism only exist in KCs containing these claws? One possible way to identify this is through use of a tool that labels the synapses of the KCs cognate PN boutons like BacTrace (Cachero et al., 2020). This would allow you to directly compare the number of claws that synapse with the same PN bouton in control vs TrpA flies. However, this system requires too many transgenes and even with recombination on multiple chromosomes I would be unable to use both MARCM and BacTrace together. Nonetheless, given my morphological analysis did not identify any informative factors, this represents an appealing/simple way to explain why certain claws are removed and why this doesn’t affect their ability to encode odours.

3.32. Activity-dependent reduction in the number of claws is not limited to the early adult CP but does disappear with age

It was possible that the initial activity-dependent claw loss we described was actually a reduction in the number of claws these neurons grow as they may still be within a CP (Dombrovski and Condron, 2021; Devaud, Acebes and Ferrús, 2001; Devaud, Keane and Ferrús, 2003; Devaud et al., 2003). It has already been established that the *Drosophila* olfactory system is sensitive to activity changes during this period and these can result in increases in total volume of glomeruli (Devaud, Acebes and Ferrús, 2001; Devaud, Keane and Ferrús, 2003; Devaud et al., 2003). However, I repeated the 4 days at 31°C experiment outside of this window and still found a reduction in the number of claws in TrpA KCs. This not only demonstrates this adaptation represents a loss of claws but also shows it is not limited to this CP and represents an adult adaptation. However, our later experiments revealed that significantly aged flies raised at both 18°C and 22°C before being moved to 31°C for 1 day lose the ability to reduce their claws in response to increased activity. It is

possible that a longer period at 31°C could induce claw loss still, but these flies may not survive this manipulation due to the combination of high temperature and their advanced age. If we assume these neurons are incapable of this adaptation is there a precedent for loss of plasticity with age? Growing evidence suggests that during natural ageing and during neurodegeneration especially, homeostatic plasticity becomes dysregulated (Taylor and Jeans, 2021). It is possible that 30-50 days is close enough to the end of the fly's lifespan that some of the homeostatic mechanisms KCs may usually possess have begun to be lost. The loss of a whole claw is extreme compared to other potential mechanisms like altering synapse number or adjusting the neurons spiking threshold, so this may be one of the first mechanisms to disappear. Ultimately, future work would need to test alternative timepoints in-between our current conditions to determine when exactly this adaptation is lost.

3.33 Is protein required for activity-dependent loss of claws?

Drawing conclusions from the current Starvation and Sugar only findings is challenging, due to the conflicting nature of the results. There is a trend of claw loss in flies starved of all nutrients for 1 day and yet flies under very similar conditions but with access to sugar show no claw loss. The low sample size in Sugar only flies limits the conclusions that can be drawn from this condition, but both conditions lack essential amino acid availability so it is possible to make some inferences. There is significant precedent for the importance of protein in plasticity, both Hebbian and homeostatic. For example, in *Drosophila* long-term olfactory memory formation requires KC protein synthesis (Tully et al., 1994; Perazzona et al., 2004; Yu, Akalal and Davis, 2006; Tonoki and Davis, 2015; Turrel et al., 2022; Wang et al., 2023), and there is a wealth of similar evidence for LTM in the mammalian hippocampus (Leal, Comprido and Duarte, 2014). Although not as prevalent, there is also plentiful evidence to support the importance of protein synthesis in homeostatic plasticity. I have already described how different homeostatic mechanisms require changes in channel expression, changes in receptor expression at specific synapses and changes in several structural proteins that accompany these, all of which require protein synthesis (Gilestro, Tononi and Cirelli, 2009; Weyhersmüller et al., 2011; Dissel et al., 2015; de Vivo et al., 2017; Mendez et al., 2018; Spano et al., 2019; Gisabella et al., 2020; Li et al., 2020a). The protein synthesis expression profiles are also quite distinct at different homeostatic timepoints and are associated with distinct adaptations (Dieterich et al., 2006; Schanzenbächer et al., 2016; Schanzenbächer, Langer and Schuman, 2018). I theorise that the results from both conditions suggest the lack of key amino acids impacts synthesis of key regulatory proteins involved in activity-

dependent claw loss. However, these conclusions could be strengthened by blocking protein synthesis directly. It is also worth acknowledging that starvation and the sugar-only manipulation occurred concurrently with incubation at 31°C to hyperactivate KCs. This leaves the possibility that stores of energy sources and amino acids were still available to these neurons, although starvation/loss of protein during KC hyperactivity still appears to be sufficient to block activity-dependent claw loss.

In future, to ascertain whether protein synthesis is involved in activity-dependent claw loss, I would incubate flies at 31°C on food containing cycloheximide, a protein synthesis inhibitor which has been effectively utilised in Drosophila research previously (Yu, Akalal and Davis, 2006). Flies raised on cycloheximide may also tolerate longer periods at 31°C, which is a major limitation of our starvation condition that prevents us from determining if more prolonged activity would induce claw loss in starved flies. Ultimately, these findings suggest protein synthesis may be important for activity-dependent loss of claws and if this effect is homeostatic, the literature supports this as a requirement for many homeostatic mechanisms. Beyond broad protein synthesis inhibition, targeting specific proteins involved in activity-dependent claw loss would be more revealing. I will discuss potential targets for KO/KD experiments in Chapter 5 when reviewing proteins implicated in homeostatic plasticity across species and those involved in KC function (5.3).

3.34 α/β and α'/β' Kenyon cells do not demonstrate activity-dependent loss of claws

Both α/β and α'/β' KCs show no significant differences in their claw counts or morphology after a prolonged period of hyperactivity. If our modelling work (Abdelrahman, Vasilaki and Lin, 2021) is correct, it is likely they have other homeostatic mechanisms to compensate for deviation from a set level of activity, and I will discuss some of these alternatives further in Chapter 4 and 5. Focusing on morphological adaptations alone for now, what key differences may be responsible for the existent of an activity-dependent claw loss mechanism in γ KCs but not in other subtypes? One key difference in morphology is the pre-existing number of claws in α/β and α'/β' subtypes, which at ~5 claws on average is significantly lower than the ~7 claws typically found in γ KCs (Caron et al., 2013). Claw removal in the former subtypes represents a loss of a significant percentage of your total claws, which while potentially tolerable in γ KCs after extreme periods of hyperactivity, may impact olfactory coding too significantly in α/β and α'/β' KCs; this is especially true if you only have 3 inputs to begin with, as several α/β and α'/β' neurons imaged did. Alternatively, it may be that other homeostatic mechanisms are more efficient in these subtypes than they are in γ KCs, meaning even after prolonged activity they are capable of restoring activity to the neurons set point. Testing a

more extreme manipulation. e.g. 8 days of TrpA activation, could induce claw loss if the neurons other mechanisms fail to lower activity effectively. However, it is unlikely flies would tolerate 8 days at such a high temperature without it significantly impacting their health, adding an additional confounding factor.

Another key difference between each of the 3 main olfactory KC subtypes is their distinct roles in odour memory. To simplify these differences, it appears that γ KCs are involved in STM, α'/β'-KCs are involved in early and so called 'mid-term' memory and α/β KCs are required for LTM formation (Yu, Akalal and Davis, 2006; Krashes et al., 2007; Wang et al., 2008; Akalal, Yu and Davis, 2011; Davis, 2011; Qin et al., 2012; Cervantes-Sandoval et al., 2013). It is possible these distinct roles may mean that different subtypes utilise different homeostatic mechanisms, although the reason for this is not apparent and is not currently explained by our model (Abdelrahman, Vasilaki and Lin, 2021) which only suggests all KC subtypes must adjust their activity back to a set point to achieve optimal odour learning. To understand this difference, further work is needed to identify alternative homeostatic mechanisms utilised by these other subtypes. For example, identification of proteins that are differentially regulated in both learning and memory and homeostatic plasticity between subtypes may shed light on the source of these differences.

3.35 Future work

During the course of the many different conditions, I have collected a vast array of images but only had time to analyse the morphology in more detail in a few of these. Future work should first focus on tracing skeletons of existing conditions like starvation and aged flies to identify any key differences. This would be especially pertinent in the 18°C aged group, which shows dramatic differences in claw and non-claw counts across both genotypes compared to the other conditions. Drosophila are sensitive to temperature, so it is possible that while looking for homeostatic adaptations I have identified a consequence of raising flies at lower temperatures (increased dendrite number) and it would be informative to analyse changes in their length and branching complexity. Additionally, my current morphological analysis could be expanded further. The current results only allow me to conclude that path length does not impact the choice of claw removal. However, it would be intriguing to measure if the volume of claws changes across both genotype and condition. I can currently conclude that claws aren't retracted before being removed, at least they don't by 12 hours of TrpA activation, but it is possible the volume of claws is decreased before removal in a way not detectable by my class 2/class 3 distinction. Furthermore, claw volume may be a key factor in determining claw removal. For example, claw volume typically correlates with the number of synapses present

at a single claw, so an effective way to reduce the cells activity would be to target the largest claws first as they may contribute a higher frequency/amplitude of mEPSCs to the neuron. Ultimately, future morphological analysis should focus on trying to identify the rationale of why certain claws are removed over others. This would not only improve our understanding of KC homeostatic mechanisms but may help reveal the different contributions individual claws make to the neuron's activity.

Labelling of key proteins involved in synaptic scaffolding could also be revealing. For example, previous work discovered that claws are actin rich (Leiss et al., 2009) so it would be interesting to label the actin in single cells that have been hyperactivated to test how this adaptation effects actin dynamics beyond its removal from claws that are lost. In fact, an experiment where key transporters of actin are fluorescently tagged and could be observed over long periods of time (Ladt, Ganguly and Roy, 2016) to determine how these dynamics change as claws are removed would be fascinating. Actin aside, the ability to image these neurons over long periods of time at 31°C would be incredibly useful as it would aid in determining the exact window in which claws can be removed and may help determine the logic of their removal. However, current live imaging techniques does not allow for the clarity needed to observe these changes and furthermore, flies do not survive during long imaging periods making any potential conclusions dubious.

3.36 Is activity-dependent loss of claws actually homeostatic?

In this chapter I have suggested that the change in claw number is homeostatic but the evidence presented so far alone is not proof of this. I can confidently say that the loss of claws is activity-dependent but it is impossible to conclude these changes are homeostatic without observing how the activity of these neurons shifts in response. In the next chapter we will see how the responses of single neurons change after prolonged hyperactivation and discuss how these findings relate to the morphological ones I have discussed so far.

4. Single cell physiological homeostatic adaptations

4.1 Introduction

For adaptations within neurons to be homeostatic, they must restore the activity of that neuron to its usual level. It is unclear whether neurons detect changes to their activity directly or whether they maintain a set level through altering some parameters in response to changes in others. However, it is generally acknowledged that these changes restore a neurons activity to a set level so it can continue to function normally. In the previous chapter, I showed that KCs respond to prolonged periods of hyperactivity by reducing the number of their claws. But what is the physiological consequence of this loss of claws? If this adaptation is homeostatic, I would expect the activity of these neurons should decrease as this would demonstrate an attempt to shift activity from a hyperactive state and move it closer to a set level. In this chapter, my primary aim was to determine how the activity of KCs changes in response to the same periods of prolonged hyperactivity used in Chapter 3. I hypothesized that I would see an associated decrease in the activity of neurons at 24 and 96 hours, the same timepoints where activity-dependent claw loss was observed.

4.2 Results

4.2.1 Labelling single cells with GCaMP8M

There are two main options for recording from single cells in *Drosophila*: electrophysiology or calcium indicators. However, electrophysiology in the MB is incredibly difficult, especially when trying to record from single cells. Kenyon cells are incredibly small with a diameter of ~4-5μm (Scheffer et al., 2020; Schlegel et al., 2024) which makes recording from their dendrites impossible and from their cell bodies very difficult. Furthermore, the cell bodies are closely associated with each other surrounding the calyx and, in the case of my experiments, it is necessary to patch a specific cell only e.g. the neuron hyperactivated for a prolonged period of time. The combination of these difficulties and our labs existing experience using calcium indicators informed my decision to use GCaMP as a proxy for activity in KCs, as we and others in the field have done previously (Li et al., 2013; Lin et al., 2014; Apostolopoulou and Lin, 2020).

However, unlike the previous morphological experiments we had not already created a genotype to label single cells with GCaMP. The MARCM genotype for labelling single cells with GFP (hsFLP, UASCD8GFP;; FRT82, GAL80/TM3-Sb; OK107) could not be used for live

imaging and there wasn't an FRT82 stock containing hsFLP available that did not contain GFP. However, we did have a double balanced hsFLP stock that I used to create a new line containing GCaMP6f and the KC driver R13F02-Gal4; this was subsequently crossed to a line containing tubp-FRT>Gal80-FRT so that offspring should have no GCaMP expression unless heatshocked. I hoped that by using an incredibly short heatshock time, only a few cells would produce sufficient Flippase to excise Gal80 and allow expression of GCaMP and other genes under the control of UAS like TrpA. However, heatshocks from 2.5 minutes-35 minutes all produced labelling of the whole MB the majority of the time. Furthermore, even flies that were not heatshocked labelled too many KCs with occasional whole MB labelling (Figure 4.1). The most likely explanation for this is that hsFLP may be active even without a heatshock resulting in excision of the Gal80 in most neurons. It is possible in MARCM the distance between FRT sites on opposite chromosomes prevents GAL80 excision occurring even without heatshock, unlike the hsFLP line where both FRT sites are very closely associated, which may increase the ease of recombination. Regardless, these findings demonstrated continuing with this genotype would not be appropriate.

Fortunately, there was a MARCM genotype available on Bloomington (hsFLP, tubp-Gal80, neoFRT19A) that I used for the creation of a single cell live imaging genotype. Taking advantage of the newest calcium indicators from Janelia (Zhang et al., 2023) I created a line containing GCaMP8m and mCherry for visualizing KC morphology, driven by the MB Gal4-driver R13F02 (hsFLP, tubp-Gal80, neoFRT19A; UASGCaMP8m, UASmCherry/Cyo; R13F02-Gal4/TM3-Ser). Using the same 35 minute heatshock time as before resulted in brains with only 1-4 KCs consistently labelled across flies (Figure 4.1). Note that because FRT19A is on the X chromosome, all offspring picked had to be female to allow the recombination necessary for MARCM to occur. By crossing this to a line containing FRT19A and UASTrpA, I could then test whether hyperactivating KCs resulted in any changes in their activity.

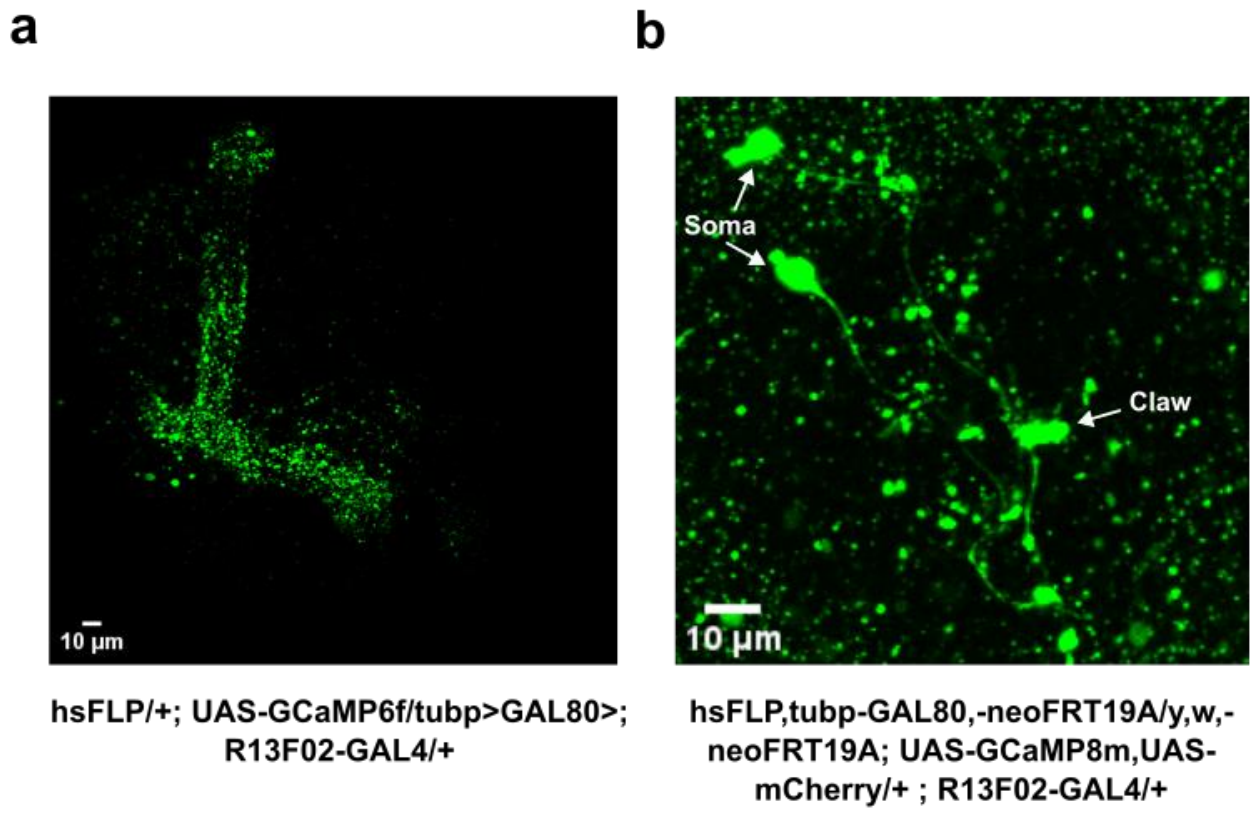

Figure 4.1. Comparing Non-MARCM and MARCM single cell live imaging genotype labelling. a) hsFLP Non-MARCM line occasionally produces whole MB labelling, even with no heatshock as in example image. **b)** MARCM single cell live imaging genotype heatshocked for 35 minutes consistently labels 1-4 KCs. Example image shows 2 KCs with GCaMP8m labelling, both somas are indicated, as is an example claw; labelling of claws/dendrites is weak. **a-b)** Scale bars shown in bottom left of both images and full offspring genotype displayed below respective images.

4.2.2 Determining appropriate stimulation method for single Kenyon cells

In our labs work on homeostatic plasticity in the whole MB (Apostolopoulou and Lin, 2020; G. Bergmann, unpublished results) we used an array of odours to stimulate the MB and determine how responses have adapted after prolonged hyperactivity. However, the stochastic nature of MARCM means using a similar method would be completely inconsistent as any KC(s) labelled may or may not respond to a given odour. Importantly, it would be unclear whether the lack of response was a result of homeostatic adaptation or that particular KC not receiving the associated inputs of that odour. To consistently produce single KC activation, I needed a stimulation method that would activate the entire MB (all KCs), so I could be confident any differences identified were a result of adaptation. I decided to use antennal nerve stimulation, a method that has been previously used to elicit whole MB

activation (Groschner et al., 2018). This technique involves cutting the antennae between the Scape and Pedicel segments to reveal the exposed nerve, which can then be stimulated with a suction electrode. The aim is to use sufficient electrical stimulation to recruit all olfactory glomeruli which should also result in activation of most/all KCs. However, to confirm what current on our constant current stimulator was sufficient to produce maximum MB response, I tested an array of different currents on flies expressing GCaMP6f in the entire MB (Figure 4.2); ORNs were also labelled with GCaMP6 to assist with suction of the nerve. Flies were pinned to a stage using wax, the head was exposed and a surgical window was cut so the MB could be visualised. I then used a 2-photon to record whole MB responses while flies were stimulated. This revealed that 1000μA produced the maximum response from the MB, with responses to 3000μA being no higher. Due to the difficulty of the technique initially, the sample size is quite low, and I was only able to test 3000μA on one fly, so it is possible higher currents could produce larger responses. However, the difference between 1000μA and lower currents is also negligible at different frequencies (Figure 4.2) and the aim of these experiments was mostly to identify a current that consistently produced large responses, while avoiding damaging the neurons after successive stimulations, which would be more likely at higher amplitudes. Ultimately, I elected to use 1000μA for all stimulations going forward as a compromise between maximum MB response and avoiding nerve damage during successive stimulations. The stimulation frequencies and time window for each pulse can be seen in tables 2.9 and 2.10

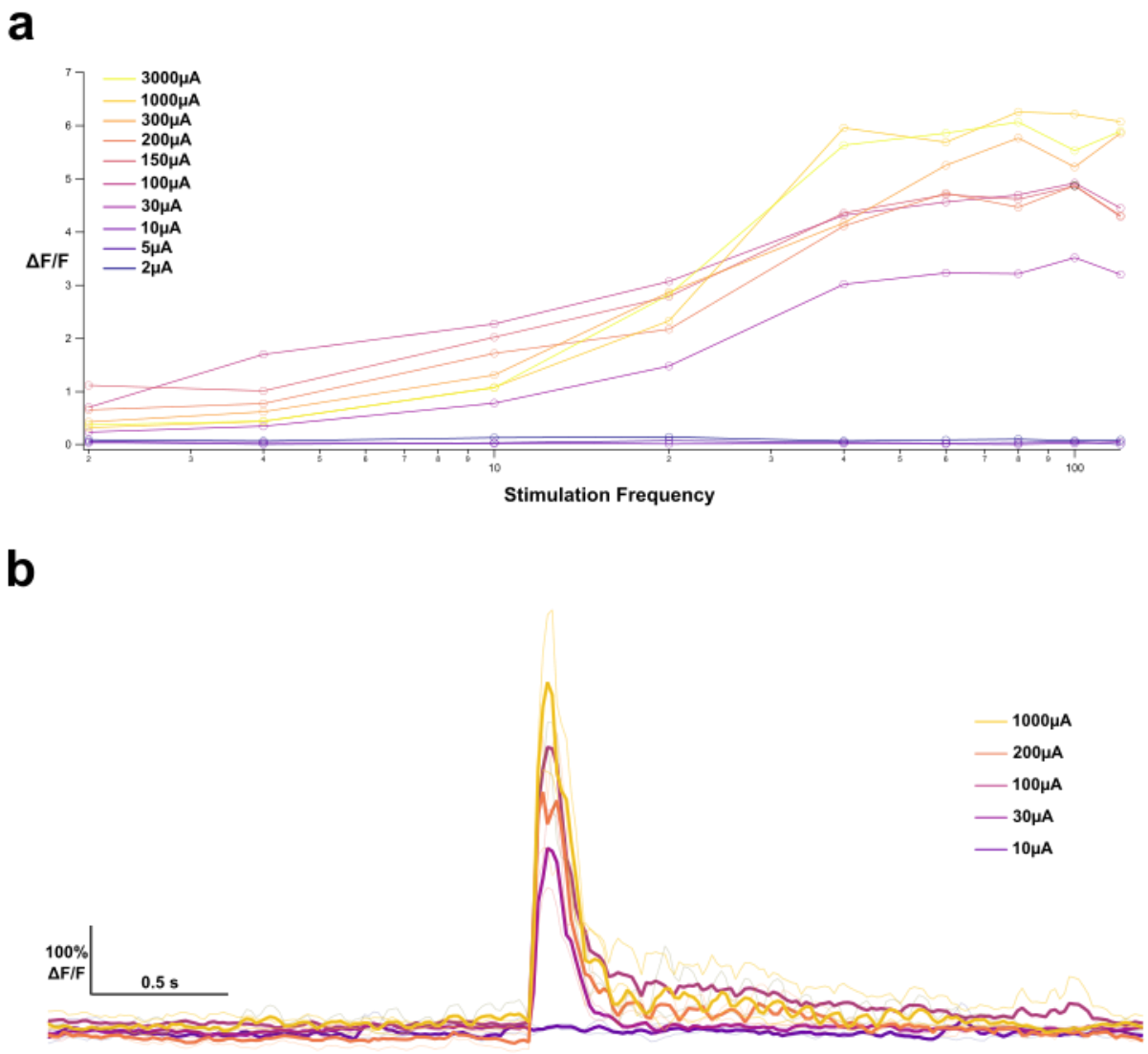

Figure 4.2. Determining appropriate current for antennal nerve stimulation to achieve whole MB activation. a) Response of a single fly to an array of different currents. The log frequency of stimulation is on the x axis and ranges from a minimum of 2Hz to a maximum of 120Hz. The y axis shows the ΔF/F response values with 1 representing 100%. **b)** Responses to different currents at 120Hz compared between two flies. Scale bar showing 100% ΔF/F on the y and 0.5 seconds on the x seen on the left.

4.2.3 Confirming TrpA response is limited to single cells

After creating the new single cell live imaging genotype, I wanted to confirm that Gal80 was correctly suppressing TrpA expression in all other KCs. To do this I created the following positive control line *LexAOP-jRGECO1A /CyO; Mb247-LexA, LexAOP -TrpA/TM3-Ser* that drives TrpA expression in the entire MB, while responses can be visualised with the red calcium indicator jRGECO1A. Response of the whole MB in my experimental genotype was

assessed by crossing the single cell live imaging line to a LexAOP-*jRGECO1A*, UASTrpA/CyO; Mb247-LexA/TM3-Ser line. Flies were pinned to the stage and a surgical window was created to visualize the MB under the 2P. The perfused external solution temperature was then gradually increased until reaching ~31°C, where the heater was then switched off; temperature often still increases after this as it takes time for the external solution to cool. The recording was ended when solution temperature reached baseline again (~22°C) and responses were then analysed to determine if they responded. This revealed that as expected positive control flies begin to respond as temperature increases at around 25°C, matching previously reported temperature response onset (Hamada et al., 2008), and reach a plateau at ~33°C (Figure 4.3), demonstrating TrpA works as expected in these flies. In contrast experimental flies don't show an obvious response that follows the increase in temperature (Figure 4.3). However, flies do often respond to increasing temperature by moving, and inexperience with proper pinning technique while conducting this experiment resulted in movement artifacts in experimental fly responses (a large peak that does not persist); see Figure 4.3b for example recording. While this does not perfectly demonstrate a complete lack of response, it is clear from reviewing the recordings that this 'peak' is caused by a brighter area of the MB moving into the viewing plane as the fly moves in response to the high temperature. I am confident this does not represent TrpA expression in the whole MB within the single cell live imaging genotype, as the pattern of response is completely different from the positive control and does not gradually rise as temperature increases, but instead has a short peak that quickly returns to baseline at the highest temperature. Regardless, these preliminary experiments demonstrated that the Gal80 was correctly repressing TrpA expression across the MB, allowing me to begin identifying any physiological adaptations to prolonged single KC activation.

a

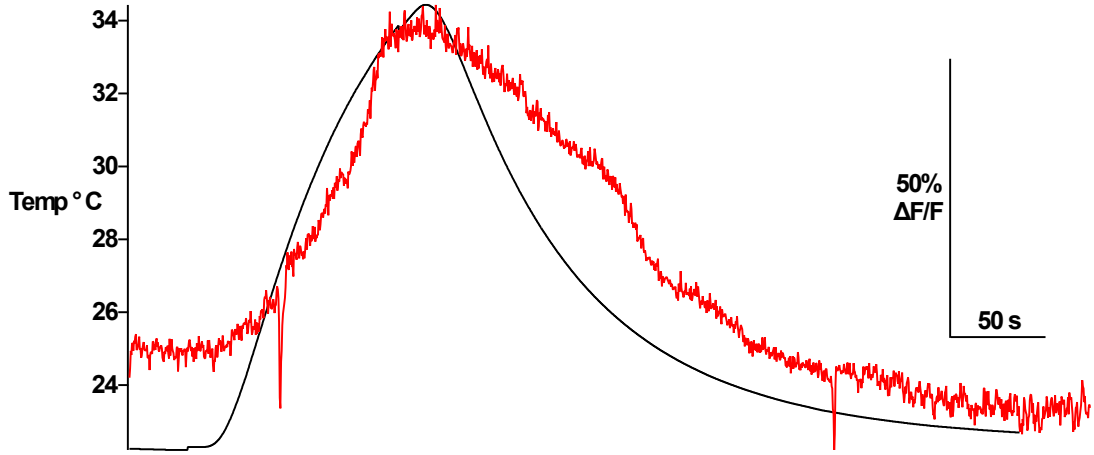

b

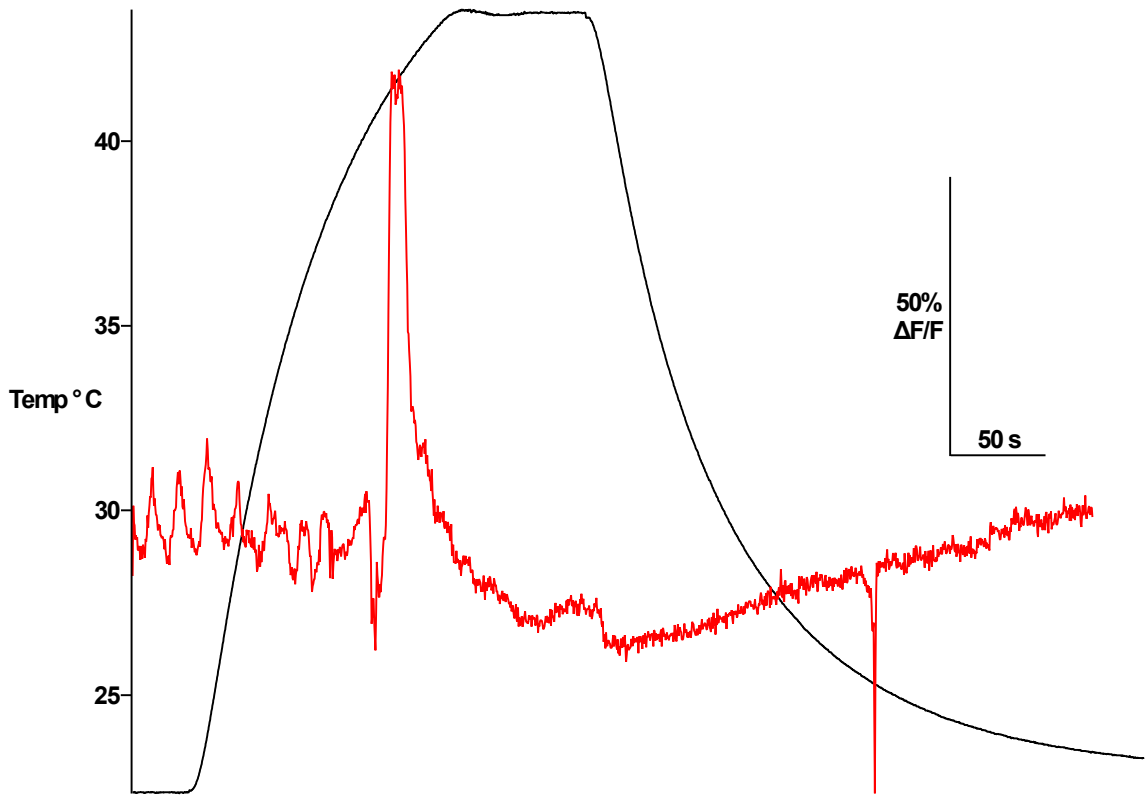

Figure 4.3. Confirming TrpA is repressed by Gal80 across the entire MB. a) jRGECO1A functional imaging recordings from single KC expressing UAS-TrpA1 (*LexAOP-jRGECO1A/Cyo; Mb247-LexA, LexAOP-TrpA/TM3-Ser*) to increasing temperature of the perfusion solution. Red line shows the ΔF/F response with a scale for this and time along the x axis shown on the right of the plot. Left y axis shows the temperature in °C which is represented by the solid black line on the plot. **b**) jRGECO1A functional imaging recordings from single KC expressing UAS-TrpA1 (*hsFLP, tubp-Gal80, neoFRT19A; UASGCaMP8M, UASmCherry/UASTrpA, LexAOP-jRGECO1A; R13F02-Gal4/MB247-LexA*). Scale and axes as in a.

4.2.4 Preliminary experiments find single γ KCs demonstrate decreased responses across all periods of hyperactivation

To determine the physiological changes that accompany activity-dependent loss of claws, I incubated flies at 31°C for 1 day and 4 days, the two periods of prolonged hyperactivity that induced this adaptation. I also repeated the 31°C 6 hour condition, to test if the neuron adapts its responses before it loses claws and identify any potential difference in the size of this adaptation across conditions. Single KCs were imaged separately in the calyx and γ lobe to distinguish between dendrite and axonal responses. A Fast Z stack was performed to record from as much of the dendrite/axon as possible while stimulating. Visually analysing the full calyx responses (Figure 4.4) shows that TrpA flies consistently have a lower response to antennal nerve stimulation at all frequencies across all 3 conditions tested (4 days, 1 day and 6 hours). A 2-way ANOVA comparing the average peak response at 120Hz between these conditions and the 22°C 1 day condition, which I will discuss later, found that only TrpA 31°C flies had significantly lower responses than control flies within their condition (Figure 4.4; Figure 4.8); the average of the peak of the response was defined as a 0.5 second window starting at onset of stimulation. There was also no significant interaction between genotype and condition, although there was a significant difference between genotype across conditions. Given the stark visual difference in response size between control and TrpA flies within each condition, it seems more likely that my ability to detect significant differences and an interaction is limited by the small sample size within the 6 hour and 4 day conditions (Figure 4.4). The percentage of brains successfully labelled is similar to the morphological experiments, and the number of these that result in successful responses is even lower. The GCaMP8M and mCherry signal in single neurons is quite dim, requiring maximum power on the 2P to visualise; this is likely due to a combination of limited fluorescence emanating from

single cells, reduced clarity through the live imaging window, and weaker baseline signal from GCaMP8m despite its improved signal to noise ratio. Additionally, antennal nerve dissection and suction had a variable success rate, with stimulation sometimes producing no response from flies across genotype/condition, likely as a result of damage to the nerve during dissection; responses from these flies were not included in analysis. Collectively, these factors and the difficulty of the technique meant a small proportion of the total flies dissected and recorded resulted in successful responses.

To compare differences in responses between genotype across all stimulation frequencies, I fit a nonlinear saturating curve, similar to a Hill function (Weiss, 1997), to the average peak responses of each genotype using the following equation: $y = k * \frac{x}{b+x}$; parameter k represents the saturation point, while b is the slope/represents how fast the saturation point is reached and x is the stimulation frequency. This equation is similar to one previously used to fit the relationship between ORN response and PN response in the *Drosophila* olfactory system (Olsen, Bhandawat and Wilson, 2010), but is applied here to describe the relationship between KC response and stimulation frequency. While their model raised x to the power of 1.5 to account for the steepness of the curve, this exponent adds another parameter and proved unnecessary in my work, as the relationship was adequately captured by the simplified equation without increasing the number of parameters. I then performed an extra sum-of-squares F test which determines whether separate curves fit to both conditions with the aforementioned parameters more adequately capture the spread of the data then a simpler model fit to data from both conditions. Significance indicates that if the null hypothesis (a single model) were true, it would be unlikely to produce data that fit the alternative hypothesis (two models) so much better; this was performed separately within each condition comparing only between genotype. Shading around fit indicates the 95% confidence interval, while the few examples of lines without shading was due to Graphpad Prism being unable to calculate these intervals, likely because the nonlinear saturating model could not be fit to that particular data set. The results of these F tests revealed that across all 3 conditions (6 hours, 1 day, 4 days), responses between genotypes significantly differed. If we further investigate the nonlinear curve (Figure 4.4) we can see the response in TrpA flies saturates at a much lower level than in controls, with 31°C 1 day demonstrating the most extreme difference between genotype; it is possible this is a result of this groups higher sample size compared to 6 hours and 4 day flies.

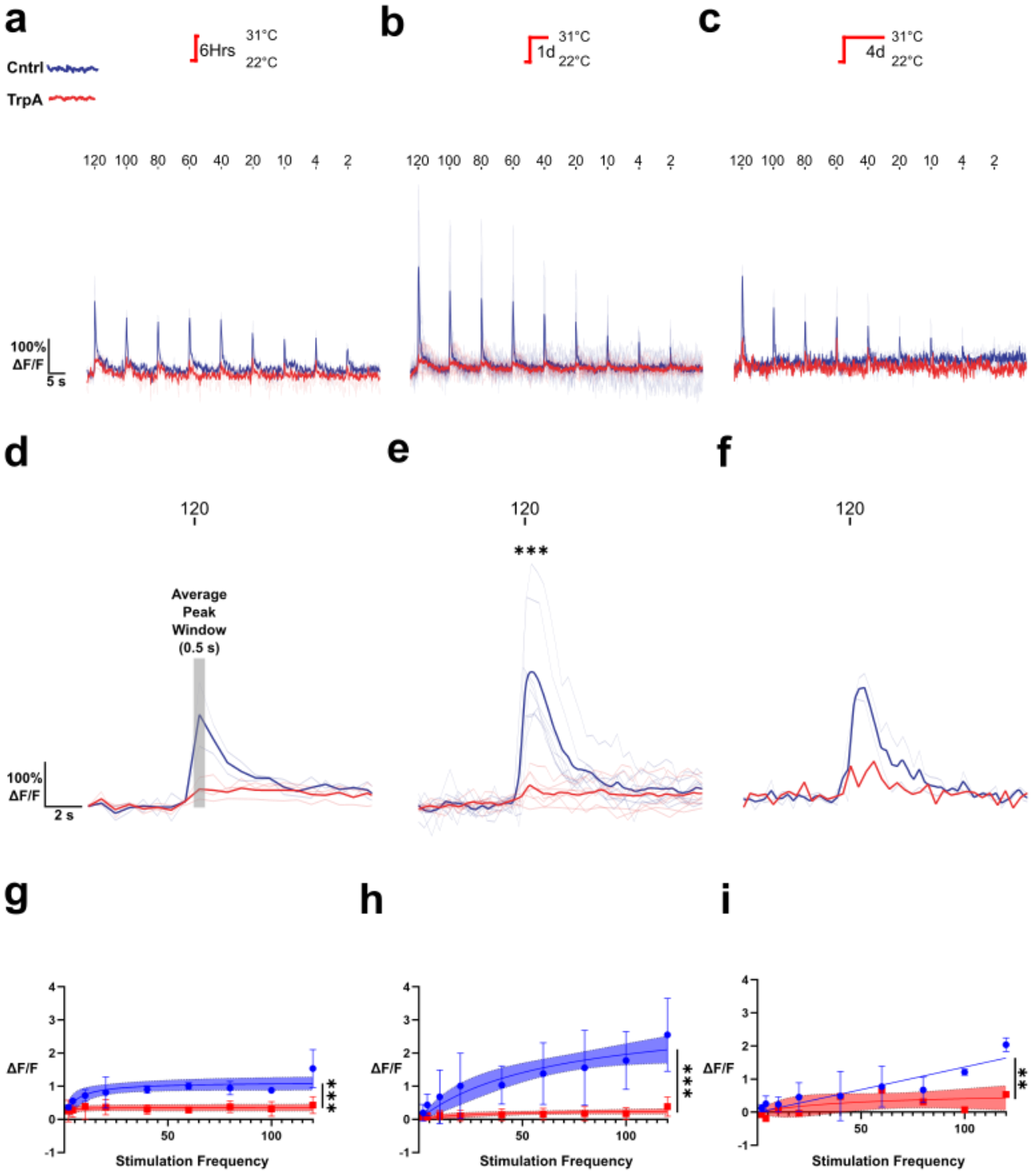
a
Cntrl
TrpA
6Hrs
31°C
22°C
b
1d
31°C
22°C
c
4d
31°C
22°C
120 100 80 60 40 20 10 4 2
100%
ΔF/F
5 s
d
e
f
120
***
Average
Peak
Window
(0.5 s)
100%
ΔF/F
2 s
g
h
i
ΔF/F
Stimulation Frequency
50
100
***

Figure 4.4. Single KC dendrite responses after 6 hours, 1 day and 4 days of TrpA activation. a-c) 6 hours (a), 1 day (b) and 4 days (c) of TrpA activation causes decreased responses in TrpA flies. Response to all stimulation frequencies (Hz) are shown. Scale bar on left applies to all traces and represents 100% ΔF/F and 0.5 seconds on the x axis. Timings of each pulse and frequency applied are shown above each peak. Conditions shown are maintained across all figures within a column. d-f) Responses at 120Hz only across all 4 conditions. 2-way ANOVA was performed across 31°C 6 hours, 1 day, 4 day and 22°C 1 day (Not shown, see Figure 4.6) conditions in dendrites. Tukey multiple comparison test with corrections was performed to compare between each group. g-i) A nonlinear saturating curve was fit to the average peak responses of each genotype using the equation $y = \frac{k*x}{b+x}$. In this model, y represents the average peak response and x is the stimulation frequency. Parameter k represents the saturation point, while b represents the stimulation frequency at which half of the saturation point is reached. An extra sum-of-squares F-test was used to compare between genotypes across conditions. Each point represents the mean response at that frequency, and error bars show the SD. a-i) *P<0.05, **P<0.01, ***P<0.001. n = Cntrl 31°C 6 hours (2), TrpA 31°C 6 hours (3), Cntrl 31°C 1 day (8), TrpA 31°C 1 day (7), Cntrl 31°C 4 days (2), TrpA 31°C 4 days (1)

Where possible after dendrites were recorded responses of axons were recorded separately, with stimulation repeated. Similar to dendrite responses, activity of TrpA axons is reduced when compared to control flies, as seen in the nonlinear saturating fits (Figure 4.5). A 2-way ANOVA again revealed a significant difference in genotype and no interaction and only 31°C 1 day control and TrpA flies had significantly different peaks at 120Hz; as before it seems likely that low n in the 6 hour and 4 day groups limits the ability to detect a significant difference on this test. However, the curve fits were significantly different on all 3 conditions (Figure 4.5), which combined with the visual differences suggests all periods of hyperactivity result in a reduced response in TrpA flies. It is worth noting that the amplitude of response is slightly lower in axons when compared to recordings from the calyx; this may represent stimulation failing to induce a spike.

Collectively, these results suggest that activity-dependent loss of claws is accompanied by a decrease in the responsiveness of these neurons, as you would expect if this adaptation was homeostatic. After all recordings/stimulations I took a Z stack of each neuron so that I could analyse their morphology later. However, the combination of low signal and the high power used to record during stimulations, means that counting claws or reconstructing the neurons from these Z stacks was impossible in most cases. This means I could not directly confirm the decreased claw count previously observed after 1 days and 4 days of TrpA activation. However, unless the difference in exact genotype abolished the claw loss adaptation, it seems likely these neurons still have fewer claws.

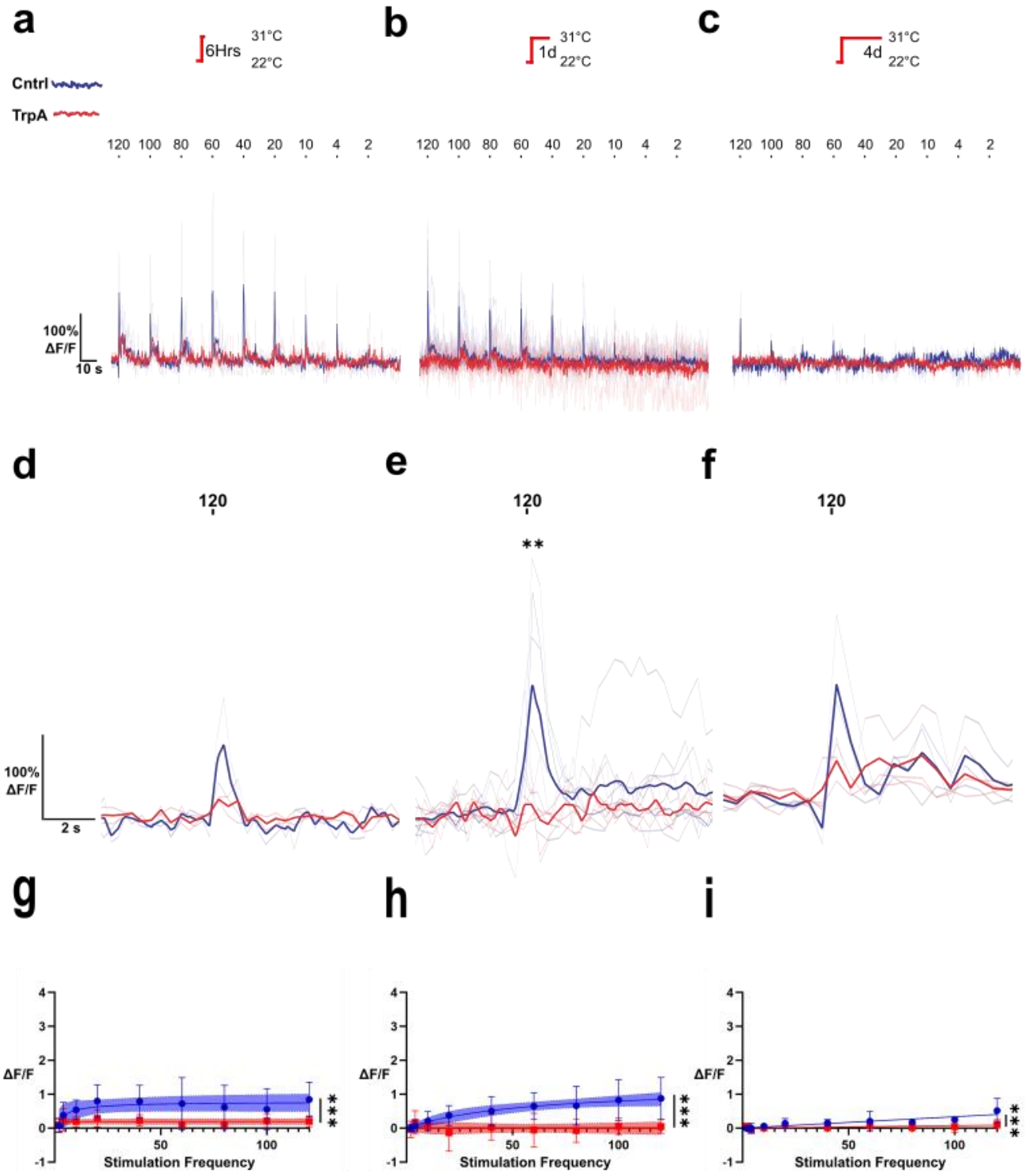
a
b
c
6Hrs
1d
4d
31°C
22°C
Cntrl
TrpA
120 100 80 60 40 20 10 4 2
100%
ΔF/F
10 s
d
e
f
120
**
2 s
g
h
i
ΔF/F
Stimulation Frequency
50
100
***

Figure 4.5. Single KC axon responses after 6 hours, 1 day and 4 days of TrpA activation. a-c) 6 hours (a), 1 day (b) and 4 days (c) of TrpA activation causes decreased responses in TrpA flies. Response to all stimulation frequencies (Hz) are shown. Scale bar on left applies to all traces and represents 100% ΔF/F and 0.5 seconds on the x axis. Timings of each pulse and frequency applied are shown above each peak. Conditions shown are maintained across all figures within a column. d-f) Responses at 120Hz only across all 3 conditions. 2-way ANOVA was performed across 31°C 6 hours, 1 day, 4 day and 22°C 1 day (Not shown, see Figure 4.6) conditions in axons. Tukey multiple comparison test with corrections was performed to compare between each group. g-i) A nonlinear saturating curve was fit to the average peak responses of each genotype using the equation $y = \frac{k*x}{b+x}$. In this model, y represents the average peak response and x is the stimulation frequency. Parameter k represents the saturation point, while b represents the stimulation frequency at which half of the saturation point is reached. An extra sum-of-squares F-test was used to compare between genotypes across conditions. Each point represents the mean response at that frequency, and error bars show the SD. a-i) *P<0.05, **P<0.01, ***P<0.001. n = Cntrl 31°C 6 hours (3), TrpA 31°C 6 hours (3), Cntrl 31°C 1 day (8), TrpA 31°C 1 day (5), Cntrl 31°C 4 days (2), TrpA 31°C 4 days (1)

4.2.5 Preliminary experiments find single α/β Kenyon cells also demonstrate slightly reduced responses after prolonged TrpA activation

Despite the lack of activity-dependent loss of claws in α/β KCs I wanted to test if they demonstrated a homeostatic decrease in response like γ KCs. The protocol for labelling α/β KCs was the same as in 3.2.8. Once eclosed flies were incubated at 31°C for 1 day and then dissected and imaged to identify differences in responses when stimulated. The calyx, α lobe and β lobe were all recorded from separately in brains with single cells labelled. However, due to inconsistent responses and poor sample size, recordings from the β lobe were discarded. This revealed that TrpA flies have lower responses in both the calyx and the α lobe, although when comparing average peak responses at 120Hz only, there was no significant difference between any group, possibly resulting from the combination of low sample size and a smaller effect in α/β KCs. However, the curve fits were significantly different across both conditions. Regardless these findings suggest that α/β KCs decrease their activity in response to prolonged hyperactivation implying, as posited in Section 3, they may have alternative compensatory mechanisms. This also assumes that loss of claws is solely responsible for the decreased response in γ KCs, which seems unlikely; more on this in this section’s discussion.

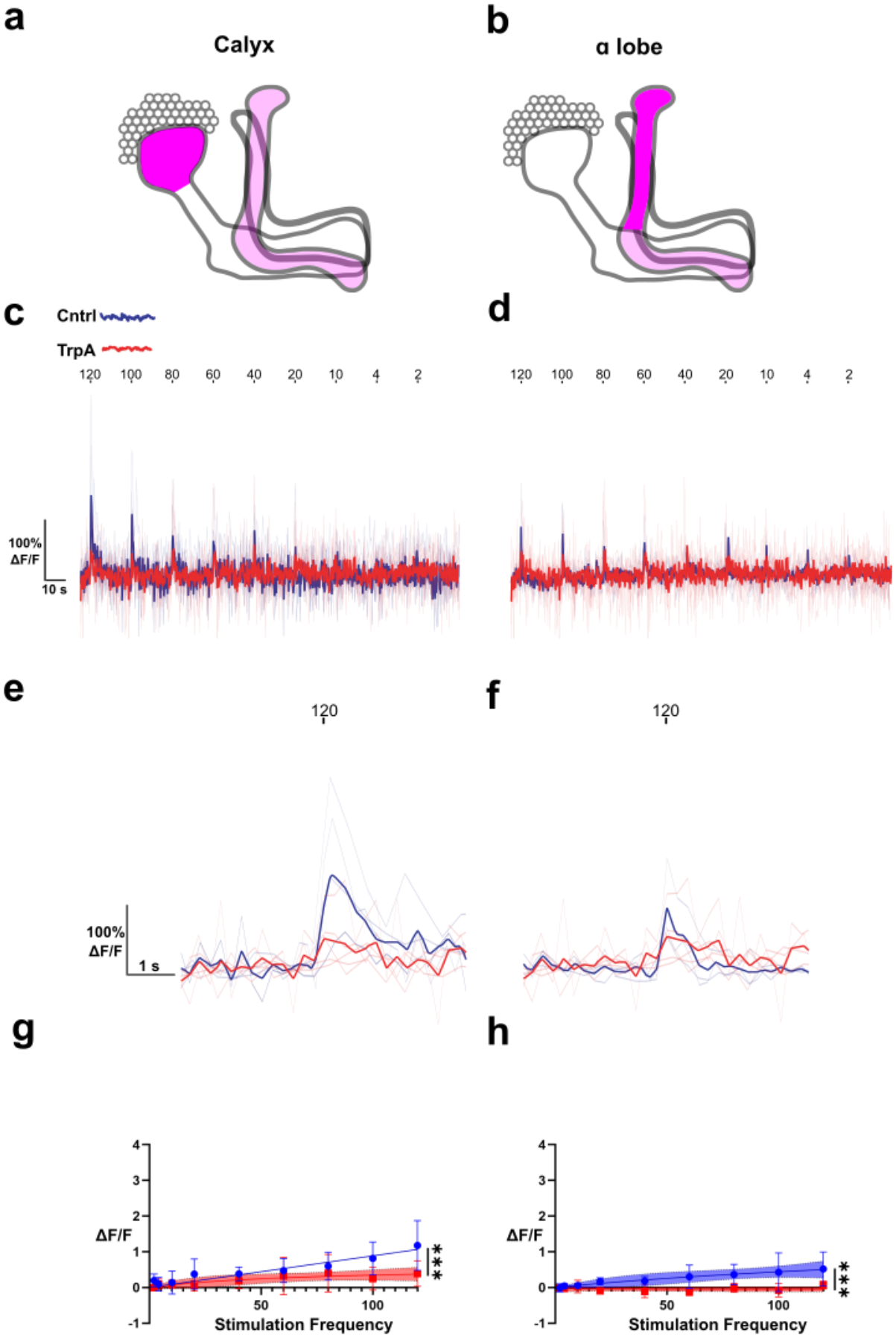
a
Calyx
b
α lobe
c
Cntrl
TrpA
120 100 80 60 40 20 10 4 2
100%
ΔF/F
10 s
d
120 100 80 60 40 20 10 4 2
e
120
100%
ΔF/F
1 s
f
120
g
ΔF/F
Stimulation Frequency
50
100
***
h
ΔF/F
Stimulation Frequency
50
100
***

Figure 4.6. Single α/β KC calyx and alpha lobe responses after 1 day of TrpA activation. a-b) Schematic diagrams of the mushroom body with the calyx (a) and α lobe (b) highlighted indicating the region responses belong to in the corresponding column. **c-d**) 1 day TrpA activation causes decreased responses in the calyx and alpha lobe of TrpA flies. Response to all stimulation frequencies (Hz) are shown. Scale bar on left applies to all traces and represents 100% ΔF/F and 0.5 seconds on the x axis. Timings of each pulse and frequency applied are shown above each peak. **e-f**) Average peak responses at 120Hz in single cells in the calyx (e) and α lobe (f). 2-way ANOVA was performed across both genotypes and between calyx and α lobe responses. Tukey multiple comparison test with corrections was performed to compare between each group. **g-h**) A nonlinear saturating curve was fit to the average peak responses of each genotype using the equation $y = \frac{k*x}{b+x}$. In this model, y represents the average peak response and x is the stimulation frequency. Parameter k represents the saturation point, while b represents the stimulation frequency at which half of the saturation point is reached. An extra sum-of-squares F-test was used to compare between genotypes across conditions. Each point represents the mean response at that frequency, and error bars show the SD. a-i) *P<0.05, **P<0.01, ***P<0.001. n = Cntrl 31°C 1 day Calyx α/β (4), TrpA 31°C 1 day Calyx α/β (5), Cntrl 31°C 1 day alpha lobe α/β (3), TrpA 31°C 1 day alpha lobe α/β (3),

4.2.6 The 22°C γ control group still shows decreased responses in TrpA flies

After analysing the 31°C 6 hour, 1 day and 4 day conditions I wanted to confirm that presence of TrpA alone did not result in any changes to responses, similar to the 22°C control experiment for my morphological results (Figure 3.4). I incubated the single cell live imaging flies at 22°C and recorded from stimulated flies as in 4.2.4. However, this surprisingly revealed that TrpA flies incubated at 22°C still demonstrated a significantly decreased response compared to controls in both dendrites and axons of single KCs (Figure 4.7), although this difference was more pronounced in dendrite responses. This suggests that TrpA may still be slightly active at 22°C despite previous findings (Hamada et al., 2008; Lin et al., 2014), which may partially result from prior experiments 'baseline response' temperature starting at 22-24°C; this means there is no lower temperature response to compare to, resulting in the conclusion these flies do not start to respond till ~25°C. If the TrpA channel is open at 22°C this is also potentially problematic for my previous experiments as all flies are raised at this temperature. This increases the likelihood that the adaptations observed were a result of activity-sensitive developmental changes and not adult homeostatic plasticity. However, the 22°C control flies in the morphological experiments showed no reduction in number of claws, suggesting this adaptation may still be a result of activity-dependent adult plasticity, or at least requires greater activity during adulthood to induce.

To determine at exactly what temperature TrpA begins to open and activate KCs in the single cell live imaging genotype, I put the perfused external solution on ice until the temperature dropped to ~17°C and imaged flies with single γ KCs labelled. I then gradually heated the solution to ~31°C while recording responses and then slowly cooled the solution back down to ~17°C again. This revealed that flies reached a peak response size at ~22°C (Figure 4.9). It is likely that this would continue to increase with temperature but the large laser power required to illuminate single KCs for an extended period of time appears to cause photobleaching, seen as a gradual decrease in response as temperature continues to increase (Figure 4.9). However, responses rapidly decrease in amplitude as temperature begins to decline, indicating likely closing of TrpA channels. Importantly, this experiment demonstrated that the calcium response of these neurons begins to increase at as low as 20°C, demonstrating that 22°C is definitely sufficient to induce TrpA channel opening and induce an increase in the neuron's activity.

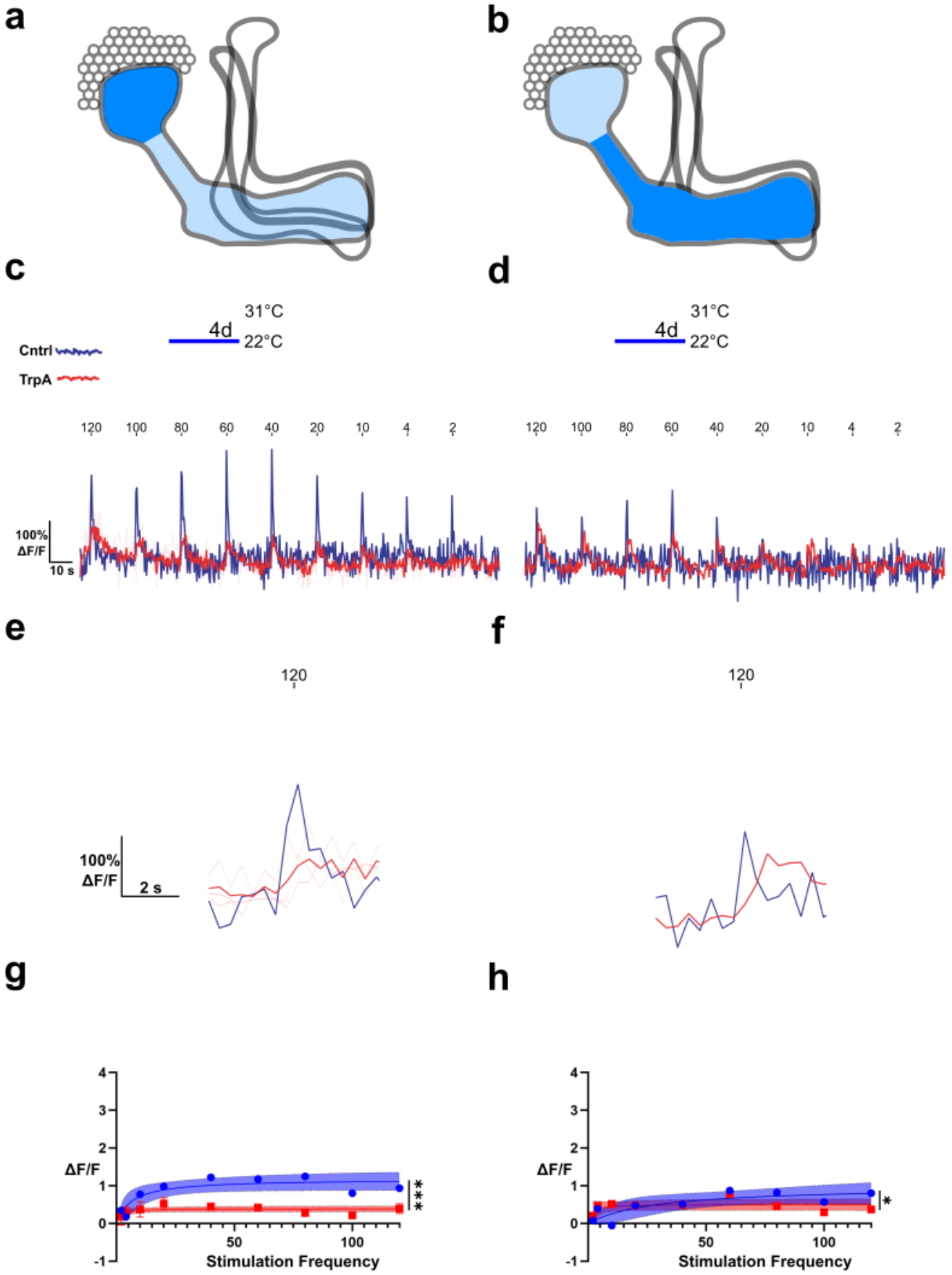
a
b
c
d
31°C
4d
22°C
Cntrl
TrpA
120
100
80
60
40
20
10
4
2
100%
ΔF/F
10 s
e
f
2 s
g
h
ΔF/F
Stimulation Frequency
50
100
***
*

Figure 4.7. Single KC dendrite and axon responses after 1 day at 22°C. a-b) Schematic diagrams of the mushroom body with the calyx (a) and γ lobe (b) highlighted indicating the region responses belong to in the corresponding column. **c-d)** 1 day at 22°C causes decreased responses in the calyx and gamma lobe of TrpA flies. Response to all stimulation frequencies (Hz) are shown. Scale bar on left applies to all traces and represents 100% ΔF/F and 0.5 seconds on the x axis. Timings of each pulse and frequency applied are shown above each peak. **e-f)** Average peak responses at 120Hz in single cells in the calyx (e) and gamma lobe (f). 2-way ANOVA was performed across 31°C 6 hours, 1 Day, 4 day and 22°C 1 day axon average peak responses. Tukey multiple comparison test with corrections was performed to compare between each group. **g-h)** A nonlinear saturating curve was fit to the average peak responses of each genotype using the equation $y = \frac{k*x}{b+x}$. In this model, y represents the average peak response and x is the stimulation frequency. Parameter k represents the saturation point, while b represents the stimulation frequency at which half of the saturation point is reached. An extra sum-of-squares F-test was used to compare between genotypes across conditions. Each point represents the mean response at that frequency, and error bars show the SD. a-i) *P<0.05, **P<0.01, ***P<0.001. n = Cntrl 22°C 1 day Calyx (1), TrpA 22°C 1 day Calyx (3), Cntrl 22°C 1 day gamma lobe (1), TrpA 22°C 1 day gamma lobe (1).

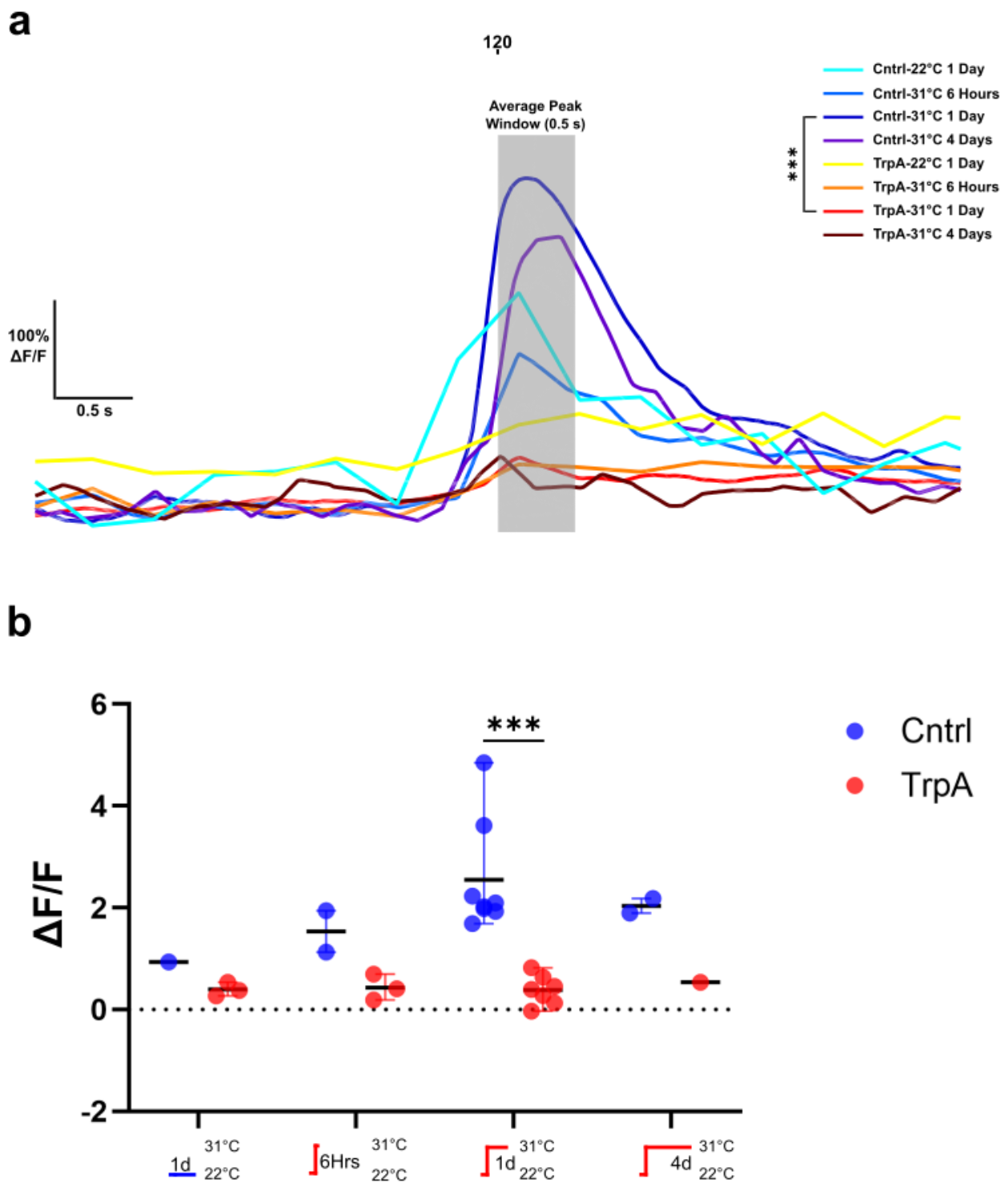
a
120
Average Peak
Window (0.5 s)
Cntrl-22°C 1 Day
Cntrl-31°C 6 Hours
Cntrl-31°C 1 Day
Cntrl-31°C 4 Days
TrpA-22°C 1 Day
TrpA-31°C 6 Hours
TrpA-31°C 1 Day
TrpA-31°C 4 Days
***
100%
ΔF/F
0.5 s
b
6
4
2
0
-2
ΔF/F
***
Cntrl
TrpA
31°C
1d
22°C
31°C
6Hrs
22°C
31°C
1d
22°C
31°C
4d
22°C

Figure 4.8. Comparing the average peak response between all conditions at flies raised at 22°C. a) Mean peak responses at 120Hz only across all 4 conditions. 2-way ANOVA was performed across 31°C 6 hours, 1 day, 4 day and 22°C 1 day (Not shown, see Figure 4.6) conditions in dendrites. Tukey multiple comparison test with corrections was performed to compare between each group. **0.5 second window in which mean response values were calculated is shown by grey shaded area. b)** Mean calyx single KC ΔF/F 120Hz responses across conditions; individual data points represent the response of an individual fly. Error bars represent the range. a-b) *P<0.05, **P<0.01, ***P<0.001. n = Cntrl 22°C 1 day Calyx (1), TrpA 22°C 1 day Calyx (3), Cntrl 31°C 6 hours (2), TrpA 31°C 6 hours (3), Cntrl 31°C 1 day (8), TrpA 31°C 1 day (7), Cntrl 31°C 4 days (2), TrpA 31°C 4 days (1)

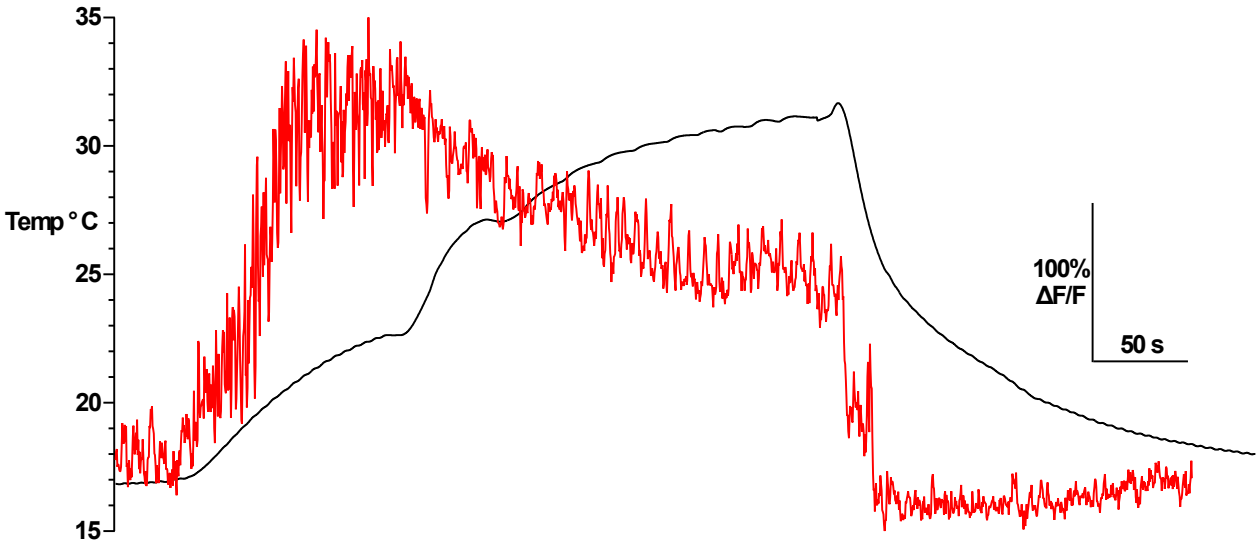

Figure 4.9. Example temperature calcium response of a single γ KC expressing TrpA. Fly was perfused on ice with an ~ temperature of 17°C. Red line shows the ΔF/F response with a scale for this and time along the x axis shown on the right of the plot. Left y axis shows the temperature in °C which is represented by the solid black line on the plot

Unfortunately, this test cannot conclusively confirm TrpA is not open at 18°C either. In fact, recordings start at ~17°C and even in the change from 17 to 18°C it appears there is a slight increase in calcium response. However, raising flies at even lower temperatures would increase experimental time even further due to slowed development and may impact their development significantly. Furthermore, it is possible lower temperatures may still induce slight TrpA opening but recording at sub-17°C temperatures is quite difficult to achieve in an open system,e.g. no fine temperature control of the room/microscope; I will discuss the implications of TrpA's unexpected sensitivity to lower temperatures in this Chapters Discussion. These results at least suggested 18°C may not significantly activate neurons expressing TrpA, so I next wanted to determine whether raising flies at 18°C would still produce the decreased response observed in 22°C TrpA flies. Additionally, now that it was clear TrpA is active at 22°C I wanted to make sure neurons were not being activated by the external temperature during stimulation. I also noticed a recurring issue where the responses of TrpA KCs rose at the beginning of the recording (Figure 4.10) causing a high initial baseline before the first antennal nerve pulse; I suspected the initial heat of the laser onset was triggering opening of TrpA channels. To assess the impact of these issues I trialled 4 different conditions while recording in flies raised at 18°C and incubated at the same temperature for the first day of adulthood. These conditions were a combination of recording while solution was cooled to ~17°C (Ice) vs no cooling (Non-ice) and adding an initial 40 seconds to the recording before stimulating (Delayed onset) vs only 5 seconds recording before the first pulse (Regular onset) (Figure 4.10). TrpA flies recorded at 17°C had almost identical responses to their control counterparts, with no significant difference on a 2 way ANOVA comparing their mean peak responses at 120Hz (Figure 4.10). In contrast, TrpA flies recorded at room temperature had slightly lower responses than controls, although this difference was not a significant on a 2-way ANOVA; only responses from TrpA flies on ice vs those not on ice significantly differed. This slight difference in response is likely a result of a small amount of TrpA activation occurring at this temperature, although why this would produce a lower response is unclear (more on this in 4.3.1). The same conditions with delayed onset had very similar findings, suggesting onset does not significantly alter the calcium response of these neurons. However, the initial rise in baseline response can be seen in the Delayed onset TrpA flies, so it seemed worthwhile to take this precaution going forward. It is worth noting that the nonlinear fit between Iced control and TrpA flies appears to differ at only lower frequencies, which could suggest TrpA still impacts excitability at lower frequencies even at 17°C. However, as demonstrated by the non-significant difference in the 120Hz 2-way ANOVA, this difference is lost at higher frequencies, suggesting this

temperature is at least more effective at reducing the impact of TrpA on excitability over 22°C. Collectively, these results suggest that flies raised at 18°C do not exhibit significantly decreased activity in TrpA-expressing KCs, as shown by the lack of difference between control and TrpA-containing genotypes under 17°C recording conditions. The slight difference seen in Non iced flies may arise from TrpA activation resulting in a higher baseline at this temperature. Following these results, future experiments were raised at 18°C, recorded at 17°C to reduce TrpA activation and had a delayed onset to solve the initial rise in baseline issue.

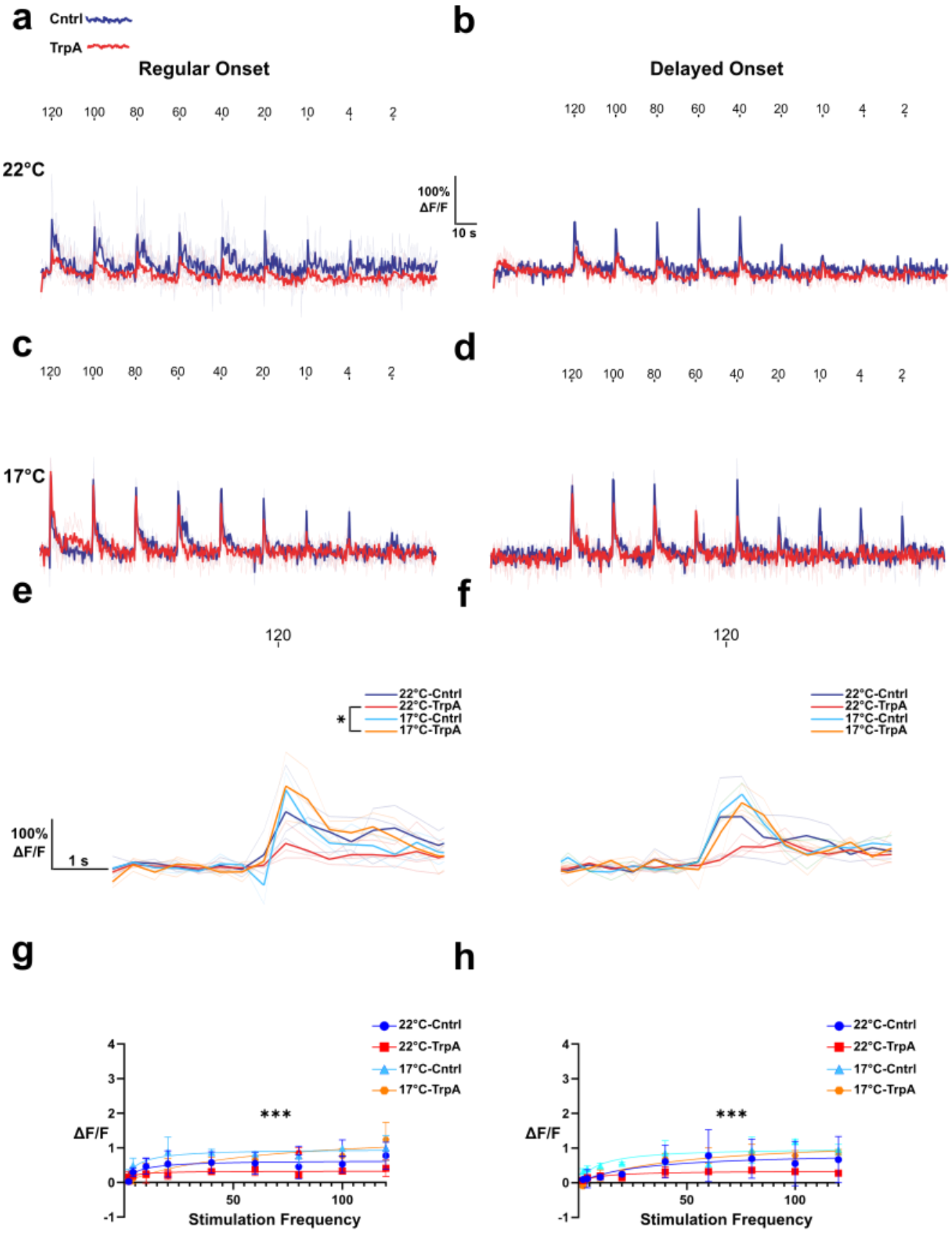
a
Cntrl
TrpA
Regular Onset
b
Delayed Onset
120 100 80 60 40 20 10 4 2
22°C
100%
ΔF/F
10 s
c
d
17°C
e
f
22°C-Cntrl
22°C-TrpA
17°C-Cntrl
17°C-TrpA
*
100%
ΔF/F
1 s
g
h
***
ΔF/F
Stimulation Frequency
50
100

Figure 4.10. Determining the effect of onset timing and recording temperature on single KC responses in flies raised at 18°C. a-d) Full dendrite responses to antennal nerve stimulation in 18°C 1 day flies recorded in different conditions. **a-h**) The left and right column show Regular onset and Delayed onset respectively while the top and bottom row (**a-d**) show responses recorded at 22°C and 17°C . Response to all stimulation frequencies (Hz) are shown. Scale bar to the left of b applies to all traces and represents 100% ΔF/F and 0.5 seconds on the x axis. Timings of each pulse and frequency applied are shown above each peak. **e-f**) Mean peak dendrite responses at 120Hz of flies recorded at 17°C or 22°C; e shows Regular onset only, while f shows Delayed onset only. 2-way ANOVA was performed across all conditions (both Temperature and Onset combinations). Tukey multiple comparison test with corrections was performed to compare between each group. **g-h**) A nonlinear saturating curve was fit to the average peak responses of each genotype and condition using the equation $y = \frac{k*x}{b+x}$. In this model, y represents the average peak response and x is the stimulation frequency. Parameter k represents the saturation point, while b represents the stimulation frequency at which half of the saturation point is reached. An extra sum-of-squares F-test was used to compare between genotypes across conditions. Plot g shows all Regular onset response curves while h shows Delayed onset curves. Each point represents the mean response at that frequency, and error bars show the SD. a-h) *P<0.05, **P<0.01, ***P<0.001. n = Cntrl 18°C Regular onset imaged at 22°C (3), TrpA 18°C Regular onset imaged at 22°C (3), Cntrl 18°C Delayed onset imaged at 22°C (2), TrpA 18°C Delayed onset imaged at 22°C (3), Cntrl 18°C Regular onset imaged at 17°C (2), TrpA 18°C Regular onset imaged at 17°C (3), Cntrl 18°C Delayed onset imaged at 17°C (2), TrpA 18°C Delayed onset imaged at 17°C (3).

4.2.7 In flies raised at 18°C, Kenyon cells hyperactivated for 1 day still decrease their responses

After confirming that TrpA is not active at 18°C and that these flies do not show decreased responses when raised at this temperature, I wanted to test whether hyperactivated KCs still decrease their responses under these recording conditions. After raising flies at 18°C I collected them after eclosion and incubated them at 31°C for 1 day before dissecting, stimulating and recording them as described previously (on ice and with delayed onset before stimulation). Although not as pronounced as the previous 31°C 1 day TrpA responses, TrpA flies still had a significantly lower dendrite response to stimulation compared to controls (Figure 4.11d). I performed a 2 way ANOVA to compare control and TrpA flies of this condition with flies raised at 18°C and recorded on ice with Delayed onset; there was no significant interaction between genotype and condition (p=0.176), although again I suspect my ability to detect this is limited by the small sample size; this limitation was a result of time constraints

at the end of the project. The slightly smaller difference in these flies compared to the previous group activated for 1 day, is likely a result of not recording on Ice previously which as seen in Figure 4.10 reduces the response of these flies. However, I cannot rule out that some combination of developmental activity and increased adult activity in these neurons is responsible for the previous more pronounced decrease in TrpA fly responses. Regardless by repeating this experiment with flies raised at 18°C, I can confirm that they still show a compensatory reduction in their responses, associated with an activity-dependent loss of claws.

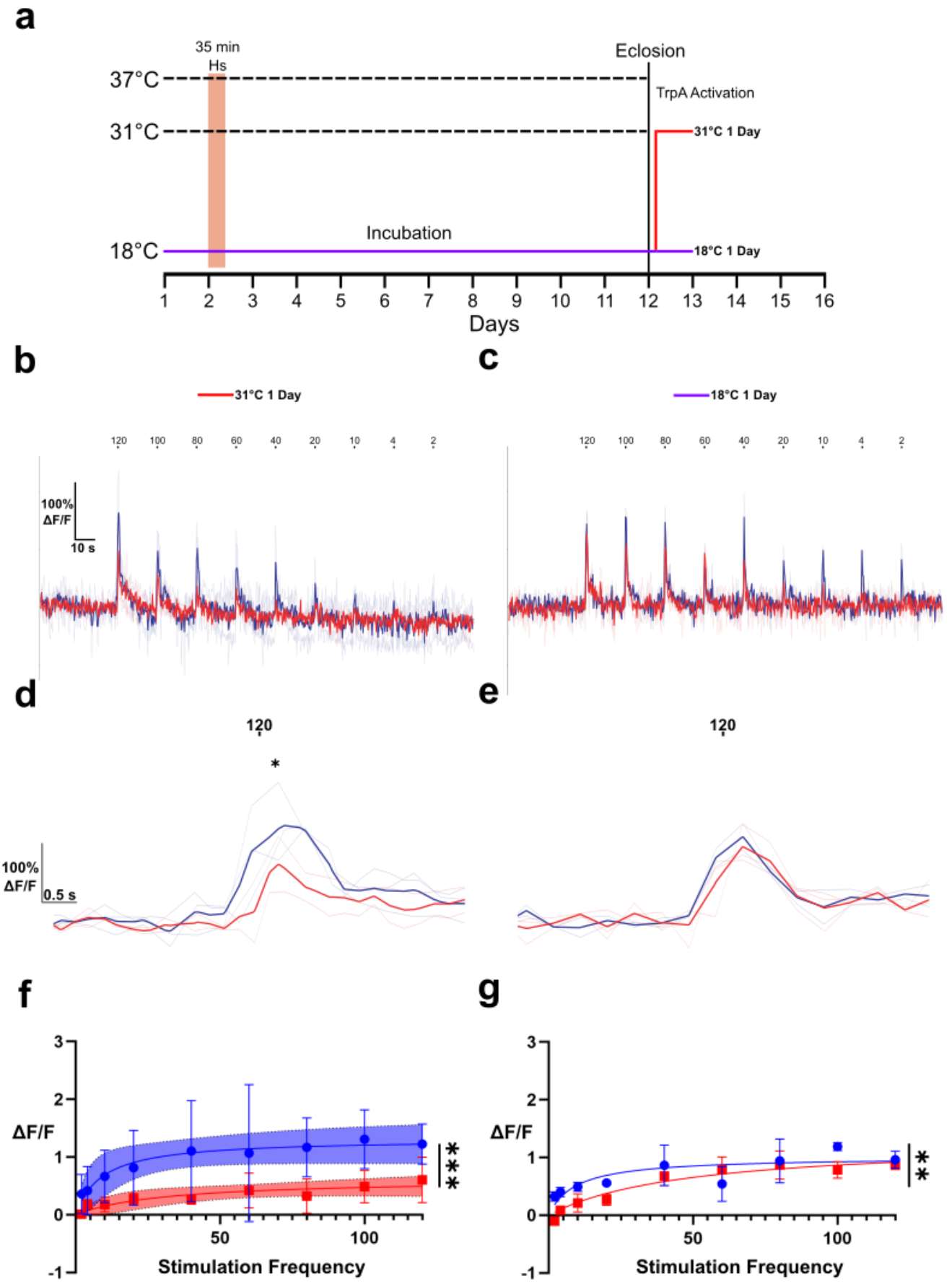
a
35 min
Hs
Eclosion
37°C
TrpA Activation
31°C
31°C 1 Day
Incubation
18°C
18°C 1 Day
1 2 3 4 5 6 7 8 9 10 11 12 13 14 15 16
Days
b
31°C 1 Day
120 100 80 60 40 20 10 4 2
100%
ΔF/F
10 s
c
18°C 1 Day
120 100 80 60 40 20 10 4 2
d
120
*
100%
ΔF/F
0.5 s
e
120
f
ΔF/F
3
2
1
0
-1
50
100
Stimulation Frequency
***
g
ΔF/F
3
2
1
0
-1
50
100
Stimulation Frequency
**

Figure 4.11. Single KC TrpA dendrites still homeostatically reduce their response when raised at 18°C and then activated for 1 day during adulthood. a) To achieve labelling of single γ KCs vials were heatshocked (Hs) 2 days after egg laying as described previously (Lee, Lee and Luo, 1999). Flies were raised at 18°C until eclosion (~12-15 days after egg laying). After eclosion flies were then incubated at 18°C for 1 day in the control condition or at 31°C for 1 day to activate TrpA and test the effect of 1 day hyperactivity on KC dendrite responses. Flies were then dissected and recorded in vivo while stimulated on ice. **b-c**) 1 day at 31°C causes decreased responses in the dendrites of TrpA flies. Response to all stimulation frequencies (Hz) are shown. Scale bar on left applies to all traces and represents 100% ΔF/F and 0.5 seconds on the x axis. Timings of each pulse and frequency applied are shown above each peak. **d-e**) Average peak dendrite responses at 120Hz in flies incubated at 31°C for 1 day (d) and at 18°C for 1 day (e). 2-way ANOVA was performed on 31°C 1 day and 18°C 1 day (ice delayed onset) flies across both genotypes. Tukey multiple comparison test with corrections was performed to compare between each group. **g-h**) A nonlinear saturating curve was fit to the average peak responses of each genotype and condition using the equation $y = \frac{k*x}{b+x}$. In this model, y represents the average peak response and x is the stimulation frequency. Parameter k represents the saturation point, while b represents the stimulation frequency at which half of the saturation point is reached. An extra sum-of-squares F-test was used to compare between genotypes across conditions. Plot g shows all Regular onset response curves while h shows Delayed onset curves. Each point represents the mean response at that frequency, and error bars show the SD. a-h) *P<0.05, **P<0.01, ***P<0.001. n = Cntrl 31°C 1 day raised at 18°C (3), TrpA 31°C 1 day raised at 18°C (2), Cntrl 18°C Ice Delayed onset (2), TrpA 18°C Ice Delayed onset (3).

4.3 Discussion

4.3.1 Interpretation of results in light of TrpA issues

Single KCs hyperactivated for 6 hours, 1 day and 4 days all show reduced calcium responses suggesting the activity-dependent loss of claws is accompanied by a homeostatic reduction in the neuron's activity. Before interpreting whether claw loss is responsible for this change, the problem of TrpA's activation at 22°C needs to be discussed. As established in the 22°C control group (Figure 4.7) and my heating experiments (Figure 4.9), TrpA begins to open and induce changes in calcium response at temperatures as low as 20°C; this is despite previous reports that neurons containing TrpA don't begin to spike until ~25-26°C (Hamada et al., 2008); this spiking onset temperature has also been confirmed by others (Pulver et al., 2009) where it was also observed TrpA-expressing neurons have a spiking frequency of 0 at 23°C. Spiking may be the important distinction here however, as both these experiments performed electrophysiological recordings on TrpA-expressing neurons, while I am measuring change in calcium response using GCaMP8m. Given TrpA is a non-specific cation channel, this means

it also allows influx of Ca2+ which could directly influence the calcium response measured by GCaMP. It is possible that at lower temperatures, a small proportion of the total channels are open producing a small and consistent influx of cations that is detected during GCaMP recordings, but is not sufficient to produce a spike and so was not detected previously (Hamada et al., 2008; Pulver et al., 2009). It is possible that this small amount of TrpA activation would result in an increased resting membrane potential, which could result in a slight increase in spiking frequency as a result of a slightly lower spiking threshold. This of course assumes no adaptations counter this change and it is currently unclear from the 22°C results whether their decreased responses are a result of an adaptation or are due to room temperature recordings activating the TrpA. It is unlikely that the lower responses to stimulation in non-iced neurons raised at 18°C is caused by any homeostatic adaptation. Instead, the combination of a higher baseline response, due to TrpA activation in these neurons at the start of the recording, and an absolute ceiling to the calcium response, as seen in the saturating nature of these responses, makes responses appear smaller even though they would likely be very similar to controls. This could be confirmed using live recording and a combination of EGTA and Ionomycin. EGTA is a calcium chelator (Miller and Smith, 1984) that could be applied to the MB to remove extracellular calcium ions and when combined with application of Ionomycin, which creates calcium permeable pores in the cell membrane (Liu and Hermann, 1978), should induce rapid efflux of intracellular calcium. If TrpA neurons have a higher base calcium level, recording with GCaMP during application of these compounds should result in a significantly larger decrease in baseline calcium response vs controls. This technique could be performed ex vivo which may help increase clarity of signal and offset its inherent difficulty.

Alternatively, if TrpA is constantly open this could decrease input resistance by producing a leak conductance. This could reduce the amplitude of EPSPs, as Ohms law (V = IR) dictates that a lower resistance means the same amount of synaptic current would produce a decreased voltage. It is unclear what net effect on the activity of the neuron would result from the theoretical combination of increased leak conductance and the aforementioned decreased spiking threshold; it would likely depend on which of these two factors was more dominant, but without electrophysiological recordings this is hard to determine. The best approach is to interpret all results in flies raised at 22°C with caution. We know that activity-dependent loss of claws does not occur in 22°C controls so it seems likely this is a result of the adult increase in activity and not a developmental rise in resting membrane potential. Furthermore, my later 31°C 1 day TrpA flies that were raised at 18°C still showed a

decreased response when recorded on ice, although this difference is slightly smaller than that observed in flies raised at 22°C. Collectively, this suggests my findings are not a result of any developmental activation of these neurons but is caused by increased activity in adults.

Interestingly few of the experiments linking morphological and physiological homeostatic adaptations discussed earlier (Section 1.7.3) increase the activity of neurons, but there are several examples to compare to. For example, hippocampal pyramidal neurons hyperactivated with the optogenetic tool channelrhodopsin-2 for 12-24 hours demonstrate a decrease in volume and number of spines, which is accompanied by a decrease in mEPSC amplitude and frequency (Goold and Nicoll, 2010; Moulin et al., 2019). From the initial experiments characterising synaptic scaling it is well established that artificially increasing activity results in a homeostatic decrease in the neurons activity to compensate(Turrigiano et al., 1998). My findings don't deviate from this trend and demonstrate a clear activity-dependent reduction in response at all time points (although the size of this difference varies between conditions). If the combination of adaptations (claw loss and decreased response) are homeostatic, they match what has been seen in other systems.

4.3.2 The link between physiological and morphological adaptations in single KCs

Returning to the key question of whether loss of claws is homeostatic, this is where my findings become less clear. I know that prolonged activity for 1-4 days causes a reduction in the number of claws in γ KCs, and this manipulation also causes a decrease in calcium responses in the single cell live imaging genotype. Recent computational modelling from our lab (P Fischer, unpublished results) predicts that dropping the KCs excitatory weights by only 20% is sufficient to completely abolish their odour responses, partially as a result of the high spiking threshold of these neurons. Following this logic, it is not unreasonable to suppose that if KCs drop 20% of their claws while their spiking threshold remains the same, this may also be sufficient to completely silence γ KCs. However, there are many other potential parameters the neuron may be adapting, including spiking threshold, that challenge the idea KC homeostatic mechanisms are as simple as reduction in number of inputs. For example, the current reversal results suggest claws can be removed but not 'reinstated'; without this possibility it is impossible for this mechanism to consistently restore neurons to a set point of activity alone. To determine the contribution claws and their loss have on the neuron's activity, future experiments could artificially manipulate the existing claw number in KCs. For example, knockdown of Tao, a kinase that regulates microtubule dynamics and dendritic branching (King et al., 2011; Hu et al., 2020) in *Drosophila*, induces an increase in the number of claws per KC and increases their odour responses (Ahmed et al., 2023). It is

possible that knockout of Tao in single KCs hyperactivated with TrpA would abolish the activity-dependent loss of claws and allow us to assess how activity changes without this adaptation. In combination with experiments in other systems demonstrating an association between dendrite loss and activity decrease (Goold and Nicoll, 2010; Moulin et al., 2019), it seems likely loss of claws influences the neurons activity, but I cannot confidently draw this conclusion with the available evidence.

To determine why some claws are removed over others, I had hoped I would be able to distinguish single claws enough in my live imaging genotype, that I could identify any changes in calcium responses in single claws. Unfortunately, the signal proved too weak to capture individual claw responses in most cases, leaving the factors influencing claw removal and their relation to the neurons activity unclear. As alluded to in the discussion of Chapter 3, it is possible that the strength of claws/number of synapses on claws could be a deciding factor in a claw's removal. For example, if you removed the 'strongest' claws this would likely be effective at reducing the neurons activity, but it is possible these claws are more valuable than others. The reason for their increased synaptic weight may be because connections with that particular PN are repeatedly active, suggesting that odour is being regularly encountered and remembering its associated valence may be important. In this scenario competing Hebbian and homeostatic factors could drive the neuron to select 'weaker' claws to remove, in a compromise between maintaining important connections while reducing the neurons activity that still results in decreased activity overall. However, there is currently no evidence for an LTP-like adult plasticity in synapse weight at the PN-KC synapses. It is equally possible that the mostly stochastic nature of the formation of PN-KC connections, means the strength of synapses is somewhat randomly determined from some acceptable range required for the KC to function e.g. spike when the majority of its PNs do. It is possible an alternative calcium indicator like GCaMP6f, would have an increased signal making it easier to distinguish individual claws, but for now I have no evidence from the responses of individual claws to help deduce the connection between claw loss and activity decrease.

Prolonged hyperactivity induces both loss of claws and decreased antennal nerve response in single KCs, but this only demonstrates a strong association between these two effects without proving that loss of claws causes the decrease in KC responses. While plausible that loss of claws could contribute to a decrease in the neuron's activity, there is a high likelihood that KCs possess other homeostatic mechanisms, so the exact contribution of claw loss to activity changes is hard to determine. In our previous work (Abdelrahman, Vasilaki and Lin, 2021) we modelled variation in three different parameters that could impact the neurons

chance of firing: the number of PN inputs per KC, the strength/weight of each connection and the KC spiking threshold. In this work I have already discussed adaptations in number of inputs, but it is equally plausible changes to the other two parameters may be responsible for the decreased activity discussed in this chapter. For example, the weight of remaining claws could be decreased through a compensatory decrease in nicotinic acetylcholine receptor (nAChR) expression and we have already extensively discussed similar forms of synaptic plasticity (Chapter 1.7.2.2). AMPARs are the homologue for this receptor in mammalian excitatory neurons and consistently demonstrate changes in expression or incorporation of different subunits in response to prolonged perturbations to activity (Ibata, Sun and Turrigiano, 2008; Gainey et al., 2009). Furthermore, blocking nicotinic receptors in *Drosophila* culture for 24 hours results in an enhancement in mEPSC amplitude produced by increased expression of Dα7-subunit-containing nAChRs in culture and brain-wide in adults (Ping and Tsunoda, 2011). This demonstrates that homeostatic adaptation of the expression of these receptors in *Drosophila* central brain excitatory neurons is possible, although it hasn't been observed in KCs. These findings suggest it is feasible that KCs could also decrease their activity by regulating expression of Dα7-subunit-containing nAChRs. However, these changes are very difficult to identify on the single cell level. As mentioned previously, fluorescent tagging of Dα7-nAChRs proved ineffective for even identifying claws and may therefore be limited as a tool to measure changes in this receptor's expression. RNA sequencing could also potentially be utilised to identify changes in expression of these receptors, but dissecting and analysing the necessary number of brains to detect changes in expression of key RNAs is likely infeasible or beyond the scope of most projects at least. Labelling and hyperactivating all KCs (or even all γ KCs only) and running RNA-seq on this would be far more feasible and would enable us to identify changes in expression that result from prolonged activity. However, it would limit our ability to compare these changes to those observed on the single cell level in this project.

It is also possible that the number or weight of inhibitory synapses, which arise from the APL in KCs, could be increased in response to prolonged hyperactivity to produce the decreased responses in TrpA flies. This was another factor considered in our prior modelling work (Abdelrahman, Vasilaki and Lin, 2021), but in this case the model suggested adjusting inhibitory weights alone would not be sufficient to achieve a set level of activity in KCs; however adaptation in this parameter may still play a role. Previous work from our lab using TrpA to hyperactivate the APL identified KCs increase their odour responses and suggested this is driven through the combination of increased KC excitation and decreased APL activity

(Apostolopoulou and Lin, 2020). These experiments were performed at the whole MB level which makes it difficult to determine if changes in activity arise from intrinsic homeostatic changes in each neuron or through alterations in the number/strength of synapses between them. However, this work and our modelling suggests adjusting inhibition through an increase in number of GABA receptors or the number of APL synapses could contribute to the decreased activity observed in single KCs hyperactivated for prolonged periods.

Changes in intrinsic parameters as discussed in Chapter 1.7.1 could also produce the observed hyperactivity-induced decreased activity. Our model proposed spiking threshold as another parameter that could be adjusted to return neurons to set activity. Alterations in expression of ion channels is the key lever on which many intrinsic homeostatic mechanisms act, which includes changes in numbers of sodium, potassium and calcium channels (Desai, Rutherford and Turrigiano, 1999; Aptowicz, Kunkler and Kraig, 2004; Li et al., 2020a; Huang et al., 2021b). Importantly these adaptations have been observed in *Drosophila*. Elevated activity in motor neurons decreases mRNA levels of para, one of the primary voltage-gated sodium channels in Drosophila. We have observed activity-dependent adaptations in this channel in our labs work (Greenin-Whitehead et al., 2025), where artificially increasing sodium influx across the whole MB with NaChBac decreased para expression. This change accompanied a decrease in the MB odour response in adults, suggesting alterations in voltage-gated Na+ channel expression may be a homeostatic mechanism in KCs to reduce their activity; reducing para expression would theoretically increase spiking threshold by reducing the influx of Na+ ions at the KC AIS. Furthermore, the effect of NaChBac on endogenous Shaker expression, a potassium channel responsible for repolarization of neurons, was also tested (Greenin-Whitehead et al., 2025). It was predicted that KCs may compensate for prolonged depolarisation caused by NachBac by increasing Shaker expression to achieve greater repolarisation. However, Shaker expression appears to be unaffected suggesting that these channels are not a target for homeostatic mechanisms in KCs. It is plausible that compensation in para expression in response to increased sodium influx may also exist at the single KC level and would produce changes in spiking threshold in KCs sufficient to restore activity to a set level. I will discuss more potential proteins that could be involved in activity-dependent claw loss mechanisms and decreased activity in Chapter 5.

4.3.3 What about α/β KCs?

Compared to γ KCs, the evidence of adapted responses after 1 day of hyperactivation is more uncertain in α/β KCs. Dendrite responses in α/β TrpA flies appear slightly reduced while the responses of axons in the α lobe are very similar to controls. Both show no significant

differences on a 2 way ANOVA but do have curves that are significantly different from one fit to both data sets. This would appear to suggest that single α/β KCs may slightly adapt their responses after a prolonged period of hyperactivity, but I cannot confidently draw this conclusion, especially after discovering the necessity of recording responses on ice. Future experiments would likely need to increase the sample size due to the relatively small size of this effect and could trial an increased stimulation period like 4 days to determine if any differences become more pronounced. Identifying this is important as our current model (Abdelrahman, Vasilaki and Lin, 2021) suggesting single KCs need to adjust their activity to maintain an average level of activity included all subtypes. If we assume this subtype is not capable of a single cell homeostatic adaptation, it would also be interesting to alter the model so that only γ KCs were capable of homeostatic plasticity, to determine whether their adaptations alone are sufficient to maintain a functional level of lifetime sparseness across the population.

One important limitation of our model to note is that 'odour responses' were determined by only two MBONS (1 approach vs 1 avoid) that connected to all 2000 KCs. In the actual MB, KC subtypes connect with distinct MBONs in their associated lobes (Figure 1.2)(Aso et al., 2014b), so it is possible that 'correctly' assigning an appetitive or aversive valence to an odour is performed at a subtype level first and a whole MB level second. If this is true, the extent to which inter-KC variability effects the ability to discriminate between odours may also occur at a subtype level. Large overlap in KCs representing multiple odours is only problematic because it results in behavioural confusion/'noisy' responses from MBONs that make it unclear exactly what odour the fly is detecting and what valence it has. Both γ and α/β KCs show decreased activity, to varying degrees, after prolonged hyperactivity but only γ KCs also demonstrates activity-dependent loss of claws. If the assumption that inter-KC variability is regulated on a subtype level is correct, what is responsible for the different compensatory mechanisms I have observed between γ and α/β KCs (and α'/β' to an extent) and why do these differences exist? One possibility is that it is more important for odours to be non-overlapping in γ KCs than in the other two subtypes. This idea is partially supported by evidence that γ KCs are the sparsest and least excitable subtype (Turner, Bazhenov and Laurent, 2008), suggesting a homeostatic mechanism may exist to maintain this high spiking threshold and sparseness. However, the behavioural/computational reason for a subtype distinction is unclear. It is well established that these subtypes have different roles in distinct phases of memory formation and consolidation (Yu, Akalal and Davis, 2006; Krashes et al., 2007; Wang et al., 2008; Akalal, Yu and Davis, 2011; Davis, 2011; Qin et al., 2012;

Cervantes-Sandoval et al., 2013). The general theory is that parallel traces/representations of learned odour associations are established across subtypes but are stronger in γ KCs earlier, but quickly weaken, while α'/β' and α/β are consolidated and α/β especially has longer lasting representations. It is possible that γ KCs role in STM means the need for odour representations to be non-overlapping is more immediate and thus requires additional compensatory mechanisms to maintain (like claw loss). It is also possible that possessing single cell compensatory mechanisms in α/β and α'/β' would be disadvantageous in some way, perhaps because 'homeostatic' mechanisms would impact too much on the Hebbian mechanisms required for long-term learning and consolidation. For example, LTM in α/β KCs requires protein synthesis and our results suggest that protein availability may be important for activity-dependent loss of claws in γ KCs. The mechanisms required for consolidation and claw loss may require opposing pathways, while long-term consolidation is not important in γ KCs and so may not have this issue. Furthermore, as discussed in Chapter 3 α/β and α'/β' KCs have fewer claws than γ KCs, which may make loss of a higher percentage of their odour information less tolerable, especially when these subtypes appear to be important for the fly's long-term odour memory. It is also possible an external homeostatic mechanism, possibly arising from the APL or through lateral connections from γ KCs, is sufficient to maintain an average level of activity in this subtype, while γ KCs require a homeostatic mechanism on the single cell level. Ultimately, this is all speculation as the reason why subtypes play distinct roles the phases of odour memory is unknown, but it is possible that by uncovering further distinctions in their compensatory mechanisms the logic behind these differences may become more clear. In this case, repeating these experiments on ice and with a greater sample size may provide more clarity.

4.3.3 Future work

The most obvious next step is to repeat the 31°C 6 hours, 4 days and 1 day α/β conditions with flies raised at 18°C, recorded on ice and with a greater sample size. This would allow us to more confidently determine whether homeostatic adaptation occurs across all 3 of these conditions. Additionally, there are a few concerns about raising flies at 18°C, principally the higher claw counts you see in the aged condition performed by Ya Yu C Wong. As mentioned earlier the Drosophila nervous system is sensitive to temperature during development and it is possible raising them at such low temperatures could introduce additional confounding factors. Therefore, it may also be worthwhile to repeat the 22°C 1 day condition but with flies recorded/stimulated while on ice, to determine whether the decreased response seen in TrpA

flies is a result of homeostatic adaptation or an increased baseline response. Determining this would provide an alternative to raising flies at 18°C if this turns out to be problematic.

The heatshock protocols for labelling γ and α/β KCs in the single cell live imaging genotype labels the correct subtype the majority of the time. In contrast, as discussed in chapter 3, the success rate is a lot lower when trying to label α'β' KCs. Combining this with the increased difficulty of live imaging dissection and achieving proper antennal nerve suction meant I omitted this subtype from my initial live imaging experiments. Additionally, the dim signal in these neurons and the inability to immunolabel the brain makes it hard to differentiate this subtype from α/β KCs. However, future experiments would benefit from identifying any changes in response after prolonged hyperactivation in this subtype too. These KCs also show no activity-dependent loss of claws so it would be informative to know whether they show a similar response to α/β TrpA neurons as this could hint that the difference in responses to γ KCs arises from the lack of this adaptation.

As part of the preparation for the single cell live imaging genotypes, I also created a genotype for labelling the majority of PNs with jRGECO1A. The plan was to use this for a future experiment where dual colour calcium imaging would be utilized to record from single KCs and their associated PNs at the same time. The hope was that I could visualize PN boutons and their connecting claws and plot these responses against each other, to determine if one or both synapses adjust their strength in response to prolonged hyperactivity in KCs. First, this would help determine whether KCs are capable of additional homeostatic adaptations, outside of loss of claws. Second, as mentioned previously it could provide insight on why certain claws are removed over others. For example, if TrpA claws demonstrate stronger responses to stimulation than controls this could suggest that weaker claws are removed first. Alternatively, this could mean claws increase their strength to adapt for the loss of a claw from the cell. Additionally, being able to image PN boutons and their associated claw at the same time could help determine whether KCs adjust their firing threshold in response to their increased activity. If we assume PN activity would remain the same, any decrease or increase in the response of claws would suggest a change in threshold. However, it is possible that PN boutons may also adapt to the increased KC activity, which these experiments would also reveal. The largest issue for these experiments is the weak GCaMP8m and likely jRGECO1A signal means it may be very difficult to distinguish individual claws and their associated PN boutons. It is possible that with time the imaging and dissection technique could be refined to improve the clarity of images, but whether this would be sufficient to record responses from these small structures is unclear. Taking

electrophysiological recordings of single KCs expressing TrpA while stimulating them could reveal more detail on how the neuron adapts. For example, you could more accurately determine whether their spiking threshold changes or could even try recording from single claws to measure how the mEPSCs arising from these dendrites is altered. However, electrophysiologically recording from single KCs would be extremely difficult and certainly wasn't within the scope of this project, while recording from single claws is likely currently impossible.

Ultimately, any future work should focus on expanding the conditions tested and confirming that TrpA is only active during the desired period. For example, measuring how responses change in aged flies or in flies that have been starved would help improve our understanding of how this adaption may work e.g. whether it is limited to early life and whether it requires protein synthesis. Further experiments should focus efforts on identifying an underlying mechanism for loss of claws and determine whether this mechanism is required for the decreased response observed in TrpA flies, which would determine whether loss of claws is solely responsible for this change. I will further discuss some potential proteins that may be involved in these mechanisms in the next chapter.

5. General Discussion

5.1 Overview of key findings and their significance

The aim of this project was to determine whether KCs show activity-dependent plasticity at the single-cell level, which would support our previous modelling work suggesting this may be necessary to maintain an average level of activity across the population (Abdelrahman, Vasilaki and Lin, 2021). I have identified two responses to prolonged hyperactivation with TrpA: The first is an activity-dependent loss of claws after 1-4 days of hyperactivity and the second is a decrease in the amplitude of response to antennal nerve stimulation. The latter demonstrates a potentially compensatory decrease in activity to restore it to a set point, although these results are still preliminary after the issues with TrpA discussed in Chapter 4. However, the extent to which claw loss contributes to decreased activity is unclear.

By utilising MARCM to label single cells, I was able to identify a previously unreported activity-dependent loss of claws that occurs after 1-4 days of hyperactivity. This adaptation was not observed at 6-12 hours, suggesting that claw loss occurs at some point between 12 and 24 hours. However, volume analysis of all claws in future experiments could reveal that the size of claws begins to decrease by this time, suggesting some aspect of this adaptation may start earlier. It also still remains unclear what factor(s) determine which claws are removed after prolonged hyperactivity. There was no significant difference in the length of claws between control and TrpA flies in the 1 or 4 day conditions, suggesting the existing length of claws does not impact decision of claw removal.

I also confirmed that loss of claws was not just a result of flexibility during the early-adult CP in Drosophila (Dombrovski and Condron, 2021; Devaud, Acebes and Ferrús, 2001; Devaud, Keane and Ferrús, 2003; Devaud et al., 2003) by incubating flies for 4 days at 22°C after eclosion before moving them to 31°C for a further 4 days. However, this adaptation does disappear with further ageing when raised at both 22°C and 18°C (Ya Yu Colin Wong) for 30 and 50 days respectively. While these results appear initially conflicting, I hypothesize that KCs have this particular adaptation earlier in life, but not as a result of an early-adult CP, and as with many forms of plasticity it is lost with more significant ageing. It is possible that the investment required to maintain the capability for this adaptation is too strenuous at a later age. If our model is correct this would further support the idea that claw loss is not the only compensatory mechanism in single KCs as it is possible maintaining an average level of activity is still necessary in later life. However, our model and most work in the MB does not account for the unidentified changes that likely accompany an ageing system. It is also

possible that single cell homeostatic plasticity in KCs is required earlier in the fly's life, but not later. I identified that only γ KCs and not α/β and α'/β' demonstrate a loss of claws and theorised these differences may pertain to the subtype's distinct roles in the stages of memory formation and consolidation. Given γ KCs are only involved in STM, it is plausible that preventing overlap between odour representations is important earlier in life when flies are still establishing the associated valences of the odours they encounter. In later life possessing this level of flexibility may not be necessary as the valences of most odours the fly will encounter have already been determined and are unlikely to significantly change. Even if an odour associated valence does change, the reason flies need to effectively distinguish between odours is to avoid odours with hazardous associations and maximise the food they can consume associated with appetitive odours. Ultimately this is only necessary to increase the fly's likelihood of successfully mating, so the need for maintaining an average level of activity across the KC population to ensure effective odour discrimination may fade with time as the probability mating has already occurred increases. Finally, I did not perform any physiological experiments on aged flies so I cannot conclude that they have lost their ability to return their activity to a set point. While loss of claws may contribute to a compensatory decrease in activity, it is plausible other homeostatic mechanisms may exist in aged flies that can still achieve this goal.

After 1 day of TrpA activation and a further day of TrpA inactivation (or minimal activation) KCs do not regain their lost claws, suggesting this adaptation is not reversible. It is possible that claws are not reinstated at the same speed in which they are removed, so future experiments should trial longer periods of TrpA inactivity after initial hyperactivation to determine if claw loss is reversible. If we assume this adaptation isn't reversible, this could raise doubt that this mechanism is homeostatic. However, this depends on whether a mechanism must act bidirectionally to be defined as homeostatic. It is equally plausible that this mechanism only acts in one direction and other mechanisms compensate for decreased activity (see 5.4.2.2).

We also discovered that activity-dependent loss of claws is affected when flies are concurrently starved or provided only sugar (Chaw C Yi, Ya Yu Colin Wong**)**. Confusingly, sugar only flies incubated at 31°C for 1 day demonstrate no claw loss, while starved flies show a non-significant decrease in claw count. It seems unlikely that the availability of only sugar completely abolishes claw loss while complete starvation only partially reduces this, and the smaller sample size in the former group may limit the conclusions we can draw from this condition. One of the nutrients both conditions lack is amino acids and in particular the 9

essential amino acids (Kosakamoto et al., 2024). These amino acids act as limiting factors for protein synthesis, causing it to slow or stop depending on the exact amino acid missing (Everson et al., 1989; Mazor et al., 2018). It is probable that removing claws requires protein synthesis as seen in other homeostatic mechanisms requiring changes to dendrite structure (Mendez et al., 2018) and further supported by the long timeframe of hyperactivity required before claw loss occurs. It is also possible that lack of lipids in both conditions could contribute to the loss of the claw reduction adaptation. Given the sugar only condition has no claw loss, it is unlikely that decreased energy availability from dietary lipids is a determining factor. However, internal triglyceride stores are rapidly depleted under starvation conditions (Chauhan, Anis and Chauhan, 2021) and are required for many essential processes in neurons including cytoskeleton rearrangement (Tracey et al., 2018) which may be necessary for claw degradation/retraction. Ultimately, future experiments would need to directly block protein synthesis to determine its contribution to activity-dependent loss of claws vs loss of lipids.

Preliminary single cell live imaging experiments revealed that hyperactivity for 6 hours, 24 hours and 1 day all resulted in decreased calcium responses in TrpA flies. However, when I performed the 22°C 1 day control this revealed that TrpA was still active despite previous reports (Hamada et al., 2008). It is possible that the number of open TrpA channels at this temperature is not sufficient to induce spiking (Pulver et al., 2009) but causes a small change in the resting membrane potential or spiking threshold; this is supported by the 22°C control in Chapter 3, which demonstrated no decrease in claw counts with TrpA. Fortunately, raising flies at 18°C and recording them at ~18°C does not result in decreased KC activity, suggesting that if TrpA is active at this temperature it is only minor. While sample size was limited due to time constraints, TrpA flies raised at 18°C and incubated at 31°C for 1 day demonstrated a significantly decreased response compared to controls. From this I conclude cautiously that KCs appear to compensate for prolonged hyperactivity by decreasing their activity. This may represent a novel homeostatic mechanism.

5.2 Are the adaptations identified homeostatic?

What evidence is required to prove an adaptation is homeostatic? If we revisit the elements of negative feedback I introduced in Chapter 1.6, a homeostatic plasticity mechanism requires a sensor to detect changes in activity from a set point or changes in key parameters, a comparator that calculates the error/difference in current activity from that set point, a controller that interprets this error and determines the correction required, and an effector that produces this correction to restore activity to its set point. One of the most well defined

homeostatic plasticity mechanisms is synaptic scaling in visual cortex neurons. TTX application causes an initial decrease in mEPSC amplitude followed by a later compensatory increase (Turrigiano et al., 1998). The homeostatic sensor in this example is decreased calcium influx which results in decreased activation of the calcium binding protein CaMKIV (Ibata, Sun and Turrigiano, 2008). CaMKIV is a transcriptional regulator (Soderling, 1999) and acts as a comparator, as the difference in baseline Ca2+ binding and reduced binding after TTX application induces changes in transcription (Ibata, Sun and Turrigiano, 2008). This cascade of changes in transcription may cause an increase in GluR2-AMPAR accumulation at synapses which acts to increase activity of the neuron (Ibata, Sun and Turrigiano, 2008; Gainey et al., 2009). Work over decades has established many of the elements of this overarching mechanism, but can we confidently conclude it is homeostatic? I argue that to demonstrate a mechanism is a form of homeostatic plasticity you must show that mechanism is necessary and sufficient to restore the neuron to a set point. However, as discussed throughout this work the factor(s) that is/are being maintained by homeostatic plasticity likely varies between neurons depending on the role it plays within a network. For example, visual deprivation causes a decrease in baseline firing rates of V1 neurons in the deprived hemisphere that slowly returns to baseline after several days (Hengen et al., 2013, 2016). This adaptation demonstrates clearly that perturbing neurons induces a change in a key factor which is then restored later, likely through several of the mechanisms we discussed above. However, the original TTX experiments did not demonstrate a return of any factor to baseline levels because TTX prevents spiking making it impossible to measure this while it is applied. If we use the highest threshold, you could conclude that although the original work showed that perturbed neurons produce an opposing compensatory change in their activity (mEPSC amplitude), they did not show any restoration to a set point. Applying a strict threshold where only mechanisms that quantitively restore perturbed activity back within a tolerable threshold are qualified as homeostatic plasticity would rule out much of the research in the field. It is perhaps better to conclude that research identifying a compensatory opposing adaptation to perturbation indicates that mechanism is likely homeostatic but can only be proved definitively so once (1) the set point/factor of the neuron in that particular system is identified and (2) you observe that mechanism restoring it to its baseline level.

In the example of KCs in the MB, our modelling work indicates that the average activity of neurons must remain roughly equal to ensure effective discrimination between odours (Abdelrahman, Vasilaki and Lin, 2021); in particular, to avoid a situation where a small minority of KCs respond to most odours while the rest of the populations remains

silent/mostly inactive. In this case, the set point is likely the average firing rate of KCs in response to all the odours the fly encounters over time, which, for reasons we will discuss later, is hard to measure with our current techniques. Instead, I will focus on whether the adaptations I have identified indicate single KCs are capable of homeostatic plasticity. Beginning with the physiological results, the decreased calcium response observed in γ KCs raised at 18°C and then hyperactivated with TrpA for 24 hours are a more obvious indication of homeostatic plasticity. In theory TrpA activation pushes the firing rate of the neuron beyond a set point and it compensates with mechanisms that produce a rebound in this activity; the 'rebound' is decreased calcium response to antennal nerve stimulation which I am using as a proxy for neural activity (more on this later). At the very least this suggests TrpA neurons reduce their evoked activity in line with previous experiments investigating homeostatic plasticity in mammals, where chronically increasing activity causes a decrease in mEPSC amplitude (Turrigiano et al., 1998; Goold and Nicoll, 2010). Although the issues with TrpA need to be further investigated and a greater sample size is required, this is strong evidence that KCs can compensate for changes in their activity. It is possible electrophysiological recordings of single KCs could be used in future to determine whether a firing rate set point is restored as a result of the decreased activity I have observed here. However, recording from single MARCM-labelled KCs would be extremely difficult and was far beyond the scope of this project. Additionally, given the extreme nature of TrpA activation, it is unlikely that any homeostatic mechanisms could restore a firing rate set point while it is active, making it difficult to definitively prove the compensation observed is homeostatic. However, the activity-dependent compensation observed does at least show the directionality one would expect if single KCs have homeostatic mechanisms that attempt to decrease activity, even if they may not fully succeed while TrpA is active.

The other adaptation I identified was an activity-dependent reduction in claws after 1-4 days hyperactivity, and this is more difficult to define as homeostatic. I posit that claw loss contributes to the decreased activity observed in my physiological results by reducing the number of inputs and therefore the number of EPSPs that can be summed to induce an AP. Modelling from our lab suggests dropping a KC's total excitatory weights by only 20% would be sufficient to completely abolish odour responses (P Fischer, unpublished results), so it is feasible that decreasing number of claws could produce a reduction in the neurons activity. However, if this isn't a homeostatic mechanism, what other processes could account for activity-dependent loss of claws? One possibility is that constant hyperactivity for 1-4 days triggers excitotoxicity apoptotic mechanisms that begin with degradation of claws. However,

some of my results argue against this conclusion. First, there is no difference in the amplitude of claw loss between 1 day and 4 days at 31°C, so if claw removal represents the beginning of apoptosis this suggests no other steps occur for 3 days. Second, KCs show no other signs of damage or morphological differences that would suggest general cell degradation although many changes like breakdown of key proteins or cytoplasmic structures cannot be detected by the techniques used. Third, α/β and α'/β' show no loss of claws or other morphological changes, so it is unclear why excitotoxicity driven apoptosis would begin with claw removal in γ KCs and not in other subtypes. It is also possible that claw loss represents a pathological mechanism that does not result in apoptosis or at least is delayed for much longer periods than those observed in this experiment (>4 days). Excitotoxicity induced cell death can occur by necrosis when calcium influx is so pronounced it causes rapid depolarization of the neuron and mitochondrial membranes which disrupts the electron transport chain; this results in a failure to produce ATP and production of ROS which quickly triggers cell death (Armada-Moreira et al., 2020). This likely would occur in under 4 days and therefore is not responsible for activity-dependent loss of claws. In contrast, weak excitotoxicity enables the neuron to homeostatically adjust intracellular calcium which can prevent cell death or result in delayed apoptosis (Armada-Moreira et al., 2020). However, this also typically occurs 6-12 hours after the cause of excitotoxicity ceases (Ankarcrona et al., 1995; Armada-Moreira et al., 2020) and given TrpA activation is constant in my work, you would expect any excitotoxicity to have triggered cell death by 4 days. It is also possible that excitotoxicity triggers targeted degradation of just claws as a result of excessive activity though, similar to my discussion of homeostatic plasticity, it is unclear why some claws would be more active than others and targeted for degradation; it is also unclear why this doesn't occur in α/β KCs. Although it is possible claw loss represents a homeostatic response to a pathological situation (See Chapter 5.512) my current findings suggest it is more likely it represents a compensatory mechanism to restore activity to a set point.

5.3 Potential proteins, regulators and pathways responsible for observed adaptations

When determining potential proteins or pathways responsible it is necessary to first explore this separately for the two adaptations I have identified; it is possible there is some overlap in pathways that could produce both loss of claws and decreased activity but we will explore this later. First, as more extensively described in Chapter 4.3.2, there are several adaptations

in receptor or ion channel expression that could cause a decrease in the KCs activity. This includes potential synaptic scaling mechanisms like decreasing synaptic weight at PN-KC synapses by reducing nAChR expression, and/or increasing weight of APL-KC synapses by increasing GABA receptor expression; there is precedent for similar changes in both mammalian and Drosophila work (Ibata, Sun and Turrigiano, 2008; Gainey et al., 2009; Ping and Tsunoda, 2011; Apostolopoulou and Lin, 2020). Intrinsic homeostatic mechanisms are also plausible and in particular we have already identified a compensatory decrease in para expression in KCs with artificially increased sodium influx via NaChBac, with no change in voltage-gated outward currents (Greenin-Whitehead et al., 2025). However, it is worth noting the mechanisms of action of TrpA and NaChBac are quite different, as TrpA increases the activity of neurons when heated (Hamada et al., 2008; Pulver et al., 2009) while NaChBac surprisingly decreases activity while potentially producing greater sodium influx and more total depolarization overall (Greenin-Whitehead et al., 2025). Any potential changes in expression of all of the above proteins would need to be investigated separately in the genotypes used in this work to confirm how prolonged TrpA activation in single cells affects them.

The morphological analysis I performed also allows me to describe what prolonged TrpA hyperactivity in single KCs does **not** cause. While I have observed activity-dependent loss of claws there is no change in the number of non-claw dendrites or in the length of either type of dendrite. I cannot rule out that claws may adapt their volume in response to hyperactivity which has also been observed in mammalian work (Keck et al., 2013; Barnes et al., 2017; Hobbiss, Ramiro-Cortés and Israely, 2018; Moulin, Rayêe and Schiöth, 2022). For example, KCs could decrease both expression of receptors on claws and that claws associated volume, or decreased volume may precede total claw removal; it is worth noting that most mammalian research has only observed changes in spine volume in response to activity blockade and not activity increase (Moulin, Rayêe and Schiöth, 2022). Working from this base of physiological and morphological findings I will now speculate on the wider regulators and pathways that may be responsible for these changes.

A recurring concept in Chapter 1 was the influence of Ca2+ influx/intracellular concentration and its impact on a host of calcium-dependent pathways implicated in homeostatic plasticity. Research in both Drosophila and mammals has demonstrated that calcium influx through voltage-gated calcium channels is necessary for several forms of homeostatic plasticity (Murthy et al., 2001; Thiagarajan, Lindskog and Tsien, 2005; Frank et al., 2006; Frank, Pielage and Davis, 2009; Müller and Davis, 2012; Frank, 2014b; Gratz et al., 2019). This

opens up an interesting avenue for future experiments to test conditional knockouts of voltage-gated calcium channels (e.g. cacophony) in single KCs expressing TrpA, to test whether calcium influx is necessary for activity-dependent loss of claws and/or decreased activity. However, there are several potential difficulties with this experiment. First, most conditional knockouts in Drosophila use a heat-sensitive form of GAL80 which is at odds with the genotypes used in this experiment which (1) recombine out GAL80 during development and (2) utilise heat to activate TrpA. These issues could be potentially solved by using the recently developed Auxin GAL80 knockout system (McClure et al., 2022), which utilises the plant hormone Auxin in fly food to trigger degradation of GAL80. However, there is no LexA alternative for Auxin or MARCM, which means I would have to use both MARCM GAL80 which is recombined out of a KC during development and later feed Auxin to induce GAL80 degradation during adulthood. These techniques are potentially compatible but would result in a delay in GFP/GCaMP and TrpA labelling until the Auxin-associated GAL80 is also removed, which could result in weaker signal or reduced TrpA expression. Alternatively, you could knockout voltage-gated calcium channels at the same time KCs are labelled with GFP and TrpA. However, this would likely have significant developmental impacts, making it impossible to determine whether any effect of calcium channel knockout on KC adaptations is due to their importance in adult homeostatic plasticity or a functional change to the neuron induced during development.

Another issue with investigating the relationship between calcium influx and KC hyperactivity adaptations is TrpA itself. This channel is a non-specific cation channel which means it also allows influx of Ca2+ when open. Any experiments that did knockout voltage-gated calcium channels in KCs would be unable to completely prevent calcium influx, which would limit the ability to conclude any change or lack of change to KC adaptations was due to missing calcium. One way to avoid this issue altogether may be to investigate changes in expression of calcium-associated proteins instead. For example, creating FLPtags of endogenous voltage-gated calcium channels may be effective at detecting differences in expression between control and TrpA flies. Many regulatory proteins with calcium affinities like the CaMKinase family are also implicated in learning, memory and homeostatic plasticity. For example, CaMKII is the only Calmodulin kinase in Drosophila and has also been implicated in homeostatic plasticity (Perry et al., 2022). Similar to the strategy used in (Ibata, Sun and Turrigiano, 2008) I could introduce a dominant negative CaMKII in adult single KCs and test if inactivating the endogenous form effects either of the adaptations I have observed. I could also use a CaMKII FLPtag to identify any changes in expression, although if it is a

homeostatic comparator/regulator it seems more likely its expression would remain the same to enable accurate detection of any differences in baseline Ca2+. Ultimately, there are many calcium-sensitive proteins in Drosophila that could be implicated in loss of claws or decreased KC activity, but I cannot explore all of them in detail here. The first step is to identify whether changes in Ca2+ influx impact the mechanisms I have identified and if so, further associated proteins can be investigated.

Earlier I raised the possibility that KO of Tao, a kinase that regulates microtubule dynamics and dendritic branching (King et al., 2011; Hu et al., 2020), could be used to block claw loss and investigate how this affects changes in the neurons activity; this could suggest that Tao is involved in regulating activity-dependent claw loss in γ KCs. Tao is a developmental regulator of dendritic arborization in Drosophila, but is also required for the maintenance of adult dendrites; KO in both development and adulthood also causes deficits in social behaviours (Hu et al., 2020). Furthermore, developmental knockdown of Tao in only KCs causes a 50% increase in claw numbers and associated increase in odour responses (Ahmed et al., 2023), demonstrating endogenous Tao plays a role in regulating dendritic arborization during KC development. Leveraging the same Auxin GAL80 strategy mentioned earlier would allow future experiments to test conditional knockdown of Tao during only adulthood in single KCs. By combining this with 1-4 days of TrpA activation this may reveal if Tao contributes to activity-dependent claw loss, although this would not show whether Tao is permissive or instructive for this compensation. Tao controls dendrite arborization partially through driving regulation of microtubule and F-actin expression, although the exact details of this mechanism is still uncertain (Hu et al., 2020). Claw loss almost certainly involves changes in cytoskeletal dynamics so investigating both actin and microtubules further could help reveal the detailed mechanisms behind this adaptation. For example, more rapid spine loss in hippocampal neurons induced by glutamate receptor activation also causes a loss of F-actin at existing spines, so it is possible all claws in TrpA-expressing neurons may show cytoskeletal changes. An ambitious experiment would be to use MARCM to label KCs as normal with the addition of UAS-LifeAct-mCherry to visualise F-actin (Riedl et al., 2008), and then perform timelapse microscopy over 24 hours at 31°C. By performing ‘snapshots’ every 1-2 hours this could enable identification of exactly when claw loss begins and the changes in actin dynamics that underpin it. However, long-term in vivo imaging in flies is challenging, though not completely impossible (Huang et al., 2018).

Beyond the building blocks of the cytoskeleton there are many other structural and supporting proteins that could be involved in the breakdown of claws. Most obviously, to

remove claws, degradation of its various components must be required, which likely involves breakdown of receptors, channels and scaffolding proteins. A potential candidate for this is the ubiquitin proteosome system which bidirectionally effects the turnover of postsynaptic density (PSD) proteins in an activity-dependent manner (Ehlers, 2003). A common scaffold protein in mammalian spines is PSD-95, the homolog of which in Drosophila is Discs Large (Dlg). These proteins connect receptors to the cytoskeleton to maintain the structural integrity of the synapse and regulate its size and shape (Bertin et al., 2022). Dlg knockouts in the MB also demonstrate short-term odour memory deficits, suggesting they may play a key role in γ KCs (Bertin et al., 2022) and making them an appealing potential regulator of claw removal or synaptic downscaling. Transport machinery may also be required for removal of proteins expressed at claws. For example, the kinesin motor protein Kif21b is important for homeostatic synaptic downscaling in hippocampal dendritic spines, where it is required for actin turnover after chronic activity (Gromova et al., 2023). Furthermore, in association with GKAP, which connects actin with the PSD, Kif21b controls removal of GluA2-containing AMPARs which induces synaptic downscaling (Shin et al., 2012; Gromova et al., 2023). Although many of the proteins mentioned relate to changes in dendrite morphology, this latter example demonstrates how several of them could easily be implicated in the compensatory decrease in activity observed in γ KCs through scaling the strength and size of claws. Although there is evidence these proteins facilitate spine removal, it is important to acknowledge that spine removal and claw removal are not identical; indeed, it may be more apt to compare claw removal to loss of a whole dendrite containing thousands of spines in mammals when considering their relative contribution to the total number of inputs.

My current findings leave the role of protein synthesis in activity-dependent claw loss uncertain, only suggesting that essential amino acids may be required. However, if future experiments go on to prove protein synthesis is necessary for the observed adaptations there are several associated proteins that could be implicated. Proteomics analysis of cultured hippocampal neurons that have undergone homeostatic plasticity identified a large number of proteins involved in post-translational modifications that demonstrate associated changes in expression (Schanzenbächer, Langer and Schuman, 2018). This could suggest these adaptations require protein synthesis and later modification of new proteins or proteins may be inactive in synapses until homeostasis-induced post-translational modifications activates them. Investigating pathologies that demonstrate neuronal hyperexcitability can help highlight proteins central to homeostatic plasticity. For example, Fragile X syndrome, caused by the loss of the RNA-binding protein FMRP, leads to cortical hyperexcitability. FMRP has multiple

roles, including the regulation of ion channels and receptors through both protein synthesis-dependent and -independent mechanisms (Bülow, Segal and Bassell, 2022). This condition causes cortical hyperexcitability partially through dysregulation of key ion channels, many of which have been implicated in homeostatic mechanisms (Bülow, Segal and Bassell, 2022). This link demonstrates that proteins crucial for regulating protein synthesis, like FMRP, are likely important for homeostatic plasticity and warrant investigation in future single KC experiments if protein synthesis is revealed to be necessary for activity-dependent adaptations.

The proteins described above are by no means an extensive list but instead highlight the many pathways that could be involved in changes to KCs activity or in activity-dependent claw loss. The best approach for future experiments would be to begin with investigations of more likely targets like calcium-associated proteins or proteins important for regulating morphology like Tao kinase. If these targets prove to be important for single KC compensatory mechanisms this will reveal more about the pathways involved in these adaptations and provide additional targets to investigate.

5.4 Limitations and future directions

5.4.1 Current limitations

5.4.1.1 Calcium imaging as a proxy for neuronal activity

In Chapter 4, I use GCaMP8M to measure changes in activity of single KCs after prolonged hyperactivation induced by TrpA. Calcium imaging is a common technique in Drosophila because genetic labelling of many cell types is easily achieved and electrophysiology is comparatively difficult, especially in the central brain. However, there are some broad issues with calcium imaging and some specific issues relevant to these experiments.

The first limitation to acknowledge is that this technique measures changes in intracellular calcium concentrations as a proxy for the neuron’s activity. While calcium influx does typically occur during EPSPs and APs, this technique is not a direct measure of neuronal spiking and there may be variation in the relationship between number of spikes and amount of calcium influx depending on the cell type being recorded. For example, GCaMP6f is effective at capturing multi-spike events but often misses single spikes and accuracy of detection decreases even further under whole population recording conditions (Huang et al., 2021a). While GCaMP6f could only resolve individual spikes that are more than 50-75ms apart (Chen

et al., 2013), GCaMP8 has a nearly 10 times faster fluorescence rise time than prior indicators and can distinguish spikes that are ~20ms apart (Zhang et al., 2023). This indicator also behaves linearly, with rise in calcium more accurately capturing the increase in AP number for the first 1-10 APs before saturating (Zhang et al., 2023). However, this method still can't accurately capture voltage fluctuations especially in KC dendrites which pre-AIS do not spike. Alternatively, genetically encoded voltage indicators are a relatively new tool for measuring neuronal activity that continues to improve and may be better suited for measuring changes in activity in single KCs. These indicators are embedded in the cell membrane and possess a voltage-sensing domain that shift with changes in the membrane voltage; this also causes a conformational change in an associated fluorescent protein which demonstrates a peak response five times faster than GCaMP6f (Yang et al., 2016). However, the current level of signal produced by voltage indicators may not have been sufficient to record from single KCs given my GCaMP8m signal was already quite weak; these indicators also have issues with excessive bleaching which would be problematic given the high laser power required to visualize KCs in my experiments (Alich et al., 2021). Furthermore, there have been reports that certain voltage indicators affect firing of APs and cause significant changes in the neurons capacitance (Alich et al., 2021). Ultimately, when interpreting findings from calcium indicators it is important to be aware that changes in intracellular calcium concentration are not a perfect proxy for activity but still allow for unparalleled access that in this experiment enabled single cell recordings of KCs, which would be extremely difficult using electrophysiology.

Another drawback of GCaMP is its capacity to act as a buffer for intracellular calcium which can impact calcium dynamics and gene expression via interference with voltage-gated calcium channels and endogenous Calmodulin nuclear translocation (Yang et al., 2018). This is of particular concern in this work for two reasons. First, as extensively covered, calcium and calcium-dependent pathways are important for many homeostatic mechanisms and are theorised to act as a sensor for chronic changes in activity (O'Leary et al., 2014). If calcium influx and associated pathways are perturbed by GCaMP, this could impact any calcium-dependent homeostatic pathways and limit our ability to compare adaptations between GCaMP and non-GCaMP containing genotypes. This problem is complicated further by TrpA, which is a non-specific cation channel that therefore also allows calcium influx (Hamada et al., 2008). This means that not only could any potential homeostatic mechanisms be affected in GCaMP-expressing flies, but the extent of KC activation by TrpA may be altered by GCaMP calcium buffering. If possible, future experiments should try to confirm that activity-

dependent claw loss still occurs in the single cell live imaging genotype, as this would suggest GCaMP does not significantly affect adaptations. There are also now alternative GCaMPs that have reduced impact on neuronal calcium dynamics that could be used in future (Yang et al., 2018). Although it has significant limitations, GCaMP was still the best tool to use in this experiment as it has improved signal compared to voltage indicators and enables unparalleled ease of recording from single KCs, especially when compared to electrophysiological alternatives.

5.4.1.2 Lack of ethologically relevant neuronal activation

It is possible the activity-dependent loss of claws represents an extreme response to an extreme perturbation and may constitute an end point of a host of 'homeostatic' mechanisms that aim to return the KCs activity to a set point. Incubating flies with TrpA-expressing KCs at 31°C for 1-4 days theoretically induces constant depolarization and spiking which the majority of neurons do not typically experience, especially KCs who fire sparsely. There are two reasons neurons must utilise homeostatic mechanisms, although they are fundamentally intertwined. First, as we have extensively discussed, restoring some factor like firing rate to a set point ensures the neuron can continue to function effectively for whatever that particular network requires e.g. maintain an average level of activity across the population to enable effective odour discrimination. Second, prolonged hyperactivity can lead to metabolic stress, ion imbalances (excessive intracellular calcium is particularly problematic), and production of ROS, all of which can cause long-term damage, excitotoxicity or at worse cell death (Chen et al., 2022; Samanta, Chakraborty and Bagchi, 2024); many of these mechanisms are implicated in neurodegeneration and disruption of circuit homeostatic plasticity has been associated with progression of behavioural symptoms (Taylor and Jeans, 2021; Chen et al., 2022; Samanta, Chakraborty and Bagchi, 2024). Fundamentally, these two aspects of neuronal homeostasis may not represent distinct processes but instead lie on a spectrum of mechanisms that respond to continued hyperactivity or different levels of perturbations. While TrpA does represent an extreme manipulation to activity, similar timeframes are used for complete AP blocking using TTX and constant activation using optogenetic manipulations (Goold and Nicoll, 2010; Michetti and Benfenati, 2024; Moulin, Rayêe and Schiöth, 2022). In fact, Hebbian and homeostatic plasticity mechanisms often seem to operate at distinct timescales to ensure temporary behaviourally-relevant changes in activity are encoded while chronic changes that could affect network function are adapted for. Of course, the delayed timeframe in homeostatic plasticity is partially due to the speed at which adaptations occur, often requiring protein synthesis or morphological restructuring. It is possible other

homeostatic mechanisms may attempt to reduce KC activity before claw loss occurs and this adaptation represents a ‘last resort’ to avoid potential pathological consequences. However, this does not mean activity-dependent claw loss is not a homeostatic mechanism and although potentially extreme, TrpA activation still enabled me to identify this novel adaptation.

Would other tools for hyperactivating single KCs have been more ethologically relevant? In our previous model we theorised that activity drift in KCs could be caused by drift in parameters relevant for regulating the neurons activity (e.g. number of channels, receptors etc), but it is more likely this would result in an increased, but not constant, spike rate; in contrast, TrpA activation theoretically causes constant depolarization. Pharmacological manipulations to increase activity like nicotinic receptor agonists or GABA receptor antagonists could not be used because it would be impossible to achieve activation of only single neurons in free-moving flies. Similar manipulations have only been achieved in cultured neurons (Ibata, Sun and Turrigiano, 2008), although this does demonstrate my results may have increased ethological relevance compared to these experiments as manipulations occur in flies with intact brains/fully functioning interconnected neural circuits.

Another alternative that also allows genetically encoded hyperactivation of single neurons, while being capable of more ‘realistic’ stimulation than TrpA is optogenetics. This tool uses light to induce responses in neurons with far greater temporal control than TrpA is capable of with temperature (Zemelman et al., 2002; Deisseroth, 2010, 2011). This technique has been used to great effect in the MB previously to identify the distinct behavioural roles of MBONs (Aso et al., 2014a) and as mentioned has been used in a few mammalian experiments to achieve chronic activation of neurons (Goold and Nicoll, 2010), so why didn’t I use this in my experiments? The main initial reason was to maintain consistency with our whole MB homeostatic experiments (Apostolopoulou and Lin, 2020; G. Bergmann, unpublished results), as using similar manipulations would at least allow for some comparison between findings. We also already had the genotype prepared for TrpA manipulation, while a single KC optogenetic alternative did not exist. Ya Yu Colin Wong has since tested CsChrimsons effectiveness at activating the whole MB using CRTC, a bidirectional reporter of neural activity that localizes to the nucleus in minutes in response to activity (Bonheur et al., 2023). KCs subjected to continuous stimulation for 30 minutes and flashing stimulation (20Hz 10ms pulse width and 100Hz 2ms) for 24 hours demonstrated overwhelmingly cytoplasmic localization of CRTC, suggesting these manipulations fail to activate KCs in intact flies. In both these conditions and no light controls, CsChrimson-expressing neurons demonstrated punctate CRTC signal and signs of decreased cell health including reduced cell body size

and disorganization of cell bodies across the MB. CsChrimson achieves neuronal activation primarily through H+ conductance which could acidify cytoplasmic pH (Vierock et al., 2017), and this may subsequently impact activity-dependent CRTC translocation. However, while reduced pulse width did appear to improve cell health, these neurons still did not demonstrate significant nuclear CRTC translocation suggesting neurons are not being activated. It is possible continuous stimulation may cause CsChrimson desensitisation, a common feature of light-gated ion channels like channelrhodopsins where there response to illumination quickly decays from a strong initial peak to a much lower steady-state current (Nagel et al., 2003; Lin, 2011); this steady-state current may not be sufficient to induce spiking in KCs. In contrast, TrpA activation produces sustained CRTC nuclear translocation at 15 minutes and 24 hours suggesting it may be a more effective tool for achieving prolonged KC activation (G. Bergmann *et al*, unpublished results). Ultimately, while I have identified issues with TrpA activation it may still represent the best method for achieving chronic single neuron activation in live flies.

5.4.2 Future directions

This section will mostly focus on exciting avenues for large future experiments, but it is worth acknowledging there are several open ended questions from my current experiments that require further work to strengthen their conclusions. This is particularly true for the single cell physiological experiments, where issues with improper TrpA activation warranted a last minute switch to raising flies at 18°C and this time constraint limited the sample size I could collect. A repeat of all the other conditions I tested in flies raised at 22°C is necessary to confirm the physiological adaptations observed still occur at other timepoints (6 hours and 4 days) and in other subtypes (α/β). In addition, morphological analysis of all conditions covered in Chapter 3 may be informative, especially in starved, sugar-only and aged flies where some of the results are quite surprising. While the lack of these extra experiments does not significantly limit the conclusions of this work in most cases, it would strengthen them and provide more certainty on single KC adult compensatory mechanisms.

5.4.2.1 Dual-colour calcium imaging

Although I have identified that single KCs demonstrate a compensatory decrease in activity, I had hoped to test how individual claws adjust their strength. As part of this aim I developed a genotype to label the majority of PNs with the red calcium indicator jRGECO1A, which in combination with single KC GCaMP labelling would have allowed me to investigate any homeostatic changes on the synaptic level. Using this dual-colour calcium imaging strategy, I would have measured the relationship between KC claw activity and the activity of their

associated PN bouton and compared between control and TrpA flies. I suspected that changes in the threshold of remaining claws may also occur as a result of compensatory mechanisms and only by measuring the activity of both bouton and connecting claw could I accurately determine this.

However, there are several issues with the feasibility of this experiment. First, the weak GCaMP signal in KCs means I was unable to effectively resolve claws in most instances. While future experimentation or use of different calcium indicators may be able to optimise single claw recording, it is unlikely they would be able to consistently record from the majority of claws on each KC. This is currently the biggest experimental limitation but could be worsened further by overlapping signal from all PNs despite use of 2-photon microscopy. Also, it was difficult to identify the associated boutons of KC claws when PN boutons were immunolabelled (Figure 3.2) and may be just as difficult to achieve with jRGECO1A labelling. While this experiment could have revealed whether thresholds of single claws adapt to prolonged hyperactivity, with the current techniques available it is likely not feasible.

5.4.2.2 Investigating bidirectional plasticity

For neurons to achieve homeostasis around a set point, they must be capable of bidirectional plasticity that induces opposing changes in the neurons activity so they can respond to perturbations of either extreme. However, I have only identified evidence of single KC compensations to hyperactivity and not hypoactivity. While the reversal experiments potentially demonstrate KCs are not capable of activity-induced increase in claws, these conclusions are currently limited by the short period at 22°C post activation and more importantly decreased activity is not necessarily the same as hypoactivity. Future experiments could test blocking activity in KCs, but given their spontaneous firing rate is already incredibly low (~0.1Hz)(Turner, Bazhenov and Laurent, 2008), it is uncertain whether this would impact activity enough to induce homeostatic mechanisms. In our model we demonstrated that poor odour discrimination performance arose from a combination of a small minority of KCs with low lifetime sparseness and a majority with high lifetime sparseness, only responding to a small number of odours or not responding at all. This suggests that this extreme could also significantly affect odour encoding, so how could future work test this? The majority of work identifying compensatory increases in activity uses pharmacological manipulation to block spiking (typically using TTX or GABA receptor agonists), however as covered in 5.4.1.2 this is not possible in free-moving *Drosophila*. Our lab has previously shown that artificially increasing inhibition, through APL TrpA activation, causes a compensatory increase in KC activity (Apostolopoulou and Lin, 2020).

Unfortunately, it is not possible to utilise the APL in this way on the single KC level without affecting the rest of the population. Experiments have successfully identified compensatory increases in activity by increasing the expression of Kir2.1, an inward-rectifier potassium channel that hyperpolarises neurons and suppresses activity (Burrone, O'Byrne and Murthy, 2002). They have also been successfully used to inhibit neurons in *Drosophila* (Zhang et al., 2021) so it would be relatively easy to achieve single cell overexpression of this channel. Alternatively, there are also inhibitory optogenetic tools like halorhodopsin (Zhang et al., 2019), but these may effect KC health similar to what we observed with CsChrimson. Overexpression of ion channels that decrease the neurons activity, like Kir2.1, is likely to be the most effective strategy for testing whether the observed adaptations are bidirectional, which represents an important step in proving these compensatory mechanisms are homeostatic.

5.4.2.3 Further modelling work

In our original model (Abdelrahman, Vasilaki and Lin, 2021) while the number of inputs was varied to test its effect on model performance, activity-dependent tuning of this parameter was never trialled. In light of my discovery of activity-dependent loss of claws as a potential compensatory mechanism, it would be informative to trial a model where number of inputs are adjusted to restore set activity to determine whether adjusting inputs alone is (1) sufficient and (2) matches the changes in number of claws I have observed. Furthermore, I only identified morphological adaptations in γ KCs and not in α/β or α'/β' so it would be interesting to adjust the model to include a subtype distinction in compensation. This would require dividing the current 2000 KCs in the model into their accurate counts for each subtype: γ ~670, α/β ~1000 and α'/β' ~ 330 (Aso et al., 2014b; Table 1). Given these subtypes also synapse with distinct MBONs, the model should also be adjusted to include individual avoid and approach MBONs for each subtype; odour decision making would be decided by the sum of all 6 MBONS, instead of the 2 used in the original model. However, we currently don't understand why these subtypes play distinct roles in odour memory formation (e.g. is this an intrinsic feature of neurons or a result of their associated MBONS), so the applicability of this potential model may be limited. Despite these limitations, this future model may help us understand the different contributions of KC subtypes in odour discrimination and determine why they may demonstrate different compensatory mechanisms.

5.5 Contribution to the field of homeostatic plasticity

In this work I have discovered a previously unidentified activity-dependent morphological compensation and demonstrated that single KCs reduce their activity in response to prolonged hyperactivity. This compensatory decrease in activity lines up with a wealth of previous mammalian homeostatic plasticity research (Michetti and Benfenati, 2024) and our own whole MB findings (Apostolopoulou and Lin, 2020; G. Bergmann, unpublished results Greenin-Whitehead et al., 2025). I was only able to demonstrate an association between claw loss and activity decrease, but this lays the groundwork for future research to establish a causal link between these adaptations. By identifying novel compensatory mechanisms in single KCs, I have provided further evidence to support our labs prior modelling work (Abdelrahman, Vasilaki and Lin, 2021) and opened up many avenues for future investigation. Furthermore, I have contributed to the incredibly limited work investigating single neuron homeostatic plasticity and demonstrated the Drosophila MB is a useful learning network to study how individual neurons regulate their own activity and morphology to maintain circuit stability.

6. Bibliography

Abbott, L. F. and Nelson, S. B. (2000). Synaptic plasticity: taming the beast. *Nature neuroscience*, 3 Suppl (S11), pp.1178–1183.

Abdelrahman, N. Y., Vasilaki, E. and Lin, A. C. (2021). Compensatory variability in network parameters enhances memory performance in the Drosophila mushroom body. *Proceedings of the National Academy of Sciences of the United States of America*, 118 (49). [Online]. Available at: doi:10.1073/pnas.2102158118.

Acuna, C., Liu, X. and Südhof, T. C. (2016). How to make an active zone: Unexpected universal functional redundancy between RIMs and RIM-BPs. *Neuron*, 91 (4), pp.792–807.

Adams, M. D. et al. (2000). The genome sequence of Drosophila melanogaster. *Science (New York, N.Y.)*, 287 (5461), pp.2185–2195.

Ahmed, M. et al. (2023). Input density tunes Kenyon cell sensory responses in the Drosophila mushroom body. *Current biology: CB*, 33 (13), pp.2742-2760.e12.

Akalal, D.-B. G., Yu, D. and Davis, R. L. (2011). The long-term memory trace formed in the Drosophila α/β mushroom body neurons is abolished in long-term memory mutants. *The Journal of neuroscience: the official journal of the Society for Neuroscience*, 31 (15), pp.5643–5647.

Albuquerque, E. X. et al. (2009). Mammalian nicotinic acetylcholine receptors: from structure to function. *Physiological reviews*, 89 (1), pp.73–120.

Albus, J. S. (1971). A theory of cerebellar function. *Mathematical biosciences*, 10 (1), pp.25–61.

Alich, T. C. et al. (2021). A dark quencher genetically encodable voltage indicator (dqGEVI) exhibits high fidelity and speed. *Proceedings of the National Academy of Sciences of the United States of America*, 118 (6), p.e2020235118.

Ankarcrona, M. et al. (1995). Glutamate-induced neuronal death: a succession of necrosis or apoptosis depending on mitochondrial function. *Neuron*, 15 (4), pp.961–973.

Antonini, A., Fagiolini, M. and Stryker, M. P. (1999). Anatomical correlates of functional plasticity in mouse visual cortex. *The Journal of neuroscience: the official journal of the Society for Neuroscience*, 19 (11), pp.4388–4406.

Antonini, A. and Stryker, M. P. (1996). Plasticity of geniculocortical afferents following brief or prolonged monocular occlusion in the cat. *The Journal of comparative neurology*, 369 (1), pp.64–82.

Apostolopoulou, A. A. and Lin, A. C. (2020). Mechanisms underlying homeostatic plasticity in the Drosophila mushroom body in vivo. *Proceedings of the National Academy of Sciences of the United States of America*, 117 (28), pp.16606–16615.

Aptowicz, C. O., Kunkler, P. E. and Kraig, R. P. (2004). Homeostatic plasticity in hippocampal slice cultures involves changes in voltage-gated Na+ channel expression. *Brain research*, 998 (2), pp.155–163.

Arendt, K. L., Sarti, F. and Chen, L. (2013). Chronic inactivation of a neural circuit enhances LTP by inducing silent synapse formation. *The Journal of neuroscience: the official journal of the Society for Neuroscience*, 33 (5), pp.2087–2096.

Ariga, H. et al. (2013). Neuroprotective function of DJ-1 in Parkinson's disease. *Oxidative medicine and cellular longevity*, 2013, p.683920.

Armada-Moreira, A. et al. (2020). Going the extra (synaptic) mile: Excitotoxicity as the road toward neurodegenerative diseases. *Frontiers in cellular neuroscience*, 14, p.90.

Armstrong, C. M. and Hille, B. (1998). Voltage-gated ion channels and electrical excitability. *Neuron*, 20 (3), pp.371–380.

Arshadi, C. et al. (2021). SNT: a unifying toolbox for quantification of neuronal anatomy. *Nature methods*, 18 (4), pp.374–377.

Artavanis-Tsakonas, S., Matsuno, K. and Fortini, M. E. (1995). Notch signaling. *Science (New York, N.Y.)*, 268 (5208), pp.225–232.

Aso, Y. et al. (2014a). Mushroom body output neurons encode valence and guide memory-based action selection in Drosophila. *eLife*, 3, p.e04580.

Aso, Y. et al. (2014b). The neuronal architecture of the mushroom body provides a logic for associative learning. *eLife*, 3, p.e04577.

Aso, Y. and Rubin, G. M. (2016). Dopaminergic neurons write and update memories with cell-type-specific rules. *eLife*, 5. [Online]. Available at: doi:10.7554/eLife.16135.

Aunis, D. and Bader, M. F. (1988). The cytoskeleton as a barrier to exocytosis in secretory cells. *The journal of experimental biology*, 139 (1), pp.253–266.

Baines, R. A. et al. (2001). Altered electrical properties in Drosophila neurons developing without synaptic transmission. *The Journal of neuroscience: the official journal of the Society for Neuroscience*, 21 (5), pp.1523–1531.

Baines, R. A. and Bate, M. (1998). Electrophysiological development of central neurons in the Drosophila embryo. *The Journal of neuroscience: the official journal of the Society for Neuroscience*, 18 (12), pp.4673–4683.

Baker, N. E. (1988). Transcription of the segment-polarity gene wingless in the imaginal discs of Drosophila, and the phenotype of a pupal-lethal wg mutation. *Development (Cambridge, England)*, 102 (3), pp.489–497.

Barnes, C. L., Bonnéry, D. and Cardona, A. (2022). Synaptic counts approximate synaptic contact area in Drosophila. *PloS one*, 17 (4), p.e0266064.

Barnes, S. J. et al. (2017). Deprivation-induced homeostatic spine scaling in vivo is localized to dendritic branches that have undergone recent spine loss. *Neuron*, 96 (4), pp.871-882.e5.

Baumann, A. et al. (1987). Molecular organization of the maternal effect region of the Shaker complex of Drosophila: characterization of an I(A) channel transcript with homology to vertebrate Na channel. *The EMBO journal*, 6 (11), pp.3419–3429.

Beggs, J. M. and Plenz, D. (2003). Neuronal avalanches in neocortical circuits. *The Journal of neuroscience: the official journal of the Society for Neuroscience*, 23 (35), pp.11167–11177.

Bender, K. J. and Trussell, L. O. (2012). The physiology of the axon initial segment. *Annual review of neuroscience*, 35 (1), pp.249–265.

Bernard, C. (1885). Leçons sur les phenomenes de la vie communs aux ani- maux et aux vegetaux. *Paris: J.-B. Bailli ere,*.

Bertin, F. et al. (2022). Dlg is required for short-term memory and interacts with NMDAR in the Drosophila brain. *International journal of molecular sciences*, 23 (16), p.9187.

Bhandawat, V. et al. (2007). Sensory processing in the Drosophila antennal lobe increases reliability and separability of ensemble odor representations. *Nature neuroscience*, 10 (11), pp.1474–1482.

Biederer, T., Kaeser, P. S. and Blanpied, T. A. (2017). Transcellular nanoalignment of synaptic function. *Neuron*, 96 (3), pp.680–696.

Bleckert, A., Photowala, H. and Alford, S. (2012). Dual pools of actin at presynaptic terminals. *Journal of neurophysiology*, 107 (12), pp.3479–3492.

Bliss, T. V. and Lomo, T. (1973). Long-lasting potentiation of synaptic transmission in the dentate area of the anaesthetized rabbit following stimulation of the perforant path. *The journal of physiology*, 232 (2), pp.331–356.

Böhme, M. A. et al. (2016). Active zone scaffolds differentially accumulate Unc13 isoforms to tune Ca(2+) channel-vesicle coupling. *Nature neuroscience*, 19 (10), pp.1311–1320.

Böhme, M. A. et al. (2019). Rapid active zone remodeling consolidates presynaptic potentiation. *Nature communications*, 10 (1), p.1085.

Boisseau, R. P., Vogel, D. and Dussutour, A. (2016). Habituation in non-neural organisms: evidence from slime moulds. *Proceedings. Biological sciences*, 283 (1829), p.20160446.

Bonheur, M. et al. (2023). A rapid and bidirectional reporter of neural activity reveals neural correlates of social behaviors in Drosophila. *Nature neuroscience*, 26 (7), pp.1295–1307.

Boothe, R. G., Kiorpes, L. and Carlson, M. R. (1985). Studies of strabismus and amblyopia in infant monkeys. *Journal of pediatric ophthalmology and strabismus*, 22 (5), pp.206–212.

Bridge, H. and Cumming, B. G. (2001). Responses of macaque V1 neurons to binocular orientation differences. *The Journal of neuroscience: the official journal of the Society for Neuroscience*, 21 (18), pp.7293–7302.

Bülow, P., Segal, M. and Bassell, G. J. (2022). Mechanisms driving the emergence of neuronal hyperexcitability in Fragile X syndrome. *International journal of molecular sciences*, 23 (11), p.6315.

Burrone, J., O'Byrne, M. and Murthy, V. N. (2002). Multiple forms of synaptic plasticity triggered by selective suppression of activity in individual neurons. *Nature*, 420 (6914), pp.414–418.

Bushey, D., Tononi, G. and Cirelli, C. (2011). Sleep and synaptic homeostasis: structural evidence in Drosophila. *Science (New York, N.Y.)*, 332 (6037), pp.1576–1581.

Butcher, N. J. et al. (2012). Different classes of input and output neurons reveal new features in microglomeruli of the adult Drosophila mushroom body calyx. *The Journal of comparative neurology*, 520 (10), pp.2185–2201.

Byers, D., Davis, R. L. and Kiger, J. A., Jr. (1981). Defect in cyclic AMP phosphodiesterase due to the dunce mutation of learning in Drosophila melanogaster. *Nature*, 289 (5793), pp.79–81.

Cachero, S. et al. (2020). BAcTrace, a tool for retrograde tracing of neuronal circuits in Drosophila. *Nature methods*, 17 (12), pp.1254–1261.

Camacho, M. et al. (2017). Heterodimerization of Munc13 C2A domain with RIM regulates synaptic vesicle docking and priming. *Nature communications*, 8 (1), p.15293.

Campbell, R. A. A. et al. (2013). Imaging a population code for odor identity in the Drosophila mushroom body. *The Journal of neuroscience: the official journal of the Society for Neuroscience*, 33 (25), pp.10568–10581.

Cancedda, L. et al. (2004). Acceleration of visual system development by environmental enrichment. *The Journal of neuroscience: the official journal of the Society for Neuroscience*, 24 (20), pp.4840–4848.

Cannon, W. B. (1929). Organization for physiological homeostasis. *Physiological reviews*, 9 (3), pp.399–431.

Caron, S. J. C. et al. (2013). Random convergence of olfactory inputs in the Drosophila mushroom body. *Nature*, 497 (7447), pp.113–117.

Castillo, P. E. (2012). Presynaptic LTP and LTD of excitatory and inhibitory synapses. *Cold Spring Harbor perspectives in biology*, 4 (2), pp.a005728–a005728.

Caston, R. M. et al. (2022). Stochastic resonance governs memory consolidation accuracy in a neural network model. *Annual International Conference of the IEEE Engineering in Medicine and Biology Society. IEEE Engineering in Medicine and Biology Society. Annual International Conference*, 2022, pp.2254–2257.

Catterall, W. A. (2000). Structure and regulation of voltage-gated Ca2+ channels. *Annual review of cell and developmental biology*, 16 (1), pp.521–555.

Catterall, W. A. and Few, A. P. (2008). Calcium channel regulation and presynaptic plasticity. *Neuron*, 59 (6), pp.882–901.

Cervantes-Sandoval, I. et al. (2013). System-like consolidation of olfactory memories in Drosophila. *The Journal of neuroscience: the official journal of the Society for Neuroscience*, 33 (23), pp.9846–9854.

Chand, A. N. et al. (2015). A distinct subtype of dopaminergic interneuron displays inverted structural plasticity at the axon initial segment. *The Journal of neuroscience: the official journal of the Society for Neuroscience*, 35 (4), pp.1573–1590.

Chauhan, V., Anis, A. and Chauhan, A. (2021). Effects of starvation on the levels of triglycerides, diacylglycerol, and activity of lipase in male and female Drosophila melanogaster. *Journal of lipids*, 2021, p.5583114.

Chen, L. et al. (2022). Homeostatic plasticity and excitation-inhibition balance: The good, the bad, and the ugly. *Current opinion in neurobiology*, 75 (102553), p.102553.

Chen, T.-W. et al. (2013). Ultrasensitive fluorescent proteins for imaging neuronal activity. *Nature*, 499 (7458), pp.295–300.

Chia, P. H., Patel, M. R. and Shen, K. (2012). NAB-1 instructs synapse assembly by linking adhesion molecules and F-actin to active zone proteins. *Nature neuroscience*, 15 (2), pp.234–242.

Chodankar, A. et al. (2020). Glomerulus-selective regulation of a critical period for interneuron plasticity in the Drosophila antennal lobe. *The Journal of neuroscience: the official journal of the Society for Neuroscience*, 40 (29), pp.5549–5560.

Cocchi, L. et al. (2017). Criticality in the brain: A synthesis of neurobiology, models and cognition. *Progress in neurobiology*, 158, pp.132–152.

Cohen, J. E. et al. (2011). MicroRNA regulation of homeostatic synaptic plasticity. *Proceedings of the National Academy of Sciences of the United States of America*, 108 (28), pp.11650–11655.

Connolly, J. B. et al. (1996). Associative learning disrupted by impaired Gs signaling in Drosophila mushroom bodies. *Science (New York, N.Y.)*, 274 (5295), pp.2104–2107.

Couto, A., Alenius, M. and Dickson, B. J. (2005). Molecular, anatomical, and functional organization of the Drosophila olfactory system. *Current biology: CB*, 15 (17), pp.1535–1547.

Crisp, S. et al. (2008). The development of motor coordination in Drosophila embryos. *Development (Cambridge, England)*, 135 (22), pp.3707–3717.

Crisp, S. J., Evers, J. F. and Bate, M. (2011). Endogenous patterns of activity are required for the maturation of a motor network. *The Journal of neuroscience: the official journal of the Society for Neuroscience*, 31 (29), pp.10445–10450.

Currie, K. P. M. (2010). G protein modulation of CaV2 voltage-gated calcium channels. *Channels (Austin, Tex.)*, 4 (6), pp.497–509.

Cynader, M. and Mitchell, D. E. (1980). Prolonged sensitivity to monocular deprivation in dark-reared cats. *Journal of neurophysiology*, 43 (4), pp.1026–1040.

da Costa, Ralf Engelmann, Martin Gleisner and Lutz Schäfer, Olivia Prazeres. (2021). A Practical Guide of Deconvolution. *Zeiss*.

Das, S. et al. (2011). Plasticity of local GABAergic interneurons drives olfactory habituation. *Proceedings of the National Academy of Sciences of the United States of America*, 108 (36), pp.E646-54.

Davis, G. W. et al. (1998). Postsynaptic PKA controls quantal size and reveals a retrograde signal that regulates presynaptic transmitter release in Drosophila. *Neuron*, 20 (2), pp.305–315.

Davis, R. L. (2011). Traces of Drosophila memory. *Neuron*, 70 (1), pp.8–19.

Daw, N. W. et al. (1992). Critical period for monocular deprivation in the cat visual cortex. *Journal of neurophysiology*, 67 (1), pp.197–202.

Deisseroth, K. et al. (2003). Signaling from synapse to nucleus: the logic behind the mechanisms. *Current opinion in neurobiology*, 13 (3), pp.354–365.

Deisseroth, K. (2010). Controlling the brain with light. *Scientific American*, 303 (5), pp.48–55.

Deisseroth, K. (2011). Optogenetics. *Nature methods*, 8 (1), pp.26–29.

Deng, L. et al. (2011). RIM proteins activate vesicle priming by reversing autoinhibitory homodimerization of Munc13. *Neuron*, 69 (2), pp.317–331.

Denk, W., Strickler, J. H. and Webb, W. W. (1990). Two-photon laser scanning fluorescence microscopy. *Science (New York, N.Y.)*, 248 (4951), pp.73–76.

Desai, N. S. et al. (2002). Critical periods for experience-dependent synaptic scaling in visual cortex. *Nature neuroscience*, 5 (8), pp.783–789.

Desai, N. S., Rutherford, L. C. and Turrigiano, G. G. (1999). Plasticity in the intrinsic excitability of cortical pyramidal neurons. *Nature neuroscience*, 2 (6), pp.515–520.

Devaud, J. M., Acebes, A. and Ferrús, A. (2001). Odor exposure causes central adaptation and morphological changes in selected olfactory glomeruli in Drosophila. *The Journal of neuroscience: the official journal of the Society for Neuroscience*, 21 (16), pp.6274–6282.

Devaud, J.-M. et al. (2003). Structural and functional changes in the olfactory pathway of adult Drosophila take place at a critical age. *Journal of neurobiology*, 56 (1), pp.13–23.

Devaud, J.-M., Keane, J. and Ferrús, A. (2003). Blocking sensory inputs to identified antennal glomeruli selectively modifies odorant perception in Drosophila. *Journal of neurobiology*, 56 (1), pp.1–12.

DiAntonio, A. et al. (1999). Glutamate receptor expression regulates quantal size and quantal content at the Drosophila neuromuscular junction. *The Journal of neuroscience: the official journal of the Society for Neuroscience*, 19 (8), pp.3023–3032.

Dickstein, D. L. et al. (2013). Dendritic spine changes associated with normal aging. *Neuroscience*, 251, pp.21–32.

Dieterich, D. C. et al. (2006). Selective identification of newly synthesized proteins in mammalian cells using bioorthogonal noncanonical amino acid tagging (BONCAT). *Proceedings of the National Academy of Sciences of the United States of America*, 103 (25), pp.9482–9487.

Dissel, S. et al. (2015). Sleep restores behavioral plasticity to Drosophila mutants. *Current biology: CB*, 25 (10), pp.1270–1281.

Dobler, T. et al. (2007). TRESK two-pore-domain K+ channels constitute a significant component of background potassium currents in murine dorsal root ganglion neurones. *The journal of physiology*, 585 (Pt 3), pp.867–879.

Doi, A. et al. (2018). High-resolution imaging in two-photon excitation microscopy using in situ estimations of the point spread function. *Biomedical optics express*, 9 (1), pp.202–213.

Dolphin, A. C. (2009). Calcium channel diversity: multiple roles of calcium channel subunits. *Current opinion in neurobiology*, 19 (3), pp.237–244.

Dombrovski, M. and Condron, B. (2021). Critical periods shaping the social brain: A perspective from Drosophila. *BioEssays: news and reviews in molecular, cellular and developmental biology*, 43 (1), p.e2000246.

Dorkenwald, S. et al. (2024). Neuronal wiring diagram of an adult brain. *Nature*, 634 (8032), pp.124–138.

Drakew, A. et al. (1996). Spine loss in experimental epilepsy: quantitative light and electron microscopic analysis of intracellularly stained CA3 pyramidal cells in hippocampal slice cultures. *Neuroscience*, 70 (1), pp.31–45.

Driscoll, H. E. et al. (2013). Pumilio-2 regulates translation of Nav1.6 to mediate homeostasis of membrane excitability. *The Journal of neuroscience: the official journal of the Society for Neuroscience*, 33 (23), pp.9644–9654.

Dudai, Y. et al. (1976). dunce, a mutant of Drosophila deficient in learning. *Proceedings of the National Academy of Sciences of the United States of America*, 73 (5), pp.1684–1688.

Dulubova, I. et al. (2005). A Munc13/RIM/Rab3 tripartite complex: from priming to plasticity? *The EMBO journal*, 24 (16), pp.2839–2850.

Dussutour, A. (2021). Learning in single cell organisms. *Biochemical and biophysical research communications*, 564, pp.92–102.

Eckstein, N. et al. (2024). Neurotransmitter classification from electron microscopy images at synaptic sites in Drosophila melanogaster. *Cell*, 187 (10), pp.2574-2594.e23.

Ehlers, M. D. (2003). Activity level controls postsynaptic composition and signaling via the ubiquitin-proteasome system. *Nature neuroscience*, 6 (3), pp.231–242.

Ellis, K. E. et al. (2024). Evolution of connectivity architecture in the Drosophila mushroom body. *Nature communications*, 15 (1), p.4872.

Evans, M. D. et al. (2013). Calcineurin signaling mediates activity-dependent relocation of the axon initial segment. *The Journal of neuroscience: the official journal of the Society for Neuroscience*, 33 (16), pp.6950–6963.

Everson, W. V. et al. (1989). Effect of amino acid deprivation on initiation of protein synthesis in rat hepatocytes. *The American journal of physiology*, 256 (1 Pt 1), pp.C18-27.

Fagiolini, M. et al. (1994). Functional postnatal development of the rat primary visual cortex and the role of visual experience: dark rearing and monocular deprivation. *Vision research*, 34 (6), pp.709–720.

Fagiolini, M. et al. (2003). Separable features of visual cortical plasticity revealed by N-methyl-D-aspartate receptor 2A signaling. *Proceedings of the National Academy of Sciences of the United States of America*, 100 (5), pp.2854–2859.

Fagiolini, M. and Hensch, T. K. (2000). Inhibitory threshold for critical-period activation in primary visual cortex. *Nature*, 404 (6774), pp.183–186.

Fayyazuddin, A. et al. (2006). The nicotinic acetylcholine receptor Dalpha7 is required for an escape behavior in Drosophila. *PLoS biology*, 4 (3), p.e63.

Fernández-Chacón, R. et al. (2001). Synaptotagmin I functions as a calcium regulator of release probability. *Nature*, 410 (6824), pp.41–49.

Ferster, D. (1981). A comparison of binocular depth mechanisms in areas 17 and 18 of the cat visual cortex. *The journal of physiology*, 311 (1), pp.623–655.

Fişek, M. and Wilson, R. I. (2014). Stereotyped connectivity and computations in higher-order olfactory neurons. *Nature Neuroscience*, 17 (2), pp.280–288. [Online]. Available at: doi:10.1038/nn.3613.

Flores, C. E. et al. (2015). Activity-dependent inhibitory synapse remodeling through gephyrin phosphorylation. *Proceedings of the National Academy of Sciences of the United States of America*, 112 (1), pp.E65-72.

Fouquet, W. et al. (2009). Maturation of active zone assembly by Drosophila Bruchpilot. *The journal of cell biology*, 186 (1), pp.129–145.

Frambach, I. et al. (2004). F-actin at identified synapses in the mushroom body neuropil of the insect brain. *The Journal of comparative neurology*, 475 (3), pp.303–314.

Frank, C. A. et al. (2006). Mechanisms underlying the rapid induction and sustained expression of synaptic homeostasis. *Neuron*, 52 (4), pp.663–677.

Frank, C. A. (2014a). Homeostatic plasticity at the Drosophila neuromuscular junction. *Neuropharmacology*, 78, pp.63–74.

Frank, C. A. (2014b). How voltage-gated calcium channels gate forms of homeostatic synaptic plasticity. *Frontiers in cellular neuroscience*, 8, p.40.

Frank, C. A., Pielage, J. and Davis, G. W. (2009). A presynaptic homeostatic signaling system composed of the Eph receptor, ephexin, Cdc42, and CaV2.1 calcium channels. *Neuron*, 61 (4), pp.556–569.

Frenkel, M. Y. and Bear, M. F. (2004). How monocular deprivation shifts ocular dominance in visual cortex of young mice. *Neuron*, 44 (6), pp.917–923.

Fu, A. K. Y. et al. (2011). APC(Cdh1) mediates EphA4-dependent downregulation of AMPA receptors in homeostatic plasticity. *Nature neuroscience*, 14 (2), pp.181–189.

Fu, M. et al. (2012). Repetitive motor learning induces coordinated formation of clustered dendritic spines in vivo. *Nature*, 483 (7387), pp.92–95.

Gainey, M. A. et al. (2009). Synaptic scaling requires the GluR2 subunit of the AMPA receptor. *The Journal of neuroscience: the official journal of the Society for Neuroscience*, 29 (20), pp.6479–6489.

Galili, D. S., Jefferis, G. S. and Costa, M. (2022). Connectomics and the neural basis of behaviour. *Current opinion in insect science*, 54 (100968), p.100968.

Ganeshina, O. et al. (2012). Depolymerization of actin facilitates memory formation in an insect. *Biology letters*, 8 (6), pp.1023–1027.

Ganeshina, O., Vorobyev, M. and Menzel, R. (2006). Synaptogenesis in the mushroom body calyx during metamorphosis in the honeybee Apis mellifera: an electron microscopic study. *The Journal of comparative neurology*, 497 (6), pp.876–897.

Ganetzky, B. and Wu, C. F. (1982). Indirect suppression involving behavioral mutants with altered nerve excitability in DROSOPHILA MELANOGASTER. *Genetics*, 100 (4), pp.597–614.

Gao, S. et al. (2008). The neural substrate of spectral preference in Drosophila. *Neuron*, 60 (2), pp.328–342.

Garber, R. L., Kuroiwa, A. and Gehring, W. J. (1983). Genomic and cDNA clones of the homeotic locus Antennapedia in Drosophila. *The EMBO journal*, 2 (11), pp.2027–2036.

Geppert, M. et al. (1994). Synaptotagmin I: a major Ca2+ sensor for transmitter release at a central synapse. *Cell*, 79 (4), pp.717–727.

Giachello, C. N. and Baines, R. A. (2017). Regulation of motoneuron excitability and the setting of homeostatic limits. *Current opinion in neurobiology*, 43, pp.1–6.

Giachello, C. N. G. and Baines, R. A. (2015). Inappropriate neural activity during a sensitive period in embryogenesis results in persistent seizure-like behavior. *Current biology: CB*, 25 (22), pp.2964–2968.

Gilbert, C. D. and Wiesel, T. N. (1992). Receptive field dynamics in adult primary visual cortex. *Nature*, 356 (6365), pp.150–152.

Gilestro, G. F., Tononi, G. and Cirelli, C. (2009). Widespread changes in synaptic markers as a function of sleep and wakefulness in Drosophila. *Science (New York, N.Y.)*, 324 (5923), pp.109–112.

Gireesh, E. D. and Plenz, D. (2008). Neuronal avalanches organize as nested theta- and beta/gamma-oscillations during development of cortical layer 2/3. *Proceedings of the National Academy of Sciences of the United States of America*, 105 (21), pp.7576–7581.

Gisabella, B. et al. (2020). Regulation of hippocampal dendritic spines following sleep deprivation. *The Journal of comparative neurology*, 528 (3), pp.380–388.

Gjorgjieva, J., Drion, G. and Marder, E. (2016). Computational implications of biophysical diversity and multiple timescales in neurons and synapses for circuit performance. *Current opinion in neurobiology*, 37, pp.44–52.

Goel, A. and Lee, H.-K. (2007). Persistence of experience-induced homeostatic synaptic plasticity through adulthood in superficial layers of mouse visual cortex. *The Journal of neuroscience: the official journal of the Society for Neuroscience*, 27 (25), pp.6692–6700.

Goel, P. et al. (2019). A screen for synaptic growth mutants reveals mechanisms that stabilize synaptic strength. *The Journal of neuroscience: the official journal of the Society for Neuroscience*, 39 (21), pp.4051–4065.

van der Goes van Naters, W. and Carlson, J. R. (2007). Receptors and Neurons for Fly Odors in Drosophila. *Current biology: CB*, 17 (7), pp.606–612.

Golic, K. G. and Lindquist, S. (1989). The FLP recombinase of yeast catalyzes site-specific recombination in the Drosophila genome. *Cell*, 59 (3), pp.499–509.

Golovin, R. M. et al. (2019). Activity-dependent remodeling of Drosophila olfactory sensory neuron brain innervation during an early-life critical period. *The Journal of neuroscience: the official journal of the Society for Neuroscience*, 39 (16), pp.2995–3012.

Goold, C. P. and Nicoll, R. A. (2010). Single-cell optogenetic excitation drives homeostatic synaptic depression. *Neuron*, 68 (3), pp.512–528.

Gotti, C. et al. (2009). Structural and functional diversity of native brain neuronal nicotinic receptors. *Biochemical pharmacology*, 78 (7), pp.703–711.

Govindarajan, A. et al. (2011). The dendritic branch is the preferred integrative unit for protein synthesis-dependent LTP. *Neuron*, 69 (1), pp.132–146.

Grabe, V. et al. (2016). Elucidating the neuronal architecture of olfactory glomeruli in the Drosophila antennal lobe. *Cell reports*, 16 (12), pp.3401–3413.

Gratz, S. J. et al. (2019). Endogenous tagging reveals differential regulation of Ca2+ channels at single active zones during presynaptic homeostatic potentiation and depression. *The Journal of neuroscience: the official journal of the Society for Neuroscience*, 39 (13), pp.2416–2429.

Greenin-Whitehead, K. et al. (2025). Ectopic sodium channel expression decreases excitability of Drosophila Kenyon cells. *The journal of physiology*, (JP288790). [Online]. Available at: doi:10.1113/JP288790.

Gromova, K. V. et al. (2023). The kinesin Kif21b binds myosin Va and mediates changes in actin dynamics underlying homeostatic synaptic downscaling. *Cell reports*, 42 (7), p.112743.

Groschner, L. N. et al. (2018). Dendritic Integration of Sensory Evidence in Perceptual Decision-Making. *Cell*, 173 (4), pp.894-905.e13.

Grubb, M. S. and Burrone, J. (2010). Activity-dependent relocation of the axon initial segment fine-tunes neuronal excitability. *Nature*, 465 (7301), pp.1070–1074.

Gruntman, E. and Turner, G. C. (2013). Integration of the olfactory code across dendritic claws of single mushroom body neurons. *Nature neuroscience*, 16 (12), pp.1821–1829.

Gu, H. and O'Dowd, D. K. (2006). Cholinergic synaptic transmission in adult Drosophila Kenyon cells in situ. *The Journal of neuroscience: the official journal of the Society for Neuroscience*, 26 (1), pp.265–272.

Guo, H. et al. (2010). Mammalian microRNAs predominantly act to decrease target mRNA levels. *Nature*, 466 (7308), pp.835–840.

Hallem, E. A. and Carlson, J. R. (2006). Coding of odors by a receptor repertoire. *Cell*, 125 (1), pp.143–160.

Hallem, E. A., Ho, M. G. and Carlson, J. R. (2004). The molecular basis of odor coding in the Drosophila antenna. *Cell*, 117 (7), pp.965–979.

Halpain, S., Hipolito, A. and Saffer, L. (1998). Regulation of F-actin stability in dendritic spines by glutamate receptors and calcineurin. *The Journal of neuroscience: the official journal of the Society for Neuroscience*, 18 (23), pp.9835–9844.

Hamada, F. N. et al. (2008). An internal thermal sensor controlling temperature preference in Drosophila. *Nature*, 454 (7201), pp.217–220.

Hamanaka, Y. and Meinertzhagen, I. A. (2010). Immunocytochemical localization of synaptic proteins to photoreceptor synapses of Drosophila melanogaster. *The Journal of comparative neurology*, 518 (7), pp.1133–1155.

Han, P. L. et al. (1992). Preferential expression of the Drosophila rutabaga gene in mushroom bodies, neural centers for learning in insects. *Neuron*, 9 (4), pp.619–627.

Handler, A. et al. (2019). Distinct Dopamine Receptor Pathways Underlie the Temporal Sensitivity of Associative Learning. *Cell*, 178 (1), pp.60-75.e19.

Hayashi, T. T. et al. (2022). Mushroom body input connections form independently of sensory activity in Drosophila melanogaster. *Current biology: CB*. [Online]. Available at: doi:10.1016/j.cub.2022.07.055.

Hebb, D. O. (1949). HEBB, D. O. Organization of behavior: A neuropsychological theory. Pp. Xix, 335. New York: John Wiley & sons, 1949. *The annals of the American Academy of Political and Social Science*, 271 (1), pp.216–217.

Heinen, S. J. and Skavenski, A. A. (1991). Recovery of visual responses in foveal V1 neurons following bilateral foveal lesions in adult monkey. *Experimental brain research*, 83 (3), pp.670–674.

Hengen, K. B. et al. (2013). Firing rate homeostasis in visual cortex of freely behaving rodents. *Neuron*, 80 (2), pp.335–342.

Hengen, K. B. et al. (2016). Neuronal firing rate homeostasis is inhibited by sleep and promoted by wake. *Cell*, 165 (1), pp.180–191.

Hensch, T. K. (2005). Critical period mechanisms in developing visual cortex. *Current topics in developmental biology*, 69, pp.215–237.

Hensch, T. K. and Quinlan, E. M. (2018). Critical periods in amblyopia. *Visual neuroscience*, 35 (E014). [Online]. Available at: doi:10.1017/s0952523817000219.

Hige, T. et al. (2015). Heterosynaptic Plasticity Underlies Aversive Olfactory Learning in Drosophila. *Neuron*, 88 (5), pp.985–998.

Hobbiss, A. F., Ramiro-Cortés, Y. and Israely, I. (2018). Homeostatic plasticity scales dendritic spine volumes and changes the threshold and specificity of Hebbian plasticity. *iScience*, 8, pp.161–174.

Holler, S. et al. (2021). Structure and function of a neocortical synapse. *Nature*, 591 (7848), pp.111–116.

Honegger, K. S., Campbell, R. A. A. and Turner, G. C. (2011). Cellular-resolution population imaging reveals robust sparse coding in the Drosophila mushroom body. *The Journal of neuroscience: the official journal of the Society for Neuroscience*, 31 (33), pp.11772–11785.

Hongpaisan, J., Winters, C. A. and Andrews, S. B. (2004). Strong calcium entry activates mitochondrial superoxide generation, upregulating kinase signaling in hippocampal neurons. *The Journal of neuroscience: the official journal of the Society for Neuroscience*, 24 (48), pp.10878–10887.

Hu, C. et al. (2020). Conserved Tao kinase activity regulates dendritic arborization, cytoskeletal dynamics, and sensory function in Drosophila. *The Journal of neuroscience: the official journal of the Society for Neuroscience*, 40 (9), pp.1819–1833.

Hu, J.-H. et al. (2010). Homeostatic scaling requires group I mGluR activation mediated by Homer1a. *Neuron*, 68 (6), pp.1128–1142.

Hu, Z., Tong, X.-J. and Kaplan, J. M. (2013). UNC-13L, UNC-13S, and Tomosyn form a protein code for fast and slow neurotransmitter release in Caenorhabditis elegans. *eLife*, 2, p.e00967.

Huang, C. et al. (2018). Long-term optical brain imaging in live adult fruit flies. *Nature communications*, 9 (1). [Online]. Available at: doi:10.1038/s41467-018-02873-1.

Huang, L. et al. (2021a). Relationship between simultaneously recorded spiking activity and fluorescence signal in GCaMP6 transgenic mice. *eLife*, 10. [Online]. Available at: doi:10.7554/eLife.51675.

Huang, W. et al. (2021b). TRESK channel contributes to depolarization-induced shunting inhibition and modulates epileptic seizures. *Cell reports*, 36 (3), p.109404.

Hubel, D. H. and Wiesel, T. N. (1962). Receptive fields, binocular interaction and functional architecture in the cat's visual cortex. *The journal of physiology*, 160 (1), pp.106–154.

Hubel, D. H. and Wiesel, T. N. (1970). The period of susceptibility to the physiological effects of unilateral eye closure in kittens. *The journal of physiology*, 206 (2), pp.419–436.

Hubel, D. H., Wiesel, T. N. and LeVay, S. (1977). Plasticity of ocular dominance columns in monkey striate cortex. *Philosophical transactions of the Royal Society of London. Series B, Biological sciences*, 278 (961), pp.377–409.

Huff, J. (2015). The Airyscan detector from ZEISS: confocal imaging with improved signal-to-noise ratio and super-resolution. *Nature methods*, 12 (12), pp.i–ii.

Ibata, K., Sun, Q. and Turrigiano, G. G. (2008). Rapid synaptic scaling induced by changes in postsynaptic firing. *Neuron*, 57 (6), pp.819–826.

Inada, K., Tsuchimoto, Y. and Kazama, H. (2017). Origins of Cell-Type-Specific Olfactory Processing in the Drosophila Mushroom Body Circuit. *Neuron*, 95 (2), pp.357-367.e4.

Ito, M. and Kano, M. (1982). Long-lasting depression of parallel fiber-Purkinje cell transmission induced by conjunctive stimulation of parallel fibers and climbing fibers in the cerebellar cortex. *Neuroscience letters*, 33 (3), pp.253–258.

Jaenisch, R. (1976). Germ line integration and Mendelian transmission of the exogenous Moloney leukemia virus. *Proceedings of the National Academy of Sciences of the United States of America*, 73 (4), pp.1260–1264.

Jaenisch, R. and Mintz, B. (1974). Simian virus 40 DNA sequences in DNA of healthy adult mice derived from preimplantation blastocysts injected with viral DNA. *Proceedings of the National Academy of Sciences of the United States of America*, 71 (4), pp.1250–1254.

Jan, L. Y. and Jan, Y. N. (1976a). L-glutamate as an excitatory transmitter at the Drosophila larval neuromuscular junction. *The journal of physiology*, 262 (1), pp.215–236.

Jan, L. Y. and Jan, Y. N. (1976b). Properties of the larval neuromuscular junction in Drosophila melanogaster. *The journal of physiology*, 262 (1), pp.189–214.

Jan, Y. N., Jan, L. Y. and Dennis, M. J. (1977). Two Mutations of synaptic transmission in Drosophila. *Proceedings of the Royal Society of London*, 198 (1130), pp.87–108.

Jayaraman, V. and Laurent, G. (2007). Evaluating a genetically encoded optical sensor of neural activity using electrophysiology in intact adult fruit flies. *Frontiers in neural circuits*, 1, p.3.

Jefferis, G. S. X. E. et al. (2004). Developmental origin of wiring specificity in the olfactory system of Drosophila. *Development (Cambridge, England)*, 131 (1), pp.117–130.

Jefferis, G. S. X. E. et al. (2007). Comprehensive maps of Drosophila higher olfactory centers: spatially segregated fruit and pheromone representation. *Cell*, 128 (6), pp.1187–1203.

Jenett, A. et al. (2012). A GAL4-driver line resource for Drosophila neurobiology. *Cell reports*, 2 (4), pp.991–1001.

Jiang, J., Foyard, E. and van Rossum, M. C. W. (2024). Reinforcement learning when your life depends on it: A neuro-economic theory of learning. *PLoS computational biology*, 20 (10), p.e1012554.

Jiang, M. et al. (1998). Spine loss and other persistent alterations of hippocampal pyramidal cell dendrites in a model of early-onset epilepsy. *The Journal of neuroscience: the official journal of the Society for Neuroscience*, 18 (20), pp.8356–8368.

Jinek, M. et al. (2012). A programmable dual-RNA-guided DNA endonuclease in adaptive bacterial immunity. *Science (New York, N.Y.)*, 337 (6096), pp.816–821.

Johnston, J., Forsythe, I. D. and Kopp-Scheinpflug, C. (2010). Going native: voltage-gated potassium channels controlling neuronal excitability. *The journal of physiology*, 588 (Pt 17), pp.3187–3200.

Jordán-Álvarez, S. et al. (2012). Presynaptic PI3K activity triggers the formation of glutamate receptors at neuromuscular terminals of Drosophila. *Journal of cell science*, 125 (Pt 15), pp.3621–3629.

Joseph, J., Dunn, F. A. and Stopfer, M. (2012). Spontaneous olfactory receptor neuron activity determines follower cell response properties. *The Journal of neuroscience: the official journal of the Society for Neuroscience*, 32 (8), pp.2900–2910.

Jürgens, G. et al. (1984). Mutations affecting the pattern of the larval cuticle inDrosophila melanogaster : II. Zygotic loci on the third chromosome. *Wilhelm Roux's archives of developmental biology*, 193 (5), pp.283–295.

Kaas, J. H. et al. (1990). Reorganization of retinotopic cortical maps in adult mammals after lesions of the retina. *Science (New York, N.Y.)*, 248 (4952), pp.229–231.

Kakihara, K. et al. (2008). Conversion of plasma membrane topology during epithelial tube connection requires Arf-like 3 small GTPase in Drosophila. *Mechanisms of development*, 125 (3–4), pp.325–336.

Kamb, A., Iverson, L. E. and Tanouye, M. A. (1987). Molecular characterization of Shaker, a Drosophila gene that encodes a potassium channel. *Cell*, 50 (3), pp.405–413.

Kaplan, W. D. and Trout, W. E., 3rd. (1969). The behavior of four neurological mutants of Drosophila. *Genetics*, 61 (2), pp.399–409.

Katz, B. and Miledi, R. (1970). Further study of the role of calcium in synaptic transmission. *The journal of physiology*, 207 (3), pp.789–801.

Kaufman, T. C., Lewis, R. and Wakimoto, B. (1980). Cytogenetic analysis of chromosome 3 in DROSOPHILA MELANOGASTER: The homoeotic gene complex in polytene chromosome interval 84a-B. *Genetics*, 94 (1), pp.115–133.

Keck, T. et al. (2008). Massive restructuring of neuronal circuits during functional reorganization of adult visual cortex. *Nature neuroscience*, 11 (10), pp.1162–1167.

Keck, T. et al. (2011). Loss of sensory input causes rapid structural changes of inhibitory neurons in adult mouse visual cortex. *Neuron*, 71 (5), pp.869–882.

Keck, T. et al. (2013). Synaptic scaling and homeostatic plasticity in the mouse visual cortex in vivo. *Neuron*, 80 (2), pp.327–334.

Kim, J. and Tsien, R. W. (2008). Synapse-specific adaptations to inactivity in hippocampal circuits achieve homeostatic gain control while dampening network reverberation. *Neuron*, 58 (6), pp.925–937.

Kim, R. H. et al. (2005). DJ-1, a novel regulator of the tumor suppressor PTEN. *Cancer cell*, 7 (3), pp.263–273.

Kim, Y.-C. et al. (2009). Oxidation of DJ-1-dependent cell transformation through direct binding of DJ-1 to PTEN. *International journal of oncology*, 35 (6), pp.1331–1341.

King, I. et al. (2011). Drosophila tao controls mushroom body development and ethanol-stimulated behavior through par-1. *The Journal of neuroscience: the official journal of the Society for Neuroscience*, 31 (3), pp.1139–1148.

Kiral, F. R. et al. (2021). Brain connectivity inversely scales with developmental temperature in Drosophila. *Cell reports*, 37 (12), p.110145.

Kirov, S. A. and Harris, K. M. (1999). Dendrites are more spiny on mature hippocampal neurons when synapses are inactivated. *Nature neuroscience*, 2 (10), pp.878–883.

Kittel, R. J. et al. (2006). Bruchpilot promotes active zone assembly, Ca2+ channel clustering, and vesicle release. *Science (New York, N.Y.)*, 312 (5776), pp.1051–1054.

Kleindienst, T. et al. (2011). Activity-dependent clustering of functional synaptic inputs on developing hippocampal dendrites. *Neuron*, 72 (6), pp.1012–1024.

Knogler, L. D., Liao, M. and Drapeau, P. (2010). Synaptic scaling and the development of a motor network. *The Journal of neuroscience: the official journal of the Society for Neuroscience*, 30 (26), pp.8871–8881.

Kosakamoto, H. et al. (2024). Context-dependent impact of the dietary non-essential amino acid tyrosine on Drosophila physiology and longevity. *Science advances*, 10 (35), p.eadn7167.

Kosik, K. S. (2006). The neuronal microRNA system. *Nature reviews. Neuroscience*, 7 (12), pp.911–920.

Kramár, E. A. et al. (2006). Integrin-driven actin polymerization consolidates long-term potentiation. *Proceedings of the National Academy of Sciences of the United States of America*, 103 (14), pp.5579–5584.

Krashes, M. J. et al. (2007). Sequential use of mushroom body neuron subsets during drosophila odor memory processing. *Neuron*, 53 (1), pp.103–115.

Kremer, M. C. et al. (2010). Structural long-term changes at mushroom body input synapses. *Current biology: CB*, 20 (21), pp.1938–1944.

Krucker, T., Siggins, G. R. and Halpain, S. (2000). Dynamic actin filaments are required for stable long-term potentiation (LTP) in area CA1 of the hippocampus. *Proceedings of the National Academy of Sciences of the United States of America*, 97 (12), pp.6856–6861.

Kuang, Q., Purhonen, P. and Hebert, H. (2015). Structure of potassium channels. *Cellular and molecular life sciences: CMLS*, 72 (19), pp.3677–3693.

Kuebler, D. and Tanouye, M. A. (2000). Modifications of seizure susceptibility in Drosophila. *Journal of neurophysiology*, 83 (2), pp.998–1009.

Ladt, K., Ganguly, A. and Roy, S. (2016). Axonal actin in action: Imaging actin dynamics in neurons. *Methods in cell biology*, 131, pp.91–106.

Lambo, M. E. and Turrigiano, G. G. (2013). Synaptic and intrinsic homeostatic mechanisms cooperate to increase L2/3 pyramidal neuron excitability during a late phase of critical period plasticity. *The Journal of neuroscience: the official journal of the Society for Neuroscience*, 33 (20), pp.8810–8819.

Lamprecht, R. (2016). The role of actin cytoskeleton in memory formation in amygdala. *Frontiers in molecular neuroscience*, 9, p.23.

Leal, G., Comprido, D. and Duarte, C. B. (2014). BDNF-induced local protein synthesis and synaptic plasticity. *Neuropharmacology*, 76 Pt C, pp.639–656.

Lee, T., Lee, A. and Luo, L. (1999). Development of the Drosophila mushroom bodies: sequential generation of three distinct types of neurons from a neuroblast. *Development* , 126 (18), pp.4065–4076.

Lee, T. and Luo, L. (2001). Mosaic analysis with a repressible cell marker (MARCM) for Drosophila neural development. *Trends in Neurosciences*, 24 (5), pp.251–254. [Online]. Available at: doi:10.1016/s0166-2236(00)01791-4.

Leiss, F. et al. (2009). Synaptic organization in the adult Drosophila mushroom body calyx. *The Journal of comparative neurology*, 517 (6), pp.808–824.

Levin, L. R. et al. (1992). The Drosophila learning and memory gene rutabaga encodes a -adenylyl cyclase. *Cell*, 68 (3), pp.479–489.

Li, B. et al. (2020a). Neuronal inactivity co-opts LTP machinery to drive potassium channel splicing and homeostatic spike widening. *Cell*, 181 (7), pp.1547-1565.e15.

Li, F. et al. (2020b). The connectome of the adult Drosophila mushroom body provides insights into function. *eLife*, 9. [Online]. Available at: doi:10.7554/eLife.62576.

Li, H. et al. (2013). Transformation of odor selectivity from projection neurons to single mushroom body neurons mapped with dual-color calcium imaging. *Proceedings of the National Academy of Sciences of the United States of America*, 110 (29), pp.12084–12089.

Liberti, W. A., 3rd et al. (2016). Unstable neurons underlie a stable learned behavior. *Nature neuroscience*, 19 (12), pp.1665–1671.

Lignani, G., Baldelli, P. and Marra, V. (2020). Homeostatic plasticity in epilepsy. *Frontiers in cellular neuroscience*, 14, p.197.

Lin, A. C. et al. (2014). Sparse, decorrelated odor coding in the mushroom body enhances learned odor discrimination. *Nature neuroscience*, 17 (4), pp.559–568.

Lin, J., Prahlad, J. and Wilson, M. A. (2012). Conservation of oxidative protein stabilization in an insect homologue of parkinsonism-associated protein DJ-1. *Biochemistry*, 51 (18), pp.3799–3807.

Lin, J. Y. (2011). A user's guide to channelrhodopsin variants: features, limitations and future developments. *Experimental physiology*, 96 (1), pp.19–25.

Lin, T. P. (1966). Microinjection of mouse eggs. *Science (New York, N.Y.)*, 151 (3708), pp.333–337.

Linford, N. J. et al. (2013). Measurement of lifespan in Drosophila melanogaster. *Journal of visualized experiments: JoVE*, (71). [Online]. Available at: doi:10.3791/50068.

Lipscombe, D., Allen, S. E. and Toro, C. P. (2013). Control of neuronal voltage-gated calcium ion channels from RNA to protein. *Trends in neurosciences*, 36 (10), pp.598–609.

Litwin-Kumar, A. et al. (2017). Optimal degrees of synaptic connectivity. *Neuron*, 93 (5), pp.1153-1164.e7.

Liu, C. and Hermann, T. E. (1978). Characterization of ionomycin as a calcium ionophore. *The journal of biological chemistry*, 253 (17), pp.5892–5894.

Liu, K. S. Y. et al. (2011). RIM-binding protein, a central part of the active zone, is essential for neurotransmitter release. *Science (New York, N.Y.)*, 334 (6062), pp.1565–1569.

Liu, P. et al. (2013). Functional analysis of a migraine-associated TRESK K+ channel mutation. *The Journal of neuroscience: the official journal of the Society for Neuroscience*, 33 (31), pp.12810–12824.

Livingstone, M. S., Sziber, P. P. and Quinn, W. G. (1984). Loss of calcium/calmodulin responsiveness in adenylate cyclase of rutabaga, a Drosophila learning mutant. *Cell*, 37 (1), pp.205–215.

Lu, H. et al. (2025). The interplay between homeostatic synaptic scaling and homeostatic structural plasticity maintains the robust firing rate of neural networks. *eLife*, 12. [Online]. Available at: doi:10.7554/eLife.88376.

Lu, J. et al. (2006). Structural basis for a Munc13-1 homodimer to Munc13-1/RIM heterodimer switch. *PLoS biology*, 4 (7), p.e192.

Lyon, P. (2015). The cognitive cell: bacterial behavior reconsidered. *Frontiers in microbiology*, 6, p.264.

Ma, H. et al. (2014). γCaMKII shuttles Ca^{2+}/CaM to the nucleus to trigger CREB phosphorylation and gene expression. *Cell*, 159 (2), pp.281–294.

Ma, Z. et al. (2019). Cortical circuit dynamics are homeostatically tuned to criticality in vivo. *Neuron*, 104 (4), pp.655-664.e4.

MacLean, J. N. et al. (2003). Activity-independent homeostasis in rhythmically active neurons. *Neuron*, 37 (1), Elsevier BV., pp.109–120.

Maffei, A. et al. (2006). Potentiation of cortical inhibition by visual deprivation. *Nature*, 443 (7107), pp.81–84.

Maffei, A., Lambo, M. E. and Turrigiano, G. G. (2010). Critical period for inhibitory plasticity in rodent binocular V1. *The Journal of neuroscience: the official journal of the Society for Neuroscience*, 30 (9), pp.3304–3309.

Maffei, A., Nelson, S. B. and Turrigiano, G. G. (2004). Selective reconfiguration of layer 4 visual cortical circuitry by visual deprivation. *Nature neuroscience*, 7 (12), pp.1353–1359.

Makino, H. and Malinow, R. (2011). Compartmentalized versus global synaptic plasticity on dendrites controlled by experience. *Neuron*, 72 (6), pp.1001–1011.

Marder, E. and Goaillard, J.-M. (2006). Variability, compensation and homeostasis in neuron and network function. *Nature reviews. Neuroscience*, 7 (7), pp.563–574.

Marsat, G. and Maler, L. (2010). Neural heterogeneity and efficient population codes for communication signals. *Journal of neurophysiology*, 104 (5), pp.2543–2555.

Martín-Peña, A. et al. (2006). Age-independent synaptogenesis by phosphoinositide 3 kinase. *The Journal of neuroscience: the official journal of the Society for Neuroscience*, 26 (40), pp.10199–10208.

Mazor, K. M. et al. (2018). Effects of single amino acid deficiency on mRNA translation are markedly different for methionine versus leucine. *Scientific reports*, 8 (1). [Online]. Available at: doi:10.1038/s41598-018-26254-2.

McClure, C. D. et al. (2022). An auxin-inducible, GAL4-compatible, gene expression system for Drosophila. *eLife*, 11. [Online]. Available at: doi:10.7554/eLife.67598.

McDonnell, M. D. and Ward, L. M. (2011). The benefits of noise in neural systems: bridging theory and experiment. *Nature reviews. Neuroscience*, 12 (7), pp.415–426.

McGinnis, W. et al. (1984). A homologous protein-coding sequence in Drosophila homeotic genes and its conservation in other metazoans. *Cell*, 37 (2), pp.403–408.

McGuire, S. E., Mao, Z. and Davis, R. L. (2004). Spatiotemporal gene expression targeting with the TARGET and gene-switch systems in Drosophila. *Science's STKE: signal transduction knowledge environment*, 2004 (220), p.l6.

Mee, C. J. et al. (2004). Regulation of neuronal excitability through pumilio-dependent control of a sodium channel gene. *The Journal of neuroscience: the official journal of the Society for Neuroscience*, 24 (40), pp.8695–8703.

Mendez, P. et al. (2018). Homeostatic plasticity in the hippocampus facilitates memory extinction. *Cell reports*, 22 (6), pp.1451–1461.

Meulener, M. C. et al. (2006). Mutational analysis of DJ-1 in Drosophila implicates functional inactivation by oxidative damage and aging. *Proceedings of the National Academy of Sciences of the United States of America*, 103 (33), pp.12517–12522.

Michelassi, F. et al. (2017). A C1-C2 module in Munc13 inhibits calcium-dependent neurotransmitter release. *Neuron*, 95 (3), pp.577-590.e5.

Michetti, C. and Benfenati, F. (2024). Homeostatic regulation of brain activity: from endogenous mechanisms to homeostatic nanomachines. *American journal of physiology. Cell physiology*, 327 (6), pp.C1384–C1399.

Miller, D. J. and Smith, G. L. (1984). EGTA purity and the buffering of calcium ions in physiological solutions. *The American journal of physiology*, 246 (1 Pt 1), pp.C160-6.

Miller, K. D. and MacKay, D. J. C. (1994). The role of constraints in Hebbian learning. *Neural computation*, 6 (1), pp.100–126.

Misonou, H. et al. (2004). Regulation of ion channel localization and phosphorylation by neuronal activity. *Nature neuroscience*, 7 (7), pp.711–718.

Misonou, H. et al. (2005). Calcium- and metabolic state-dependent modulation of the voltage-dependent Kv2.1 channel regulates neuronal excitability in response to ischemia. *The Journal of neuroscience: the official journal of the Society for Neuroscience*, 25 (48), pp.11184–11193.

Misonou, H., Mohapatra, D. P. and Trimmer, J. S. (2005). Kv2.1: a voltage-gated k+ channel critical to dynamic control of neuronal excitability. *Neurotoxicology*, 26 (5), pp.743–752.

Modell, H. et al. (2015). A physiologist's view of homeostasis. *Advances in physiology education*, 39 (4), pp.259–266.

Modi, M. N., Shuai, Y. and Turner, G. C. (2020). The Drosophila Mushroom Body: From Architecture to Algorithm in a Learning Circuit. *Annual review of neuroscience*, 43, pp.465–484.

Mohapatra, D. P. et al. (2009). Regulation of intrinsic excitability in hippocampal neurons by activity-dependent modulation of the KV2.1 potassium channel. *Channels (Austin, Tex.)*, 3 (1), pp.46–56.

Morishita, H. and Hensch, T. K. (2008). Critical period revisited: impact on vision. *Current opinion in neurobiology*, 18 (1), pp.101–107.

Moulin, T. C. et al. (2019). Chronic in vivo optogenetic stimulation modulates neuronal excitability, spine morphology, and Hebbian plasticity in the mouse hippocampus. *Hippocampus*, 29 (8), pp.755–761.

Moulin, T. C., Rayêe, D. and Schiöth, H. B. (2022). Dendritic spine density changes and homeostatic synaptic scaling: a meta-analysis of animal studies. *Neural regeneration research*, 17 (1), pp.20–24.

Movshon, J. A. and Van Sluyters, R. C. (1981). Visual neural development. *Annual review of psychology*, 32 (1), pp.477–522.

Muller, H. J. (1918). Genetic variability, twin hybrids and constant hybrids, in a case of balanced lethal factors. *Genetics*, 3 (5), pp.422–499.

Muller, H. J. (1927). Artificial transmutation of the gene. *Science (New York, N.Y.)*, 66 (1699), pp.84–87.

Müller, M. et al. (1993). Reversible loss of dendritic spines and altered excitability after chronic epilepsy in hippocampal slice cultures. *Proceedings of the National Academy of Sciences of the United States of America*, 90 (1), pp.257–261.

Müller, M. et al. (2012). RIM controls homeostatic plasticity through modulation of the readily-releasable vesicle pool. *The Journal of neuroscience: the official journal of the Society for Neuroscience*, 32 (47), pp.16574–16585.

Müller, M. and Davis, G. W. (2012). Transsynaptic control of presynaptic Ca^{2+} influx achieves homeostatic potentiation of neurotransmitter release. *Current biology: CB*, 22 (12), pp.1102–1108.

Müller, M., Genç, Ö. and Davis, G. W. (2015). RIM-binding protein links synaptic homeostasis to the stabilization and replenishment of high release probability vesicles. *Neuron*, 85 (5), pp.1056–1069.

Murthy, M. and Turner, G. (2013). Whole-cell in vivo patch-clamp recordings in the Drosophila brain. *Cold Spring Harbor protocols*, 2013 (2), pp.140–148.

Murthy, V. N. et al. (2001). Inactivity produces increases in neurotransmitter release and synapse size. *Neuron*, 32 (4), pp.673–682.

Nagel, G. et al. (2003). Channelrhodopsin-2, a directly light-gated cation-selective membrane channel. *Proceedings of the National Academy of Sciences of the United States of America*, 100 (24), pp.13940–13945.

Nakagaki, T., Yamada, H. and Tóth, A. (2000). Maze-solving by an amoeboid organism. *Nature*, 407 (6803), p.470.

Nakai, J., Ohkura, M. and Imoto, K. (2001). A high signal-to-noise Ca(2+) probe composed of a single green fluorescent protein. *Nature biotechnology*, 19 (2), pp.137–141.

Nakanishi, H. et al. (1997). Neurabin: a novel neural tissue-specific actin filament-binding protein involved in neurite formation. *The journal of cell biology*, 139 (4), pp.951–961.

Nelson, J. I., Kato, H. and Bishop, P. O. (1977). Discrimination of orientation and position disparities by binocularly activated neurons in cat straite cortex. *Journal of neurophysiology*, 40 (2), pp.260–283.

Nüsslein-Volhard, C. and Wieschaus, E. (1980). Mutations affecting segment number and polarity in Drosophila. *Nature*, 287 (5785), pp.795–801.

O'Leary, T. et al. (2014). Cell types, network homeostasis, and pathological compensation from a biologically plausible ion channel expression model. *Neuron*, 82 (4), pp.809–821.

Olsen, S. R., Bhandawat, V. and Wilson, R. I. (2010). Divisive normalization in olfactory population codes. *Neuron*, 66 (2), pp.287–299.

Orr, B. O., Fetter, R. D. and Davis, G. W. (2017). Retrograde semaphorin–plexin signalling drives homeostatic synaptic plasticity. *Nature*, 550 (7674), pp.109–113.

Orr, B. O., Fetter, R. D. and Davis, G. W. (2022). Activation and expansion of presynaptic signaling foci drives presynaptic homeostatic plasticity. *Neuron*, 110 (22), pp.3743-3759.e6.

Oswald, M. C. et al. (2018). Reactive oxygen species regulate activity-dependent neuronal plasticity in Drosophila. *eLife*, 7. [Online]. Available at: doi:10.7554/eLife.39393.

Papazian, D. M. et al. (1987). Cloning of genomic and complementary DNA from Shaker, a putative potassium channel gene from Drosophila. *Science (New York, N.Y.)*, 237 (4816), pp.749–753.

Park, H. and Kaang, B.-K. (2019). Balanced actions of protein synthesis and degradation in memory formation. *Learning & memory (Cold Spring Harbor, N.Y.)*, 26 (9), pp.299–306.

Park, K.-S. et al. (2006). Graded regulation of the Kv2.1 potassium channel by variable phosphorylation. *Science (New York, N.Y.)*, 313 (5789), pp.976–979.

Parker, L. et al. (2011). Drosophila as a model for epilepsy: bss is a gain-of-function mutation in the para sodium channel gene that leads to seizures. *Genetics*, 187 (2), pp.523–534.

Parnas, M., Manoim, J. E. and Lin, A. C. (2024). Sensory encoding and memory in the mushroom body: signals, noise, and variability. *Learning & memory (Cold Spring Harbor, N.Y.)*, 31 (5), p.a053825.

Paul, L. A. and Scheibel, A. B. (1986). Structural substrates of epilepsy. *Advances in neurology*, 44, pp.775–786.

Perazzona, B. et al. (2004). The role of cAMP response element-binding protein in Drosophila long-term memory. *The Journal of neuroscience: the official journal of the Society for Neuroscience*, 24 (40), pp.8823–8828.

Perin, M. S. et al. (1990). Phospholipid binding by a synaptic vesicle protein homologous to the regulatory region of protein kinase C. *Nature*, 345 (6272), pp.260–263.

Perry, S. et al. (2022). A glutamate receptor C-tail recruits CaMKII to suppress retrograde homeostatic signaling. *Nature communications*, 13 (1), p.7656.

Petersen, S. A. et al. (1997). Genetic analysis of glutamate receptors in Drosophila reveals a retrograde signal regulating presynaptic transmitter release. *Neuron*, 19 (6), pp.1237–1248.

Pilauri, V. et al. (2005). Gal80 dimerization and the yeast GAL gene switch. *Genetics*, 169 (4), pp.1903–1914.

Ping, Y. and Tsunoda, S. (2011). Inactivity-induced increase in nAChRs upregulates Shal K(+) channels to stabilize synaptic potentials. *Nature neuroscience*, 15 (1), pp.90–97.

Plaçais, P.-Y. and Preat, T. (2013). To favor survival under food shortage, the brain disables costly memory. *Science (New York, N.Y.)*, 339 (6118), pp.440–442.

Prusky, G. T. and Douglas, R. M. (2003). Developmental plasticity of mouse visual acuity. *The European journal of neuroscience*, 17 (1), pp.167–173.

Pulver, S. R. et al. (2009). Temporal dynamics of neuronal activation by Channelrhodopsin-2 and TRPA1 determine behavioral output in Drosophila larvae. *Journal of neurophysiology*, 101 (6), pp.3075–3088.

Qin, H. et al. (2012). Gamma neurons mediate dopaminergic input during aversive olfactory memory formation in Drosophila. *Current biology: CB*, 22 (7), pp.608–614.

Radulescu, C. I. et al. (2023). Age-related dysregulation of homeostatic control in neuronal microcircuits. *Nature neuroscience*, 26 (12), pp.2158–2170.

Ramesh, N. et al. (2021). Antagonistic interactions between two Neuroligins coordinate pre- and postsynaptic assembly. *Current biology: CB*, 31 (8), pp.1711-1725.e5.

Ramesh, N. et al. (2023). An antagonism between Spinophilin and Syd-1 operates upstream of memory-promoting presynaptic long-term plasticity. *eLife*, 12. [Online]. Available at: doi:10.7554/eLife.86084.

Reddy-Alla, S. et al. (2017). Stable positioning of Unc13 restricts synaptic vesicle fusion to defined release sites to promote synchronous neurotransmission. *Neuron*, 95 (6), pp.1350-1364.e12.

Reiter, L. T. et al. (2001). A systematic analysis of human disease-associated gene sequences in Drosophila melanogaster. *Genome research*, 11 (6), pp.1114–1125.

Riedl, J. et al. (2008). Lifeact: a versatile marker to visualize F-actin. *Nature methods*, 5 (7), pp.605–607.

Rohrbough, J. and Broadie, K. (2002). Electrophysiological analysis of synaptic transmission in central neurons of Drosophila larvae. *Journal of neurophysiology*, 88 (2), pp.847–860.

Romer, S. H. et al. (2014). Redistribution of Kv2.1 ion channels on spinal motoneurons following peripheral nerve injury. *Brain research*, 1547, pp.1–15.

Romer, S. H., Deardorff, A. S. and Fyffe, R. E. W. (2016). Activity-dependent redistribution of Kv2.1 ion channels on rat spinal motoneurons. *Physiological reports*, 4 (22), p.e13039.

Rosenblatt, F. (1958). The perceptron: a probabilistic model for information storage and organization in the brain. *Psychological review*, 65 (6), pp.386–408.

Rosenmund, C. and Stevens, C. F. (1996). Definition of the readily releasable pool of vesicles at hippocampal synapses. *Neuron*, 16 (6), pp.1197–1207.

Rosenzweig, M. et al. (2005). The Drosophila ortholog of vertebrate TRPA1 regulates thermotaxis. *Genes & development*, 19 (4), pp.419–424.

Rozenfeld, E. et al. (2023). Homeostatic synaptic plasticity rescues neural coding reliability. *Nature communications*, 14 (1), p.2993.

Rubin, G. M. and Spradling, A. C. (1982). Genetic transformation of Drosophila with transposable element vectors. *Science (New York, N.Y.)*, 218 (4570), pp.348–353.

Rumelhart, D. E., Hinton, G. E. and Williams, R. J. (1986). Learning representations by back-propagating errors. *Nature*, 323 (6088), pp.533–536.

Ryan, X. P. et al. (2005). The Rho-specific GEF Lfc interacts with neurabin and spinophilin to regulate dendritic spine morphology. *Neuron*, 47 (1), pp.85–100.

Sachse, S. et al. (2007). Activity-dependent plasticity in an olfactory circuit. *Neuron*, 56 (5), pp.838–850.

Sakamoto, H. et al. (2018). Synaptic weight set by Munc13-1 supramolecular assemblies. *Nature neuroscience*, 21 (1), pp.41–49.

Samanta, S., Chakraborty, S. and Bagchi, D. (2024). Pathogenesis of neurodegenerative diseases and the protective role of natural bioactive components. *Journal of the American Nutrition Association*, 43 (1), pp.20–32.

Sato, M. and Stryker, M. P. (2008). Distinctive features of adult ocular dominance plasticity. *The Journal of neuroscience: the official journal of the Society for Neuroscience*, 28 (41), pp.10278–10286.

Schanzenbächer, C. T. et al. (2016). Nascent proteome remodeling following homeostatic scaling at hippocampal synapses. *Neuron*, 92 (2), pp.358–371.

Schanzenbächer, C. T., Langer, J. D. and Schuman, E. M. (2018). Time- and polarity-dependent proteomic changes associated with homeostatic scaling at central synapses. *eLife*, 7. [Online]. Available at: doi:10.7554/eLife.33322.

Scheffer, L. K. et al. (2020). A connectome and analysis of the adult Drosophila central brain. *eLife*, 9. [Online]. Available at: doi:10.7554/eLife.57443.

Schiavo, G. et al. (1996). Calcium-dependent switching of the specificity of phosphoinositide binding to synaptotagmin. *Proceedings of the National Academy of Sciences of the United States of America*, 93 (23), pp.13327–13332.

Schlegel, P. et al. (2024). Whole-brain annotation and multi-connectome cell typing of Drosophila. *Nature*, 634 (8032), pp.139–152.

Schneider, D. (2000). Using Drosophila as a model insect. *Nature reviews. Genetics*, 1 (3), pp.218–226.

Seeburg, D. P. et al. (2008). Critical role of CDK5 and Polo-like kinase 2 in homeostatic synaptic plasticity during elevated activity. *Neuron*, 58 (4), pp.571–583.

Seeburg, D. P. and Sheng, M. (2008). Activity-induced Polo-like kinase 2 is required for homeostatic plasticity of hippocampal neurons during epileptiform activity. *The Journal of neuroscience: the official journal of the Society for Neuroscience*, 28 (26), pp.6583–6591.

Segal, M. (1995). Morphological alterations in dendritic spines of rat hippocampal neurons exposed to N-methyl-D-aspartate. *Neuroscience letters*, 193 (2), pp.73–76.

Shepherd, J. D. and Huganir, R. L. (2007). The cell biology of synaptic plasticity: AMPA receptor trafficking. *Annual review of cell and developmental biology*, 23 (1), pp.613–643.

Shew, W. L. and Plenz, D. (2013). The functional benefits of criticality in the cortex. *The Neuroscientist: a review journal bringing neurobiology, neurology and psychiatry*, 19 (1), pp.88–100.

Shin, S. M. et al. (2012). GKAP orchestrates activity-dependent postsynaptic protein remodeling and homeostatic scaling. *Nature neuroscience*, 15 (12), pp.1655–1666.

Siksou, L. et al. (2007). Three-dimensional architecture of presynaptic terminal cytomatrix. *The Journal of neuroscience: the official journal of the Society for Neuroscience*, 27 (26), pp.6868–6877.

Silva, B. et al. (2022). Glia fuel neurons with locally synthesized ketone bodies to sustain memory under starvation. *Nature metabolism*, 4 (2), pp.213–224.

Sinha, S. R., Wu, L.-G. and Saggau, P. (1997). Presynaptic calcium dynamics and transmitter release evoked by single action potentials at mammalian central synapses. *Biophysical journal*, 72 (2), pp.637–651.

Slomowitz, E. et al. (2015). Interplay between population firing stability and single neuron dynamics in hippocampal networks. *eLife*, 4. [Online]. Available at: doi:10.7554/eLife.04378.

Soderling, T. R. (1999). The Ca-calmodulin-dependent protein kinase cascade. *Trends in biochemical sciences*, 24 (6), pp.232–236.

Spano, G. M. et al. (2019). Sleep deprivation by exposure to novel objects increases synapse density and axon-spine interface in the hippocampal CA1 region of adolescent mice. *The Journal of neuroscience: the official journal of the Society for Neuroscience*, 39 (34), pp.6613–6625.

Srinivasan, S. et al. (2023). Effects of stochastic coding on olfactory discrimination in flies and mice. *PLoS biology*, 21 (10), p.e3002206.

Steinmetz, C. C. and Turrigiano, G. G. (2010). Tumor necrosis factor-α signaling maintains the ability of cortical synapses to express synaptic scaling. *The Journal of neuroscience: the official journal of the Society for Neuroscience*, 30 (44), pp.14685–14690.

Stellwagen, D. and Malenka, R. C. (2006). Synaptic scaling mediated by glial TNF-alpha. *Nature*, 440 (7087), pp.1054–1059.

Stepanyants, A., Hof, P. R. and Chklovskii, D. B. (2002). Geometry and structural plasticity of synaptic connectivity. *Neuron*, 34 (2), pp.275–288.

Stern, E. A., Maravall, M. and Svoboda, K. (2001). Rapid development and plasticity of layer 2/3 maps in rat barrel cortex in vivo. *Neuron*, 31 (2), pp.305–315.

Stevens, C. F. (2015). What the fly's nose tells the fly's brain. *Proceedings of the National Academy of Sciences of the United States of America*, 112 (30), pp.9460–9465.

Strausfeld, N. J., Sinakevitch, I. and Vilinsky, I. (2003). The mushroom bodies ofDrosophila melanogaster: An immunocytological and golgi study of Kenyon cell organization in the calyces and lobes. *Microscopy Research and Technique*, 62 (2), pp.151–169. [Online]. Available at: doi:10.1002/jemt.10368.

Stürner, T. et al. (2025). Comparative connectomics of Drosophila descending and ascending neurons. *Nature*. [Online]. Available at: doi:10.1038/s41586-025-08925-z.

Südhof, T. C. (2012). The presynaptic active zone. *Neuron*, 75 (1), pp.11–25.

Taylor, H. B. C. and Jeans, A. F. (2021). Friend or foe? The varied faces of homeostatic synaptic plasticity in neurodegenerative disease. *Frontiers in cellular neuroscience*, 15, p.782768.

Tedford, H. W. and Zamponi, G. W. (2006). Direct G protein modulation of Cav2 calcium channels. *Pharmacological reviews*, 58 (4), pp.837–862.

Tempel, B. L. et al. (1987). Sequence of a probable potassium channel component encoded at Shaker locus of Drosophila. *Science (New York, N.Y.)*, 237 (4816), pp.770–775.

Thiagarajan, T. C., Lindskog, M. and Tsien, R. W. (2005). Adaptation to synaptic inactivity in hippocampal neurons. *Neuron*, 47 (5), pp.725–737.

Tierney, A. J. and Harris-Warrick, R. M. (1992). Physiological role of the transient potassium current in the pyloric circuit of the lobster stomatogastric ganglion. *Journal of neurophysiology*, 67 (3), pp.599–609.

Tjia, M. et al. (2017). Pyramidal neurons in different cortical layers exhibit distinct dynamics and plasticity of apical dendritic spines. *Frontiers in neural circuits*, 11. [Online]. Available at: doi:10.3389/fncir.2017.00043.

Tonoki, A. and Davis, R. L. (2015). Aging impairs protein-synthesis-dependent long-term memory in Drosophila. *The Journal of neuroscience: the official journal of the Society for Neuroscience*, 35 (3), pp.1173–1180.

Tononi, G. and Cirelli, C. (2003). Sleep and synaptic homeostasis: a hypothesis. *Brain research bulletin*, 62 (2), pp.143–150.

Tononi, G. and Cirelli, C. (2006). Sleep function and synaptic homeostasis. *Sleep medicine reviews*, 10 (1), pp.49–62.

Tononi, G. and Cirelli, C. (2014). Sleep and the price of plasticity: from synaptic and cellular homeostasis to memory consolidation and integration. *Neuron*, 81 (1), pp.12–34.

Tracey, T. J. et al. (2018). Neuronal lipid metabolism: Multiple pathways driving functional outcomes in health and disease. *Frontiers in molecular neuroscience*, 11. [Online]. Available at: doi:10.3389/fnmol.2018.00010.

Tully, T. et al. (1994). Genetic dissection of consolidated memory in Drosophila. *Cell*, 79 (1), pp.35–47.

Turner, G. C., Bazhenov, M. and Laurent, G. (2008). Olfactory representations by Drosophila mushroom body neurons. *Journal of neurophysiology*, 99 (2), pp.734–746.

Turrel, O. et al. (2022). Transient active zone remodeling in the Drosophila mushroom body supports memory. *Current biology: CB*, 32 (22), pp.4900-4913.e4.

Turrigiano, G., Abbott, L. F. and Marder, E. (1994). Activity-dependent changes in the intrinsic properties of cultured neurons. *Science (New York, N.Y.)*, 264 (5161), pp.974–977.

Turrigiano, G. G. et al. (1998). Activity-dependent scaling of quantal amplitude in neocortical neurons. *Nature*, 391 (6670), pp.892–896.

Venken, K. J. T. et al. (2006). P[acman]: a BAC transgenic platform for targeted insertion of large DNA fragments in D. melanogaster. *Science (New York, N.Y.)*, 314 (5806), pp.1747–1751.

Vierock, J. et al. (2017). Molecular determinants of proton selectivity and gating in the red-light activated channelrhodopsin Chrimson. *Scientific reports*, 7 (1), p.9928.

de Vivo, L. et al. (2017). Ultrastructural evidence for synaptic scaling across the wake/sleep cycle. *Science (New York, N.Y.)*, 355 (6324), pp.507–510.

Voglis, G. and Tavernarakis, N. (2006). The role of synaptic ion channels in synaptic plasticity. *EMBO reports*, 7 (11), pp.1104–1110.

Vosshall, L. B., Wong, A. M. and Axel, R. (2000). An olfactory sensory map in the fly brain. *Cell*, 102 (2), pp.147–159.

Walter, A. M., Böhme, M. A. and Sigrist, S. J. (2018). Vesicle release site organization at synaptic active zones. *Neuroscience research*, 127, pp.3–13.

Wang, B.-S., Sarnaik, R. and Cang, J. (2010). Critical period plasticity matches binocular orientation preference in the visual cortex. *Neuron*, 65 (2), pp.246–256.

Wang, C.-M. et al. (2023). Forgotten memory storage and retrieval in Drosophila. *Nature communications*, 14 (1), p.7153.

Wang, J. W. et al. (2003). Two-photon calcium imaging reveals an odor-evoked map of activity in the fly brain. *Cell*, 112 (2), pp.271–282.

Wang, Y. et al. (2008). Imaging of an early memory trace in the Drosophila mushroom body. *The Journal of neuroscience: the official journal of the Society for Neuroscience*, 28 (17), pp.4368–4376.

Watt, A. J. et al. (2000). Activity coregulates quantal AMPA and NMDA currents at neocortical synapses. *Neuron*, 26 (3), pp.659–670.

Watt, A. J. et al. (2004). A proportional but slower NMDA potentiation follows AMPA potentiation in LTP. *Nature neuroscience*, 7 (5), pp.518–524.

Weiss, J. N. (1997). The Hill equation revisited: uses and misuses. *FASEB journal: official publication of the Federation of American Societies for Experimental Biology*, 11 (11), pp.835–841.

Weiss, J. T. and Donlea, J. M. (2021). Sleep deprivation results in diverse patterns of synaptic scaling across the Drosophila mushroom bodies. *Current biology: CB*, 31 (15), pp.3248-3261.e3.

Weyhersmüller, A. et al. (2011). Rapid active zone remodeling during synaptic plasticity. *The Journal of neuroscience: the official journal of the Society for Neuroscience*, 31 (16), pp.6041–6052.

Wierenga, C. J., Ibata, K. and Turrigiano, G. G. (2005). Postsynaptic expression of homeostatic plasticity at neocortical synapses. *The Journal of neuroscience: the official journal of the Society for Neuroscience*, 25 (11), pp.2895–2905.

Wiesel, T. N. and Hubel, D. H. (1963). Single-cell responses in striate cortex of kittens deprived of vision in one eye. *Journal of neurophysiology*, 26, pp.1003–1017.

Williams, S. R. and Stuart, G. J. (2003). Role of dendritic synapse location in the control of action potential output. *Trends in neurosciences*, 26 (3), pp.147–154.

Willmore, B. and Tolhurst, D. J. (2001). Characterizing the sparseness of neural codes. *Network (Bristol, England)*, 12 (3), pp.255–270.

Wu, C. F. et al. (1983). Potassium currents in Drosophila: different components affected by mutations of two genes. *Science (New York, N.Y.)*, 220 (4601), pp.1076–1078.

Wu, H. et al. (2018). The MICALs are a family of F-actin dismantling oxidoreductases conserved from Drosophila to humans. *Scientific reports*, 8 (1). [Online]. Available at: doi:10.1038/s41598-017-17943-5.

Wu, J. S. and Luo, L. (2006). A protocol for mosaic analysis with a repressible cell marker (MARCM) in Drosophila. *Nature protocols*, 1 (6), pp.2583–2589.

Wu, L.-G. and Chan, C. Y. (2022). Multiple roles of actin in exo- and endocytosis. *Frontiers in synaptic neuroscience*, 14, p.841704.

Wu, X. and Hammer, J. A. (2021). ZEISS airyscan: Optimizing usage for fast, gentle, super-resolution imaging. In: *Confocal Microscopy*. Methods in molecular biology (Clifton, N.J.). New York, NY: Springer US. pp.111–130.

Wu, Y. K. et al. (2020). Homeostatic mechanisms regulate distinct aspects of cortical circuit dynamics. *Proceedings of the National Academy of Sciences of the United States of America*, 117 (39), pp.24514–24525.

Xu, T. and Rubin, G. M. (1993). Analysis of genetic mosaics in developing and adult Drosophila tissues. *Development (Cambridge, England)*, 117 (4), pp.1223–1237.

Xue, M., Atallah, B. V. and Scanziani, M. (2014). Equalizing excitation-inhibition ratios across visual cortical neurons. *Nature*, 511 (7511), pp.596–600.

Yadav, A. et al. (2012). Morphologic evidence for spatially clustered spines in apical dendrites of monkey neocortical pyramidal cells. *The Journal of comparative neurology*, 520 (13), pp.2888–2902.

Yang, H. H. et al. (2016). Subcellular imaging of voltage and calcium signals reveals neural processing in vivo. *Cell*, 166 (1), pp.245–257.

Yang, J.-Y. et al. (2023). Restructuring of olfactory representations in the fly brain around odor relationships in natural sources. *bioRxiv*. [Online]. Available at: doi:10.1101/2023.02.15.528627.

Yang, Y. et al. (2018). Improved calcium sensor GCaMP-X overcomes the calcium channel perturbations induced by the calmodulin in GCaMP. *Nature communications*, 9 (1). [Online]. Available at: doi:10.1038/s41467-018-03719-6.

Yao, C. A., Ignell, R. and Carlson, J. R. (2005). Chemosensory coding by neurons in the coeloconic sensilla of the Drosophila antenna. *The Journal of neuroscience: the official journal of the Society for Neuroscience*, 25 (37), pp.8359–8367.

Yasuyama, K., Meinertzhagen, I. A. and Schürmann, F.-W. (2002). Synaptic organization of the mushroom body calyx in Drosophila melanogaster. *The Journal of comparative neurology*, 445 (3), pp.211–226.

Yoon, B.-J. et al. (2009). Essential role for a long-term depression mechanism in ocular dominance plasticity. *Proceedings of the National Academy of Sciences of the United States of America*, 106 (24), pp.9860–9865.

Yu, D., Akalal, D.-B. G. and Davis, R. L. (2006). Drosophila alpha/beta mushroom body neurons form a branch-specific, long-term cellular memory trace after spaced olfactory conditioning. *Neuron*, 52 (5), pp.845–855.

Zavitz, D. et al. (2021). Connectivity patterns that shape olfactory representation in a mushroom body network model. *bioRxiv*, bioRxiv. [Online]. Available at: doi:10.1101/2021.02.10.430647.

Zeldenrust, F., Gutkin, B. and Denéve, S. (2021). Efficient and robust coding in heterogeneous recurrent networks. *PLoS computational biology*, 17 (4), p.e1008673.

Zemelman, B. V. et al. (2002). Selective photostimulation of genetically chARGed neurons. *Neuron*, 33 (1), pp.15–22.

Zhang, C. et al. (2019). Optimized photo-stimulation of halorhodopsin for long-term neuronal inhibition. *BMC biology*, 17 (1), p.95.

Zhang, Y. et al. (2021). Clock neurons gate memory extinction in Drosophila. *Current biology: CB*, 31 (6), pp.1337-1343.e4.

Zhang, Y. et al. (2023). Fast and sensitive GCaMP calcium indicators for imaging neural populations. *Nature*, 615 (7954), pp.884–891.

Zhao, C., Dreosti, E. and Lagnado, L. (2011). Homeostatic synaptic plasticity through changes in presynaptic calcium influx. *The Journal of neuroscience: the official journal of the Society for Neuroscience*, 31 (20), pp.7492–7496.

Zheng, Z. et al. (2020). Structured sampling of olfactory input by the fly mushroom body. *Current biology: CB*, 32, pp.3334-3349.e6.

Zipfel, W. R., Williams, R. M. and Webb, W. W. (2003). Nonlinear magic: multiphoton microscopy in the biosciences. *Nature biotechnology*, 21 (11), pp.1369–1377.